



THE UNIVERSITY OF QUEENSLAND
AUSTRALIA

**Production and *in vitro* Evaluation of
Macroporous Alginate Hydrogel
Fibres for Nerve Tissue Engineering**

SHARON CHIEN-YU LIN

B. Biotech (Drug Design and Development) Hons.

*A thesis submitted for the degree of Doctor of Philosophy at
The University of Queensland in 2015*

Australian Institute for Bioengineering and Nanotechnology
Pharmacy Australia Centre of Excellence

Abstract

The prospects for successful peripheral nerve repair using fibre guides are considered to be enhanced by use of a scaffold material which provides a good substrate for attachment and growth of glial cells and regenerating neurons. Alginate polymers exhibit a highly favourable balance of properties and exhibit the unique property of forming hydrogels under mild crosslinking conditions. As a result alginate has been widely applied for cell encapsulation. However the polysaccharide exhibits extremely poor cell adhesion properties, which limits its application for tissue regeneration.

Alginate fibres were modified by gelatin a) to improve cell adhesion b) to investigate the potential for polypeptide growth factor incorporation in the fibres and c) to provide a method for macropore production by extraction of the gelatin particles from the fibres (**Chapter 2**). Incubation of hydrated alginate fibres in 0.5% w/w gelatin solution at 37 °C resulted in low protein loading (1.7% w/w) and rapid release of gelatin (90% of the initial load) over 24 h in distilled water at 37 °C. In comparison, incubation of hydrated alginate fibres in 5% w/v gelatin solution resulted in approximately 9% w/w protein loading and gradual protein release (80% of initial content) over 9 days. Alginate fibres incorporating gelatin particles were successfully produced by wet spinning suspensions of gelatin particles in 1.5% (w/v) alginate solution. Gelatin loading of the starting suspension of 40.0, 57.0 and 62.5% w/w resulted in gelatin loading of the hydrated alginate fibres of 16, 21 and 24% w/w respectively. Around 45 – 60% of the gelatin content of hydrated fibres was released in 1 h in distilled water at 37 °C, suggesting that a macromolecular structure for cell growth would be rapidly established in cell culture. Furthermore, the residual gelatin is expected to form a favourable surface for nerve cell adhesion and axonal extension.

The production of macroporous alginate fibres for cell encapsulation (**Chapter 3**) was achieved by wet spinning suspensions of gelatin particles in alginate solution into CaCl₂ crosslinking solution, followed by protein extraction in distilled water. Confocal laser scanning microscopy (CLSM) and image analysis provided detailed qualitative and quantitative information on pore size and size distribution. CLSM and image analysis also provided measurements of the connectivity of macropores within the hydrogel scaffold which is essential to permit a high level of cell ingrowth.

The ability of plain alginate fibres and macroporous alginate fibres to maintain viability of encapsulated cells and to promote cell growth was assessed using fibroblasts in **Chapter 4**. Swiss 3T3 mouse fibroblasts were encapsulated in alginate fibres by wet spinning cell suspensions of alginate solutions. Increasing the cell concentration of the spinning solution from 1.4×10^4 to 1.5×10^6 cells/mL resulted in no significant improvement of fibroblast extension and growth. Human adult dermal fibroblasts (HDFa) were incorporated in macroporous alginate fibres by wet spinning alginate solutions containing both gelatin microparticles and suspended cells (cell concentration 3×10^5 cells/mL). Cell distribution was evaluated using CLSM (following staining with Calcein-AM) at an excitation wavelength of 488 nm. Fibroblast-loaded macroporous alginate fibres were characterised by a cell density of approximately 360 cells/mm³ which was significantly higher (*P<0.05) than that of non-macroporous fibres (approximately 140 cells/mm³). Cell viability was maintained for time periods of at least 12 days. This finding indicates a potential for repair of soft tissue by encapsulating cells or genetically modified, growth factor-secreting variants in alginate fibres.

Encapsulation of nerve cells (primary DRG) in macroporous alginate fibres and cell

development within the fibre are described in **Chapter 5**. Marked outgrowth of DRGs was evident within the fibre at day 11 in cell culture, indicating that macropores and channels created within the alginate hydrogel by gelatin extraction were providing a favourable environment for nerve cell development. Evidence of neurite contact was obtained at day 9. These findings indicate that macroporous alginate fibres encapsulating nerve cells may provide a useful strategy for nerve repair.

Retinal degeneration including retinitis pigmentosa (RP) and age related macular degeneration (AMD) caused by progressive and eventual death of photoreceptor cells can eventually lead to blindness. Macroporous alginate fibres were produced incorporating cone photoreceptor-derived (661W) cells to investigate their potential as tissue engineering scaffolds for retinal repair (**Chapter 6**). Significantly higher cell proliferation (* $P < 0.05$) was evident within macroporous fibres at day 14 in cell culture compared with non-macroporous fibres. Cell flattening and elongation with formation of cell extensions/projections was extensive in 2D culture on tissue culture plastic (TCP) but was not observed in 3D culture within the fibres, indicating that a suitable pore/channel structure for photoreceptor cell development was not created within the alginate hydrogel at 14 days in cell culture.

Declaration by Author

This thesis is composed of my original work, and contains no material previously published or written by another person except where due reference has been made in the text. I have clearly stated the contribution by others to jointly-authored works that I have included in my thesis.

I have clearly stated the contribution of others to my thesis as a whole, including statistical assistance, survey design, data analysis, significant technical procedures, professional editorial advice, and any other original research work used or reported in my thesis. The content of my thesis is the result of work I have carried out since the commencement of my research higher degree candidature and does not include a substantial part of work that has been submitted *to qualify for the award of any* other degree or diploma in any university or other tertiary institution. I have clearly stated which parts of my thesis, if any, have been submitted to qualify for another award.

I acknowledge that an electronic copy of my thesis must be lodged with the University Library and, subject to the policy and procedures of The University of Queensland, the thesis be made available for research and study in accordance with the Copyright Act 1968 unless a period of embargo has been approved by the Dean of the Graduate School.

I acknowledge that copyright of all material contained in my thesis resides with the copyright holder(s) of that material. Where appropriate I have obtained copyright permission from the copyright holder to reproduce material in this thesis.



Sharon Chien-Yu Lin

February 2015

Publications during candidature

PUBLICATIONS

D. M. Hariyadi, **S.C.-Y. Lin**, Y. Wang, T. Bostrom, B. Bhandar and A.G.A. Coombes, Diffusion loading and drug delivery characteristics of alginate gel microparticles produced by a novel impinging aerosols method. *Journal of Drug Targeting* 18(10):831-41 (2010) (IF: 3)

D. M. Hariyadi, Y. Wang, **S.C.-Y. Lin**, T. Bostrom, B. Bhandar and A.G.A. Coombes, Novel alginate gel microspheres produced by impinging aerosols for oral delivery of proteins. *Journal of Microencapsulation* 29(3):250-61 (2012) (IF: 1.9)

POSTERS

Sharon Chien-Yu Lin, Yiwei Wang, Sally Firth, Allan Coombes. *Characterisation of alginate fibres for controlled delivery of proteins in nerve regeneration*. Tissue Engineering & Regenerative Medicine International Society Asia-Pacific (TERMIS-AP) Meeting, Taipei, 2008.

Sharon Chien-Yu Lin, Yiwei Wang, Sally I Firth, Allan Coombes. *Characterisation of alginate fibres for controlled delivery of proteins in nerve regeneration*. The Australasian Pharmaceutical Science Association (APSA) Conference. ANU, Canberra, 2008.

Sharon Chien-Yu Lin, David Wertheim, Paul Tomlins, Elzbieta Gurdak, *Cell Immobilisation in Alginate Fibres for Soft Tissue Engineering*. APSA Conference, Brisbane, 2010.

Publications included in this thesis

No publication included in this thesis.

Contributions by others to the thesis

No contributions by others.

Statement of parts of the thesis submitted to qualify for the award of another degree

No part of thesis submitted to qualify for the award of another degree.

Acknowledgements

My exhilarating, frustrating but totally absorbing PhD project would not have started if not for my outstanding and experienced director of studies at the Pharmacy Australia Centre of Excellence (PACE), Professor Allan Coombes, who provided invaluable professional guidance throughout the course of my PhD studies. I have learned a great deal from his supervision and knowledge. I am greatly indebted to him for his continuous encouragement and helpful advice. Sincerely and heartily, I would like to thank him with great gratitude and appreciation.

Special thanks are also due to my current supervisor Professor Traian Chirila (Chief Scientist, Queensland Eye Institute) and co-supervisor Associate Professor Idriss Blakey (Australian Research Council (ARC) Future Fellow, Australian Institute for Bioengineering and Nanotechnology (AIBN)). I would have lost the opportunity of completing my thesis if not for their tremendous support, encouragement and invaluable discussions during my thesis review.

I am grateful to my former co-supervisor at PACE, Dr Sally Firth for providing advice, expertise and tuition in immunolabelling and fluorescence microscopy. I am indebted to Dr Paul Tomlins (Research Group Leader) and Dr Elzbieta Gurdak for their valuable time and supervision in confocal laser scanning (CLSM) image acquisition at the National Physical Laboratory (NPL), Teddington, UK. I thank Dr Xiong-Wei Li (Research Fellow, School of Pharmacy, University of London) for his support and assistance in obtaining valuable and high quality cell culture data.

Professor David Wertheim (Director of the Scientific Analysis and Visualisation Centre (SAVIC) at Kingston University, London) merits very special thanks and appreciation, not only for his diligent efforts in providing an enriching experience in CLSM image analysis but also for being a wonderful host during my research visit to the UK.

I would like to express my appreciation to Dr Yiwei Wang of the ANZAC Medical Research Institute, Sydney and Dr Fiona Li of the Queensland Eye Institute for their insightful comments, advice and instruction on cell culture during my PhD studies.

I greatly appreciate the advice and technical assistance with tensile testing given by Dr Grant Edwards, from the AIBN and I acknowledge the support of Dr Daniel Sangermani, Manager of the Centre for Advanced Light Microscopy (CALM), the University of Queensland, in providing access to the FluoView confocal laser scanning microscope. Special thanks are also due to Luke Hammond, Manager of the Queensland Brain Institute (QBI) Microscopy Facility for his efforts in helping me acquire expertise in image analysis using the CLSM.

I would also like to express my appreciation to Dr James St John, Group Leader, Olfactory Ensheathing Cell Biology, National Adult Stem Cell Research Centre (NASCRC), Griffith University and Susan Scott, research assistant at NASCRC for generously supplying Swiss 3T3 fibroblasts and for their insightful advice and technical assistance with cell culture.

I am grateful to the University of Queensland for the award of a Graduate School Research Travel Grant in 2010, which allowed me to visit the National Physical

Laboratory in London, one of the UK's leading research organisations, to analyse the macroporous structure of alginate hydrogel fibres and its influence on cell growth. I also appreciate the encouraging and supportive research environment provided by the Pharmacy Australia Centre of Excellence and the Queensland Eye Institute and the advice and assistance of their dedicated staff members from academic and administrative disciplines.

My life at the University of Queensland and the short visit to the NPL, Kingston University, London and the School of Pharmacy, University of London were enriched by many people around me. Thanks especially to my colleagues, Dr Dewi M. Hariyadi, Honours Student, Ms Ee Li Yu and my wonderful supporting friends, Jessica Xin Liu, Cymin Lien and all Movenpick Southbank colleagues.

To my best friend and boyfriend Christopher Lam Shang Leen, I cannot thank you enough for your love, encouragement, patience, and sacrifice. You have always been my support, my cheerleader, and the best "cook" in the house. Thank you for always listening and calming me down during frustrating times, and for keeping me company during those long nights of writing.

Most importantly, I wish to express my deepest gratitude to my sister, brother, auntie and especially my parents and grandparents. Their support and selfless affection made my studies possible. If it were not for them, this work would not have happened.

Keywords

alginate, hydrogel, fibres, gelatin, tissue engineering, nerve regeneration, soft tissue repair, macropores, image analysis

Australian and New Zealand Standard Research Classifications (ANZSRC)

ANZSRC code: 090301 Biomaterials, 60%

ANZSRC code: 060106 Cellular Interactions (incl. Adhesion, Matrix, Cell Wall), 40%

Fields of Research (FoR) Classification

FoR code: 0903 Biomedical Engineering, 60%

FoR code: 0601, Biochemistry and Cell Biology, 40%

Table of Contents

Abstract.....	i
Declaration by Author	iv
Acknowledgements	vii
Table of Contents	xi
List of Figures and Tables	xv
List of Abbreviations.....	xxviii
CHAPTER 1	1
Introduction.....	1
1.1 LITERATURE REVIEW	2
1.1.2 Extracellular matrix and the design of artificial scaffolds	2
1.1.3 Nerve structure and regeneration	4
1.1.4 Polymers used for scaffold manufacture.....	10
1.1.5 Alginate	17
1.1.6 Cell encapsulation in alginate polymers	25
1.1.7 Scaffold design and manufacture for tissue engineering	25
1.1.8 Cell interaction with polymeric scaffolds	31
1.1.9 Cell migration	33
1.1.10 Cell adhesion and integrin receptors.....	34
1.1.11 Growth factors and nerve regeneration	35
Specific Research Objectives	37
CHAPTER 2.....	39
Production of Alginate Fibres for Nerve Tissue Engineering	39
ABSTRACT.....	39
2.1 INTRODUCTION	41
2.2 MATERIALS	43
2.3 METHODS	43
2.3.1 Wet spinning of alginate fibres	43
2.3.2 Gelatin modification of alginate fibres	44
2.3.3 Incorporation of gelatin in alginate fibres as a porogen for producing	

macropores	45
2.3.4 Determination of the gelatin loading of alginate fibres	46
2.3.5 Gelatin release from gelatin-modified alginate fibres	47
2.3.6 Gelatin release from hydrated alginate fibres containing gelatin particles	48
2.3.7 Tensile properties of dried alginate fibres	48
2.3.8 Morphology of hydrated alginate fibres using cryo-scanning electron microscopy	50
2.3.9 Morphology of dried alginate fibre using scanning electron microscopy	51
2.4 RESULTS AND DISCUSSION.....	51
2.4.1 Dimensions and morphology of alginate fibres	51
2.4.2 Tensile properties of dried alginate fibres	55
2.4.3 Gelatin modification of alginate fibres by incubation in gelatin solution.....	56
2.4.4 Gelatin loading and release from alginate fibres spun into gelatin/CaCl ₂ solution	60
2.4.5 Gelatin loading and release from fibres wet spun from a mixed alginate/gelatin solution	61
2.4.6 Incorporation of gelatin particles in alginate fibres to produce macropores	62
2.5 CONCLUSION.....	64
CHAPTER 3.....	66
Production and Characterisation of a Macroporous Structure in Alginate Fibres for Nerve Repair	66
ABSTRACT.....	66
3.1 INTRODUCTION	66
3.2 MATERIALS	72
3.3 METHODS	72
3.3.1 Production of macroporous alginate fibres	72
3.3.2 Gelatin particle size distribution	72
3.3.3 Morphology of macroporous alginate fibres.....	73
3.3.4 Preparation of alginate fibre cryosections.....	73
3.3.4 FluoView Confocal Laser Scanning Microscopy (CLSM).....	74
3.3.5 Quantitative analysis of the internal pore structure of alginate fibres	74
3.4 RESULTS AND DISCUSSION.....	77
3.5 CONCLUSIONS.....	93

CHAPTER 4.....94

Cell Encapsulation of in Alginate Hydrogel Fibres Using Wet Spinning

Techniques94

ABSTRACT..... 94

4.1 INTRODUCTION 95

4.2 MATERIALS 97

4.3 METHODS 98

 4.3.1 Culture of Swiss 3T3 fibroblasts..... 98

 4.3.2 Encapsulation of Swiss 3T3 fibroblasts in alginate fibres by wet spinning..... 99

 4.3.3 Encapsulation of Swiss 3T3 fibroblasts-in macroporous alginate fibres 100

 4.3.4 Imaging of Swiss 3T3 mouse fibroblasts encapsulated in alginate fibres using confocal laser scanning microscopy..... 102

 4.3.5 Encapsulation of human adult dermal fibroblasts (HDFa) in macroporous alginate fibres 102

 4.3.6 Viability assay of HDFa cells encapsulated in macroporous alginate fibres using Calcein-AM staining 103

 4.3.7 Cell Staining..... 104

 4.3.8 Imaging of encapsulated HDFa in alginate fibres using CLSM..... 106

 4.3.9 Image compilation and data analysis following Calcein-AM staining of HDFa 107

4.4 RESULTS AND DISCUSSION..... 109

 4.4.1 Encapsulation of Swiss 3T3 fibroblasts in alginate fibres. 109

 4.4.2 Incorporation of Swiss 3T3 fibroblasts in macroporous alginate fibres 115

 4.4.3 Incorporation of HDFa in macroporous alginate fibres 117

4.5 CONCLUSION..... 121

CHAPTER 5..... 122

Encapsulation of Primary Rat Dorsal Root Ganglia in Macroporous Alginate

Fibres for Nerve Regeneration..... 122

ABSTRACT..... 122

5.1 INTRODUCTION 122

5.2 MATERIALS 127

5.3 METHODS 127

5.3.1 Preparation of cryo-sectioned mouse retinal tissue	127
5.3.2 Immunolabelling of retinal tissue	128
5.3.3 Imaging of immunolabelled mouse retinal tissue	130
5.3.4 Encapsulation of primary rat DRG cells in non-macroporous and macroporous alginate fibres	130
5.3.5 Immunolabelling of DRG cells encapsulated in alginate fibres	134
5.3.6 Assay of viability of primary rat DRG cells encapsulated in alginate fibres using Calcein-AM staining	134
5.4 RESULTS AND DISCUSSION.....	135
5.5 CONCLUSION.....	147
CHAPTER 6.....	148
Encapsulation of 661W Cone Photoreceptor Cells in Macroporous Alginate Fibre Scaffolds for Retinal Regeneration	148
ABSTRACT.....	148
6.1 INTRODUCTION	148
6.2 MATERIALS	151
6.3 METHODS	152
6.3.1 661W cell growth on tissue culture plastic (TCP)	152
6.3.2 Encapsulation of 661W cells in non-macroporous alginate fibres ...	153
6.3.3 Encapsulation of 661W cells in macroporous alginate fibres.....	153
6.3.4 Measurement of cell viability using the alamarBlue® Assay.....	154
6.3.5 Immunolabelling of 661W cells grown on TCP or encapsulated in alginate fibres using β -tubulin III antibody	156
6.3.6 Fluorescent labelling of 661W cell nuclei	157
6.3.7 Assay of viability of 661W cells encapsulated in alginate fibres using Calcein-AM staining.....	158
6.4 RESULTS AND DISCUSSION.....	159
6.5 CONCLUSIONS.....	168
CHAPTER 7.....	169
Overall Conclusions and Future Work	169
REFERENCES.....	174

List of Figures and Tables

Figure 1.1 Biodegradable three-dimensional scaffold used to promote cell attachment, proliferation and differentiation. The scaffold with or without cells and/or biological signalling molecules (e.g. growth factors, cytokines, chemokines and genes) is applied to a defect *in vivo* to induce tissue and organ regeneration.

Figure 1.2 Peripheral motor neuron [5].

Figure 1.3 Schematic drawing of a peripheral nerve [12].

Figure 1.4 Cross-sectional anatomy of a peripheral nerve. Inset at left shows an unmyelinated fibre. Inset at bottom shows a myelinated fibre [13].

Figure 1.5 A photomicrograph of nerve tissue. A single neuron and numerous smaller supporting cells can be seen [14].

Figure 1.6 Types of peripheral nerve injuries [15].

Figure 1.7 Schematic diagram of peripheral nerve regeneration. (A) Normal neuron, (B) Appearance at 2 weeks, (C) 3 weeks, and (D) 3 months after injury. (E) Appearance several months after neuron injury with unsuccessful nerve regeneration [20].

Figure 1.8 Chemical structures of silicone elastomer and polyethylene.

Figure 1.9 Chemical structure of poly(L-lactic acid), polyglycolic acid and poly- ϵ -caprolactone.

Figure 1.10 Laminin molecular structure consisting of three large polypeptides α , β_1 and β_2 crosslinked by disulfide bonds [40].

Figure 1.11 The modular structure of fibronectin and its binding domains [41].

Figure 1.12 Simplified chemical structure of collagen showing the main amino acid.

Figure 1.13 Chemical structure of gelatin.

Figure 1.14 Chemical structure of chitosan.

Figure 1.15 Chemical structure of alginate.

Figure 1.16 (A) Chemical structure of the two monomeric units of alginate. (B)

Structures in Figure 1.16A expressed as ‘chair’ forms.

Figure 1.17 The chemical structure of the M block, G block and MG copolymer of alginate.

Figure 1.18 Production of sodium alginate.

Figure 1.19 Viscosity of 1% alginate solution at different temperatures (adapted from [61]).

Figure 1.20 Gel formation via G blocks of alginate polymers: egg-box model [65].

Figure 1.21 Properties of a nerve guidance channel or conduit. Adapted from [29].

Figure 1.22 Schematic architecture of integrin heterodimeric adhesive receptors consisting of α - and β -subunits. The ligand binding site is provided by the N-terminal domain of the α - and β -integrin subunits (the β -propeller and the β A domain, respectively) which are assembled in most integrins by non-covalent interactions to form a “head”. It is known that in eight α integrin subunits (α 1, α 2, α 10, α 11, α L, α M, α X and α D), the α A domain, which is homologous to the β A domain of the β -integrin subunit, is inserted into the β -propeller domain. This is the main ligand-binding site in these integrins [128].

Figure 2.1 Production of alginate fibres by wet spinning.

Figure 2.2 (A) Optical micrograph of hydrated fibre. (B) Cryo-scanning electron micrograph of hydrated fibre. (Pore size approx. 1 μ m). The fibre was produced by wet spinning a 1% alginate solution through a syringe needle (0.6 \times 32 mm) into 0.5 M CaCl₂ solution.

Figure 2.3 (A) Dried alginate fibre and (B) its oriented surface. Fibres produced by wet spinning from a 1.2 \times 38 mm needle and dehydrated by ethanol treatment.

Figure 2.4 (A) Stress–strain curves of alginate fibres dried using ethanol treatment. (B) Stress–strain curves of alginate fibres dried at 60 °C (n = 5).

Figure 2.5 Gelatin loading of alginate fibres (n = 10, mean ± SD) following incubation in 2% w/v gelatin solution at 37 °C for 48 h. (1) Hydrated alginate fibres. Mean gelatin loading using BCA assay = 9.3% w/w (standard deviation: 0.9). (2) Alginate fibres dried in ethanol. Mean gelatin loading using BCA assay = 15.4% w/w (standard deviation: 11.6).

Figure 2.6 (A) Gelatin release from hydrated alginate fibres ($\mu\text{g}/\text{mg}$ fibre) and (B) Cumulative release of gelatin from hydrated alginate fibres (% w/w) in distilled water at 37 °C over 9 days. Mean fibre weight was 294 ± 26 mg. Fibres were incubated in 0.5, 1, 2 and 5% w/v gelatin solution at 37 °C for 48 h before release testing. Corresponding gelatin loading of fibres was 1.7, 8.9, 8.5 and 9.7% w/w.

Figure 2.7 (A) Gelatin release from alginate fibres dried using ethanol ($\mu\text{g}/\text{mg}$ fibre) in distilled water at 37 °C over 9 days. (B) Cumulative release (% w/w) of gelatin from alginate fibres dried using ethanol. Mean fibre weight was 24 ± 9 mg. Fibres incubated in 0.5, 1, 2 and 5% w/v gelatin at 37 °C for 48 h. Corresponding gelatin loading of fibres was 0.4, 10.6, 24.5 and 72.8% w/w. Release medium: distilled water at 37 °C.

Figure 2.8 (A) Gelatin release ($\mu\text{g}/\text{mg}$ fibre) and (B) cumulative gelatin release (% w/w) from alginate fibres over 9 days in distilled water at 37 °C. (1) Fibres were manufactured by extruding alginate solution (1% w/w) into 0.5 M CaCl_2 crosslinking solution containing dissolved gelatin (2% w/v). (2) Dried alginate fibres were prepared using ethanol treatment.

Figure 2.9 (A) Gelatin release ($\mu\text{g}/\text{mg}$ fibre) and (B) cumulative gelatin release (% w/w) from alginate fibres over 9 days in distilled water at 37 °C. (1) Fibres were manufactured by spinning a mixture of gelatin (2% w/v) and alginate (1% w/v) solution (gelatin:alginate volume ratio 1:1) into 0.5 M CaCl_2 solution. (2) Dried alginate fibres

were prepared by ethanol treatment. Total gelatin loading of (1) hydrated and (2) dried fibres was 1.7 and 1.2% w/w, respectively.

Figure 2.10 (A) Gelatin release ($\mu\text{g}/\text{mg}$ fibre) and (B) cumulative gelatin release (% w/w) from hydrated gelatin-loaded alginate fibres over 2 days in distilled water at 37 °C. Fibres were produced from suspensions of sieved gelatin particles ($<90\ \mu\text{m}$) in alginate solution with gelatin contents of 40.0, 57.0 and 62.5% w/w. The corresponding (actual) loading of gelatin in the spun fibres was 16, 21 and 24% w/w.

Figure 2.11 (A) Gelatin release ($\mu\text{g}/\text{mg}$ fibre) and (B) cumulative gelatin release (% w/w) from dried gelatin-loaded alginate fibres over 2 days in distilled water at 37 °C. Fibres were produced from suspensions of sieved gelatin particles ($<90\ \mu\text{m}$) in alginate solution with gelatin contents of 40.0, 57.0 and 62.5% w/w and were dried using ethanol. The corresponding (actual) loading of gelatin in the spun fibres was 12.4, 18.0 and 36.0% w/w.

Figure 3.1 Micro-CT image of a bioactive glass scaffold produced by a sol–gel foaming process, with streak lines showing the calculated paths of fluid flow [194].

Figure 3.2 Sequential images of an alginate fibre selected from a z-axis stack (slides 95 – 100). (A) pre-processed fluorescence confocal images (B) binary image of the pore phase and (C) binary image of the fibre boundary. Images obtained from a hydrated gelatin-extracted macroporous alginate fibre produced by wet spinning a 62.5% (w/w) gelatin particle suspension in alginate solution. Actual gelatin loading of fibre = 24% w/w.

Figure 3.3 Optical micrograph of a gelatin particle-loaded alginate fibre produced by wet spinning a 57% w/w suspension of gelatin particles in alginate solution.

Corresponding gelatin loading of dried spun fibre = 21% w/w.

Figure 3.4 Scanning electron micrographs of (A) unsieved, (B) sieved gelatin particles in a size range <90 microns. Magnified view at top right.

Figure 3.5 Optical micrographs of gelatin particles suspended in 1.5% w/v alginate solution. (A) unsieved (B) sieved particles before homogenisation (C) unsieved and (D) sieved particles following homogenisation in 1.5% alginate solution for 30 s at 4 °C.

Figure 3.6 Distribution of gelatin particle size. (A) smallest and largest dimensions of unsieved and sieved particles and (B) smallest and largest dimensions of unsieved (control) and sieved particles following homogenisation in 1.5% (w/v) alginate solution for 30 s at 4 °C.

Figure 3.7 Scanning electron micrographs (A and B) of a dried gelatin-extracted alginate fibre produced by wet spinning a 57% w/w suspension of gelatin particles in alginate solution. Macropores are partially visible (arrowed).

Figure 3.8 Cryosection images of hydrated alginate fibres without incorporation of gelatin particles (A and B) reveal a smooth gel surface. The internal macroporous structure (arrowed) of an alginate fibre produced by gelatin extraction (C and D) shows macropores of irregular shape corresponding to the original gelatin particles. Fibres were stained by methylene blue for visualisation using inverted optical microscopy.

Figure 3.9 Wavelength intensity of alginate fibres (A) before and (B) after gelatin extraction in distilled water. Fibres spun from 57% w/w gelatin particle suspension in alginate solution.

Figure 3.10 CLSM images of alginate fibre (A) differential interference contrast (DIC) and (B) autofluorescence. Fibre spun from 1.5% alginate solution through a syringe needle into 0.5 M CaCl₂ solution.

Figure 3.11 CLSM image of a 21% w/w gelatin particle-loaded alginate fibre produced by wet spinning a 57% w/w suspension of gelatin particles in alginate solution. (A) differential interference contrast (DIC) and (B) autofluorescence.

Figure 3.12 CLSM microscopy of hydrated gelatin-extracted macroporous alginate fibres. (A) DIC, (B) autofluorescence, (C) 3D reconstruction showing isolated regions of macropore coalescence and (D) 3D projection view. The fibre was produced by extracting gelatin particles from a 16% w/w gelatin-loaded alginate fibre produced by wet spinning a 40% w/w gelatin particle suspension in alginate solution.

Figure 3.13 CLSM image analyses of hydrated macroporous alginate fibres - frequency distribution of equivalent macropore diameter following extraction of (A) 16%, (B) 21% and (C) 24% w/w gelatin particle-loaded alginate fibres.

Figure 3.14 3D visualization of hydrated 24% w/w gelatin-loaded alginate fibre after protein extraction. (A) pore volume and (B) volume of fibre body.

Figure 3.15 Regions of pore coalescence (highlighted in red) identified by CLSM analysis of (A) 16%, (B) 21% and (C) 24% (w/w) gelatin-loaded alginate fibres after protein extraction. (D) Magnified view of a region of pore coalescence.

Figure 3.16 Determination of tortuosity in a porous material using the arc-chord ratio. (A) Tortuosity of a path through a porous structure (B) Tortuosity determined by the ratio of the pore length (L) to the displacement of the ends of the pore (X). (C) On compression the magnitude of L remains constant, but displacement X is reduced to X', resulting in an increase in tortuosity [221]. (D) Example of tortuosity pathway through a macroporous alginate fibre.

Figure 4.1 Cell encapsulation in a hydrogel tissue-engineered scaffold. The hydrogel acts as a temporary extracellular matrix (ECM) and neo-tissue replaces the scaffold [236].

Figure 4.2 Preparation of Swiss 3T3 fibroblast-loaded alginate hydrogel fibres by wet spinning.

Figure 4.3 Preparation of Swiss 3T3 fibroblast-loaded macroporous alginate fibres.

Figure 4.4 Calcein-acetoxymethyl ester (Calcein-AM) [240].

Figure 4.5 Analysis of HDFa cell distribution and density in macroporous alginate fibre after 12 days of cell culture. Cells were stained using Calcein-AM prior to analysis (viable cells emit strong green fluorescence). (A) Live cells that are in focus on each 2D plane were counted within a 1 mm^2 area in each image section and were marked in green. (B) Counted cells from each slide were labelled in different colour (red) to avoid double counting. (C) The sum of green-labelled cells in all image sections was used to determine the overall cell density.

Figure 4.6 Internal cell to cell distance measured for HDFa-loaded alginate fibres (1 mm^3). (A) non-macroporous alginate fibre, (B) macroporous alginate fibre.

Figure 4.7 Optical micrograph of (A) control cell-free alginate fibres and (B) Swiss 3T3 fibroblasts encapsulated in alginate fibres at day 10 in culture. Fibres produced by spinning cell-alginate solution (cell density of 1.4×10^4 cells/mL in 1.5% w/v alginate solution) into 0.5 M filtered CaCl_2 solution.

Figure 4.8 CLSM images of (A) Swiss 3T3 fibroblasts encapsulated in alginate fibres after 8 weeks in cell culture. (B) Magnified view of elongated fibroblasts in selected field of view. Fibre produced by spinning cell-alginate solution (cell density of 1.4×10^4 cells/mL in 1.5% w/v alginate solution) into 0.5 M filtered CaCl_2 solution. Cells stained with DAPI to label the cell nucleus (blue) and rhodamine to label the actin filaments (pink).

Figure 4.9 Optical micrographs of (A) hydrated cell-free alginate fibres, (B) Swiss 3T3 fibroblasts encapsulated in alginate fibres at day 17 of cell culture (C) day 23 of cell culture (D) magnified view of elongated fibroblasts (arrowed) in selected field of view. (E and F) fractured fibre at day 17 of cell culture. Alginate fibre produced by spinning suspension of fibroblasts in alginate solution (cell density 1.5×10^6 cells/mL in 1.5% w/v alginate solution) into 0.5 M CaCl_2 solution.

Figure 4.10 Cell morphology and organization of 3T3 Fibroblasts encapsulated in

GelMA hydrogel. (A) Rhodamine B stained GelMA hydrogel construct shows patterned and unpatterned regions. (B) Representative phase contrast images of 3T3-fibroblasts (10×10^6 cells/mL) encapsulated in patterned (top row) and unpatterned regions (bottom row) of the hydrogel on days 1, 3 and 5 of culture. Cell elongation increases over time for all hydrogels, while alignment is only induced in patterned constructs [263].

Figure 4.11 Optical micrographs of (A) cell-free gelatin particle-loaded alginate fibre before particle extraction (B) cell-free gelatin particle-loaded alginate fibres following particle extraction (C) macroporous alginate fibres incorporating Swiss 3T3 fibroblasts at day 7 of cell culture (D) magnified view of elongated fibroblasts (arrowed) in selected field of view, (E) macroporous alginate fibres incorporating Swiss 3T3 fibroblasts at day 13 of cell culture, (F) magnified view of contacting fibroblasts (arrowed) in selected field of view. Macroporous alginate fibres produced by wet spinning suspension of Swiss 3T3 fibroblasts and gelatin particles in alginate solution into 0.5 M CaCl_2 (cell density 1.5×10^6 cells/mL, gelatin particle 57% w/w, 1.5% w/v alginate solution).

Figure 4.12 Human adult dermal fibroblast cell (HDFa) density in non-macroporous and macroporous alginate fibres. HDFa were suspended in alginate solution with or without gelatin particles at 3×10^5 cells/mL. Wet spun fibre samples subjected to Calcein-AM staining and cell density determined using CLSM. (One way ANOVA * $P < 0.05$, $n = 5$).

Figure 4.13 CLSM image at day 12 in cell culture of HDFa cells loaded in macroporous alginate fibres. WGA- and DAPI-labelled HDFa cells in (A) non-macroporous alginate fibre, (B) macroporous alginate fibre. Live/dead staining with Calcein-AM of HDFa cells in (C) non-macroporous alginate fibre, (D) macroporous alginate fibre. 3D visualisation of DAPI- and WGA-labelled HDFa cells

in (E) non-macroporous alginate fibre, (F) macroporous alginate fibre.

Non-macroporous HDFa-containing alginate fibre produced by spinning cell suspension in alginate solution (cell density of 1.3×10^6 cells/mL in 1.5% w/v alginate solution) into CaCl_2 solution. Macroporous HDFa-containing fibre produced by spinning suspension of HDFa fibroblasts and gelatin particles in alginate solution into CaCl_2 solution (cell density 1.3×10^6 cells/mL, gelatin particle 57% w/w, 1.5% w/v alginate solution).

Figure 4.14. Flowchart illustrating the method of Thevenot et al. to quantify 3D cell distribution and infiltration [268].

Figure 5.1 Schematic representation of a neuron and detailed view of the growth cone with its main cytoskeletal components (actin filaments and microtubules) [284].

Figure 5.2 Serial dilutions of the primary antibody (TU-20) in blocking solution.

Figure 5.3 Sensory peripheral neurons are called pseudounipolar neurons [288].

Figure 5.4 Preparation of non-macroporous (blue arrowed) and macroporous (black arrowed) alginate fibres encapsulating primary rat DRG cells.

Figure 5.5 Bright field microscopy images of DRGs encapsulated in a non-macroporous alginate fibre at Day 1 (A), Day 5 (B), Day 11 (C) and Day 15 (D) in cell culture.

Figure 5.6 Bright field microscopy of DRGs encapsulated in a alginate fibre by wet spinning suspensions of cells and gelatin particles in alginate solution at Day 1 (A), Day 2 (B), Day 5 (C), Day 9 (D), Day 11 (E) and Day 15 (F) in cell culture.

Figure 5.7 Morphology of DRGs encapsulated in alginate fibre and observed using inverted microscopy. (A–C) Early stage of neurite outgrowth at day 1 – 5, (D) a pseudounipolar-DRG-like neuron (E–F) DRGs aggregate in balls and extend multiple neurites becoming a densely branching network after 9 days, (G–I) evidence of neuronal contacts.

Figure 5.8 CLSM characterisation of dendritic outgrowth from rat DRG cells contained in a macroporous alginate fibre at day 15 in cell culture. (A) Superimposed DIC/autofluorescent and (B) autofluorescent images of the neurites.

DRG-containing fibre produced by wet spinning 1.5% w/v alginate solution containing DRGs (cell density 6.25×10^3 cells/mL) and gelatin particles (57% w/w) into 0.5 M CaCl₂ solution. Autofluorescence produced using UV at excitation wavelength 350 nm and emission maximum 460 nm.

Figure 5.9 Rat dorsal root ganglion cells at 5 days in cell culture, subjected to live/dead assay by staining with Calcein-AM. Cells were seeded on 6-well plate at densities of 6.25×10^3 cells/mL. The DRG cells display outgrowth and varied cell soma size (7 – 20 μ m).

Figure 5.10 Live/dead staining assay using Calcein-AM of rat DRGs encapsulated in non-macroporous alginate fibre at (A) day 2, (B) day 5 in culture. Rat DRGs encapsulated in macroporous alginate fibre at (C) day 2 and (D) day 5 in culture. DRG-containing macroporous alginate fibre produced by wet spinning alginate solution (1.5% w/v) containing DRG (cell density 6.25×10^3 cells/mL) and gelatin particles (57% w/w) into 0.5 M CaCl₂ solution. Gelatin particles omitted for production of DRG-containing non-macroporous fibres.

Figure 5.11 Imaging of mouse retinal tissues, labelled with Vectashield Anti-fade containing DAPI and TU-20, using fluorescence microscopy. Cryosections of mouse retina tissue were incubated for 24 h at 4 °C with anti- β -tubulin (TU-20) at dilution (A) 1:100, (B) 1:250, (C) 1:500 and (D) 1:1000. Cryosections were fixed in 4% paraformaldehyde for 15 min. and washed with copious D-PBS followed by incubation with primary antibodies (TU-20) for 24 h at 4 °C and with the secondary antibody (Cy3-conjugated Affinipure Donkey Anti-Mouse IgG) for 1 h at room temperature.

Figure 5.12 TU-20 was used as a marker to differentiate encapsulated neurons from glia. (A) Hematoxylin and eosin stain of normal rat retina [293]. (B) Cryosections of mouse retinal tissue labelled with anti- β -tubulin (TU-20) 1:250 dilution).

Figure 5.13 TU-20 (mouse monoclonal anti-tubulin-III antibody)-labelled DRG cells in a macroporous alginate fibre at day 15 of cell culture. (A) Superimposed DIC and fluorescence (arrowed black) and (B) TU-20 labelled images revealed neurites (arrowed white) encapsulated in the alginate fibre. Magnified view of highly branched neurite displayed in the selected field. DRG-containing alginate fibre produced by wet spinning 1.5% w/v alginate solution containing DRGs (cell density 6.25×10^3 cells/mL and gelatin particles 57% w/w) into 0.5 M CaCl_2 solution.

Figure 6.1 Photoreceptor cells in the retina of the eye [294].

Figure 6.2 The reduction reaction of resazurin dye.

Figure 6.3 Hoechst 33342 stain for nucleic acid [309].

Figure 6.4 Phase contrast microscopy images of 661W culture on TCP at Day 0 (A), Day 3 (B) and Day 6 (C) in cell culture. Cells were seeded on 6-well plates at a density of 4.5×10^3 cells/mL.

Figure 6.5 Fluorescence imaging of 661W cells cultured on TCP labelled with TUJ-1 (A) Hoechst dye reveals nuclear DNA in blue (B) resulting composite image (C) at day 7 in culture. Cells were seeded on 6-well plates at a density of 4.5×10^3 cells/mL. Formalin fixed 661-W cells were permeabilized with 0.1% Triton X-100 in D-PBS for 15 minutes at room temperature and blocked with 5% NGS + 0.1% Triton X-100 for 15 minutes at room temperature. Cells were probed with primary antibody (TUJ-1) at 1:200 dilution for 24 h at 4 °C and with the secondary antibody (goat anti-rabbit IgG (H+L), Alexa Fluor® 594 conjugate) at 1:500 dilution for 1 h at room temperature. Nuclei (blue) were stained with Hoechst 33342 dye at 1:500 dilution for 15 minutes.

Figure 6.6 Differential interference contrast (DIC) images of 661W cells

encapsulated in a non-macroporous alginate fibre at Day 0 (A), Day 6 (B), Day 10 (C) and Day 13 (D) in cell culture. Cell concentration of alginate spinning solution 2.5×10^4 cells/mL.

Figure 6.7 Differential interference contrast (DIC) images of 661W cells

encapsulated in a macroporous alginate fibre at Day 1 (A), Day 6 (B), Day 10 (C) and Day 13 (D) in cell culture. Cell concentration of alginate spinning solution 2.5×10^4 cells/mL.

Figure 6.8 Fluorescence imaging of 661W cells encapsulated in non-macroporous fibre

labelled with TUJ-1 (A) Hoechst 33342 dye (B) superimposed image (C) and in macroporous fibre labelled with TUJ-1 (D) Hoechst dye (E) superimposed image (F).

661W-containing macroporous alginate fibre produced by wet spinning 1.5% w/v alginate solution containing 661W cells (density 2.5×10^4 cells/mL) and gelatin particles 57% (w/w) into 0.5 M CaCl_2 solution. Non-macroporous fibres produced by omitting the gelatin particles.

Figure 6.9 Live/dead staining assay using Calcein-AM of 661W cells encapsulated in

non-macroporous alginate fibre (A) and macroporous alginate fibre (B) at day 14 in culture. 661W-containing macroporous alginate fibre produced by spinning alginate solution (1.5% w/v) containing 661W cells (density 2.5×10^4 cells/mL) and gelatin particles (57% w/w) into 0.5 M CaCl_2 solution. Gelatin particles omitted for production of 661W-containing non-macroporous fibres.

Figure 6.10 Resazurin assay of 661W cell proliferation in culture on TCP (cells were

seeded on 6-well plates at a density of 4.5×10^3 cells/mL) (i) encapsulated in non-macroporous alginate fibre (ii) and encapsulated in macroporous alginate fibre (iii) (cell concentration of spinning solution 2.5×10^4 cells/mL). (Mean \pm SEM, One way ANOVA * $P < 0.05$, n = 6).

Table 1.1 Characteristics of an ideal tissue scaffold (adapted from [4]).

- Table 1.2** Properties of biodegradable synthetic polymers [25-26].
- Table 1.3** Tissue engineering scaffold manufacturing techniques adapted from [4].
- Table 1.4** Capabilities and limitations of SFF fabrication techniques.
- Table 1.5** Selective synthetic peptide sequences of extracellular matrix proteins used in tissue engineering applications. Adapted from [30].
- Table 1.6** Neural responses to neurotrophic factors.
- Table 2.1** Diameters of hydrated and dried alginate fibres. Fibres were spun from 1% w/v alginate solution into 0.5 M CaCl₂ solution. Flow rate of alginate solution to needle = 2 mL/min.
- Table 2.2** Tensile properties of dried alginate fibres (n = 5, mean ± SD).
- Table 3.1** Optimal pore size for cell infiltration and host tissue ingrowth [168].
- Table 3.2** Size distribution of gelatin particles (n = 50, mean ± SEM).
- Table 3.3** Equivalent pore diameters of alginate fibre scaffolds determined by CLSM image analysis.
- Table 3.4** Macroporosity of gelatin-extracted alginate fibres determined by CLSM image analysis.
- Table 4.1** Natural and synthetic polymer-based hydrogels for tissue engineering.
- Table 4.2** Cell density and inter-cell spacing of HDFa cells encapsulated in alginate fibre.
- Table 5.1** A Summary of different approaches for nerve regeneration *in vitro*.

List of Abbreviations

ACH	Anisotropic capillary hydrogels
AMD	Age related macular degeneration
APA	Alginate-polylysine-alginate
BCA	Bicinchoninic acid
BDNF	Brain-derived neurotrophic factor
CaCl ₂	Calcium chloride
Calcein-AM	Calcein acetoxymethyl ester
CAM	Cell adhesion molecule
CLSM	Confocal laser scanning microscopy
CN	Cyanide
CNS	Central nervous system
CTAB	Cetyltrimethylammonium bromide
Cryo-SEM	Cryo-scanning electron microscopy
DAPI	4,6-diamidino-2-phenylindole
DIC	Differential interference contrast
DMEM	Dulbecco's modified Eagle's medium
DMSO	Dimethyl sulfoxide
D-PBS	Dulbecco's phosphate-buffered saline
DRGs	Dorsal root ganglions
dsDNA	Double-stranded DNA
ECM	Extracellular matrix
FN	Fibronectin
GCL	Ganglion cell layer

H ₂ O ₂	Hydrogen proxide
hMSCs	Human mesenchymal stem cells
HDFa	Human dermal fibroblasts, adult
IEP	Isoelectric point
INL	Inner nuclear layer
LN	Laminin
micro-CT	Micro-computed tomography
MgCl ₂	Magnesium chloride
MPa	Megapascals
MSCs	Mesenchymal stem cells
MT	Micelle templating
NA	Numerical aperture
NGF	Nerve growth factor
NGS	Normal goat serum
NHDF	Normal human dermal fibroblasts
NP	Nucleus pulposus
NSF-1	Neural survival factor-1
OCT	Optimum cutting temperature
PBS	Phosphate-buffered saline
PEG	Poly(ethylene glycol)
PHEMA	Poly(2-hydroxyethylmethacrylate)
PLA	Poly(lactic acid)
PLLA	Poly-L-lactide acid
PLG	Poly(lactide-co-glycolide)
PLGA	Poly(lactic-co-glycolic acid)
PMMA	Poly(methylmethacrylate)

PNGM TM	Primary neuron growth medium
PNS	Peripheral nervous system
RGD	Arginine-glycine-aspartic acid
RP	Retinitis pigmentosa
RPCs	Retinal progenitor cells
SCs	Schwann cells
SEM	Scanning electron microscopy
TCP	Tissue culture plate
UV	Ultraviolet
VN	Vitronectin
XMT	X-ray microtomography
WGA	Wheat germ agglutinin

CHAPTER 1

Introduction

In the last few decades, the concept of tissue engineering has evolved rapidly into a new field of medical therapy and an alternative to conventional transplantation methods. There is no precise definition of tissue engineering; it covers a broad range of applications, including the introduction of biological entities *in vivo* (e.g. cells, growth factors) that facilitate tissue regeneration and the use of synthetic components (implants) to replace, or repair damaged and diseased tissue [1]. Five percent of all open wounds in the extremities caused by sports and road accidents are complicated by peripheral nerve trauma. Moreover, during complicated births, peripheral nerves may be disrupted because of traction [2]. Nerve regeneration is a complex biological phenomenon. When the nervous system is impaired, recovery is difficult and malfunctions in other parts of the body may occur, because mature neurons do not undergo cell division. Present clinical treatments favour autologous nerve grafting. However, this approach usually results in limited functional recovery, partial denervation at donor sites and the requirement for multiple surgical operations [3]. Immunosuppression is required for allografts and xenografts, and there is a high possibility of disease transmission [3]. Tissue engineering is expected to overcome these limitations by developing new approaches to encourage nerve growth and repair. Neural tissue engineering has focused mainly on the following three key components that govern new tissue formation: (i) introduction of nerve cells at the injury site, (ii) provision of an artificial extracellular matrix (ECM) for cell attachment, proliferation and differentiation, and (iii) controlled delivery of growth factors to mimic physiological processes.

The following literature review describes nerve structure, function and repair to highlight the challenges of producing functional and effective nerve replacements. The review presents the principles of tissue engineering and considers the various synthetic and natural polymers used to produce 3D cell support scaffolds and their surface modification by cell adhesion molecules for enhancing cell attachment and growth. The review describes the various approaches that have been applied to date for tissue engineering of nerves including the controlled release of growth factors. Specific attention is given to the advantages of alginate as a biomaterial for cell encapsulation to establish the rationale for the studies described in this thesis of alginate fibres for nerve repair.

1.1 LITERATURE REVIEW

1.1.2 Extracellular matrix and the design of artificial scaffolds

The natural ECM is a complex structural entity that surrounds and supports cells within mammalian tissues. The ECM is often referred to as connective tissue and comprises a cross-linked network of proteins and glycosaminoglycans, which provides a three-dimensional (3D) environment to organize cells in space. Furthermore, the ECM provides cells with environmental signals to direct site-specific cellular regulation, leading to tissue regeneration and organogenesis. The body is remarkably efficient at self-repair; however, in many cases such as excessive skin loss caused by severe injuries or non-union bone fractures, the self-repair process may be inadequate to completely regenerate the tissue. Therefore, one of the principal strategies of tissue engineering attempts to achieve healing through the introduction of cells, the use of synthetic implants, or a combination of both techniques. Cell provision by itself may be inadequate to induce tissue growth, since the supplied cells require their own supportive matrix to integrate with existing tissue. Thus, the

incorporation of cells within a scaffold or artificial ECM is necessary to promote cell attachment, proliferation and differentiation (Figure 1.1). Biomaterials selected for 3D scaffold production should be biocompatible, biodegradable, non-toxic, non-immunogenic, mechanically strong, sterilizable and capable of production in an economical and scalable manner (Table 1.1) [4].

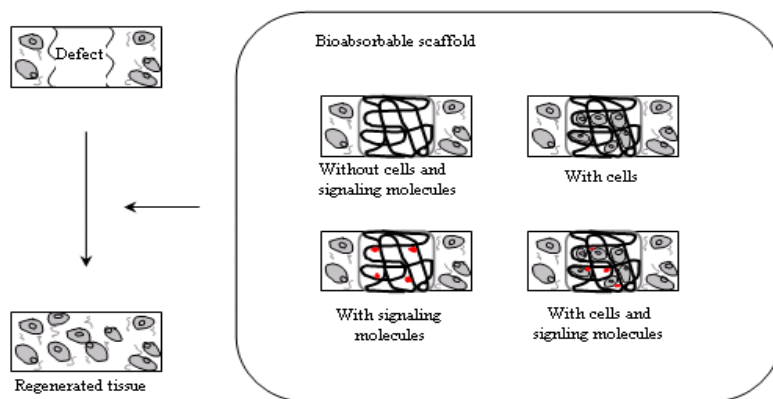


Figure 1.1 Biodegradable three-dimensional scaffold used to promote cell attachment, proliferation and differentiation. The scaffold with or without cells and/or biological signalling molecules (e.g. growth factors, cytokines, chemokines and genes) is applied to a defect *in vivo* to induce tissue and organ regeneration.

Table 1.1 Characteristics of an ideal tissue scaffold (adapted from [4]).

<i>Characteristics</i>	<i>Requirement</i>
<i>Biocompatible</i>	Biologically compatible with host tissue (i.e. should not provoke immune rejection, inflammation or toxicity)
<i>Biodegradable</i>	Degradation rate should match tissue regeneration rate and degradation products must be non-toxic to tissues
<i>Promotes vascularisation</i>	Provide channels for blood supply by vascularization to promote and maintain tissue regeneration
<i>Corrosion resistant</i>	Stability against corrosion at physiological pH and body temperature
<i>Porosity with interconnected pores</i>	Maximise space for cell adhesion, growth, ECM secretion, revascularization. Allows adequate nutrient and oxygen supply without compromising mechanical strength
<i>3D structure</i>	Provides framework to restore original volume of host tissue
<i>High surface area to volume ratio</i>	Promote cellular ingrowth and transport of nutrients and oxygen
<i>Surface modifiable</i>	Improve cell adhesion using functionalised chemical or biomolecular groups or by adsorption of cell adhesion molecules
<i>Adequate mechanical strength</i>	Withstand <i>in vivo</i> stress and surgical implantation
<i>Sterilizable</i>	Prevent contamination by microorganisms
<i>Growth factor delivery</i>	Modulate cell behaviour and function

1.1.3 Nerve structure and regeneration

The anatomical divisions of the nervous system are the central nervous system (CNS), which includes the brain and spinal cord, and the peripheral nervous system (PNS), which includes the neural tissue outside the CNS. The nervous system includes all of the neural tissue in the body, and its basic functional unit is the individual cell or neuron. A typical neuron is composed of a cell body, dendrites, an axon and a synapse (Figure 1.2). The cell body is comprised of a large nucleus with a prominent nucleolus, which contains genetic material in the form of chromosomes and other organelles, including neurofilaments, neurotubules and neurofibrils. The dendrites are branched projections that extend out from the cell body to receive electrochemical signals from other neurons. After receiving the signals, the axon (a long, slender projection)

propagates an electrical impulse known as an action potential that stimulates the release of neurotransmitters, such as acetylcholine, amino acids (glutamate, gamma-aminobutyric acid), monoamines (dopamine) and neuropeptides at the distal terminations of the branches of an axon called synaptic terminals to allow communication between neurons and other cells. Synaptic terminals are separated from neighbouring neurons by a small gap called a synapse, across which impulses are sent.

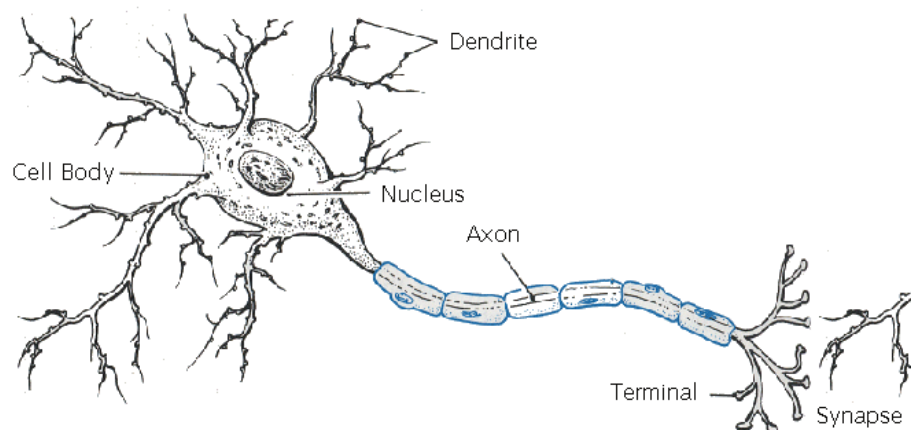


Figure 1.2 Peripheral motor neuron [5].

Axons within a peripheral nerve are the lengthy extension of cell bodies located in the dorsal root ganglia (sensory neurons), autonomic ganglia (autonomic neurons), or the ventral horn of the spinal cord of brain stem (motor neurons). Since their terminals are quite distant from the cell bodies, axons are insulated from each other, bundled together, and protected by three connective tissue layers – the endoneurium, the perineurium, and the epineurium (Figure 1.3). Axons, Schwann cells, and endoneurial components are bundled by a sheath of perineurium to form a nerve fascicle. Within the endoneurium, all axons are intimately associated with Schwann cells. As shown in

Figure 1.4, the myelin of each myelinated axon is formed from the plasma membrane of a Schwann cell wrapped tightly multiple times around the axon. However, the myelin sheath is not continuous. Individual myelinating Schwann cells cover about 100 micrometres of an axon corresponding to approximately 10,000 Schwann cells along a 1 metre length of the axon which can be up to a metre or more in length. The gaps between adjacent Schwann cells are called nodes of Ranvier (Figure 1.4) [6]. Bundles of axons bathed in endoneurial fluid are grouped into fascicles by dense connective tissue called perineurium. The perineurium is formed by up to 15 layers of flat perineurial cells interspersed with layers of type I and type II collagen fibrils and elastic fibres in circumferential, oblique, and longitudinal orientations [7]. These layers of collagen and perineurial cells provide mechanical strength, making the perineurium the primary load-bearing portion of the nerve [8-10]. Nerve fascicles are held together and surrounded by epineurium. The epineurial layer includes bundles of type I and type III collagen fibrils and elastic fibres, as well as fibroblasts, mast cells, and fat cells. It usually encases multiple nerve fascicles, as well as blood vessels which supply the nerve [11]. Supporting cells or neuroglia (also known as glial cells) separate and protect the neurons to provide a supportive framework for neural tissue (Figure 1.5). Various glial cells are present in the CNS and PNS, and each type plays distinctive roles in the nervous system. Four types of neuroglial cells including ependymal cells, astrocytes, oligodendrocytes and microglia are found in the CNS. Satellite cells and Schwann cells (SC) are found in the PNS.

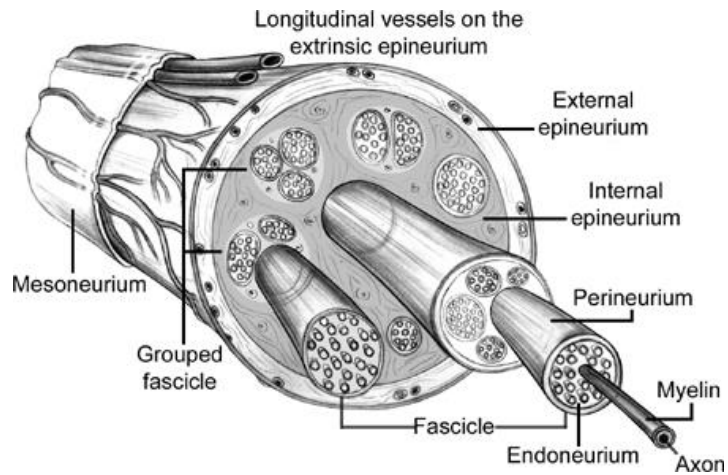


Figure 1.3 Schematic drawing of a peripheral nerve [12].

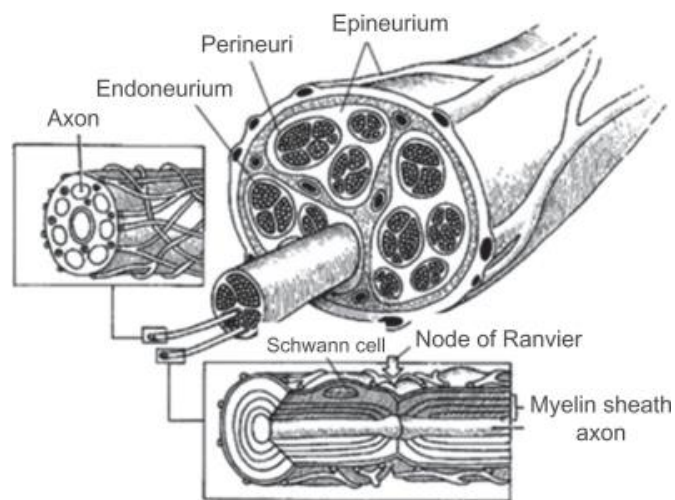


Figure 1.4 Cross-sectional anatomy of a peripheral nerve. Inset at left shows an unmyelinated fibre. Inset at bottom shows a myelinated fibre [13].

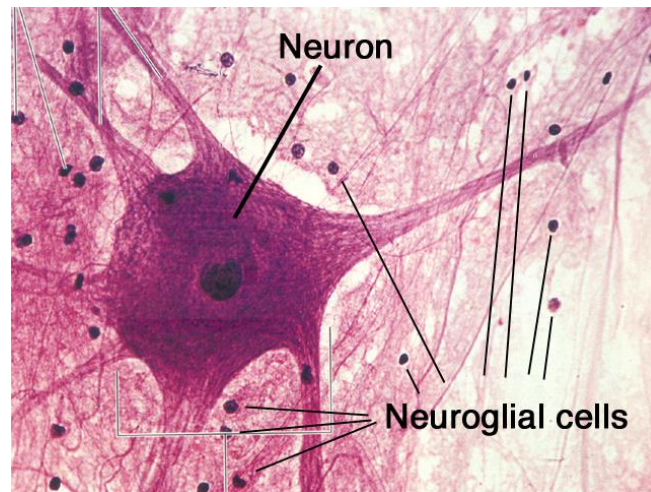


Figure 1.5 A photomicrograph of nerve tissue. A single neuron and numerous smaller supporting cells can be seen [14].

The nervous system allows information to be received and transmitted throughout the body. Thus, the brain, spinal cord and peripheral nerve tissue pose unique challenges when designing tissue engineering scaffolds to serve as replacements for injured or diseased tissue. Peripheral injuries are the most common type of nerve injury in daily life and mainly result from trauma to the upper extremities leading to loss of motor or sensory function (Figure 1.6).

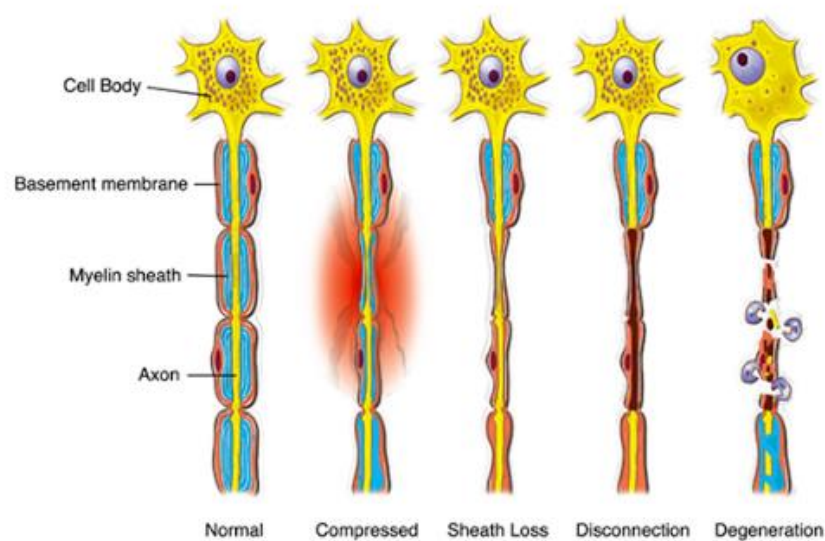


Figure 1.6 Types of peripheral nerve injuries [15].

Injury to the PNS immediately elicits Wallerian degeneration (Figure 1.7). During nerve repair, the axon distal to the injury site degenerates, and macrophages migrate into the basal lamina to engulf the debris at the distal segment. SCs then proliferate from the proximal nerve segment and form a solid cellular cord that follows the path of the original axon. As the neurons recover, the axon's neurolemma (the outermost layer of the neuron made of Schwann cells) does not degenerate and remains as a hollow tube. Within 96 hours after the injury, macrophages produce interleukin-1, which stimulates Schwann cells (SCs) to secrete growth factors that attracts the proximal axonal sprouts to grow (at 3 to 4 mm/day) towards the distal end of the lesion. SCs then form a myelin sheath around the re-innervating axonal sprout to re-establish the synaptic contacts. However, if the axon stops growing or deviates in a new direction, neuronal function may be lost. Short nerve gaps resulting from injury may be functionally repaired by end-to-end suturing whereas tubular structures are necessary for bridging larger gaps [16, 17]. Nerve autografts are the gold standard for clinical repair of large lesion gaps in the peripheral nervous system. Nerve segments are taken from another part of the body (the donor site) and inserted into the lesion to provide endoneurial tubes for axonal regeneration across the gap. However, these treatments are limited by tissue availability, donor site morbidity and potential mismatching of nerve fascicles leading to a negative effect on the recovery of nerve function [17-19].

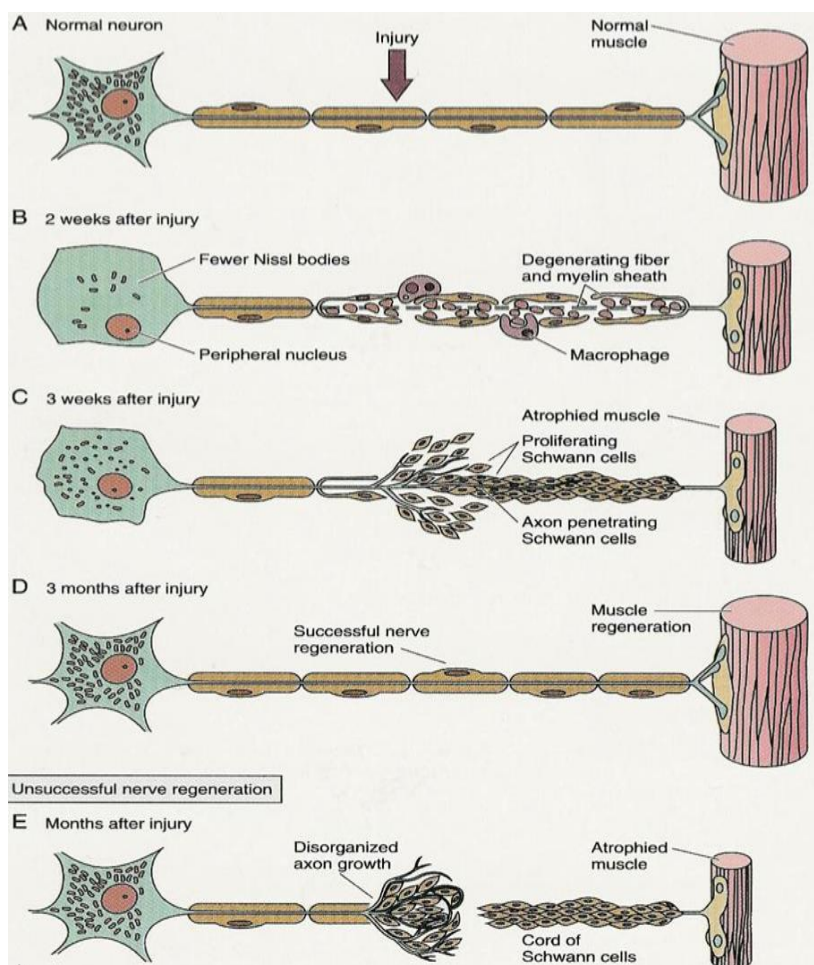


Figure 1.7 Schematic diagram of peripheral nerve regeneration. (A) Normal neuron, (B) Appearance at 2 weeks, (C) 3 weeks, and (D) 3 months after injury. (E) Appearance several months after neuron injury with unsuccessful nerve regeneration [20].

1.1.4 Polymers used for scaffold manufacture

Both natural and synthetic polymers have been applied as tissue engineering scaffolds for nerve repair in various forms including films, micro/nanoparticles, fibres, inserts or matrices. Synthetic polymers include those based on non-degradable silicone elastomers as well as biodegradable materials such as poly(L-lactic acid) (PLLA), polyglycolic acid (PGA) and poly(ϵ -caprolactone) (PCL). Natural polymers include laminin, fibronectin, collagen and gelatin and polysaccharides such as chitosan and alginate.

1.1.4.1 Synthetic polymers used in tissue engineering

The synthetic polymers investigated for manufacture of cell-support scaffolds (or artificial ECM) maybe classified into two main groups: (i) non-biodegradable materials and (ii) biodegradable materials. Silicone tubes have been used extensively for nerve regeneration. They are not biodegradable or permeable to large molecules, but create an isolated environment for nerve regeneration that allows the study of the effect of different ECM analogues on, for example, axonal elongation. Non-degradable artificial nerve guides have also been fabricated using silicone [21] and polyethylene (PE) [22] (Figure 1.8). However, the major drawbacks of non-biodegradable materials include chronic foreign body reaction caused by excessive scar tissue formation and lack of flexibility in certain cases such as PE.

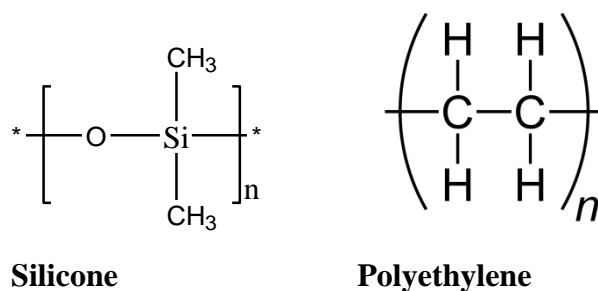


Figure 1.8 Chemical structures of silicone elastomer and polyethylene.

Many studies have focussed on the use of biodegradable synthetic polymers to address the problems associated with non-biodegradable polymeric scaffolds (Figure 1.9). Polymers such as PLLA [23, 24], PGA [25] and poly-ε-caprolactone (PCL) [26, 27] have good biocompatibility and low antigenicity and have been reported as suitable for nerve regeneration. They are intended to produce temporary support structures that resorb progressively over time as the nerve regenerates. Copolymerization has been used to obtain materials with tailored characteristics in

terms of degradation behaviour, mechanical performance, thermal properties and wettability [28] (Table 1.2). The repair of nerve defects generally requires up to 1 year for nerve regeneration and maturation; thus, during the regeneration period, it is possible that resorption and permeation of nerve guides produced from semi-crystalline polymers such as PLLA and PCL would decrease because of an increase in crystallinity over time. Polymer crystallinity affects the permeability and biodegradation of nerve guides because of the increase in packing density of polymer chains, which restricts fluid ingress. Moreover, crystalline debris formed during degradation may cause an inflammatory response that might jeopardize regeneration and recovery of nerve function [29].

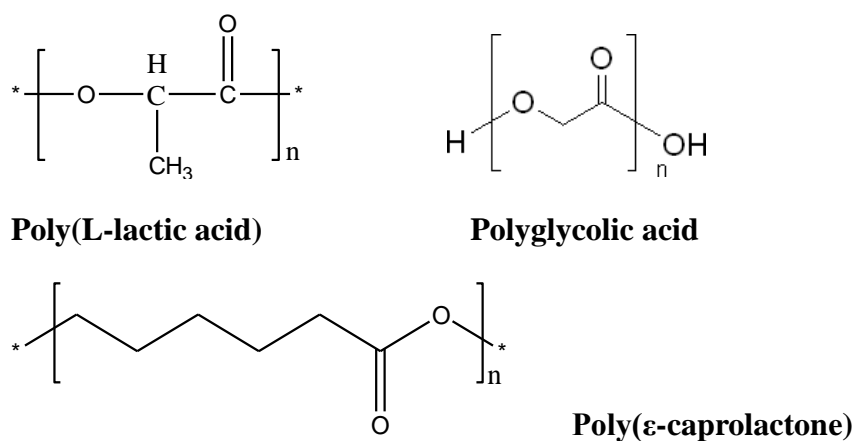


Figure 1.9 Chemical structure of poly(L-lactic acid), polyglycolic acid and poly-ε-caprolactone.

Table 1.2 Properties of biodegradable synthetic polymers [30, 31].

Biodegradable Synthetic Polymer	Thermal & Mechanical Properties			Processing Method	Degradation Time (Month)
	Melting Point (°C)	Glass Transition (°C)	Strength (Mpa)		
<i>Poly-L-lactic acid</i> (PLLA)	173-178	60-65	45-70	E, IM, CM, SC	>24
<i>Polyglycolic acid</i> (PGA)	220-225	35-40	60.8-71.8	E, IM, CM, SC	6 to 12
<i>Poly(ε-caprolactone)</i> (PCL)	60-65	-65-60	23	E, IM, CM, SC	>24

E = extrusion, IM = injection moulding, CM = compression moulding, SC = solvent casting.

1.1.4.2 Natural polymers used in tissue engineering

Natural polymers have been widely used as biomaterials in tissue engineering for several decades. Components of the natural ECM such as laminin, fibronectin and collagen have been used extensively for nerve reconstruction [32] because of their biocompatibility, lack of toxicity and innate cell adhesion capabilities. There has also been growing interest in the use of gelatin and polysaccharides such as chitosan, agarose and alginate for nerve repair.

Laminin (Figure 1.10) is the first ECM protein expressed during embryogenesis and contains various cell-binding domains such as RGD (Arg-Gly-Asp), YIGSR (Tyr-Ile-Gly-Srg-Arg) and IKVAV (Ile-Lys-Val-Ala-Val) on the α chain [33]. Several studies have found that laminin assists in the guidance of developing neurites and promotes neurite outgrowth [34, 35]. Labrador et al. [36] found that collagen and laminin gels contained in a silicone nerve guide, promoted nerve regeneration across 4-mm and 6-mm gaps of mice sciatic nerve. Evidence of laminin-mediated physical and chemical guidance for SCs and enhanced adhesion and alignment on a micropatterned biodegradable polymer substrate *in vitro* was reported by Miller et al. [37].

Fibronectin (Figure 1.11) is a dimeric glycoprotein that is composed of several rod-like domains, one of which (type III repeat) contains the RGDs sequence (Arg-Gly-Asp-Ser), which regulates cell adhesion [28]. Fibronectin has been found to play a key role in axonal growth by regulating neurite attachment and outgrowth [38, 39].

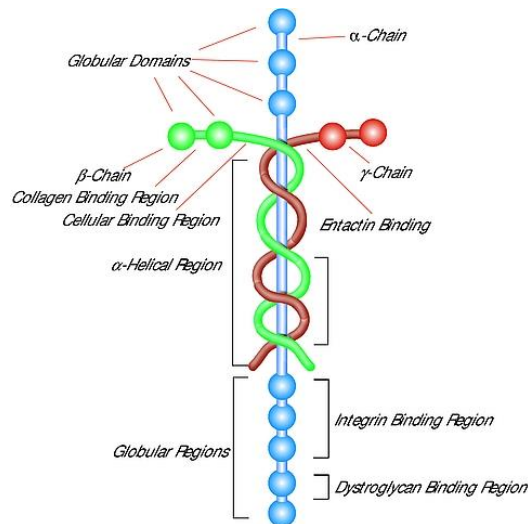


Figure 1.10 Laminin molecular structure consisting of three large polypeptides α , β_1 and β_2 crosslinked by disulfide bonds [40].

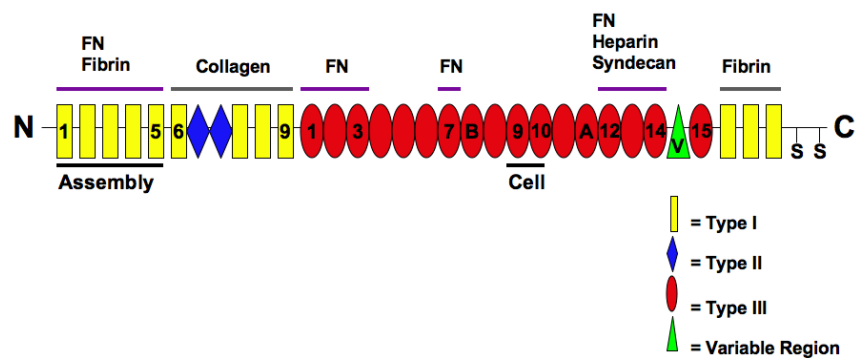


Figure 1.11 The modular structure of fibronectin and its binding domains [41].

Collagen (Figure 1.12) is one of the most widely used natural polymers for manufacturing tissue scaffolds due to its advantageous properties of biocompatibility, biodegradability non-toxicity and cell-adhesion. Although more than 28 types of collagen exist, the most abundant types in native tissue are types I and III. However, collagen extracted chemically from natural tissues is capable of inducing immunogenic responses upon implantation [4]; it has a relatively high cost and tends to exhibit a more rapid deterioration in mechanical properties compared with the natural non-processed forms.

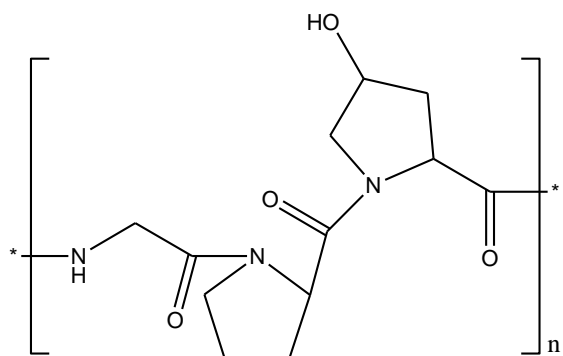


Figure 1.12 Simplified chemical structure of collagen showing the main amino acid.

Gelatin (Figure 1.13) is derived from collagen and has become a material of choice in tissue engineering, because it is not antigenic under physiological conditions. Gelatin has a lower cost than collagen and is easier to prepare in the form of concentrated solutions. Moreover, gelatin is biodegradable and has excellent biocompatibility, plasticity and cell-adhesiveness [28]. Gelatin is extensively used for pharmaceutical purposes in the form of hard- and soft-shell gelatin capsules for drug administration. It was also the first biodegradable material to be tested as a nerve guide [42]. Gelatin contains primary carboxyl groups along the chain backbones that give it the potential to covalently bind to growth factors via an appropriate cross-linking agent [43-45]. For example, the water-soluble cross-linking agent carbodiimide was used by Chen et al. [46] to bind to the amine groups of the nerve growth factor (NGF) to carboxyl groups on the surface of tricalcium phosphate and glutaraldehyde-crosslinked gelatin. SCs successfully attached to the material *in vitro*, and NGF was released during biodegradation.

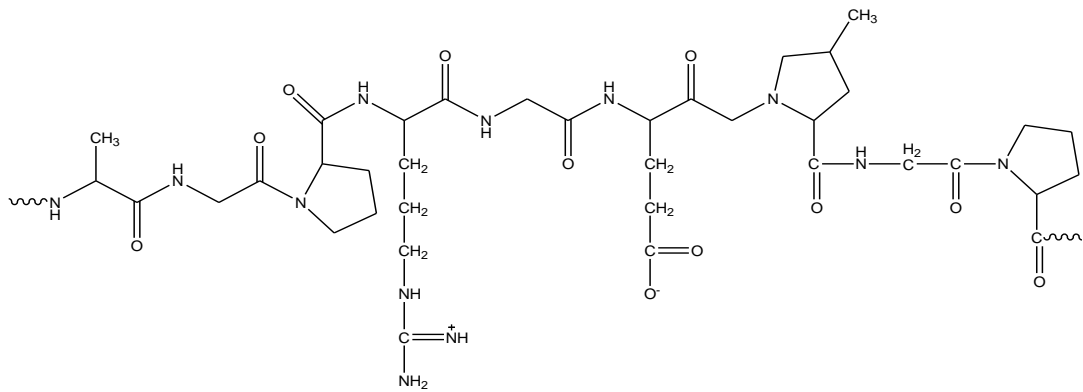


Figure 1.13 Chemical structure of gelatin.

Chitosan (Figure 1.14) is a copolymer of D-glucosamine and N-acetyl-D-glucosamine, obtained from N-deacetylation of chitin. Chitosan has been widely investigated for tissue engineering and drug delivery because of its biodegradability and biocompatibility, anti-tumour [47] and anti-bacterial activities [48]. Chitosan has a molecular structure similar to that of the glycosaminoglycans in the basal membranes of tissues and ECM that permits interactions between chitosan and extracellular adhesion molecules such as laminin, fibronectin and collagen. Moreover, chitosan has been studied as a candidate material for guiding nerve regeneration. Studies have shown that chitosan fibres support adhesion [49], migration, and proliferation of SCs as well as peripheral nerve reconstruction when used in a chitosan–laminin 3D scaffold [50].

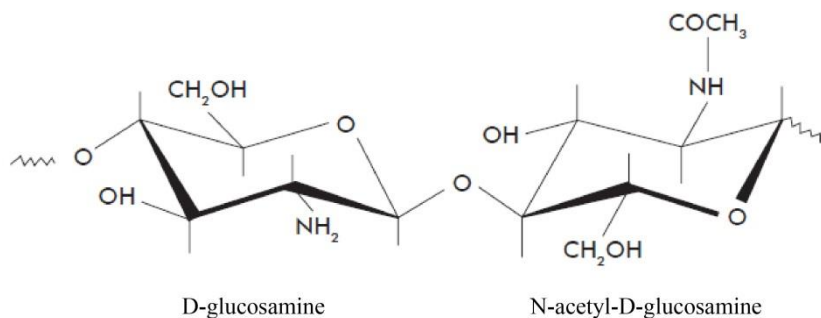


Figure 1.14 Chemical structure of chitosan.

1.1.5 Alginate

Alginate (Figure 1.15), also known as alginic acid, is abundant in the cell wall of brown algae. The properties of alginate vary among species, and the main commercial sources are *Ascophyllum*, *Durvillaea*, *Ecklonia*, *Laminaria*, *Lessonia*, *Macrocystis*, *Sagassum* and *Turbinaria*.

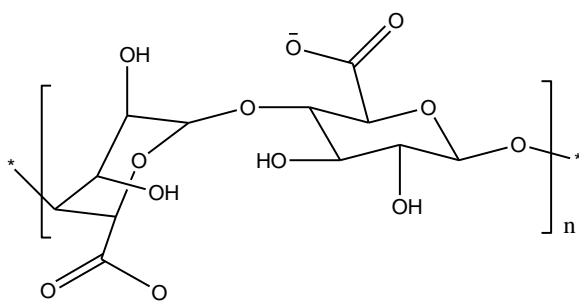


Figure 1.15 Chemical structure of alginate.

The Food Chemical Codex [51] gives specifications for alginate and its propylene glycol ester as well as its ammonium, calcium, potassium and sodium salts. These four salts have been granted GRAS (generally recognized as safe) status in the USA, and propylene glycol alginate has been approved as an emulsifier, stabilizer or thickener in food [52]. Alginate is widely used in textile printing (as a viscosity modifier), paper production (for surface sizing), the food industry (as a viscosity enhancing agent) and the pharmaceuticals industry (as a disintegrating agent in tablets). More recently, because of its good biocompatibility, alginate has been fabricated using numerous techniques into films, membranes, fibres, micro/nanoparticles, capsules and reservoir devices for tissue engineering and/or drug delivery.

Structure of alginate

Alginate is a linear anionic polysaccharide that consists of various ratios of L-guluronic and D-mannuronic acid units linked by 1,4-glycosidic bonds (Figure 1.16A). The classical Haworth chemical structures for the monomers and 3D ‘chair’ arrangement are shown in Figure 1.15. The alginate polymer is formed by linking each monomer at the C-1 and C-4 positions through the ether–oxygen bridge. Alginates are not random copolymers; according to the algae source, the polymer chain comprises three types of regions or blocks. The G blocks contain only units derived from L-guluronic acid, the M blocks contain D-mannuronic acid and the MG blocks contain a combination of D-mannuronic and L-guluronic acid units, each of which have different conformational preferences and behaviour [53-55] (Figure 1.17). As examples, the M/G ratio of alginate from *Ascophyllum rodosum* is approximately 1.56, whereas that from *Laminaria hyperborea* is approximately 0.62. Thus, the M and G blocks actually exhibit a different shape; the M block features equatorial groups at C-1 and C-4, and forms a relatively planar structure similar to a ribbon. On the other hand, the G block features axial groups at C-1 and C-4, and the resulting MG copolymer chain are buckled (Figure 1.16).

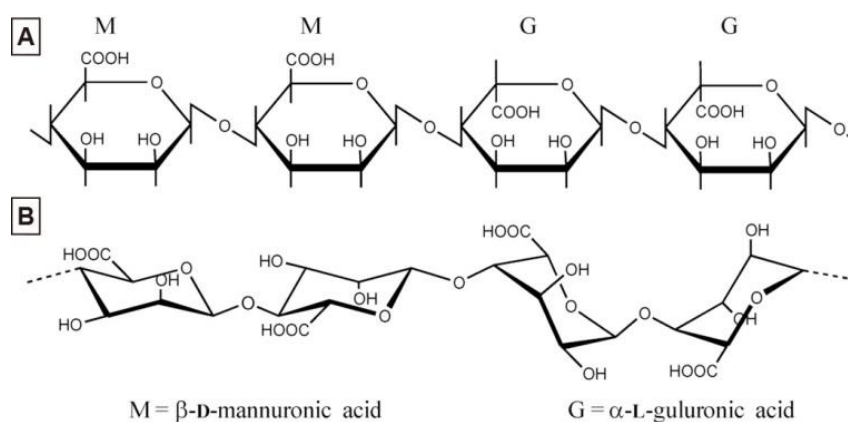


Figure 1.16 (A) Chemical structure of the two monomeric units of alginate. (B)

Structures in Figure 1.16A expressed as ‘chair’ forms.

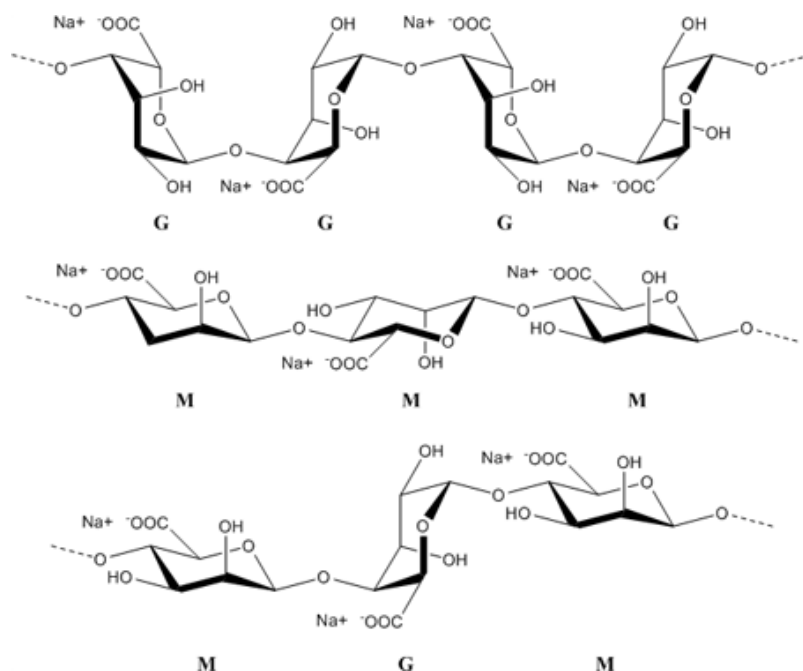


Figure 1.17 The chemical structure of the M block, G block and MG copolymer of alginate.

Sodium alginate

Sodium alginate is the sodium salt of alginate, and its empirical chemical formula is $\text{NaC}_6\text{H}_7\text{O}_6$. The chemistry of the processes used to make sodium alginate from brown seaweed is relatively simple (Figure 1.18).

Sodium alginate can be produced by two different processes: the calcium alginate process and the alginate process (Figure 1.18). In the former process, calcium alginate is formed as an intermediate along with alginic acid. In the second approach, no calcium alginate is formed, only alginate. Both methods have advantages and disadvantages. The calcium alginate process is performed by size reduction of the raw material via treatment with formalin solution followed by acid treatment to convert the insoluble calcium and magnesium salts into insoluble alginic acid and finally into soluble sodium alginate by reaction with sodium carbonate and sodium hydroxide. In

brown seaweed, alginate is present mainly as the calcium salt of alginate, although magnesium, potassium and sodium salts may also be present. Treatment with formaldehyde removes the remaining phenolic compounds and discoloration. The seaweed particles are then extracted with alkali to convert the alginate to a soluble form (sodium alginate) so that it can be separated from the rest of the seaweed. This step offers the advantage of control over the viscosity of the final product. Use of higher temperatures and longer extraction times can further break down the uronic acid chains resulting in lower viscosity sodium alginate. The extracted sodium alginate is separated from the alkali-insoluble seaweed residue by flotation and filtration. Since evaporation of the solution is not practical, sodium alginate extract is typically precipitated as a calcium salt or alginate (alginic acid) using HCl after bleaching to improve the colour and odour. Finally, the purified and concentrated solid alginate obtained from the original alkaline extract is converted to solid sodium alginate using sodium carbonate. As sodium alginate forms, it dissolves in the small amount of water present to give a heavy paste, which is oven-dried and milled to an appropriate particle size, usually around 60 mesh.

The alginate process is similar to the calcium alginate process. The first five stages (from size reduction of the raw material to separation of insoluble seaweed residue) are identical. Rather than precipitation of calcium alginate, the extracted sodium alginate undergoes bleaching and clarification followed by treatment with a dilute mineral acid (HCl or H₂SO₄) to form a gelatinous precipitate of alginate. Following precipitation, the alginate gel is dehydrated by mixing with methanol or ethanol. The final step is to convert alginate to sodium alginate. Alginate is suspended in methanol or ethanol at room temperature, and a strong sodium hydroxide solution (40%) is added to exchange the H⁺ and Na⁺ ions. The final product is obtained by grinding. There are several drawbacks to the alginate method, including the difficulty in

separating alginate from the gelatinous precipitate, the relatively low overall yield of alginate, and costly and time-consuming nature of the process.

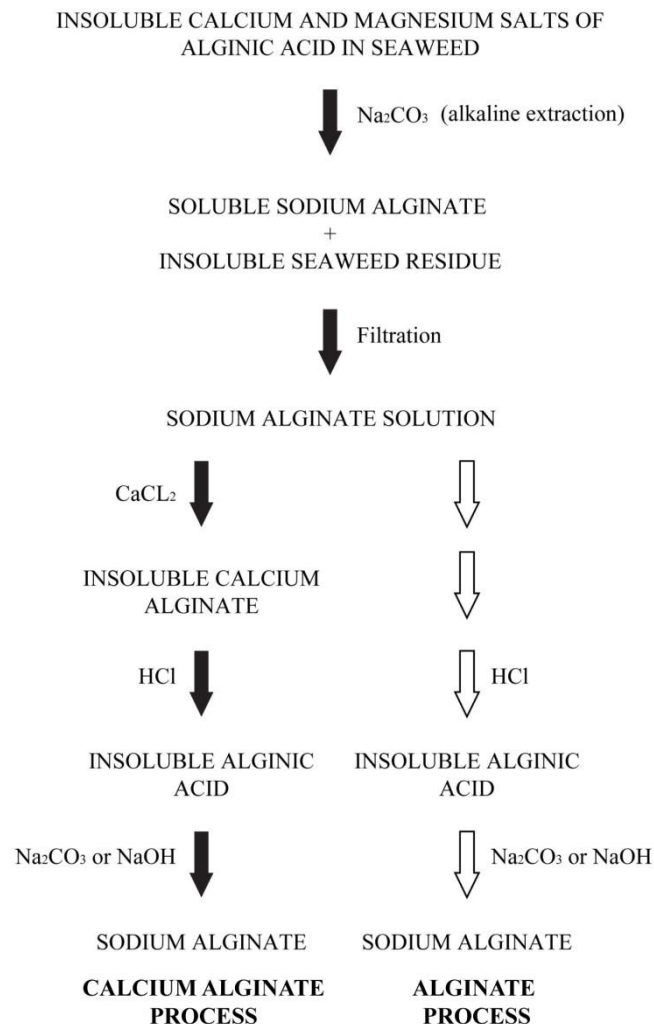


Figure 1.18 Production of sodium alginate.

Rheological properties of alginate

The physical properties of alginate depend on the relative proportion of the three types of blocks (M, G and M/G) [56-59]. The degree of polymerisation (DP) and molecular weight of sodium alginate relate directly to the viscosity of alginate solutions. Sodium alginate is manufactured in various grades, usually described as low, medium and high viscosity. Manufacturers are able to control the molecular

weight (DP) and provide products with a viscosity of 10–1,000 mPa.s (1% solution) and DP of 100–1,000 units. Low viscosity sodium alginate may be stored at 10–20 °C for 3 years without any change in properties. Medium viscosity alginate shows 10% loss at 25 °C and 45% loss at 33 °C after a year. High viscosity alginate is less stable [60]. The viscosity of alginate solution can be affected by several factors including molecular weight, concentration, temperature, pH and the presence of calcium ions. Furthermore, the higher the molecular weight of soluble alginate, the greater is the viscosity of its solution. McDowell [60] derived a useful empirical equation relating the viscosity and concentration of an alginate solution for various alginates over at least a hundredfold change in viscosity:

$$\log_{10} \text{ viscosity} = a\sqrt{(\text{concentration})} - b$$

Where **a** is a constant related to degree of polymerization (DP) of the alginate sample and **b** is a constant for a particular type of alginate [60]. The viscosity of alginate solutions decreases with increase in temperature at a rate of about 2.5% per °C (Figure 1.19) [61]. The viscosity usually returns to a slightly lesser value than the original on cooling. However, depolymerisation may occur with a subsequent permanent loss of viscosity if alginate solutions are kept above 50 °C for too long. Alginate solutions are most stable at pH 5 – 9. The viscosity of alginate solutions is usually unaffected at pH 5 – 11. Under acidic conditions, the free $-\text{COO}^-$ ions in the polymer protonate to $-\text{COOH}$, resulting in a reduction of the electrostatic repulsion between chains as hydrogen bond formation occurs, and thereby, a higher viscosity [52]. Gelation usually occurs at pH 3 – 4. However, if the pH is maintained above 11, slow depolymerisation may occur with a resulting decrease in viscosity.

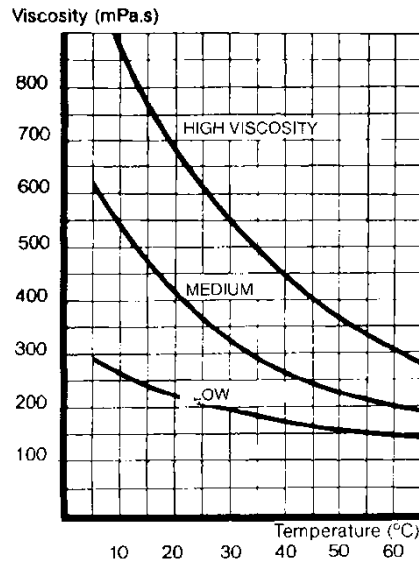


Figure 1.19 Viscosity of 1% alginate solution at different temperatures (adapted from [61]).

Alginate – Calcium complex

Low concentration (0.2 – 1.2%) of calcium ions in an alginate solution will increase the viscosity (7 – 20%), whereas a higher concentration will cause gelation [62]. Most commercial alginates made by the calcium alginate process contain residual quantities of calcium. The effect of calcium on the viscosity of a calcium-containing alginate can be estimated by measuring the viscosity of a solution before and after the addition of a sequestering agent, such as sodium hexametaphosphate, which removes the calcium ions as a complexed phosphate ion. The effect of calcium on the viscosity of an alginate solution is difficult to predict and is usually determined by experimentation. The viscosity will depend on the uronic acid composition and DP of alginate; alginates with higher molecular weights and/or higher M/G ratios having higher viscosity.

Calcium is a popular divalent ion for alginate gel formation, because it is commonly found in the salt form, is of low cost, readily available and non-toxic. Addition of sodium alginate solution to calcium chloride solution results in hydrogel formation.

Blocks of guluronic acid residues along the alginate chain molecule bind to Ca^{2+} cations to generate a 3D network of alginate strands held together by ionic interactions. Gel formation is related to the content of guluronic acid which creates a cavity that acts as a binding site for the cation [63]. Grant et al. proposed an ‘egg-box’ model in 1973 that requires the cooperative binding of two or more chains, shown in Figure 1.20 [64, 65]. The resulting network is affected by the frequency and length of contiguous guluronic acid residues as well as the concentration and type of the cation [66]. Alginates high in guluronic acid residues form stiffer and more porous gels, thus maintaining their integrity for extended time periods. Moreover, these gels do not undergo excessive swelling and subsequent shrinkage during cationic cross linking [67]. In contrast, alginates rich in mannuronic acid residues, form softer and less porous gels that disintegrate rapidly with time [67].

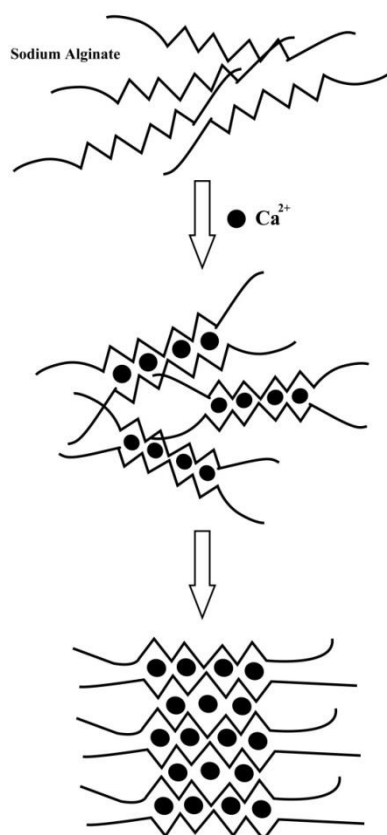


Figure 1.20 Gel formation via G blocks of alginate polymers: egg-box model [65].

1.1.6 Cell encapsulation in alginate polymers

Alginate polymers have been widely investigated for cell encapsulation but the effects of alginate composition on the growth characteristics and metabolic activity of encapsulated cells have yet to be completely assessed. Although alginates with high guluronic acid content produce stronger hydrogels, recent studies have shown that such alginates may hinder cell growth and diminish the metabolic activity of the culture for a period of up to 40 days before the encapsulated cultures recover and proliferate [68-70]. Conversely, high mannuronic acid content alginates provide an environment that supports cell growth [68-70]. Simpson et al. [71] hypothesized that the strength of the alginate gel network is the principle factor responsible for differences in the growth characteristics of encapsulated cells in different alginates. They varied the calcium concentration at the time of gelation or during culture and found that increasing the concentration of the CaCl_2 solution increased the gel strength. At the same time, cell growth characteristics were impeded in alginates with a high guluronic acid content [71]. In contrast, the gel strength of alginates with a high mannuronic acid content was not affected by changes in the concentration of CaCl_2 , because of the low fraction of crosslinking sites provided by the guluronic acid residues.

1.1.7 Scaffold design and manufacture for tissue engineering

Tissue engineering scaffolds are usually fabricated to provide a synthetic replacement for the natural ECM and a temporary support structure for growing cells and tissues. Numerous techniques have been employed to prepare scaffolds with controlled morphology, shape, size, pore structure and physicochemical and mechanical properties to optimise cell–scaffold interaction during tissue regeneration. These

techniques include solvent casting/particulate leaching, phase separation, solid free-form fabrication (SFF) and electrospinning [4, 16, 72, 73] (Table 1.3). A major challenge of scaffold manufacture is controlling the pore structure (pore size, geometry, connectivity and orientation) to permit in-growth of regenerating tissue. Solvent casting and particulate leaching are able to produce highly porous structures. However, these methods are limited to the production of thin membranes (2 – 3 mm), because of the difficulty in ensuring complete removal of embedded particles. In addition, they have been unsuccessful in controlling the internal architecture to a high degree of accuracy or homogeneity. Phase separation involves dissolving a polymer such as a poly(α -hydroxy acid), PLA in a solvent such as dioxane, dichloromethane or acetone and producing polymer separation or hardening by freezing, gelation, solvent extraction and drying [72]. The advantage of these methods is that bioactive molecules can often be incorporated into the matrices without loss of activity and the morphology and properties of the resultant scaffolds can be varied depending on the phase separation mechanism [72, 74].

Table 1.3 Tissue engineering scaffold manufacturing techniques adapted from [4].

Manufacturing techniques	General description	Advantage	Disadvantage
<i>Self-assembly</i>	Atoms, molecules and supramolecular aggregates organize and arrange themselves into an ordered structure through weak non-covalent bonds; typically involves a bottom-up approach	Mimics the biological process	Complex process, limited to a few polymers
<i>Phase separation</i>	Involves various steps, typically polymer dissolution, freezing gelation, solvent extraction and drying, to form porous, foam-like structures	Simple process, controllable mechanical properties and pore structure	Limited to a few polymers, long processing times
<i>Electrospinning</i>	Employs electrostatic forces for production of polymer nanofibre scaffolds; typically involves a top-down approach.	Simple and cost-effective process, capable of producing long and continuous fibres, films or membranes produced with control over fibre orientation, versatile and applicable to many polymers	Use of high-voltage apparatus

More recently, rapid prototyping or SFF fabrication techniques have been used to manufacture porous scaffolds, based on the principle that a material in powdered or liquid form is solidified one layer at a time to build up a 3D structure. The principal systems include fused deposition modelling (FDM) [75-81], selective laser sintering (SLS) [76-82], 3D printing [76-83] and precision extrusion [77, 80, 84, 85]. In general, SFF fabrication is very time consuming and requires sophisticated equipment. Each technique offers its own advantages such as achieving controlled pore size, complete pore interconnectivity. However, some techniques are associated with major disadvantages including the requirement for toxic organic solvents, heat input and lack of mechanical strength of the finished scaffold (Table 1.4). Over the last few years, electrospinning has attracted great attention for production of fibrous scaffolds that attempt to mimic the structural features of native ECM using various biomaterials, particularly polymeric materials [4]. Electrospinning is a simple and versatile technique that essentially employs electrostatic forces to produce polymer fibres that range in diameter from a few microns to tens of nanometres [86]. This method is able to produce fine scaffolds with precise fibre orientation, large surface area and controlled pore geometry that favours cell growth *in vitro* and *in vivo* [4].

Table 1.4 Capabilities and limitations of SFF fabrication techniques.

Technique	Pore Size (μm)	Porosity (%)	Advantages	Limitations	Ref.
Extrusion-based processing Fused Deposition Modelling (FDM)	250-1000	<80	High porosity; solvent free; good mechanical strength; cost effective; complete pore interconnectivity	Needs filament preparation; limited choice of filament materials; high processing temperatures; limited to large pore sizes	[75-81]
Powder-based processing Selective Laser Sintering (SLS)	45-100	<40	High surface area to volume ratio; solvent free	High processing temperatures; limited to small pore sizes; expensive machinery	[76-82]
Three Dimensional Printing (3DP)	45-100	<45-60	Easy process; cost effective; independent control of porosity and pore size; complete pore interconnectivity	Use of toxic organic solvents; lack of mechanical strength; limited to small pore sizes	[76-83]
Precision Extruding Deposition (PED)	200-300	<70	High porosity; no requirement of filament preparation; control of pore size	High heat effect on material; rigid filament	[77, 80, 84, 85]

1.1.7.1 Scaffold production for nerve regeneration

Regenerated nerve tissues should ideally mimic the structure of nerve fascicles and permit the transfer of electrical impulses along the axons to the synaptic terminals (Figure 1.21) [29]. To successfully regenerate nerves (and other tissues) using tissue engineering approaches, the scaffold material, pore size and structure, degradation characteristics and mechanical properties must be optimised to promote cell attachment, growth, differentiation and organisation during tissue formation. Scaffolds for nerve guidance and nerve regeneration have been fabricated predominantly as hollow tubes, aiming to mimic the endoneurium nerve architecture (Figure 3). These methods include fibre extrusion [87, 88], magnetic polymer fibre alignment [89, 90], injection moulding [91, 92], phase separation [93] and freeze-drying and lyophilizing [94]. Flynn et al. [95] developed a fibre templating technique involving solubilization (using acetone) of PCL fibres which were

embedded in poly(2-hydroxyethyl methacrylate) (pHEMA) hydrogels to create oriented pHEMA scaffolds for neural tissue engineering. Longitudinally oriented channels (diameters of 100 – 200 μm and 300 – 400 μm) were created within the hydrogel to act as conduits, providing support and contact guidance for extending axons and invading cells [87].

High-strength magnetic fields have been employed to align collagen gels in the form of 4 mm diameter rods during the self-assembly of type I collagen monomers into fibrils [90]. Dubey et al. [90] reported that a magnetically aligned type I collagen gel directed the invasion of neurites and SCs from dorsal root ganglia cultured on the gel surface, and consequently, increased the depth of invasion relative to a control collagen gel. This behaviour was attributed to a contact guidance response of growth cones and SCs to the aligned collagen fibrils. Thus, by pre-filling a tube with a magnetically aligned collagen gel, the desired directionality of cell growth was induced by the alignment of collagen fibrils along the tube axis. It was also reported that tubes filled with collagen gels, which were not pre-aligned, yielded fewer myelinated axons [95] and poorer functional recovery [96] compared to saline-filled tubes in the repair of a 4-mm gap in the mouse sciatic nerve. Sunback et al. [91] used a novel pressure injection moulding technique to generate a porous poly(DL-lactide-co-glycolide) (DL-PLGA) nerve conduit by thermally induced phase transition. Conduits were produced with different channel configurations and diameters ranging from 1.35 mm (single channel) to 0.08 mm (hundred channels). The porous conduit provided increased surface area for SC migration, adherence and axonal elongation. It was reported that approximately 2.5- and 12.5-times more SCs adhered in a monolayer at the luminal surfaces of the 7- and 100-channel conduits, respectively, compared with a single-channel conduit [91].

Freeze-drying has been investigated for producing porous polymeric scaffolds by

utilising the water present in hydrogels to form ice crystals that are subsequently removed by sublimation to create a particular micro-architecture [94]. Stokols et al. [94] utilised freeze-drying to create nerve guidance scaffolds from agarose, with uniaxial linear pores of 125 ± 25 and $119 \pm 26 \mu\text{m}$ for the hydrated and dry scaffolds, respectively. NGF-loaded agarose conduits induced neurite extension in a greater number of PC12 cells (cell line derived from a pheochromocytoma of the rat adrenal medulla) ($43 \pm 8.1\%$) in comparison to the control in the absence of NGF ($5.0 \pm 3.1\%$) after 4 weeks of cell culture at 37°C [94]. Other studies have investigated the use of extruded or spun hollow fibres of biomaterials such as collagen and PCL combined with multiple growth stimuli to enhance neuron regeneration, adhesion, viability and extension.

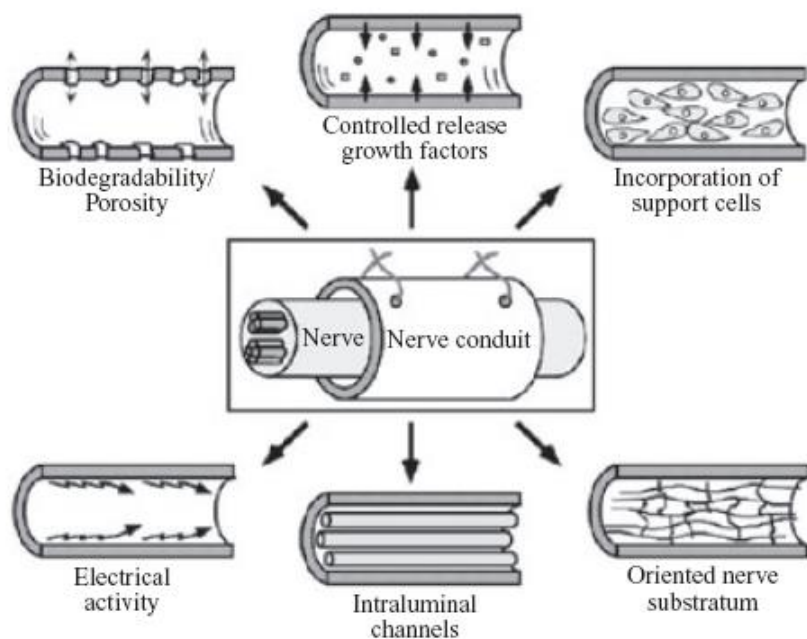


Figure 1.21 Properties of a nerve guidance channel or conduit. Adapted from [29].

1.1.8 Cell interaction with polymeric scaffolds

Successful tissue engineering requires an understanding of the effect of the scaffold structure on cell viability, growth and function. The cellular response to a material surface is governed by a number of factors that include surface chemistry, topography, surface charge, structural heterogeneity, scaffold mechanical properties and the physiological environment [97]. The growth and function of many tissue-derived cells requires their attachment and spreading on a surface; thus the strength of cell adhesion has been found to be an important determinant of the rate of cell spreading, cell migration and differentiated cell function [97]. Several studies have shown that cell adhesion appears to be maximised on surfaces with intermediate (water) wettability. For example, decreased adhesion of platelets and fibroblasts was observed on highly hydrophilic copolymers [98, 99]. Cell adhesion is enhanced on positively charged surfaces [99]. Other reports have identified specific chemical groups at the polymer surface, such as hydroxyl ($-OH$) and carboxyl ($-COOH$) [100, 101] or surface C–O functionalities [102], as important factors in modulating the fate of surface-attached cells. Curtis et al. [100] modified non-polar polystyrene by introducing hydrophilic ($-OH$) moieties into polystyrene surface chains resulting in significant improvements of adhesion of baby hamster kidney (BHK) and leukocyte cells compared with the non-treated control. For most surfaces, adhesion requires the presence of serum components, in particular cell adhesion molecules (CAMs) such as fibronectin and laminin [103].

The surface morphology of an implanted material can also significantly affect cell behaviour. Cultured cells react differently to rough and smooth surfaces. In many cases, cells orient and migrate along fibres or ridges in the surface. This phenomenon was termed contact guidance in early studies on neuronal cell cultures [104].

Fibroblasts have also been observed to orient on grooved surfaces, particularly when the texture dimensions are 1 – 8 μm [105].

Several studies have used advanced approaches to create sophisticated synthetic and/or natural polymeric scaffolds to mimic natural repair processes. However, polymeric scaffolds may not interact with cells in a desired manner because their surface chemistry may not promote adequate cell adhesion [106] and may induce toxic and inflammatory reactions [107]. In addition, the rate of polymer resorption is an important factor since the scaffold should provide sufficient support throughout the repair process. Cell adhesion problems can be resolved by surface modification to enhance cell attachment and cell growth and limit toxic effects.

Many studies have used ECM proteins such as fibronectin, vitronectin and laminin for surface modification of scaffolds because of the presence of cell binding domains, such as RGD sequences along the protein chain. Enhancing fibronectin adsorption from bovine calf serum-containing culture media on poly-ethyleneterephthalate (PET) and polystyrene surfaces by introducing the oxygen-rich functional group (i.e. C–O, C=O, and O=C–O groups) was shown to facilitate spreading and subsequent replication of Swiss mouse 3T3 fibroblasts and MM14 mouse skeletal myoblasts in culture [102]. Campos et al. [106] developed a fibronectin-functionalized, electrospun, poly(d,l-lactide-co-glycolide) (PLGA) scaffold for periodontal ligament regeneration to overcome the hydrophobicity of the polyester. Yao et al. [107] coated PLGA scaffolds with collagen type I or laminin to ameliorate neurite growth. Liu et al. [108] improved cell adhesion by crosslinking gelatin with poly(α -hydroxy acids) PLLA films in a gelatin/dioxane/water mixture. Chemically modified PLLA films showed a 45% increase in MC3T3E1 osteoblast cell number on the gelatin modified film surface compared with the control 4 h and 1 day after cell seeding [108]. Dhoot et al. [109] modified the surface of alginate gels by coating with laminin and by covalent

attachment of laminin-derived peptide YIGSR (Tyr–Ile–Gly–Ser–Arg) peptide. The modified alginate gels elicited significant increases (> 60%) in NB2a neuroblastoma cell attachment compared with unmodified alginate gel (1.5%) [109]. Specific cell adhesion fragments (short peptides) have proven in certain cases to be advantageous over the long chain native ECM proteins such as fibronectin (FN), vitronectin (VN), and laminin (LN) for cell adhesion [110, 111]. Short peptides are more advantageous because, unlike the long chains that fold randomly upon adsorption causing the active protein domains to be sterically unavailable, short peptides remain stable and do not hide the receptor binding domains when adsorbed. Another advantage of short peptides is that they can be produced more economically due to the smaller size [35]. The selective synthetic peptide sequences used in tissue engineering applications are summarised in Table 1.5.

Table 1.5 Selective synthetic peptide sequences of extracellular matrix proteins used in tissue engineering applications. Adapted from [35].

Synthetic Peptide Sequences	Origin	Function	Ref.
RGD	Fibronectin, Vitronectin	Cell adhesion	[112, 113]
KQAGDV		Smooth muscle cell adhesion	[114]
YIGSR	Laminin B1	Cell adhesion	[115, 116]
REDV	Fibronectin	Endothelial cell adhesion	[117, 118]
IKVAV	Laminin	Neurite extension	[115, 119]
RNIAEIIKDI	Laminin B2	Neurite extension	[119]
KHIFSDDSE	Neural cell adhesion molecules	Astrocyte adhesion	[120]
VPGIG	Elastin	Enhance elastic modulus of artificial ECM	[118]
FHRRIKA	Heparin binding domain	Improve osteoblastic mineralization	[121]
KRSR	Heparin binding domain	Osteoblast adhesion	[122]
NSPVNSKIPKACCVPTLSAI	BMP-2	Osteoinduction	[123]
APGL		Collagenase mediated degradation	[124]
VRN		Plasmin mediated degradation	[124]
AAAAAAAAA		Elastase mediated degradation	[125]

1.1.9 Cell migration

Migration of individual cells over or within a tissue engineering scaffold is important to fully colonise the scaffold and complete the repair process. Cell migration may occur in association with the surface of a material by contact guidance or through an

ensemble of other cells. In neuronal regeneration, SCs provide the natural substrate for axon migration [126, 127]. They produce structural and cell adhesive ECM molecules such as laminin and collagen, and express many cell adhesion molecules and neurotrophin factors that can serve as guidance cues for axonal growth [49].

1.1.10 Cell adhesion and integrin receptors

Over the past few decades, various receptor–ligand systems for cell–cell and cell–matrix binding have been identified and characterised. Some of the most common cell surface molecules involved in cell adhesion and motility are the integrins which are heterodimeric membrane proteins, consisting of non-covalently associated α and β subunits (Figure 1.22) [128]. Each member of the integrin family can be characterised by the combination of subunits involved; for example, $\alpha_1\beta_1$ binds to collagen and laminin, $\alpha_5\beta_1$ to fibronectin, and β_2 to ligands on cell surfaces. Integrin binding is Ca^{2+} dependent. Integrin-mediated cell adhesion is usually associated with cell–matrix interactions where the extracellular domain of the integrin receptor binds to an ECM protein and the cytoplasmic integrin domain binds to the protein cytoskeleton. Therefore, integrin receptors provide a critical connection between the extracellular and intracellular environments. Matrix proteins such as fibronectin, collagen, laminin, vitronectin, thrombospondin, tenascin and entactin contain the three amino acid sequence, arginyl-glycyl-aspartic acid (RGD). The short amino acid sequences, identified by analysis of active fragments of ECM molecules, appear to compete for the integrin receptor site and bind to receptors on cell surfaces to mediate cell adhesion. Moreover, different integrins bind selectively to different proteins at RGD-containing sites, suggesting that binding is also affected by polypeptide domains adjacent to the RGD domain, but specific to each protein.

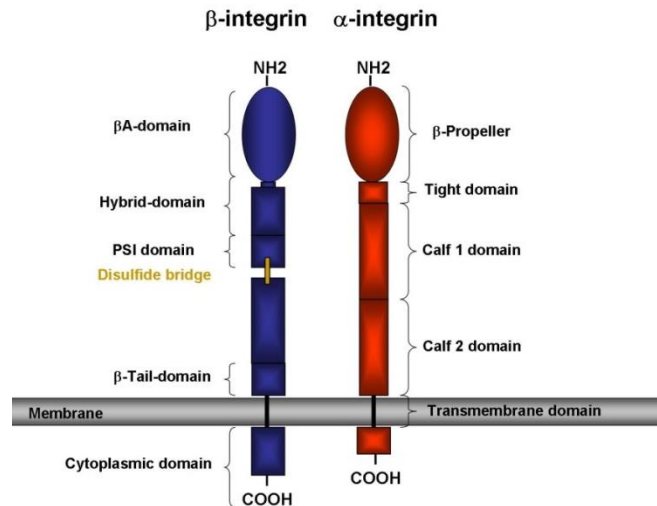


Figure 1.22 Schematic architecture of integrin heterodimeric adhesive receptors consisting of α - and β -subunits. The ligand binding site is provided by the N-terminal domain of the α - and β -integrin subunits (the β -propeller and the β A domain, respectively) which are assembled in most integrins by non-covalent interactions to form a “head”. It is known that in eight α integrin subunits ($\alpha 1$, $\alpha 2$, $\alpha 10$, $\alpha 11$, αL , αM , αX and αD), the αA domain, which is homologous to the βA domain of the β -integrin subunit, is inserted into the β -propeller domain. This is the main ligand-binding site in these integrins [128].

1.1.11 Growth factors and nerve regeneration

The effect of neurotrophic factors in neural development, axonal survival, outgrowth and branching has been examined in detail at various levels, from molecular interactions to macroscopic tissue responses, in the PNS and CNS. Various types of neurotrophic factors are active at the site of neural injuries, including neurotrophins such as NGF, brain-derived neurotrophic factor, neurotrophin-3 and neurotrophin-4/5. Furthermore, cytokines and insulin derivatives, ciliary neurotrophic factor, glial cell line-derived growth factor and acidic and basic fibroblast growth factors induce important neurotrophic effects [43, 129-131] (Table 1.6).

Table 1.6 Neural responses to neurotrophic factors.

Neurotrophic factors	Neural response promoted
BDNG, NT-3, NT-4/5, CNTF, GDNF	Motor neuron survival
BDNG, NT-3, NT-4/5, CNTF, GDNF	Motor neuron outgrowth
NGF, NT-4/5, GDNF	Sensory neuron survival
NGF, BDNF, NT-3	Sensory neuron outgrowth
NGF, NT-3, CNTF, FGFs	Spinal cord regeneration
NGF, NT-3, NT-4/5, CNTF, GDNF, FGFs	Peripheral nerve regeneration
NGF, NT-3, GDNF, FGFs	Sensory nerve growth across the PNS – CNS transition zone

*BDNG, brain-derived nerve growth factor; NT-3, neurotrophin-3; N/T-4/5, neurotrophin-4/5; CNTF, ciliary neurotrophic factor; GDNF, glial cell line-derived growth factor; aFGF/bFGF, acidic and basic fibroblast growth factor.

Consequently, the controlled release of neurotrophic factors from tissue engineering scaffolds has been studied with the aim of enhancing nerve regeneration. Several delivery systems such as polymer matrices [132], microspheres [133, 134], viral vectors [135, 136] and liposomes [137] may be used to supply neurotrophic factors in conjunction with the use of nerve guides or scaffolds, but challenges exist in delivering the necessary quantities and types of neurotrophic compounds at the rates conducive to regeneration. Ideally, a delivery system should improve the molecular stability of growth factors, control the rate of release and achieve cell targeting.

Specific Research Objectives

The prospects for successful peripheral nerve repair using tissue engineering principles are considered to be enhanced by use of a 3D scaffold which promotes attachment and growth of regenerating neurons and glial cells. The overall aim of the research described in this thesis was to evaluate *in vitro* the potential of alginate polysaccharide fibres as tissue engineering scaffolds for nerve repair.

The specific objectives were as follows:

1. To produce alginate fibres by wet spinning and modify them with gelatin a) to produce an adhesive surface for nerve cell adhesion b) to investigate the potential for polypeptide growth factor incorporation in the fibres and c) to provide a method for macropore production by extraction of gelatin particles from the fibres. The latter approach was aimed at producing macropores of sufficient size and connectivity to permit proliferation of nerve cells, neurite outgrowth and axonal extension to restore nerve function.
2. To characterise in detail the 3D structure of macroporous alginate fibres (pore dimensions, porosity, interconnected pores) using confocal laser scanning microscopy and image analysis to elucidate the relationship between macropore structure and formulation parameters and to permit subsequent correlations with the growth of encapsulated nerve cells.
3. To establish wet spinning techniques for encapsulation of fibroblasts in alginate fibres and cell growth behaviour in culture as a precursor to experiments with nerve cells.
4. To encapsulate dorsal root ganglion (DRG) cells in macroporous alginate fibres and investigate in cell culture the extent of neurite outgrowth and the formation of neuronal contacts throughout the scaffold.

5. To encapsulate photoreceptor-derived (661W) cells in macroporous alginate fibres and investigate their capacity to function as carriers for photoreceptor cells for applications in retinal regeneration.

CHAPTER 2

Production of Alginate Fibres for Nerve Tissue Engineering

ABSTRACT

The prospects for successful peripheral nerve repair using fibre guides are considered to be enhanced by use of a scaffold material which provides a good substrate for attachment and growth of glial cells and regenerating neurons. Alginate polymers exhibit a highly favourable balance of properties and form hydrogels under mild crosslinking conditions. As a result, alginate has been widely applied for cell encapsulation. However, the polysaccharide exhibits extremely poor cell adhesion properties, which limits its application for tissue regeneration. Experimental nerve guides were thus produced from alginate fibres with the dual aim of providing a favourable substrate for cell adhesion and a delivery system for growth factors. Firstly, the diameters of the hydrated and dried fibres produced by extrusion of alginate solution into CaCl_2 crosslinking solution through syringe needles of various sizes were determined using light microscopy and scanning electron microscopy (SEM). The mean diameter of hydrated fibres could be increased from approximately 450 to 1300 μm by increasing the internal diameter of the needle used for fibre spinning. A major reduction in diameter by a factor of up to 10 occurred upon drying the fibres using ethanol treatment. A syringe needle with a size of 0.6 \times 32 mm was subsequently selected for further experiments, since the spun fibres were easier to handle, and the dried fibres rehydrated efficiently. Tensile testing showed that alginate fibres dried with ethanol exhibited a mean tensile stiffness that was approximately 10 times higher (26.2 MPa) than that of fibres dried at 60 °C (2.1 MPa), with a doubling of the tensile strength and reduction in failure extension. This behaviour may be

explained by rapid dehydration of the alginate fibres in ethanol, when compared with heating at 60 °C, which causes molecular extension and alignment. SEM examination of alginate fibres dried by ethanol treatment revealed a rough-textured, oriented surface that is expected to improve nerve cell adhesion. Alginate fibres were modified by gelatin a) to improve cell adhesion b) to investigate the potential for polypeptide growth factor incorporation in the fibres and c) to provide a method for macropore production by extraction of the gelatin particles from the fibres. Thus alginate fibres were a) incubated in 0.5, 1, 2 and 5% w/v gelatin solution b) wet spun into gelatin/CaCl₂ solution c) wet spun from a mixed alginate/gelatin solution d) wet spun from alginate solution containing dispersed (undissolved) gelatin particles. Incubation of hydrated alginate fibres in 0.5% w/w gelatin solution at 37 °C resulted in low protein loading (1.7% w/w) and rapid release of gelatin (90% of the initial load) over 24 h in distilled water at 37 °C. In comparison, incubation of hydrated alginate fibres in 5% w/v gelatin solution resulted in approximately 9% w/w protein loading and gradual protein release (80% of initial content) over 9 days. The approach of wet spinning alginate solution into CaCl₂ crosslinking solution containing dissolved gelatin was unsuccessful and resulted in extremely low or non-detectable protein loading (0 – 0.03% w/w) in the resulting fibres. Wet spinning a co-solution of alginate and gelatin into CaCl₂ crosslinking solution resulted in low protein loadings of 1.2 – 1.7% w/w for both hydrated and dried fibres. Major release (>70% initial content) occurred in 24 h. Alginate fibres incorporating gelatin particles were successfully produced by wet spinning suspensions of gelatin particles in 1.5% (w/v) alginate solution. Gelatin loading of the starting suspension of 40.0, 57.0 and 62.5% w/w resulted in gelatin loading of the hydrated alginate fibres of 16, 21 and 24% w/w respectively. Around 45 – 60% of the gelatin content of hydrated fibres was released in 1 h in distilled water at 37 °C, suggesting that a macromolecular structure for cell

growth would be rapidly established in cell culture. Furthermore, the residual gelatin is expected to form a favourable surface for nerve cell adhesion and axonal extension.

2.1 INTRODUCTION

The prospects for successful peripheral nerve repair using fibre guides are considered to be enhanced by using a scaffold material that provides a good substrate for attachment and growth of glial cells and regenerating neurons [16]. Various synthetic and natural biomaterials have been considered as cell supporting matrices. As a result, bicomponent fibres have been produced from synthetic polymers such as poly(ϵ -caprolactone) (PCL) in combination with the cell adhesion molecule collagen, to promote binding with $\alpha_1\beta_1$ integrin receptors on the surface of axons and neuroglial cells, and thus, improve nerve repair [138]. Polymers of natural origin are attractive options for scaffold production due to their presence in ECM in some cases (e.g. collagen), their chemical versatility and biocompatibility. Alginate is a naturally occurring anionic, hydrophilic polysaccharide, derived primarily from brown seaweed and bacteria, which has been investigated extensively as a biomaterial. Alginate has been applied in the form of hydrogels for bone regeneration [139, 140], microspheres for bioactive and controlled release drug delivery [141-143], freeze-dried sponges to stimulate axonal regeneration [144], foams loaded with antimicrobial agent [145] and fibres as a carrier to deliver zinc [146], silver [147] and other active compounds that are beneficial for wound healing [148, 149]. Alginate exhibits excellent biocompatibility and biodegradability and can be easily modified via chemical and physical reactions to obtain derivatives having various structures, properties, function and applications [150]. Cell adhesion plays a critical role in cell migration, proliferation and differentiation. However, naturally derived polysaccharides do not readily promote cellular attachment and function due to an absence of ligands in the

chain structure that can bind with cell surface receptors. Thus alginate has been commonly modified using the amino acid sequence arginine-glycine-aspartic acid (RGD), derived from ECM proteins including fibronectin [151], laminin [152], and collagen [153] to provide cell anchorage via integrin cell surface receptors [154]. Addition of fibronectin to alginate hydrogel was shown to improve Schwann cell viability and proliferation *in vitro* [151]. Laminin-coated and YIGSR peptide conjugated alginate hydrogel (peptide/alginate ratios of 1 mg/g) improved NB2a neuroblastoma cell attachment by 44 and 60% respectively compared with the control [152]. Alginate-gelatin crosslinked (ADA-GEL) hydrogel (synthesized by covalent crosslinking of alginate di-aldehyde (ADA) with gelatin) was developed to support normal human dermal fibroblasts (NHDF) cell attachment, spreading and proliferation [140].

Gelatin is derived from collagen by breaking the natural triple-helix structure into single-strand molecules by hydrolysis and has been widely used for the production of cell support structures because of its cell adhesion properties and biocompatibility. The presence of acidic and positively charged lysine and arginine residues in the denatured collagen molecule promote electrostatic binding with negatively charged cell surfaces. In addition, specific cell adhesion (RGD) sequences along the protein molecule bind with cell surface integrin receptors (see Chapter 1, Section 1.1.10). Indirect cell–gelatin binding is also possible via interactions between integrin cell surface receptors and the RGD domain of fibronectin following formation of a fibronectin/gelatin interface.

This chapter describes the production and characterisation of wet-spun alginate fibres and their modification using gelatin to investigate their potential as scaffold material for nerve regeneration. Alginate fibres were modified by gelatin a) to improve cell adhesion b) to investigate the potential for polypeptide growth factor incorporation in

the fibres and c) to provide a method for macropore production by extraction of gelatin particles from the fibres. The latter approach was intended to provide a connected macropore structure that would allow axonal growth throughout the fibre from neurons encapsulated in the fibres during wet spinning.

2.2 MATERIALS

Sodium alginate (Protanal RF 6650, G:M 2:1, pH 6.0 – 8.0) was obtained from IMCD Australia Limited. Calcium chloride (dried, 0.5 M, UniLab), gelatin from porcine skin (type A bloom 300, average molecular mass 50-100 kDa), bicinchoninic acid (BCA) reagents were purchased from Sigma-Aldrich Chemicals Australia.

2.3 METHODS

2.3.1 Wet spinning of alginate fibres

Sodium alginate was dissolved in distilled water at a concentration of 1% w/v, and 0.5 mL of the alginate solution was wet spun into 50 mL of 0.5 M CaCl₂ solution through a syringe needle (0.6 × 32 mm). A syringe pump was used to feed the alginate solution into the needle tip at a rate of 2 mL/min. The alginate fibres (30 – 35 cm) were collected from the spinning bath, transferred to 20 mL of 0.5 M CaCl₂ solution and incubated for 1 h. After treatment, the fibres were rinsed in distilled water and used in the hydrated (wet) form for further investigations or dried with absolute ethanol. The hydrated alginate fibres were dried with ethanol by immersion in an ethanol bath for 30 s at 25 °C, followed by transfer to the bench top to allow ethanol evaporation for 5 min (Figure 2.1). The treatment was repeated three times and ethanol was allowed to evaporate at room temperature for 30 min.

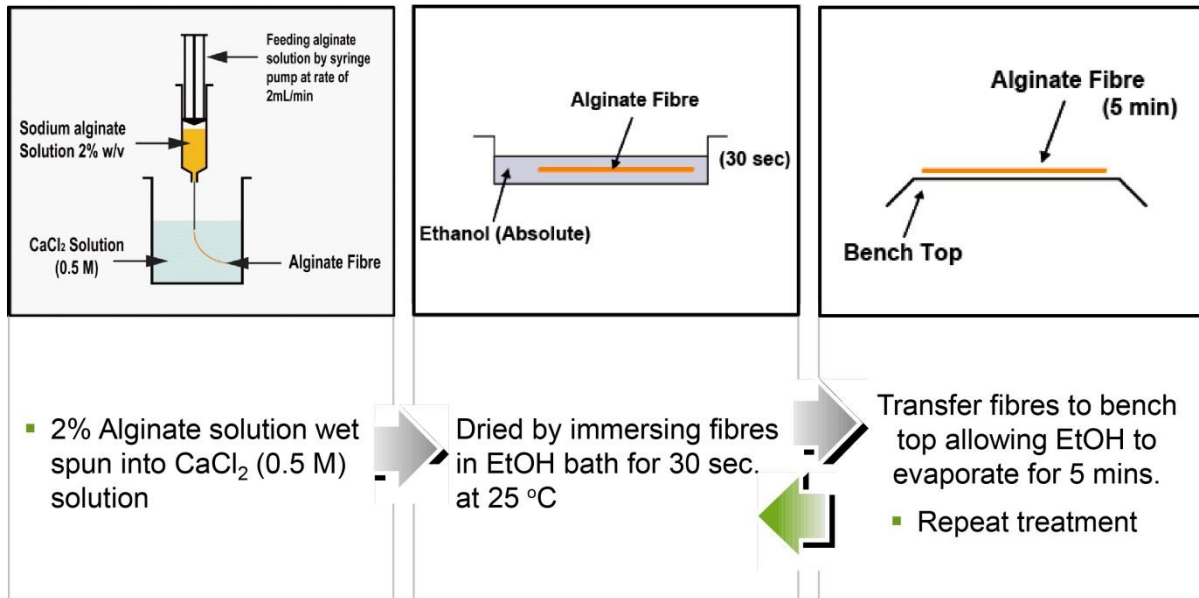


Figure 2.1 Production of alginate fibres by wet spinning.

2.3.2 Gelatin modification of alginate fibres

Wet-spun sodium alginate fibres were modified using gelatin a) to improve nerve cell adhesion to the fibres b) to investigate the potential for polypeptide growth factor incorporation in the fibres and c) to provide a method for macropore production by extraction of gelatin particles from the fibres which would permit axonal growth.

2.3.2.1 Surface modification of alginate fibres with gelatin

Gelatin was dissolved in distilled water (40 °C) to produce solutions of concentrations of 0.5, 1, 2 and 5% w/v respectively. Hydrated and dried alginate fibres (approximately 15-cm in length, produced according to the procedure described in Section 2.3.1) were incubated in 20 mL of the respective concentration of gelatin solution at 37 °C for 48 h. The fibres were rinsed with distilled water twice before further testing.

2.3.2.2 Alginate fibre spinning into a co-solution of gelatin and CaCl₂

Sodium alginate was dissolved in distilled water at a concentration of 1% w/v. Gelatin type A was dissolved in 0.5 M CaCl₂ (40 °C) solution at a concentration of 2% w/v. Alginate solution (0.5 mL) was wet spun into the gelatin/CaCl₂ solution through a syringe needle (0.6 × 32 mm). A syringe pump was used to feed the alginate solution into the needle tip at a rate of 2 mL/min. The alginate fibres were collected and transferred to 20 mL of 0.5 M CaCl₂ solution and incubated for 1 h. After treatment, the fibres were rinsed once in distilled water. Hydrated or ethanol-dried fibres were assayed for protein content using the BCA assay (Section 2.3.4).

2.3.2.3 Fibre spinning using co-solutions of alginate and gelatin

Gelatin type A was dissolved in distilled water (40 °C) at a concentration of 2% w/v and then added into an alginate solution (1% w/v) at a ratio of 1:1 (gelatin solution: alginate solution). The gelatin/alginate solution (0.5 mL) was wet spun into 0.5 M CaCl₂ solution through a needle (0.6 × 32 mm). A syringe pump was used to feed the solution into the needle tip at a rate of 2 mL/min. The alginate fibres were collected and transferred to 20 mL of 0.5 M CaCl₂ solution and incubated for 1 h. After treatment, the fibres were rinsed in distilled water. Hydrated or ethanol-dried fibres were tested for protein content using the BCA assay (Section 2.3.4).

2.3.3 Incorporation of gelatin in alginate fibres as a porogen for producing macropores

Wet-spun sodium alginate fibres were modified by incorporation of gelatin particles with the aim of producing a connected macroporous structure that would facilitate neurite outgrowth and axonal regeneration from encapsulated neurons. Gelatin

powder was passed through a <90 micron mesh sieve, and either 100, 200 or 250 mg of sieved powder were homogenised in cold (4 °C) 1.5% w/v alginate solution (10 mL) at speed 2 for 30 s using a homogeniser (IKA Ultra-Turrax® T25 basic). This produced suspensions with gelatin:alginate (w/w) ratios of 2:3, 4:3 and 5:3, respectively (corresponding to 40.0, 57.0 and 62.5% gelatin loading as a fraction of the total polymer content). The suspensions were wet spun through a syringe needle (0.6 × 32 mm) into 0.5 M CaCl₂ solution to produce hydrated alginate fibres containing increasing amounts of gelatin particles. Fibre samples were rinsed in distilled water and dehydrated by immersion in ethanol as described in Section 2.3.1.

2.3.4 Determination of the gelatin loading of alginate fibres

Gelatin-modified alginate fibres (n = 10) were dissolved in 0.2 M sodium citrate solution (3 mL), and the gelatin concentration was determined using the bicinchoninic acid (BCA) protein assay (Sigma) by comparison with a calibration curve generated using serial dilutions of gelatin in distilled water (concentrations of 1000, 900, 800, 600, 500, 400, 300 and 250 µg/mL). Gelatin loading of the fibres was subsequently expressed as % w/w of the dried fibre. The bicinchoninic acid assay (BCA assay), also known as the Smith assay, after its inventor, Paul K. Smith at the Pierce Chemical Company [155], is a biochemical assay for determining the total concentration of protein in a solution (0.5 µg/mL to 1.5 mg/mL). The total protein concentration is measured using the colour change of the sample solution from green to purple in response to protein concentration. The BCA assay primarily relies on two reactions. First, the peptide bonds in protein reduce Cu²⁺ ions from cupric sulfate to Cu⁺ (a temperature dependent reaction). The amount of Cu²⁺ reduced is proportional to the amount of protein present in the solution. Next, two molecules of bicinchoninic acid

chelate with each Cu^+ ion, forming a purple-coloured product that strongly absorbs light at a wavelength of 562 nm. The bicinchoninic acid Cu^+ complex is influenced in protein samples by the presence of cysteine/cystine, tyrosine, and tryptophan side chains. At higher temperatures (37 to 60 °C), peptide bonds assist in the formation of the reaction product. Incubating the BCA assay at higher temperatures is recommended as a way to increase assay sensitivity while minimizing the variation caused by unequal amino acid composition [156]. The amount of protein present in a solution is quantified by measuring the absorption spectra and comparing with protein solutions of known concentration.

2.3.5 Gelatin release from gelatin-modified alginate fibres

Triplicate samples of the three types of fibres (i) alginate/gelatin fibres prepared by spinning from blended solutions (ii) alginate fibres incubated in gelatin solution and (iii) alginate fibres spun into gelatin/ CaCl_2 solution were placed in distilled water (3 mL) in 10 mL (capped) centrifuge tubes and retained at 37 °C for 9 days. The release medium was replaced completely by distilled water on days 1, 3, 5, 7 and 9. The concentration of gelatin in the release medium was determined using the BCA protein assay by comparison with a calibration curve produced using series dilution of gelatin in distilled water (concentrations of 1000, 900, 800, 600, 500, 400, 250 and 220 $\mu\text{g/mL}$). Gelatin release from the fibres was subsequently expressed as the weight of gelatin released (μg) versus time (days) and cumulative release (% w/w) versus time. Cumulative gelatin release was calculated from the released amount and the weight of gelatin remaining in the fibres at day 9. The fibres were broken down with 0.2 M sodium citrate (1.5 mL) and the residual gelatin content was obtained by comparison with a calibration curve of gelatin in sodium citrate.

2.3.6 Gelatin release from hydrated alginate fibres containing gelatin particles

Cumulative gelatin release from fibres spun from suspensions having gelatin:alginate ratios of 2:3, 4:3 and 5:3 respectively, was measured for triplicate samples of hydrated and dried fibres respectively. Samples were retained in distilled water (3 mL) at 37 °C for 48 h and the release medium was replaced completely with fresh distilled water at 20, 40 and 60 min as well as 24 h and 48 h. Gelatin concentration in the release medium was determined by the BCA protein assay (Sigma). The fibres were broken down on day 3 with 0.2 M sodium citrate (1.5 mL) to obtain the residual gelatin content. The amount of gelatin released from the fibres at each time interval and the residual gelatin content following breakdown of the fibres (Section 2.3.2) were determined using a calibration curve produced using a series dilution of gelatin in distilled water (concentrations of 1000, 900, 800, 600, 500, 400, 250 and 220 µg/mL). Cumulative gelatin release (% w/w) versus time (h) was calculated from the amount released at each time interval and the residual gelatin content.

The gelatin loading of the fibres was calculated as a percentage (w/w) of the dried fibres:

$$\text{Gelatin Loading of Fibre} = \frac{\text{Total Weight of Gelatin Released} + \text{Remaining Gelatin}}{\text{Weight of the Freeze-Dried-Gelatin-Loaded Fibre}} \times 100$$

2.3.7 Tensile properties of dried alginate fibres

Fibre nerve guides which are intended to provide a support scaffold for cells *in vitro* and eventual surgical implantation are required to possess adequate strength and stiffness to permit surgical placement without breakage. The tensile properties of alginate fibres dried by two different techniques (ethanol drying and drying at 60 °C) were determined to compare the effect of drying techniques on fibre strength, stiffness

and elongation. The alginate fibres were prepared as described in Section 2.3.1. Following incubation in the second 20 mL volume of 0.5 M CaCl₂ solution for 1 h, the alginate fibres were rinsed with distilled water and dried in an incubator at 60 °C for 30 min or dried using ethanol as described in Section 2.3.1. Fibres were cut to a length of 9 – 10 cm for examination of tensile properties. The diameter of fibres dried with ethanol (circular cross section, approximately 85 µm) and the width of those dried at 60 °C (flat rectangular cross section, approximately 1 mm dimension) were measured using optical microscopy (Olympus BH-2 Trinocular Microscope) at 10× magnifications, calibrated with a 1-mm scale slide. Fibres were tested using an Instron 5543 tensile testing machine. Uniaxial testing of the dried alginate fibres was performed in tension mode using the ramp force procedure. A ramp force of 0.1 N/min was applied using a 5 N load cell. Fibre extension was measured using an optical encoder. Stress versus strain curves were generated for different samples (n = 5) and used to determine the tensile modulus (stiffness, tensile strength and fibre failure extension).

Young's modulus (modulus of elasticity)

Young's modulus is the most common *elastic modulus*, also known as the modulus of elasticity. It is a measure of the *stiffness* of an *elastic* material and is calculated from the ratio of stress (force per unit area) along an *axis* to the *strain* (ratio of deformation over initial length) along that axis in the range of stress in which Hooke's law holds [157].

Strain

Strain is "deformation of a solid due to stress" - change in dimension divided by the original value of the dimension - and can be expressed as

$$\varepsilon = dL / L \quad (1)$$

where

$\varepsilon = \text{strain (m/m)}$

$dL = \text{elongation or compression (offset) of the object (m)}$

$L = \text{length of the object (m)}$

Stress

Stress is force per unit area and can be expressed as

$$\sigma = F / A \quad (2)$$

where

$\sigma = \text{stress (N/m}^2\text{)}$

$F = \text{force (N)}$

$A = \text{cross-sectional area of object (m}^2\text{)}$

Young's Modulus (Tensile Modulus)

Young's modulus or tensile modulus (E) is expressed as

$$E = \text{stress / strain} = (F / A) / (dL / L)$$

2.3.8 Morphology of hydrated alginate fibres using cryo-scanning electron microscopy

The morphology of hydrated alginate fibres was examined using a Philips XL30 scanning electron microscope (SEM). The XL30 has an Oxford CT1500 Cryo transfer system fitted for cryo-scanning electron microscopy (cryo-SEM) that allows suitable hydrated specimens to be examined frozen. The samples were mounted on an aluminium stub using a small amount of graphite paste and then introduced into the air lock of the cryo-preparation chamber, where evacuation was initiated. The specimen was immediately transferred to the cold stage of the preparation chamber, pre-cooled to approximately $-180\text{ }^{\circ}\text{C}$, and sputter-coated with platinum in an argon

atmosphere inside the chamber before examination at a voltage of 5 kV.

2.3.9 Morphology of dried alginate fibre using scanning electron microscopy

The morphology of dried alginate fibres was examined using a Philips XL30 scanning electron microscope (SEM). Samples were mounted on carbon stubs and sputter-coated with platinum using an Eiko-Sputter coater automatic mounting press prior to examination at a voltage of 10 kV.

2.4 RESULTS AND DISCUSSION

2.4.1 Dimensions and morphology of alginate fibres

In the current study, alginate fibres were prepared successfully and reproducibly by wet spinning solutions of 1% w/w alginate (G:M ratio 2:1) into 0.5 M CaCl₂ crosslinking solution (Section 2.3.1). The ratio of guluronic/mannuronic acid, the length of the guluronic acid residues, and the molecular weight of the polymer [66] all significantly affect the crosslink characteristics of the gel. In the egg-box model of alginate postulated by Grant et al. [64] described earlier (Chapter 1, Section 1.1.5), the guluronic acid sequences along the alginate molecule primarily bind to each other via calcium ions. Gel properties are known to be influenced by the concentration of alginate solution, the duration of gelation, the molarity of the divalent crosslinking solution [158, 159] and method of sterilization [160]. Therefore, alginate featuring a high guluronic acid content (G:M ratio 2:1) was selected based on previous studies [160, 161], in order to provide mechanically stable cell support [71]. Furthermore, Bohari et al. [162] reported that as the concentration of alginate increased to 2 and 5%, major 3T3 fibroblast cell death (30–50%) occurred within the hydrogel matrix at day one while cell viability was maintained in excess of 90% when encapsulated using 0.5

or 1% alginate solution. This behaviour was explained by the higher viscosity of alginate solution at higher concentration which exerts high shear stresses that damage the cells during homogenisation in sodium alginate solution [163]. Based on the work of Bohari et al. [162] alginate solution at a concentration of 1 – 1.5% w/w was used in the present study as an optimum concentration for subsequent spinning of cell-containing fibres.

Experimental fibre nerve guides were initially produced entirely from alginate with the aim of providing a substrate for modification by cell adhesion proteins. The diameters of the hydrated and dried fibres produced using needle sizes of 1.1 × 38 mm, 0.6 × 32 mm and 0.3 × 13 mm were measured using light microscopy and scanning electron microscopy (SEM). The mean diameter of hydrated fibres could be varied from approximately 450 µm to 1300 µm by increasing the internal diameter of the needle used for fibre spinning (Table 2.1). A major reduction in diameter by a factor of up to 10 occurred upon drying the fibres using ethanol (Table 2.1). Dried fibres spun from the smaller syringe needle were found to rehydrate more rapidly than the larger fibres because of the lower fibre volume. A syringe needle with a size of 0.6 × 32 mm was subsequently selected for further experiments, since the fibres generated (typically around 700 µm in diameter) were easier to handle, and the dried fibres rehydrated efficiently.

Table 2.1 Diameters of hydrated and dried alginate fibres. Fibres were spun from 1% w/v alginate solution into 0.5 M CaCl₂ solution. Flow rate of alginate solution to needle = 2 mL/min.

Syringe needle	Hydrated fibre diameter (µm)	Dried fibre dimension (µm)
19G × 1.5" (1.1 × 38 mm)	1300 ± 100	120 ± 10
23G × 1.25" (0.6 × 32 mm)	680 ± 30	87 ± 5
30G × 0.5" (0.3 × 13 mm)	447 ± 6	40 ± 3

*Values are mean ± SD of five individually prepared fibres for each needle size.

2.4.1.1 Alginate fibre morphology

The optical micrograph of a hydrated alginate fibre in Figure 2.2A reveals the translucent appearance and uniform structure. The longitudinal ripples or flow lines visible are probably formed by passage of the alginate solution through the syringe needle. The cryo-scanning electron micrograph in Figure 2.2B reveals the fine textured microporous structure of the hydrated alginate fibre. The pore size was approximately 1 µm. The microporous structure of the alginate fibre is expected to be highly inter-connected and therefore advantageous to permit nutrient supply to encapsulated cells and allow oxygen exchange in the inner regions of the scaffold to maintain cell viability. SEM examination of the alginate fibres dried by ethanol treatment revealed a rough-textured, oriented surface (Figure 2.3).

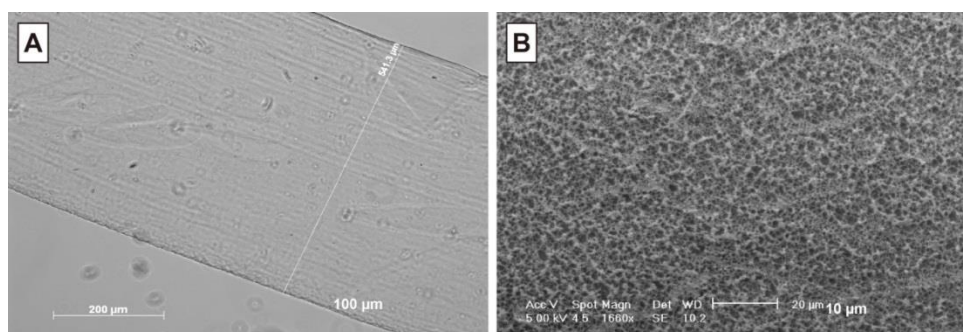


Figure 2.2 (A) Optical micrograph of hydrated fibre. (B) Cryo-scanning electron

micrograph of hydrated fibre. (Pore size approx. 1 μm). The fibre was produced by wet spinning a 1% alginate solution through a syringe needle (0.6 \times 32 mm) into 0.5 M CaCl_2 solution.

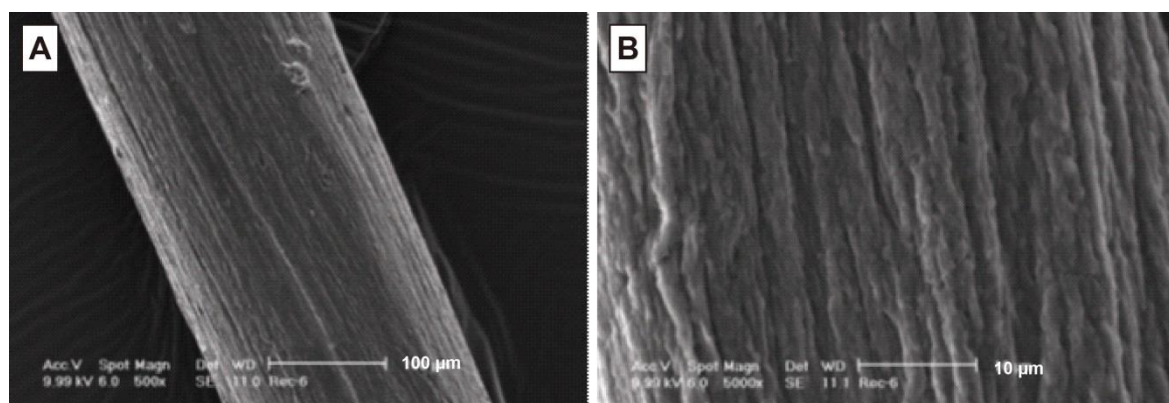


Figure 2.3 (A) Dried alginate fibre and (B) its oriented surface. Fibres produced by wet spinning from a 1.2 \times 38 mm needle and dehydrated by ethanol treatment.

Interactions between biomaterials and cells are known to be influenced by the surface characteristics of the material, including topography, charge and chemical composition. It is generally accepted that rough, textured and porous surfaces stimulate cell attachment, differentiation and the formation of extracellular matrix [164-167]. For example, connective tissue cells, endothelium epithelium, peripheral nerves, and bone cells attach to rough surfaces move easily than to smooth surfaces of various polymer and metallic implants [168-170]. One explanation for this phenomenon is that a rough surface increases the effective surface area for cell attachment and promotes mechanical interlocking (bonding strength) by tissue ingrowth [171, 172]. The rough-textured, oriented surface of dried alginate fibres produced in the present study (Figure 2.3) may therefore be advantageous for promoting nerve cell adhesion and guiding axonal extension.

2.4.2 Tensile properties of dried alginate fibres

In tissue engineering, it is preferable to use biomaterials with a modulus or stiffness close to that of the target tissue to prevent possible stress-shielding effects and to maintain sufficient mechanical support for cells during *in vitro* and/or *in vivo* cell growth and tissue remodelling. The Young's modulus of alginate fibres dried with ethanol was found to be 26.2 ± 15.2 MPa, a factor of 10 greater than alginate fibres dried at $60\text{ }^{\circ}\text{C}$ (2.1 ± 0.4 MPa) (Table 2.2). These values are comparable to those of human articular cartilage ($0.7 - 15.3$ MPa) [74]. The mean tensile strength of the fibres was 0.95 MPa when dried with ethanol and 0.4 MPa when dried at $60\text{ }^{\circ}\text{C}$, while the extension at failure was approximately 46 and 80%, respectively. The fibres dried with ethanol exhibited a tensile stiffness that was approximately 10 times higher than that of the fibres dried at $60\text{ }^{\circ}\text{C}$, with a doubling of the tensile strength and reduction in failure extension. This behaviour may be explained by rapid dehydration of the alginate fibres in ethanol, compared with heating at $60\text{ }^{\circ}\text{C}$, which causes molecular extension and alignment.

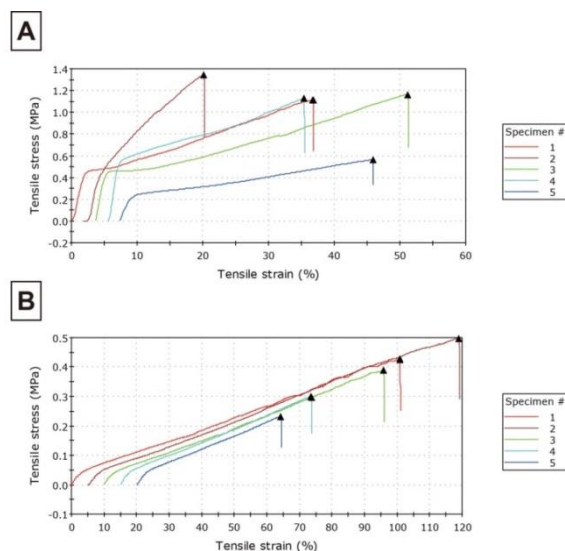


Figure 2.4 (A) Stress–strain curves of alginate fibres dried using ethanol treatment. (B) Stress–strain curves of alginate fibres dried at $60\text{ }^{\circ}\text{C}$ ($n = 5$).

Table 2.2 Tensile properties of dried alginate fibres (n = 5, mean \pm SD).

Drying technique	Young's modulus (Tensile stiffness) (MPa)	Ultimate tensile stress (MPa)	Extension at break (%)
Ethanol treatment	26.2 \pm 15.2	0.95 \pm 0.3	46.8 \pm 23.8
Heating at 60 °C	2.1 \pm 0.4	0.4 \pm 0.1	80.7 \pm 29.0

2.4.3 Gelatin modification of alginate fibres by incubation in gelatin solution

Surface modification of hydrated and dried alginate fibres by gelatin was investigated by immersion of fibres in gelatin solution of different concentration (0.5, 1, 2 and 5% w/v) (Section 2.3.2.1) with the aim of improving the adhesion of nerve cells to potential fibre nerve guides and the adhesion of myofibroblasts to the external surface of tissue engineered nerves to form a biomimetic epineurium (Figure 1.3, Chapter 1). The hydrated fibres (produced as described in Section 2.3.1) following incubation of the fibres in 2% gelatin solution (20 mL) at 37 °C for 48 h were found to exhibit a fairly uniform gelatin loading of 9.3 \pm 0.9% w/w (Figure 2.5). However, the gelatin loading of alginate fibres dried by ethanol treatment (Section 2.3.1) was inconsistent (15.4 \pm 11.6% w/w) and varied by a factor of 10 from 3.4 – 40% w/w (Figure 2.5).

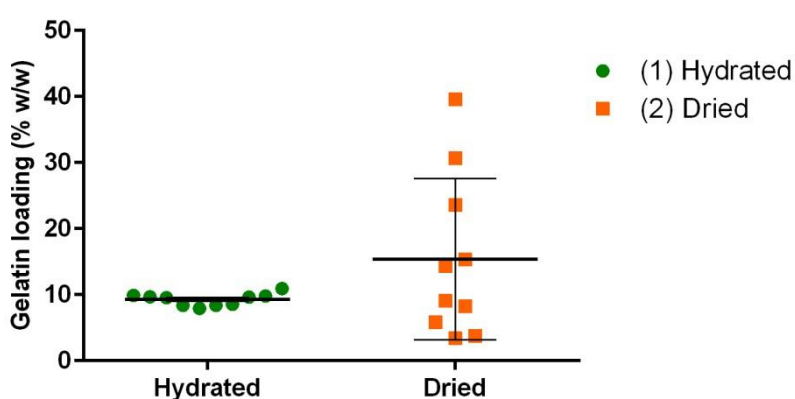


Figure 2.5 Gelatin loading of alginate fibres (n = 10, mean \pm SD) following incubation in 2% w/v gelatin solution at 37 °C for 48 h. (1) Hydrated alginate fibres.

Mean gelatin loading using BCA assay = 9.3% w/w (standard deviation: 0.9). (2)
Alginate fibres dried in ethanol. Mean gelatin loading using BCA assay = 15.4% w/w
(standard deviation: 11.6).

2.4.3.1 Gelatin release from hydrated alginate fibres modified by protein adsorption

Hydrated alginate fibres that were incubated in 0.5% w/v gelatin solution were characterised by a low protein loading (1.7% w/w) and high burst release (90% of the protein content) on day 1 (Figure 2.6B). Hydrated alginate fibres that were modified by incubation in 1, 2 and 5% w/v gelatin solution resulted in a similar gelatin loading (8.9, 8.5 and 9.7% w/w respectively), and gradual protein release occurred over 9 days (Figure 2.6B). This behaviour may be explained by the higher concentration of gelatin present in the incubation solution, which results in more efficient chain entanglement and hence entrapment of gelatin molecules at the fibre surface. It is apparent from Figure 2.6 that gelatin release is delayed from fibres incubated in higher concentration gelatin solutions (2 and 5% w/v) where around 50% of the absorbed protein is retained by the fibre at day 3, suggesting that a cell-adhesive surface may be provided for improved cell-attachment and growth.

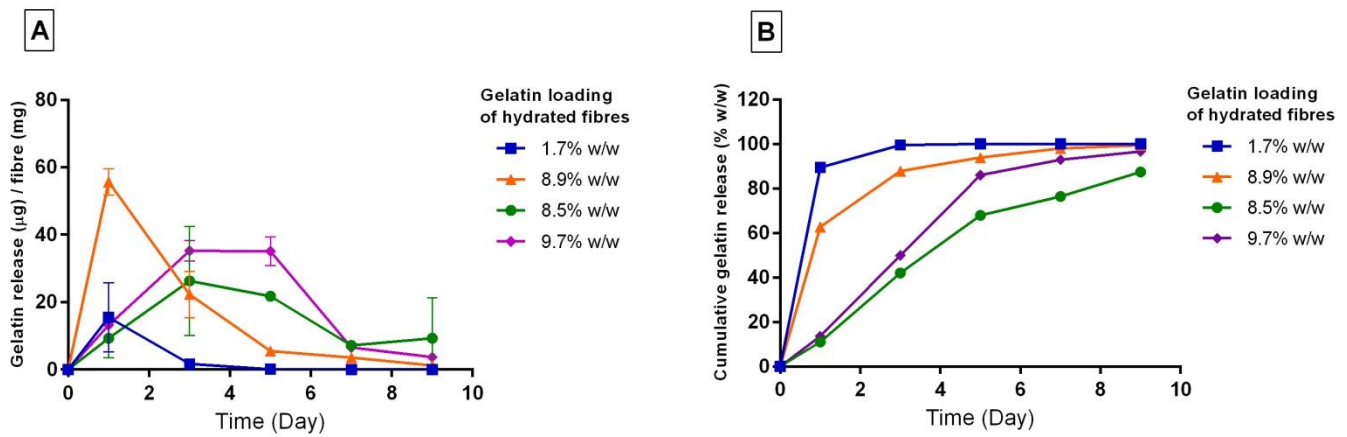


Figure 2.6 (A) Gelatin release from hydrated alginate fibres ($\mu\text{g}/\text{mg}$ fibre) and (B) Cumulative release of gelatin from hydrated alginate fibres (% w/w) in distilled water at $37\text{ }^{\circ}\text{C}$ over 9 days. Mean fibre weight was 294 ± 26 mg. Fibres were incubated in 0.5, 1, 2 and 5% w/v gelatin solution at $37\text{ }^{\circ}\text{C}$ for 48 h before release testing. Corresponding gelatin loading of fibres was 1.7, 8.9, 8.5 and 9.7% w/w.

2.4.3.2 Gelatin release from dried alginate fibres modified by protein adsorption

Incubation of dried alginate fibres in gelatin solutions of increasing concentration (0.5, 1, 2 and 5% w/v) resulted in a corresponding increase of adsorbed protein (0.4, 10.6, 24.5 and 72.8% w/w, respectively). As in the case of the hydrated fibres, this behaviour suggests that association of protein molecules in solution was leading to enhanced protein density at the fibre surface. However, the increased protein adsorption on dry fibres may result from rehydration effects and requires further study. Insertion of gelatin molecules in completely rehydrated alginate fibres is controlled by protein diffusion from the incubation medium, whereas protein transport into the rehydrating fibre may be assisted by fluid flow effects and may be an important determinant of the protein loading of dried fibres. Gelatin adsorption on dried fibres exhibited a pronounced burst effect (100% of the protein load) observed for fibres modified using low gelatin solution concentration (0.5% w/v) (Figure 2.7B). Gradual

release of gelatin occurred from the fibres over 9 days in distilled water when the dried fibres had been incubated in gelatin solutions of 1, 2 and 5% w/v. A major decrease in the cumulative release to around 20% at 9 days was measured for fibres incubated in gelatin solutions with the highest concentration (5% w/v) (Figure 2.7B). Taken together, these findings suggest that surface modification of alginate fibres by gelatin may be maintained sufficiently to enhance nerve cell attachment and extension along fibre guides. Surface modification by gelatin may also be useful for adhesion of myofibroblasts to form a surface layer on tissue engineered nerve substitutes that mimics the epineurium.

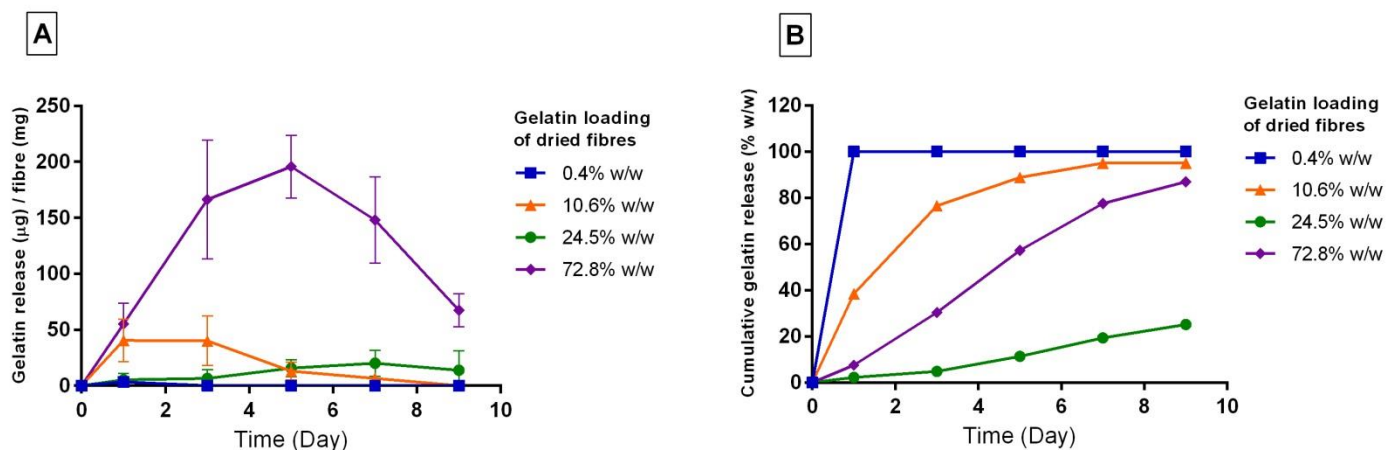


Figure 2.7 (A) Gelatin release from alginate fibres dried using ethanol ($\mu\text{g}/\text{mg}$ fibre) in distilled water at $37\text{ }^\circ\text{C}$ over 9 days. (B) Cumulative release (% w/w) of gelatin from alginate fibres dried using ethanol. Mean fibre weight was 24 ± 9 mg. Fibres incubated in 0.5, 1, 2 and 5% w/v gelatin at $37\text{ }^\circ\text{C}$ for 48 h. Corresponding gelatin loading of fibres was 0.4, 10.6, 24.5 and 72.8% w/w. Release medium: distilled water at $37\text{ }^\circ\text{C}$.

2.4.4 Gelatin loading and release from alginate fibres spun into gelatin/CaCl₂ solution

Attempts were made to modify alginate fibres with cell-adhesive gelatin molecules by wet spinning alginate solution into CaCl₂ crosslinking solution containing dissolved gelatin. The aim was to entrap protein in the fibre surface during the process of alginate gelation induced by crosslinking with divalent Ca²⁺ ions. This approach was unsuccessful and resulted in extremely low or non-detectable protein loading in the resulting alginate fibres (0% for dried fibres, 0.03% w/w for hydrated fibres) (Figure 2.8). The working range of the standard BCA assay protocol was limited to 200 – 1,000 mg/ml (20 – 100 mg of total protein). In addition, complete loss of protein occurred rapidly in 24 h in distilled water (Figure 2.8B).

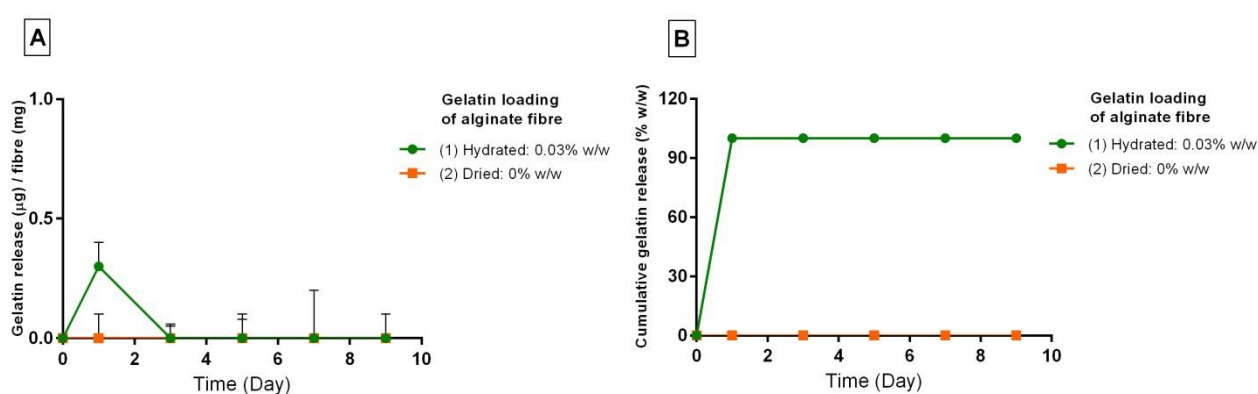


Figure 2.8 (A) Gelatin release (µg/mg fibre) and (B) cumulative gelatin release (% w/w) from alginate fibres over 9 days in distilled water at 37 °C. (1) Fibres were manufactured by extruding alginate solution (1% w/w) into 0.5 M CaCl₂ crosslinking solution containing dissolved gelatin (2% w/v). (2) Dried alginate fibres were prepared using ethanol treatment.

2.4.5 Gelatin loading and release from fibres wet spun from a mixed alginate/gelatin solution

Attempts were made to modify alginate fibres with gelatin molecules by wet spinning a co-solution of alginate and gelatin into CaCl_2 crosslinking solution. Dried alginate/gelatin fibres were prepared by ethanol treatment (Section 2.3.1). Low protein loadings of 1.7 and 1.2% w/w were obtained for hydrated and dried gelatin-loaded fibres respectively with major release of more than 70% of the protein content occurring in 24 h (Figure 2.9). The loading and release behaviour was similar to hydrated fibres modified with gelatin by incubation in low concentration (0.5%) gelatin solution (Figure 2.6B).

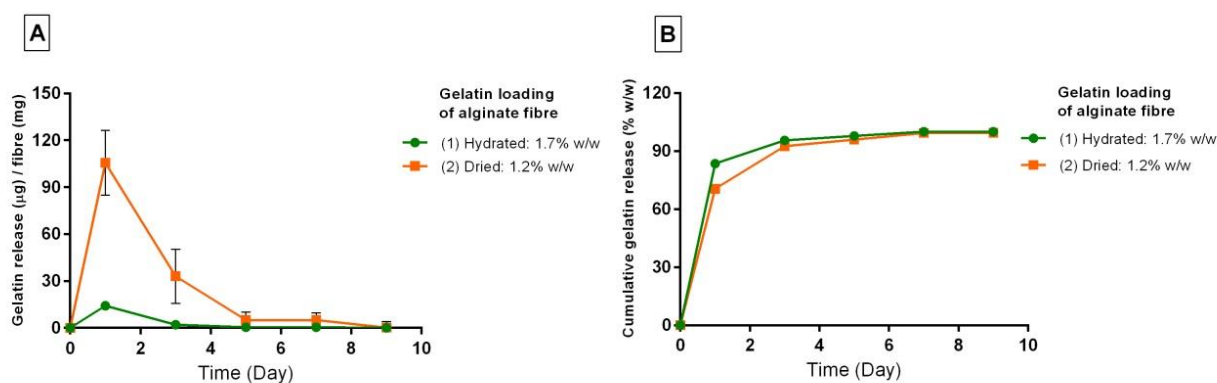


Figure 2.9 (A) Gelatin release ($\mu\text{g}/\text{mg}$ fibre) and (B) cumulative gelatin release (% w/w) from alginate fibres over 9 days in distilled water at 37 °C. (1) Fibres were manufactured by spinning a mixture of gelatin (2% w/v) and alginate (1% w/v) solution (gelatin:alginate volume ratio 1:1) into 0.5 M CaCl_2 solution. (2) Dried alginate fibres were prepared by ethanol treatment. Total gelatin loading of (1) hydrated and (2) dried fibres was 1.7 and 1.2% w/w, respectively.

2.4.6 Incorporation of gelatin particles in alginate fibres to produce macropores

Alginate fibres were successfully loaded with gelatin particles by wet spinning suspensions of gelatin particles in 1.5% (w/v) alginate solution. The aim was to create a macroporous network within the alginate fibre by extraction of the protein porogen to facilitate proliferation of nerve cells and axonal extension throughout the fibre with the formation of synaptic contacts. Three gelatin particle:alginate ratios (2:3, 4:3, 5:3) were investigated, equivalent to a gelatin content of 40.0, 57.0 and 62.5% in the starting suspension, to explore the potential for controlling the macropore content of the fibre and pore connectivity. The ratios were calculated as follows.

Gelatin: 0.25 g

1.5% alginate solution (10 mL): 0.15 g/10 mL

Ratio: gelatin (0.25 g):alginate (0.15 g) = 5:3 (w/w)

Note. Gelatin particle size and shape are characterised and presented in Chapter 3 (Figure 3.4, Table 3.3).

Gelatin loading of the starting suspension of 40.0, 57.0 and 62.5% (w/w) resulted in actual gelatin loading of the hydrated alginate fibres of 16, 21 and 24% w/w respectively (Figure 2.10). Hydrated fibres exhibited a burst release of around 45 – 60% of the gelatin content in 1 h and only minor additional amounts of gelatin were released in 48 h (Figure 2.10B). This behaviour suggests that a macromolecular structure for cell growth would be rapidly established in cell culture. In addition, the plateau of gelatin release vs. time for the hydrated fibres is noteworthy and suggests that a fraction of the gelatin content may be bound within the alginate fibre, where it may function to improve cell adhesion. In comparison, the gelatin loading of alginate

fibres dried using ethanol treatment was 12.4, 18.0 and 36.0% w/w respectively (Figure 2.11). Gelatin release from dry fibres was reduced to 3 – 20% in the first hour and to 10 – 30% over 48 h (Figure 2.11B). As expected, the gelatin content was retained more effectively by the dried fibres compared with the hydrated fibres reflecting the time required for fibre rehydration and the corresponding lag time for dissolution of the gelatin particles.

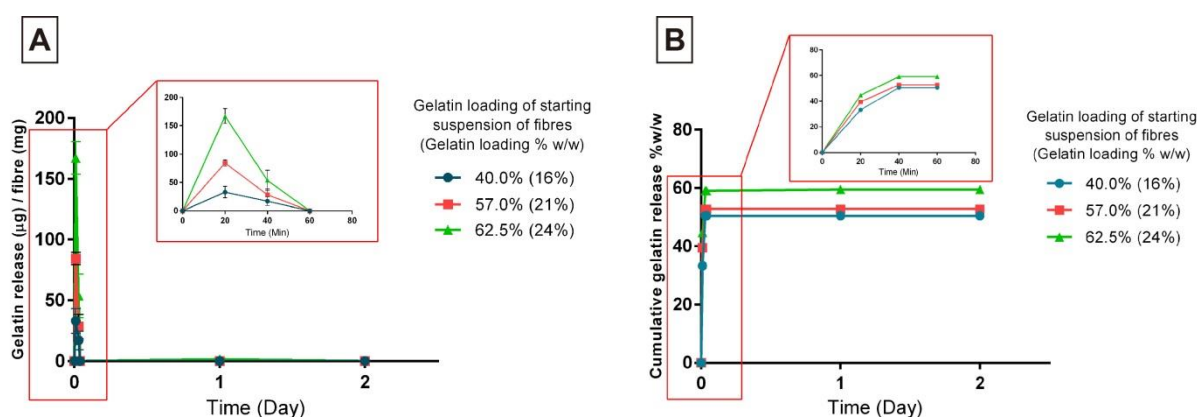


Figure 2.10 (A) Gelatin release ($\mu\text{g}/\text{mg}$ fibre) and (B) cumulative gelatin release (% w/w) from hydrated gelatin-loaded alginate fibres over 2 days in distilled water at 37 °C. Fibres were produced from suspensions of sieved gelatin particles ($<90 \mu\text{m}$) in alginate solution with gelatin contents of 40.0, 57.0 and 62.5% w/w. The corresponding (actual) loading of gelatin in the spun fibres was 16, 21 and 24% w/w.

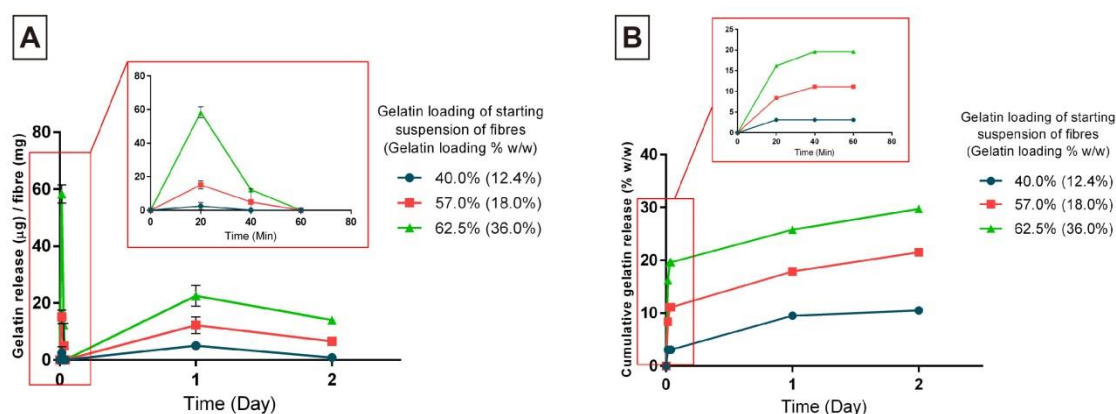


Figure 2.11 (A) Gelatin release ($\mu\text{g}/\text{mg}$ fibre) and (B) cumulative gelatin release (% w/w) from dried gelatin-loaded alginate fibres over 2 days in distilled water at 37°C . Fibres were produced from suspensions of sieved gelatin particles ($<90\ \mu\text{m}$) in alginate solution with gelatin contents of 40.0, 57.0 and 62.5% w/w and were dried using ethanol. The corresponding (actual) loading of gelatin in the spun fibres was 12.4, 18.0 and 36.0% w/w.

2.5 CONCLUSION

Wet-spun alginate fibres were successfully modified by gelatin via a) protein adsorption b) wet spinning into gelatin/ CaCl_2 solution c) wet spinning from a mixed alginate/gelatin solution and d) by suspending gelatin particles in the alginate spinning solution. Gelatin surface modification of hydrated and dried alginate fibres by adsorption from gelatin solution resulted in retention of 50% and 90% respectively of the protein content after incubation in distilled water at 37°C for 3 – 4 days. This behaviour indicates a method for improving nerve cell adhesion to tissue engineering scaffolds prepared from alginate fibres. Alginate fibres incorporating gelatin particles up to a loading of 24% w/w were successfully produced by wet spinning suspensions of gelatin particles in alginate solution. Around 45 – 60% of the gelatin content of hydrated fibres was released in 1 h in distilled water at 37°C , suggesting that a

macroporous structure potentially advantageous for nerve cell growth would be rapidly established in cell culture. Furthermore the residual gelatin is expected to form a favourable surface for nerve cell adhesion and axonal extension.

CHAPTER 3

Production and Characterisation of a Macroporous Structure in Alginate Fibres for Nerve Repair

ABSTRACT

The production of macroporous alginate fibres with transverse dimensions of around 400 μm for nerve cell encapsulation was achieved by wet spinning suspensions of gelatin particles in alginate solution into CaCl_2 crosslinking solution, followed by gelatin extraction in distilled water. Confocal laser scanning microscopy (CLSM) and image analysis provided detailed qualitative and quantitative information on pore size and size distribution and provided an estimate of pore connectivity and maximum porosity (14.6%). CLSM also revealed that protein residues lined the macropore cavities and had migrated into the body of the alginate scaffolds. This finding provides evidence for macropore surface modification by cell adhesion molecules, which is potentially advantageous for nerve cell growth and axonal extension.

3.1 INTRODUCTION

One of the primary aims of tissue engineering scaffolds is to support cell attachment and growth so that cells are able to proliferate and occupy the whole volume of the scaffold. This establishes a need for scaffold structures that are not only biocompatible and biodegradable but also possess optimum porosity, pore size and pore connectivity conducive to cell–cell contact and proliferation. A major restraint on progress in tissue engineering results from unsatisfactory scaffold pore structures that impede tissue ingrowth, nutrient supply to cells and metabolite dispersion. As a result numerous studies have focused on establishing the critical macropore size for cell

infiltration into various scaffolds produced using different biomaterials (Tables 3.1) [173].

Table 3.1 Optimal pore size for cell infiltration and host tissue ingrowth [173].

Cell/tissue type	Optimal pore size (μm)	Scaffold material	Ref.
Human skin fibroblasts	<160 μm	PLA/PLG	[174]
Bone	450 μm	P.P.M.M.	[175]
Bone	>100–150 μm	Bioceramic	[176]
Fibrocartilaginous tissue	150–300 μm	Polyurethane	[177]
Adult mammalian skin cells	20–125 μm	Collagen–glycosaminoglycan (CG)	[178]
Osteogenic cells	100–150 μm	Collagen–GAG	[179]
Smooth muscle cells	60–150 μm	PLA	[180]
Endothelial cells	<80 μm	Silicon nitride	[181]

The most common techniques used to create porosity in a biomaterial are salt leaching, gas foaming, phase separation, freeze-drying and sintering [182-184]. The most versatile methods involve incorporating water-soluble particulates as porogens in polymer matrices formed using solution or melt processing [185-187]. Studies have shown that the porosity and pore size of the scaffolds can be controlled by alternating both the size and amount of leachable particles. However, enhancing porosity in tissue engineering scaffolds, while facilitating tissue ingrowth and the exchange and diffusion of nutrients and gases, may also adversely reduce the mechanical strength of the scaffolds [188, 189]. Therefore, balancing the porosity, pore morphology, pore interconnectivity and mechanical properties is of key importance in scaffold fabrication. Nam et al. [190] showed that macropores with a size of 100–200 μm , generated between layers of PCL electrospun meshes after salt leaching, promoted cartilage/CFK2 cell infiltration to a depth of 4 mm with cellular coverage of up to 70%. In contrast, cellular infiltration through the non-modified meshes was minimal (approximately 160 μm) over the same culture duration [185].

Yang et al. reported that PLA and PLGA scaffolds (produced by salt leaching) having a pore size smaller than 160 μm facilitated growth of human skin fibroblasts [191]. Porous poly(methylmethacrylate) (PMMA) resin when implanted into skeletal and non-skeletal sites *in vivo* showed connective tissue ingrowth for a pore size of 100 μm and osseous tissue ingrowth in pores of 450 μm [192]. The issue of pore interconnectivity within scaffolds has attracted less attention than pore size, but plays a key role in determining the extent of tissue ingrowth. Pore structures often consist of irregularly shaped voids and connecting channels (connects) that can be difficult to define due to merging of adjacent cavities, resulting in the presence of fenestrations (windows) in the void walls [186]. Regardless of the type of material, it is vital to be able to characterise the pore network of scaffolds in 3D to determine the potential for cell ingrowth. Ma and Cho [193] prepared paraffin spheres as porogens (size range 250–500 μm) to create spherical pores with well-controlled pore connectivity and porosity of 95% in biodegradable PLLA and PLGA polymer foams. Jones et al. [194] applied micro-CT to characterise the size, geometry and connectivity of macropores in bioactive glass scaffolds produced by a sol–gel foaming process and intended for bone repair (Figure 3.1). The pore structure was analysed by applying computer algorithms and then validated against mercury intrusion porosimetry and 3D image analysis [195]. The study also showed that micro-CT could be used to generate finite element models to predict scaffold mechanical properties and permeability. Soliman et al. [196] determined scaffold porosity from measurements of the void fraction in top-view scanning electron micrographs of electrospun scaffolds composed of poly(ϵ -caprolactone). The SEM images were converted to black and white binary images, and the percentage of white pixels in each image was determined to define the pore phase [196]. However, this approach does not yield actual information regarding the internal pore structure. Few studies have attempted to characterise the

fragile, hydrogel materials applied in soft tissue regeneration because of poor image resolution. Partap et al. [197] applied mercury intrusion porosimetry (MIP) and helium pycnometry to determine a porosity range for alginate hydrogels of 83 – 97% and a pore volume range of 4.5 – 20.3 cm³/g. X-ray microtomography (XMT) and scanning electron microscopy (SEM) provided information on pore size, (i.e., monodisperse pores with a diameter of 32.5–164 μm) and 2D and 3D morphology.

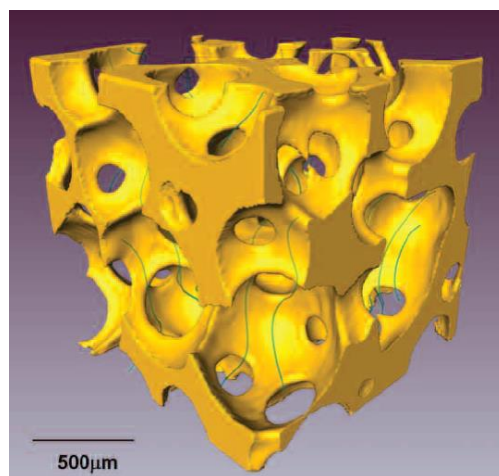


Figure 3.1 Micro-CT image of a bioactive glass scaffold produced by a sol–gel foaming process, with streak lines showing the calculated paths of fluid flow [194].

The porosity of alginate tissue engineering scaffolds has also been investigated using electron microscopy [198, 199], gel permeation chromatography and diffusion measurements [200]. By studying electron micrographs of thin sections of alginate scaffolds, Smidsrød [199] found that the alginate gel core consists of pores ranging from 5 to 200 nm, whereas the gel network on the surface featured pores with a narrower size range (5 – 16 nm). In addition, gels prepared from alginate with a high guluronic acid (G) content have been reported to display open pore structures and therefore allow high rates of protein diffusion [199]. The porosity of alginate scaffolds is affected by various factors such as the drying method, physical properties,

concentration of alginate solution, pH and nature of the cross-linking agent. Exchanging the divalent crosslinking calcium ions with strontium or barium reduces the porosity slightly, because the gel network is resistant to swelling [200]. The nanoscale porosity in alginate gels allows small molecules such as glucose and other nutrients to diffuse freely, which explains the success of alginate microspheres for encapsulation of cells such as pancreatic islets [201]. Although the diffusion of nutrients and oxygen and the elimination of waste products of cell metabolism would be expected to occur freely in alginate hydrogel scaffolds, encapsulated cells are required to be within 100 μm of a capillary to survive. The utility of alginate hydrogels as tissue engineering scaffolds also depends on the achievement of cell–cell contact and cell proliferation, which would be hindered by an absence of or insufficient macroporosity and pore interconnectivity. To overcome this limitation, many techniques have been applied to produce macroporous alginate matrices, including freeze-drying [202], particulate leaching (e.g. using supercritical fluids) [202, 203], gas foaming [204, 205] and micelle templating (MT) [196]. Partap et al. dispersed self-assembled cetyltrimethylammonium bromide (CTAB) surfactant micelles in the cross-linking (alginate – calcium) solution as a pore-forming template, followed by addition of adipic acid to yield porous alginate hydrogels. The MT hydrogel displayed controlled porosity of 83 – 97% and pore size distribution ranging from 32.5 – 164.0 μm [196].

As mentioned previously (Chapter 2, Section 2.1), a major limitation of alginate hydrogels for cell support involves the lack of inherent cell adhesive properties leading to minimal interaction between encapsulated cells/tissue and the surrounding alginate hydrogel [202]. Cells in general do not present surface receptors for most hydrogel-forming polymers. Attempts to resolve this shortcoming have involved modifying synthetic scaffolds [203] and hydrogels [204] with ECM proteins such as

fibronectin (FN), vitronectin (VN), laminin (LN) and collagen for binding with cell adhesive receptors. Zhang et al. [204] reported that bone marrow stromal cells grow and migrate into electrospun PCL/gelatin scaffolds to twice the infiltration depth (114 μm) compared with PCL scaffolds. Brynda et al. [205] modified the surface of poly(2-hydroxyethylmethacrylate) (PHEMA)-based hydrogels with collagen I attached with fibronectin and showed that the attachment of mesenchymal stromal cells (MSCs) and astrocytes improved markedly compared with unmodified hydrogels. Furthermore, the attachment of fibronectin and laminin to the collagen layer resulted in extensive cell growth compared with the poor adhesion and lack of proliferation displayed by the unmodified hydrogel.

This chapter describes the production and characterisation of macroporous alginate fibres for specific application in nerve repair and for general application in soft tissue engineering such as tendon reconstruction. A wet spinning technique is described for producing macropores within alginate fibres via extraction of incorporated gelatin particle porogens. The aim was to provide macropores of sufficient size and interconnectivity to permit proliferation of nerve cells such as Schwann cells and neurons and axonal outgrowth so that electrical connections and nerve function are established. The use of gelatin was also anticipated to provide residual cell adhesion molecules following particle extraction to enhance cell attachment to the scaffold. The 3D structure of the alginate fibres was characterised in detail using confocal laser scanning microscopy and image analysis to quantitatively define pore dimensions and porosity and to trace interconnected pores within the fibres. These investigations were designed to elucidate the relationship between pore structure and formulation parameters to enable subsequent correlations with the growth of encapsulated nerve cells.

3.2 MATERIALS

Sodium alginate (Protanal RF 6650; G:M, 2:1) was obtained from IMCD Australia Limited. Calcium chloride (dehydrate, UniLab), Gelatin from porcine skin (Type A, Bloom 300, average molecular mass 50 – 100 kDa) was purchased from Sigma.

3.3 METHODS

3.3.1 Production of macroporous alginate fibres

Gelatin powder was passed through a <90 micron mesh sieve, and either 100, 200 or 250 mg of sieved powder were homogenised in cold (4 °C) 1.5% w/v alginate solution (10 mL) at speed 2 for 30 s using a homogeniser (IKA Ultra-Turrax® T25 basic). This approach produced alginate solution with gelatin particle contents of 40.0, 57.0 and 62.5% w/w (corresponding to 16, 21 and 24% w/w (actual) loading of gelatin in the spun fibres (described in Chapter 2, Section 2.4.6)). The resulting suspensions were wet spun into 0.5 M CaCl₂ solution (50 mL) using a syringe needle (0.6 × 32 mm) to produce alginate fibres containing increasing amounts of gelatin particles. A suspension flow rate of 2 mL/min was applied using a syringe pump (Harvard Apparatus PHD 2000). The gelatin-loaded alginate fibres were rinsed and triplicate samples were retained in distilled water (15 mL) at 37 °C for 2 days to extract gelatin, thereby producing an internal macroporous structure.

3.3.2 Gelatin particle size distribution

The particle size (smallest and largest dimensions) of the sieved and unsieved gelatin powder was measured before and after homogenisation of gelatin powder suspensions in alginate solution (1.5% w/v) for 30 s, using an IKA Ultra-Turrax® T25 basic.

Images and particle size measurements were acquired using an optical microscope (Olympus BH-2 trinocular microscope).

3.3.3 Morphology of macroporous alginate fibres

The morphology of dried gelatin-extracted alginate fibres was examined using a Philips XL 30 scanning electron microscope (SEM). Samples were mounted on carbon stubs and sputter-coated with platinum using an Eiko-Sputter coater automatic mounting press prior to examination at a voltage of 10 kV.

3.3.4 Preparation of alginate fibre cryosections

Alginate fibres without incorporation of gelatin particles were prepared as described previously (Chapter 2, Section 2.3.1) and macroporous alginate fibres were prepared following extraction of 21% w/w gelatin particle-loaded fibres (Section 3.3.1). Prepared fibres were stained with 1% w/v methylene blue solution (20 mL) overnight for subsequent visualization under the optical microscope. Fibres were rinsed with distilled water and placed into a pre-labeled cryomold. Each cryomold was then filled with cryo-embedding media (Tissue Tek® O.C.T. Compound) and frozen at $-80\text{ }^{\circ}\text{C}$ for 24 h. Frozen blocks were transferred to a cryostat (Leica microsystems CM1850) at $-20\text{ }^{\circ}\text{C}$ prior to sectioning to allow the temperature to equilibrate to the temperature of the cryostat. Frozen fibre blocks were longitudinally sectioned along the flat plane of the construct. The first 10 – 15 sections (each 20 μm thick) were discarded followed by sectioning to produce 8 μm thick (middle) sections. Samples were collected onto glass slides prior to examination using an inverted optical microscope (CKX 41; Olympus) equipped with a digital camera (DP21; Olympus) and DP Controller software (Olympus).

3.3.4 FluoView Confocal Laser Scanning Microscopy (CLSM)

A FluoView FV1000 confocal microscope (Olympus Corporation, Japan) was used to visualize and record images of alginate fibre sections placed in 2-well Lab-Tek chamber slides (Permanox®) in contact with distilled water. To acquire stacks of 2D parallel images, laser excitation at 405 nm and emission detection at 415 – 515 nm were used in conjunction with a 10× objective lens with a numerical aperture (NA) of 0.4. The image size was 640 × 640 pixels, with each pixel corresponding to 1.9884 μm in the x and y directions. Images were acquired using a z-axis spacing of 4 μm. The image datasets were saved as .oif files and exported to .tif files for further analysis.

3.3.5 Quantitative analysis of the internal pore structure of alginate fibres

Analysis of transverse 2D confocal images (Figure 3.2A) obtained using a z-axis spacing of 4 μm provided a quantitative estimation of pore size distribution in alginate fibres following gelatin extraction for correlation with the initial particle size distribution. Software developed at Kingston University London based on MATLAB (The MathWorks Inc., Natick, MA, USA) was used to pre-process the 2D confocal images of the alginate fibres prior to 3D visualization of the pore structure. In summary, the 2D images were first converted to a grey scale and processed using thresholding to detect the pore boundary and form a binary image (Figure 3.2B and 3.2C). The grey-scale images were filtered and the contrast was adjusted so that the applied threshold could be used to detect the dark regions of the pores. The threshold level was adjusted manually to best define the pores in each image [206]. Higher level processing involved the removal of small objects and the removal of the image border region prior to calculation of the pore area [206]. Pores on the borders of the images

were not included because they may not be complete and hence their shape would not be accurately represented.

3D images of the pores were constructed using Amira v 5.3.1 software (Visage Imaging GmbH, Berlin, Germany). In this system, a network is used to obtain an isosurface representation of the pores and a partial outline of the fibre. Once the 2D CLSM shadow images were converted to grey scale using MATLAB, sequential grey-scale images (typically 110 slices) were processed to produce a 3D image using the Amira software v 5.3.1 programme. In addition, individual pores were shown in grey and interconnected pores were highlighted in red. The macroporosity (%) of alginate scaffolds produced by extraction of gelatin particles from 16, 21 or 24% w/w (actual) gelatin-loaded fibres was analysed using in-house computed algorithms. The porosity was calculated by comparing the volume of the pore phase with the total volume of the fibre section. It was difficult to obtain high-quality images all the way through the fibre thickness using CLSM because the diameter was typically 850 – 900 μm . Thus a stack of approximately 100 images was selected for 3D reconstruction and analysis of macroporosity. In addition, the pore data for two sections from an image stack were used to provide a measure of the frequency distribution of equivalent pore diameters in the macroporous alginate fibre; the two sections were located towards either end of the image stack to prevent inclusion of the same pores twice.

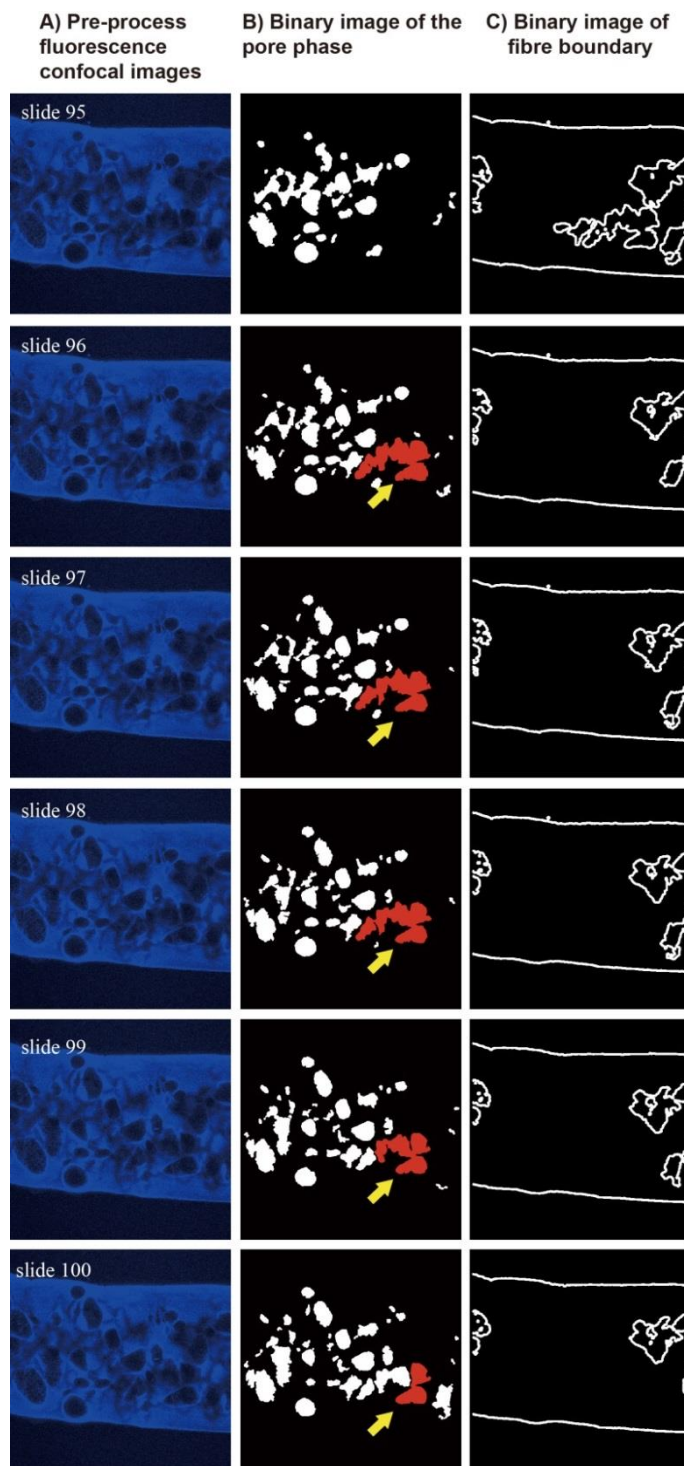


Figure 3.2 Sequential images of an alginate fibre selected from a z-axis stack (slides 95 – 100). (A) pre-processed fluorescence confocal images (B) binary image of the pore phase and (C) binary image of the fibre boundary. Images obtained from a hydrated gelatin-extracted macroporous alginate fibre produced by wet spinning a 62.5% (w/w) gelatin particle suspension in alginate solution. Actual gelatin loading of fibre = 24% w/w.

3.4 RESULTS AND DISCUSSION

Macroporous alginate fibres were successfully produced by wet spinning suspensions of gelatin particles in 1.5% (w/v) alginate solution at gelatin:alginate loading ratios of 5:3, 4:3 and 2:3 (w/w). Fibres were spun into 0.5 M CaCl₂ cross-linking solution followed by protein extraction in distilled water at 37 °C to produce the macroporous form. High protein loadings of 16, 21 and 24% (w/w) were obtained in the dried fibres corresponding to gelatin loadings of 40.0, 57.0 and 62.5%, respectively, in the starting suspension used for fibre spinning. An even distribution of gelatin particles was apparent in the fibres and they tended to be localized at the centre of the alginate fibre (Figure 3.3).



Figure 3.3 Optical micrograph of a gelatin particle-loaded alginate fibre produced by wet spinning a 57% w/w suspension of gelatin particles in alginate solution. Corresponding gelatin loading of dried spun fibre = 21% w/w.

The starting gelatin powder was composed of particles of irregular shape (block, wedge and cuboid forms; Figure 3.4). Prior to fibre spinning, the gelatin powder was passed through a 90- μ m mesh sieve to obtain a particle size range <90 μ m. This size was selected since a variety of mammalian cells appear to proliferate within 100 μ m

pores, Table 3.1). The particle size of the sieved powder was measured before and after homogenisation for 30 s in alginate solution to determine the effect of shear conditions and the aqueous environment on the size of the particles incorporated within the fibre and thus on the expected macropore dimensions.

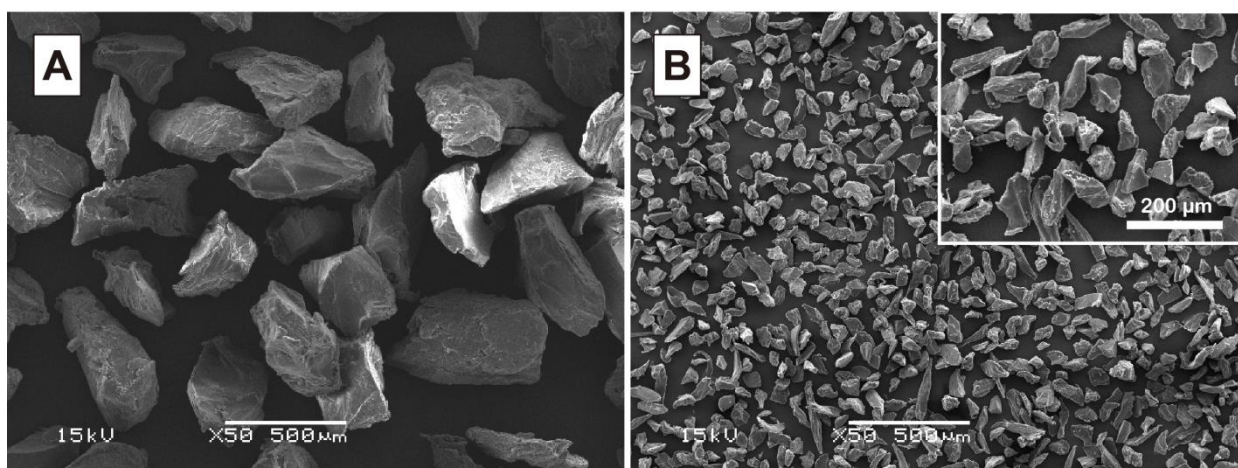


Figure 3.4 Scanning electron micrographs of (A) unsieved, (B) sieved gelatin particles in a size range <90 microns. Magnified view at top right.

Approximately 50 gelatin particles were randomly selected for measurement of the size distribution of unsieved (control) and sieved particles before and after homogenisation in alginate solution (Figure 3.5). The smallest and largest dimensions (μm) were measured by optical microscopy. The results in Table 3.2 and Figure 3.6 show that the sieved gelatin particles exhibited dimensions as small as $57 \pm 3 \mu\text{m}$ and as large as $102 \pm 6 \mu\text{m}$ (Table 3.2). However, following homogenisation in alginate solution for 30 s at 4°C (intentionally to prevent gelatin from swelling too much), the smallest and largest dimensions of the sieved gelatin particles increased by approximately three fold. This behaviour can be explained by the tendency of gelatin below a temperature of $35 - 40^\circ\text{C}$ to swell and absorb 5 – 10 times its weight of water [207].

Table 3.2 Size distribution of gelatin particles (n = 50, mean ± SEM).

n = 50 p < 0.0001 (vs. Control)	Unsieved		Sieved <90 μm	
	Small dimension (μm)	Large dimension (μm)	Small dimension (μm)	Large dimension (μm)
<i>Gelatin particles</i>	375 ± 17	511 ± 22	57 ± 3	102 ± 6
<i>Gelatin particles (following homogenisation in alginate solution)</i>	462 ± 22	600 ± 24	209 ± 7	276 ± 10

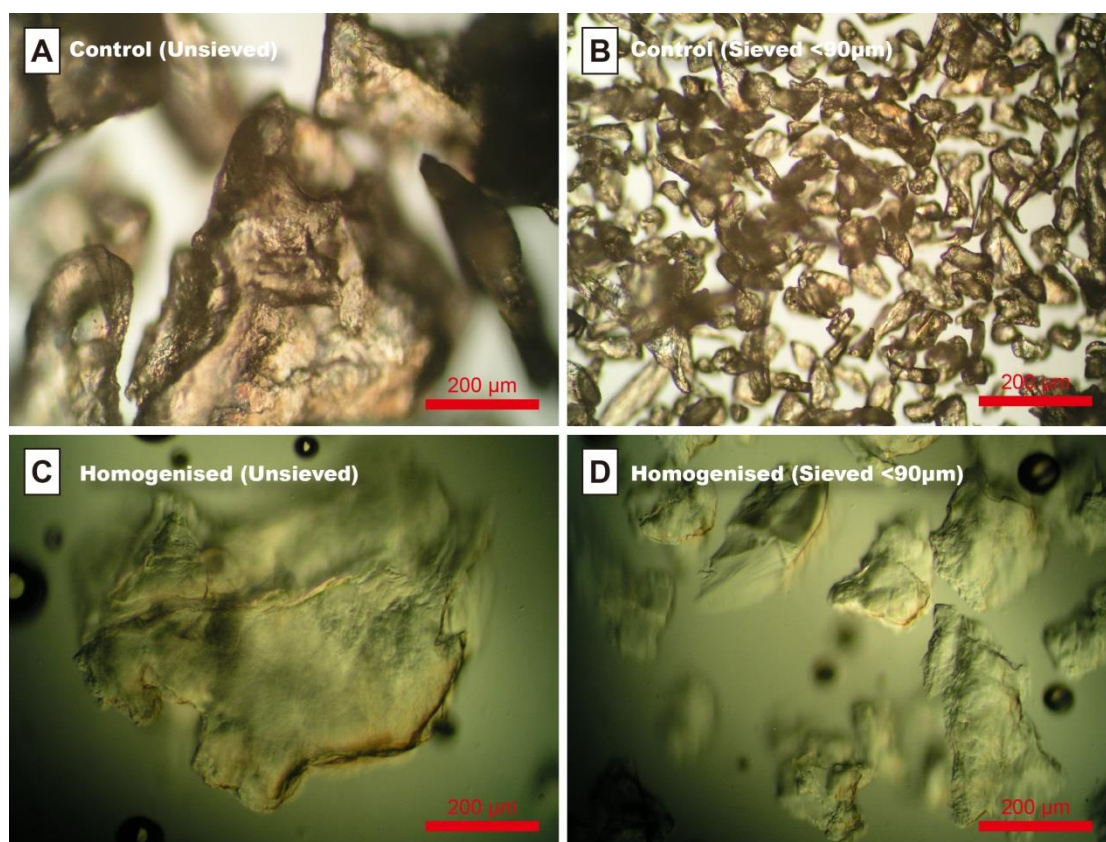


Figure 3.5 Optical micrographs of gelatin particles suspended in 1.5% w/v alginate solution. (A) unsieved (B) sieved particles before homogenisation (C) unsieved and (D) sieved particles following homogenisation in 1.5% alginate solution for 30 s at 4 °C.

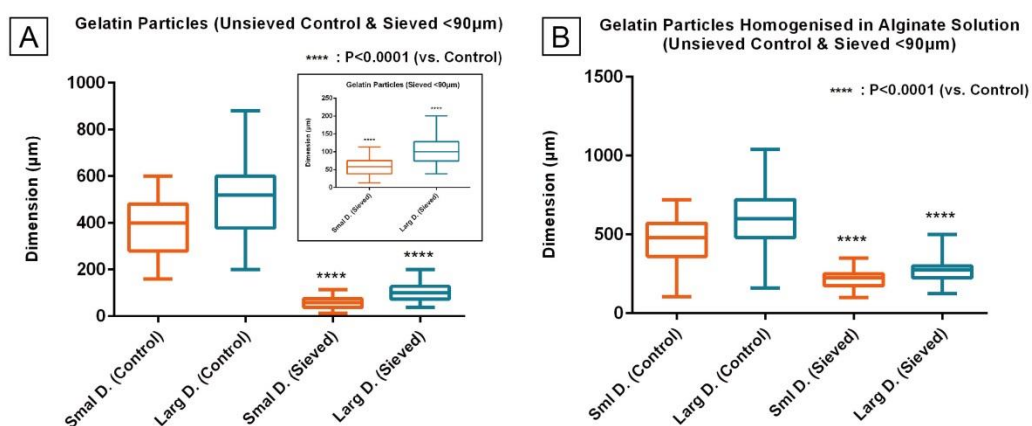


Figure 3.6 Distribution of gelatin particle size. (A) smallest and largest dimensions of unsieved and sieved particles and (B) smallest and largest dimensions of unsieved (control) and sieved particles following homogenisation in 1.5% (w/v) alginate solution or 30 s at 4 °C.

SEM examination of dried alginate fibres produced by wet spinning 1.5% w/v alginate solution alone (without suspended gelatin particles) into 0.5 M CaCl₂ solution revealed a uniform fibre shape, a fibre diameter of approximately 200 µm and a rough-textured oriented or fibrillar surface (Chapter 2, Figure 2.11). Fibres were dried by treatment with ethanol. The pore size of the hydrated alginate fibres revealed by cryo-SEM was approximately 1 µm (Chapter 2, Figure 2.10B). The microporous structure of the alginate fibres is advantageous for the transport of metabolites, the supply of nutrients to cells and oxygen exchange in the inner regions of the scaffold to maintain cell viability. This feature is especially advantageous for the complex tissue engineering of organs. In comparison, alginate fibres produced by wet spinning alginate solution containing suspended gelatin particles exhibited a distorted, bulbous form after gelatin extraction and drying (Figure 3.7A, arrowed) with cross-sectional dimensions of approximately 350 µm (Figure 3.7). A macropore is partly visible in the

fibre cross-section (Figure 3.7B, arrowed). Cryo-sectioning of hydrated fibres revealed the internal macroporous structure (arrowed) produced by gelatin extraction (Figure 3.8C & 3.8D) while the plain alginate fibre (without incorporation of gelatin) exhibited a smooth gel texture (Figure 3.8A & 3.8B). The macroporous fibres appear to have retained a macropore size around 150 – 200 μm as defined by the gelatin particles. The cryosection images in Figure 3.8B also reveal the fibre surface discontinuities and depressions produced by solubilisation of gelatin particles which were located at the fibre surface and the consequent local thinning of the fibre.

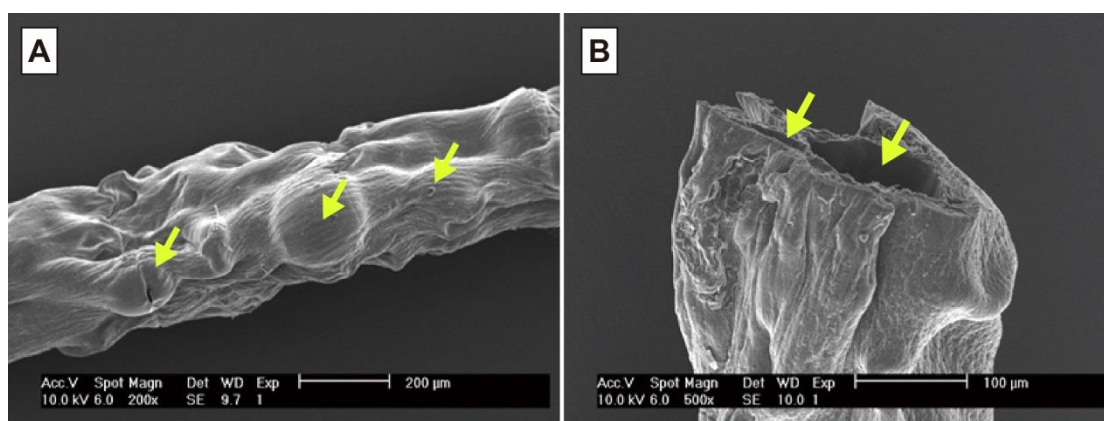


Figure 3.7 Scanning electron micrographs (A and B) of a dried gelatin-extracted alginate fibre produced by wet spinning a 57% w/w suspension of gelatin particles in alginate solution. Macropores are partially visible (arrowed).

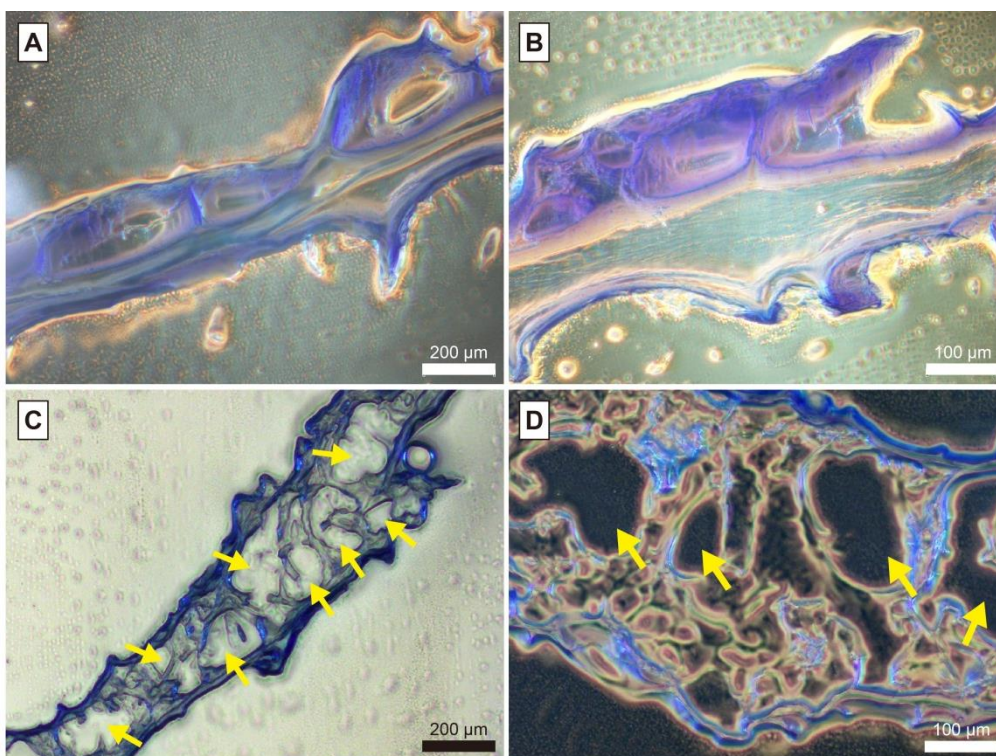


Figure 3.8 Cryosection images of hydrated alginate fibres without incorporation of gelatin particles (A and B) reveal a smooth gel surface. The internal macroporous structure (arrowed) of an alginate fibre produced by gelatin extraction (C and D) shows macropores of irregular shape corresponding to the original gelatin particles. Fibres were stained by methylene blue for visualisation using inverted optical microscopy.

FluoView CLSM

FluoView CLSM analysis was capable of resolving the macroporous structure of gelatin particle-loaded alginate fibres (Figure 3.11B). Z-stack images were originally recorded at an excitation wavelength of 405 nm using an emission detection range of 415–445 nm. However, the intensity of the autofluorescence signal was weak in some planes of the image stacks, which created difficulty in 3D reconstruction, because the software was unable to clearly define the pore boundaries. To ascertain the optimum excitation wavelength and emission detection wavelengths, wavelength scanning was

performed for gelatin-loaded and gelatin-extracted fibre samples to determine the maximum autofluorescence emission wavelength. The scan was set at an excitation wavelength of 405 nm and an emission detection range of 400 – 700 nm. Both gelatin-loaded (Figure 3.9A) and gelatin-extracted (Figure 3.9B) alginate fibre samples displayed two peaks at wavelengths of approximately 450 and 490 nm, respectively, with the non-extracted samples exhibiting a higher intensity signal (Figure 3.9A).

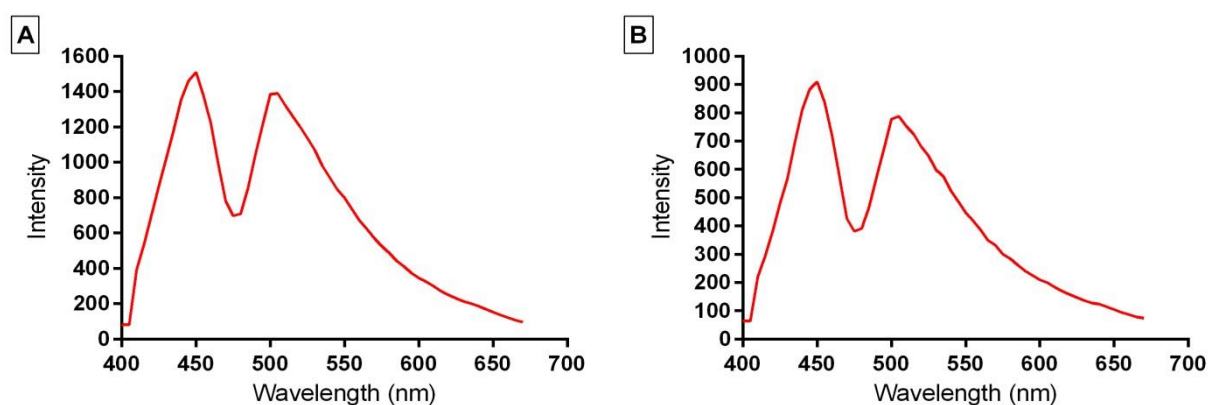


Figure 3.9 Wavelength intensity of alginate fibres (A) before and (B) after gelatin extraction in distilled water. Fibres spun from 57% w/w gelatin particle suspension in alginate solution.

CLSM image acquisition was subsequently performed using an emission detection range of 415 – 515 nm to deliver optimum intensity and improved image quality at lower laser power, thereby preventing damage to the sample. CLSM visualisation at the original emission settings of 415 – 445 nm required setting the laser power to 100% to acquire clear images; however, subsequent operation at the higher bandwidth settings only required 50% of the laser power.

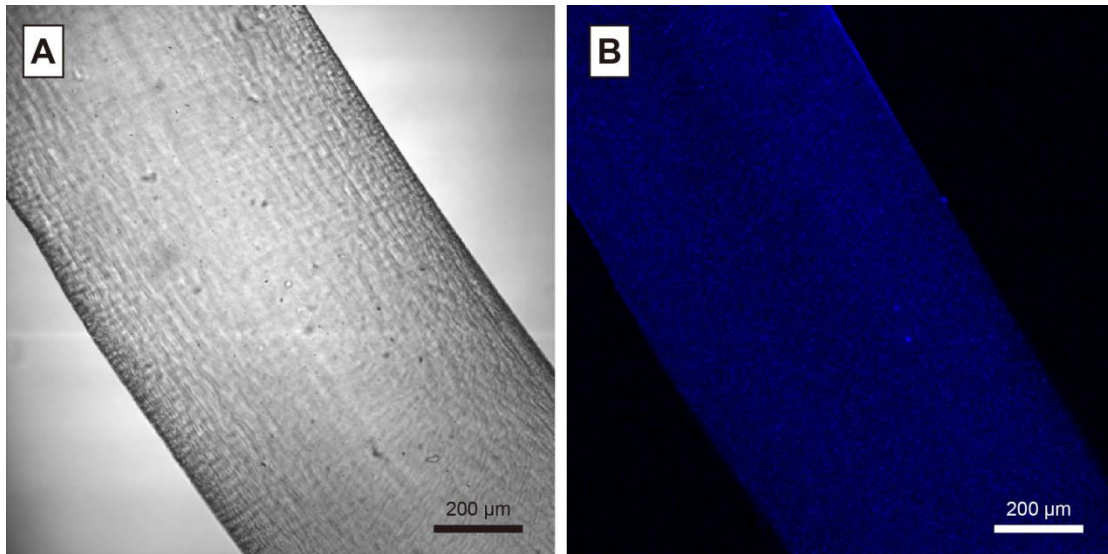


Figure 3.10 CLSM images of alginate fibre (A) differential interference contrast (DIC) and (B) autofluorescence. Fibre spun from 1.5% alginate solution through a syringe needle into 0.5 M CaCl₂ solution.

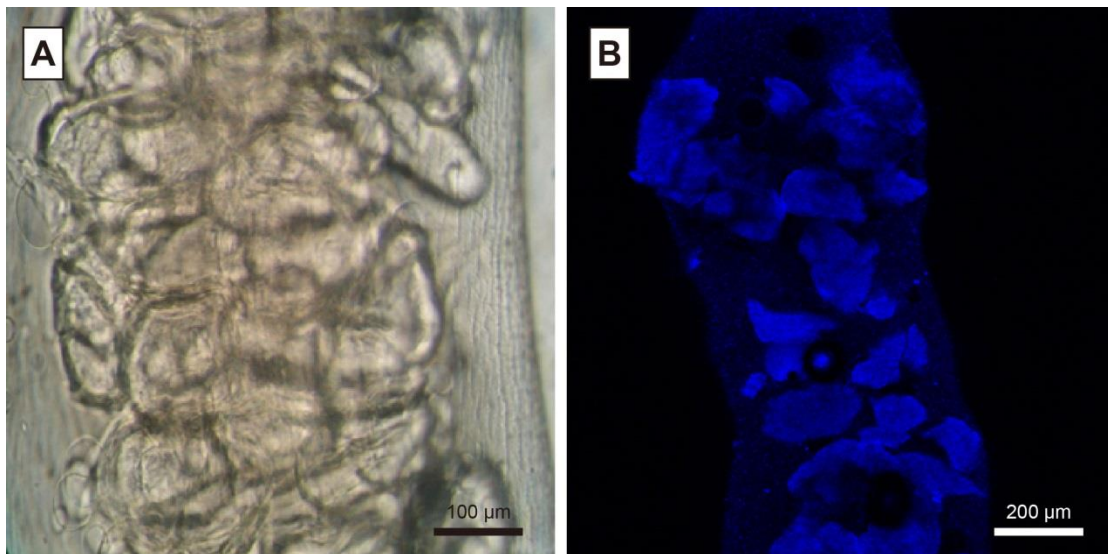


Figure 3.11 CLSM image of a 21% w/w gelatin particle-loaded alginate fibre produced by wet spinning a 57% w/w suspension of gelatin particles in alginate solution. (A) differential interference contrast (DIC) and (B) autofluorescence.

CLSM micrographs of both gelatin-free and gelatin particle-loaded alginate fibres displayed intense autofluorescence (Figure 3.10B, 3.11B). Autofluorescence emission

is commonly reported in cells and originates from biological entities such as mitochondria and lysosomes when certain molecules are excited by UV/visible radiation of suitable wavelengths [208]. The most commonly observed autofluorescent molecules are NADPH and flavins. However, the extracellular matrix can also contribute to autofluorescence, because of the intrinsic properties of proteins such as collagen and elastin [209, 210]. The emission spectra of these molecules are mainly confined within 300 – 600 nm. The intrinsic fluorescence of proteins occurs at 280 – 350 nm, requires excitation between 250 and 280 nm and is related to the aromatic amino acids tryptophan, tyrosine and phenylalanine [210]. Among the endogenous fluorophores, collagen and elastin have a relatively high quantum yield. They fluoresce broadly between 400 – 600 nm with excitation occurring at 300 – 400 nm [211, 212]. Gelatin contains approximately 1% tyrosine, 2 – 3% phenylalanine and no tryptophan [213]. Phenylalanine is not excited in most cases, because of its low quantum yield; hence, the emission in gelatin mainly results from tyrosine. Liu et al. [214] reported that gelatin exhibited an intense blue fluorescence at 415 nm and proposed that it may be affected by the steric arrangement of tyrosine residues. Skjåk-Bræk et al. [215] suggested that alginate autofluorescence may be caused by phenolic compound impurities present in most commercially available alginates. The process of sodium alginate production has been described in Chapter 1 (Section 1.1.5). Formaldehyde pretreatment is performed prior to alkaline extraction to remove phenolic compounds and discoloration [216]. However, small amounts of phenolic materials can persist in alginates. Analysis of purified alginates by fluorescence spectroscopy by Skjåk-Bræk et al. [208] and Kuhnreiber et al. [217] revealed the continued presence of residues that exhibit emission at 450 nm.

The present CLSM study showed that the gelatin particle-loaded alginate fibres exhibited higher emission intensity than alginate (Figure 3.9). This behaviour

advantageously caused the gelatin particles to stand out against the background fluorescence of the alginate phase (Figure 3.11B) thus facilitating analysis of particle distribution in the fibres. Interestingly, CLSM micrographs of gelatin-extracted fibres (Figure 3.12B) showed a bright blue ring around the pore structures (black colouring). This observation suggests that protein residues lined the pore cavity following protein extraction and had migrated into the body of the alginate fibre to a depth of around 20–30 μm . This finding is consistent with the gelatin release behaviour observed for gelatin particle-loaded hydrated fibres (Chapter 2, Section 2.4.6) where 50% of the gelatin content was retained at 48 h. As a protein, gelatin exhibits amphoteric behaviour due to the presence of terminal amino and carboxyl groups and is positively charged below its isoelectric point (IEP) (Gelatin Type A exhibits an IEP of pH 7–9) [218, 219]. On the other hand, alginate is uncharged at pH 2 due to complete protonation and becomes more negatively charged with increasing pH until it is fully deprotonated at pH > 6.5. Velings and Mestdagh's [220] finding on the interactions governing protein/alginate association suggests that alginate and protein interact electrostatically in nature. Similarly, it is expected that gelatin binds electrostatically with the alginate fibre to surface modify the macropores and provide a cell adhesion property that would be anticipated to be highly advantageous for attachment and growth of encapsulated nerve cells and axonal extension.

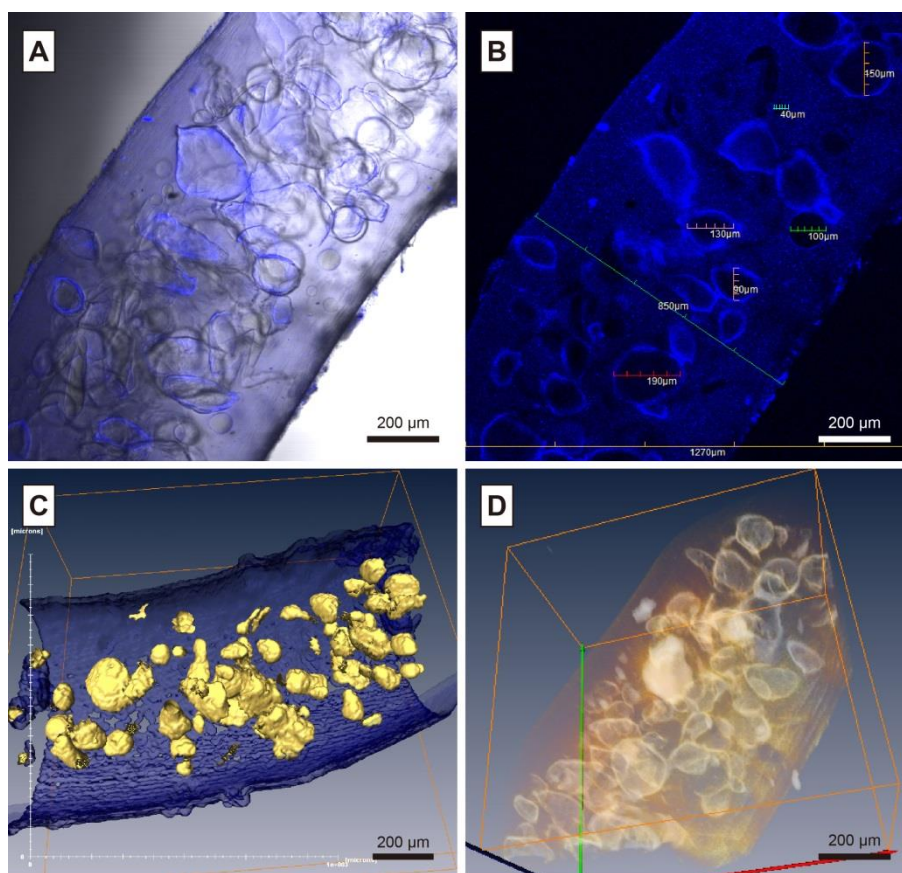


Figure 3.12 CLSM microscopy of hydrated gelatin-extracted macroporous alginate fibres. (A) DIC, (B) autofluorescence, (C) 3D reconstruction showing isolated regions of macropore coalescence and (D) 3D projection view. The fibre was produced by extracting gelatin particles from a 16% w/w gelatin-loaded alginate fibre produced by wet spinning a 40% w/w gelatin particle suspension in alginate solution.

Analysis of sequential CLSM image slices provided detailed quantitative information on the range of pore sizes and frequency distribution of pore sizes in the alginate fibre scaffold (in terms of equivalent pore diameter) (Figure 3.13). The 24% w/w gelatin-loaded alginate fibre after particle extraction exhibited a median pore diameter of 56 μm and a wide range of pore diameters (9 – 228 μm), with the majority between 36 – 87 μm (Table 3.3). Gelatin-loaded fibres (16% w/w) after particle extraction exhibited a similar pore diameter and pore size range. The equivalent macropore

diameter of 21% gelatin-loaded alginate fibres following extraction of gelatin was found to measure around 70 μm (Table 3.3). It is also apparent on inspection of the frequency distribution curve in Figure 3.13B that the majority of the macropores (around 90%) are grouped in the range 25 – 100 μm . In comparison less than 75% of the macropores are in a similar size range for 16 and 24% gelatin loaded fibres following extraction. The macropore size distribution in Figure 3.13 revealed that around 50% of the macropores are smaller than 50 μm in diameter for all gelatin loadings. The narrowest pore size distribution was obtained in 21% gelatin loaded alginate fibres, demonstrating a capacity for controlling macropore structure by adjusting fibre spinning conditions.

Table 3.3 Equivalent pore diameters of alginate fibre scaffolds determined by CLSM image analysis.

Gelatin loading of fibre (% w/w)	Sieved particle size (μm)	No. of pores analysed	Median equivalent pore diameter (Inter-Quartile-Range)	Total range equivalent pore diameter (μm)
16		68	47 (35 – 87)	22 – 209
21	<90 μm	54	69 (40 – 90)	23 – 332
24		61	56 (36 – 87)	9 – 228

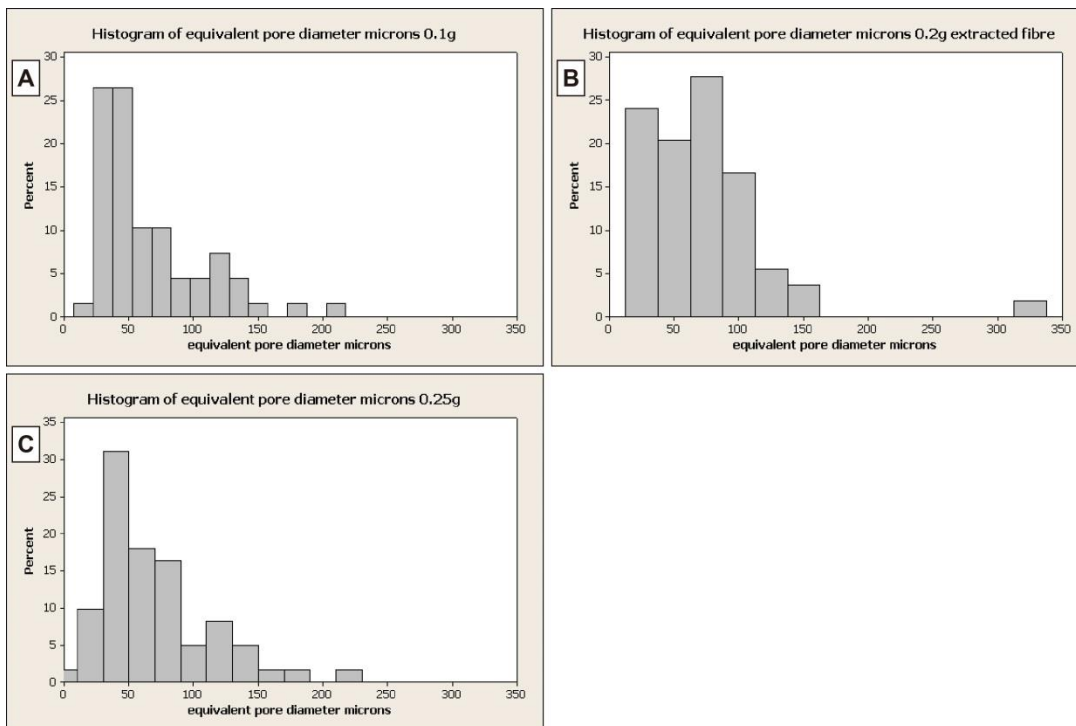


Figure 3.13 CLSM image analyses of hydrated macroporous alginate fibres - frequency distribution of equivalent macropore diameter following extraction of (A) 16%, (B) 21% and (C) 24% w/w gelatin particle-loaded alginate fibres.

Analyses of fibre macroporosity was carried out based on 3D image reconstructions generated using Amira software (Figure 3.14) and computed algorithms to define the pore volume (Figure 3.14A) within a corresponding fibre volume (Figure 3.14B). The macroporosity of alginate fibres prepared by extracting gelatin particles has been summarised in Table 3.4. A maximum porosity of 14.6% was obtained following particle extraction from 21% w/w gelatin-loaded fibres. Contrary to expectations increasing the gelatin loading of the alginate spinning solution did not increase the fibre porosity. It is interesting that maximum porosity coincided with fibres showing the narrowest pore size distribution (i.e. 90% pore < 100 μm , Figure 3.13B). The relatively low macroporosity values reflect the low efficiency of incorporation of gelatin particles in the alginate fibres (16 – 24% w/w) and suggest that particles have

been excluded from the extruded liquid filament or thread on passage through the syringe needle. Macropores produced by dissolution of gelatin particles that were embedded near the fibre surface are visible in the 3D section view in Figure 3.12D. It is also evident from the cryosections in Figure 3.8C and 3.8D that some particles were located at the fibre surface and produced curved indentations on dissolution, rather than complete internal macropores.

Table 3.4 Macroporosity of gelatin-extracted alginate fibres determined by CLSM image analysis.

Gelatin loading of fibre (% w/w)	Gelatin loading of spinning suspension (%)	Pore volume	Fibre volume	% Porosity
16	40	4.6×10^7	4.0×10^8	11.3
21	57	2.4×10^7	1.6×10^8	14.6
24	62.5	2.7×10^7	2.3×10^8	12.1

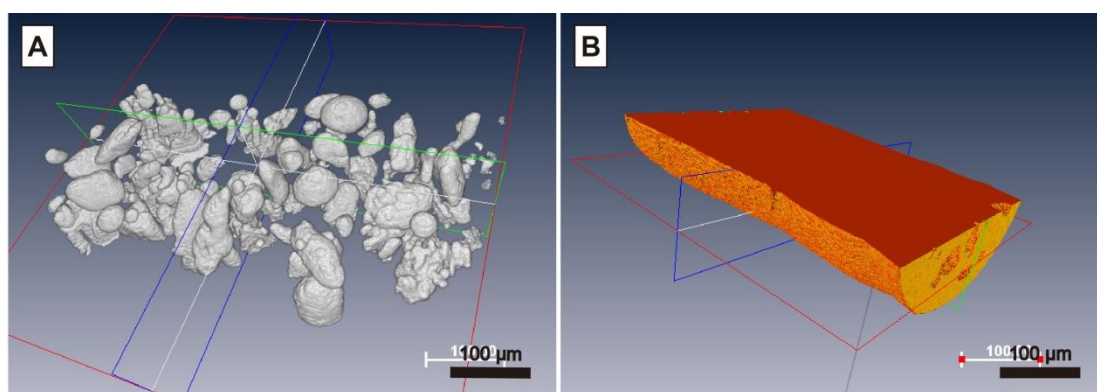


Figure 3.14 3D visualization of hydrated 24% w/w gelatin-loaded alginate fibre after protein extraction. (A) pore volume and (B) volume of fibre body.

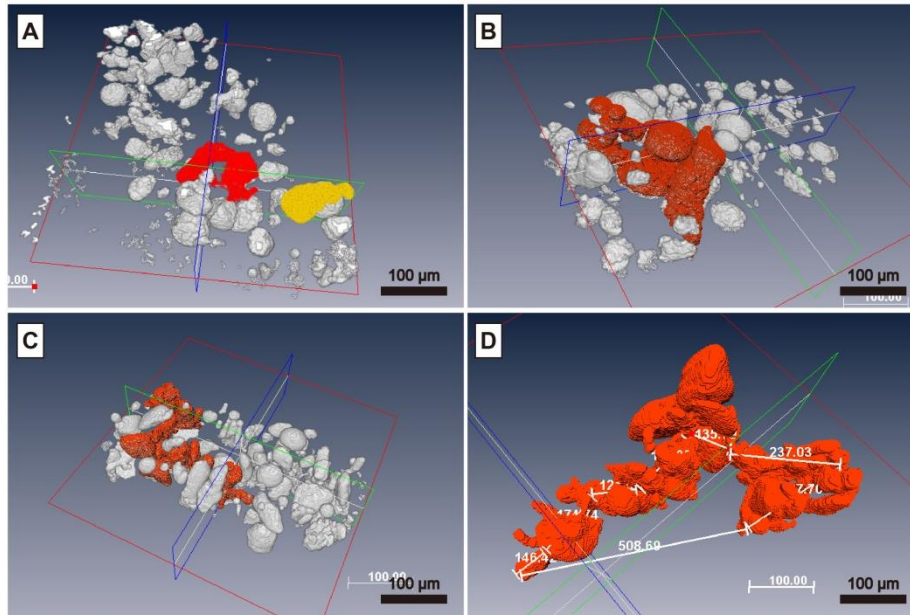


Figure 3.15 Regions of pore coalescence (highlighted in red) identified by CLSM analysis of (A) 16%, (B) 21% and (C) 24% (w/w) gelatin-loaded alginate fibres after protein extraction. (D) Magnified view of a region of pore coalescence.

Macropore interconnectivity is essential to allow cell ingrowth throughout a scaffold and its eventual replacement by regenerated tissue. Macropore connectivity was assessed using the concept of ‘tortuosity’ (τ), which describes the pore path length through the material. Tortuosity can be estimated by the arc-chord ratio, which is the ratio of the actual pore length (L) to the distance between the ends of pore (X) (Figure 3.16) [220].

$$\tau = \frac{L}{X}$$

The potential for quantifying macropore connectivity in the alginate fibre scaffolds was evaluated by tracing regions of macropore coalescence in selected 3D image presentations (Figure 3.15). As expected, alginate fibres with high gelatin particle loadings (Figure 3.15B and 3.15C) displayed a greater probability of pore coalescence than fibres with low gelatin loadings (Figure 3.15A). Connected pore lengths of 252

μm , $607 \mu\text{m}$ and $509 \mu\text{m}$ were measured for macroporous fibres produced by extraction of 16, 21 and 24% gelatin-loaded fibres respectively. Again it is interesting to note that the 21% w/w gelatin-loaded fibres displaying the narrowest pore size distribution (90% $<100 \mu\text{m}$, Figure 3.13B) resulted in the highest macropore interconnectivity. This finding indicates opportunities for improving pore connectivity for cell infiltration or axon extension by controlling the particle size distribution and content of porogens. However, it should be borne in mind that the dimensions of interconnecting channels (connects) and fenestrations or windows in the pore surface must also be of sufficient size to allow cell ingrowth and these structural features can be difficult to analyse.

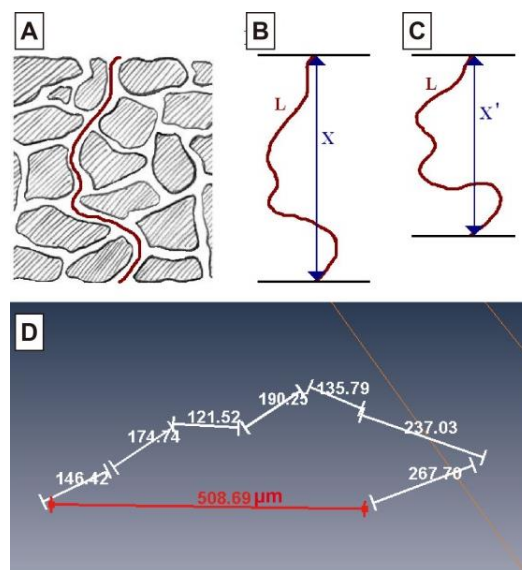


Figure 3.16 Determination of tortuosity in a porous material using the arc-chord ratio. (A) Tortuosity of a path through a porous structure (B) Tortuosity determined by the ratio of the pore length (L) to the displacement of the ends of the pore (X). (C) On compression the magnitude of L remains constant, but displacement X is reduced to X' , resulting in an increase in tortuosity [221]. (D) Example of tortuosity pathway through a macroporous alginate fibre.

3.5 CONCLUSIONS

Macroporous alginate fibres for application in nerve tissue engineering were produced by wet spinning suspensions of gelatin particles in alginate solution followed by extraction of gelatin. CLSM image analysis exploited the autofluorescence properties of alginate and gelatin to provide detailed 3D reconstructions of the pore structure, macropore dimensions, pore size distribution, porosity and pore connectivity for correlation with fibre spinning conditions and subsequent cell ingrowth behaviour. CLSM also revealed modification of the alginate macropore surface by gelatin, which is expected to be advantageous for nerve cell adhesion and axonal extension.

CHAPTER 4

Cell Encapsulation of in Alginate Hydrogel Fibres Using Wet Spinning Techniques

ABSTRACT

The ability of plain alginate fibres and macroporous alginate fibres to maintain viability of encapsulated cells and to promote cell growth was assessed using fibroblasts. Swiss 3T3 mouse fibroblasts were encapsulated in alginate fibres by wet spinning cell suspensions of alginate solutions. Optical micrographs and cell staining (DAPI staining of nuclei and rhodamine staining of actin filaments) showed that cells were evenly distributed in the fibre and the majority remained as rounded cells with a few adopting a spindle-shaped structure characteristic of fibroblasts. Encapsulated cells remained viable over 50 days and were capable of continuing growth outside the fibre after this time period. Increasing the cell concentration of the spinning solution from 1.4×10^4 to 1.5×10^6 cells/mL resulted in no significant improvement of fibroblast extension and growth. This behaviour may be explained by efficient encapsulation of the cell within a closed hydrogel environment which only permits exchange of nutrients metabolites and oxygen to maintain cell survival. Human adult dermal fibroblasts (HDFa) were incorporated in macroporous alginate fibres by wet spinning alginate solutions containing both gelatin microparticles and suspended cells (cell concentration 3×10^5 cells/mL). Cell distribution was evaluated using CLSM (following staining with Calcein-AM) at an excitation wavelength of 488 nm. Fibroblast-loaded macroporous alginate fibres were characterised by a cell density of approximately 360 cells/mm^3 which was significantly higher (* $P < 0.05$) than that of non-macroporous fibres (approximately 140 cells/mm^3). Cell viability was maintained

for time periods of at least 12 days. This finding indicates a potential for repair of soft tissue by encapsulating cells or genetically modified, growth factor-secreting variants in alginate fibres.

4.1 INTRODUCTION

The primary aim of tissue engineering is to replace or facilitate regeneration of damaged or diseased tissues by applying combinations of biomaterials, cells and bioactive molecules. Conventional strategies for tissue repair frequently involve tissue transplantation from autogeneic (from the host), allogeneic (from the same species) and xenogeneic (from a different species) sources [222]. However, these approaches are associated with several drawbacks, such as limited tissue availability, immunogenicity and disease transmission and it is necessary therefore to find an alternative. Studies conducted in the last two decades have increasingly utilised polymeric matrices to control and guide wound healing and tissue regeneration, to elicit specific cellular interactions, functions and tissue responses, and most importantly, to serve as scaffolds to support cell transplantation.

Hydrogels have been applied as cell support scaffolds for tissue engineering of cartilage [203, 223-226], cornea [227], skin [228, 229], tendon [230], vascular [231] and neural tissue [232-235] (Table 4.1). Cells are usually suspended in an aqueous precursor solution prior to encapsulation (Figure 4.1) [236]. Thus, the gelation process must be mild to avoid cell damage. The hydrogel scaffold in turn must be biocompatible and ideally biodegradable, while maintaining sufficient strength and stiffness to provide mechanical support for cell growth and tissue formation.

Table 4.1 Natural and synthetic polymer-based hydrogels for tissue engineering.

Material	Used cells	Application	Ref.
<i>Natural</i>			
Hyaluronic acid (HA)	Fibroblasts	Skin	[228]
Collagen	Astroglial cells	Neural	[234]
Gelatin	Mesenchymal stem cells	Cartilage	[231]
Chitosan	Chondrocyte, Foetal mouse cortical cells (FMCCs)	Cartilage, Neural	[226, 233]
Agarose	Corneal stromal cells	Cornea	[227]
Alginate	Chondrocytes	Cornea, Neural	[227, 235]
<i>Synthetic</i>			
Poly(ethylene oxide) (PEO)	Chondrocytes	Cartilage	[223]
Poly(vinyl alcohol) (PVA)	Chondrocytes	Cartilage	[205, 224]
Poly(ethylene glycol) (PEG)	Primary human fibroblasts, Pheochromocytoma PC12 cells	Cartilage, Neural	[225, 232]

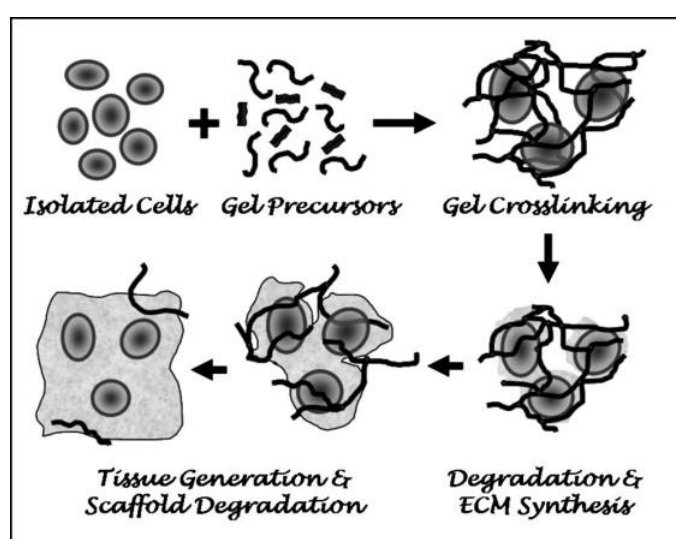


Figure 4.1 Cell encapsulation in a hydrogel tissue-engineered scaffold. The hydrogel acts as a temporary extracellular matrix (ECM) and neo-tissue replaces the scaffold [236].

Many studies of cell encapsulation have utilised hydrogels formed from the linear polysaccharide, alginate, due to its biocompatibility and low toxicity. The most common technique involves suspension of cells in alginate solution prior to gelation under mild aqueous conditions involving crosslinking of guluronic acid sequences along the alginate chain molecule with divalent metal cations such as Ca^{2+} . Lim and Sun [237] in 1980 first reported success in encapsulating pancreatic islets in

alginate-polylysine-alginate (APA) microcapsules for the treatment of diabetes. Microencapsulated islets implanted into diabetic rats remained viable and glucose levels were controlled for up to three weeks. Maysinger et al. [238] described the encapsulation of genetically engineered rat fibroblasts producing nerve growth factor (NGF) in alginate polylysine-alginate gels intended for treatment of brain injury. Peirone et al. [239] encapsulated recombinant cells (epithelial cells, fibroblasts, and myoblasts) in three kinds of alginate-based microcapsules for delivery of therapeutic gene products and showed high cell viability (65 – 90%) in culture.

Alginate composition and strength of the gel network are known to affect the growth of encapsulated cells. Alginates consisting of higher guluronic acid content have been reported to hinder cell growth and reduce metabolic activity for up to 40 days before recovery and proliferation [68, 70]. Use of a high crosslinking solution (CaCl_2) concentration has also been shown to increase the gel strength, which may hinder cell elongation or proliferation [71].

This chapter describes investigations of cell encapsulation in alginate fibres for application in tissue engineering. Fibre wet spinning techniques and cell culture conditions were established using fibroblasts not only as a precursor to experiments with nerve cells (Chapter 5) but also of the lower cost and robustness of these cells compared with nerve cells. The investigations were also useful for exploring the potential of cell-encapsulated alginate fibres for a) soft tissue repair in general and b) sustained delivery of growth factors or hormones produced in-situ by genetically modified cells.

4.2 MATERIALS

Sodium alginate (Protanal RF 6650, G:M 2:1) was obtained from IMCD Australia Limited. Calcium chloride (dehydrate) was purchased from UniLab. Gelatin from

porcine skin (Type A, Bloom 300, average molecular mass 50 – 100 kDa) and Dulbecco's phosphate-buffered saline (D-PBS; with MgCl₂ and CaCl₂, liquid, sterile filtered, suitable for cell culture, D8662) were purchased from Sigma. Complete culture medium prepared from Dulbecco's modified Eagle medium (DMEM; Invitrogen) supplemented with 10% foetal bovine serum and 1% penicillin and Calcein-AM (C3100-MP) were purchased from Invitrogen. Paraformaldehyde and dimethyl sulphoxide (DMSO; anhydrous, ≥99.9%) were purchased from Sigma-Aldrich. Phalloidin - FluoProbes® 415 FP-BP1240, 300 units* (Interchem) was purchased from Thermo Scientific. Wheat germ agglutinin (WGA) conjugates and 4,6-diamidino-2-phenylindole (DAPI) were purchased from Invitrogen. Swiss 3T3 fibroblasts were contributed by the National Centre for Adult Stem Cell Research (NCASCR), Griffith University, Brisbane, Australia. Human adult dermal fibroblasts (HDFa) were contributed by the National Physical Laboratory, Teddington, UK.

4.3 METHODS

4.3.1 Culture of Swiss 3T3 fibroblasts

Swiss 3T3 fibroblasts were cultured in a humidified incubator at 37 °C under 5% CO₂ in complete culture medium prepared from DMEM supplemented with 10% foetal bovine serum and 1% penicillin. The cells were cultured for 7 days and then detached with trypsin–ethylenediaminetetraacetic acid (EDTA; Invitrogen). Trypsin–EDTA (3 mL) was added to the culture flask, which was then placed in an incubator for 3–5 min. Following trypsin treatment, DMEM (3 mL) was added to deactivate the enzyme. Cell density was determined using a haemocytometer. The cell suspension was centrifuged at 1000 rpm for 8 min to obtain a cell pellet, which was resuspended in complete culture medium (2 mL) to obtain the required cell concentration for

subsequent encapsulation of fibroblasts in alginate fibres.

4.3.2 Encapsulation of Swiss 3T3 fibroblasts in alginate fibres by wet spinning

Sodium alginate was dissolved in distilled water at a concentration of 2% w/w and filtered using a syringe filter (0.2 μm 33 mm Millex Filter Units, Millipore). Swiss 3T3 fibroblasts were suspended in complete culture medium (6.2×10^4 cells/mL, 3 mL) and added to the filtered alginate solution (10 mL) to obtain a cell density of 1.4×10^4 cells/mL in 1.5% w/v alginate solution. Cell–alginate solution (0.5 mL) was wet spun into 0.5 M filtered CaCl_2 solution (50 mL) through a syringe needle (0.6 \times 32 mm). A syringe pump was used to feed the cell–alginate solution into the needle tip at a rate of 2 mL/min. Alginate fibres were collected from the spinning bath and rinsed in distilled water. The fibres spun from 0.5 mL cell-alginate solution were cultured in complete culture medium (5 mL) contained in 6-well tissue culture plate for 8 weeks. A schematic of the cell encapsulation process is shown in Figure 4.2.

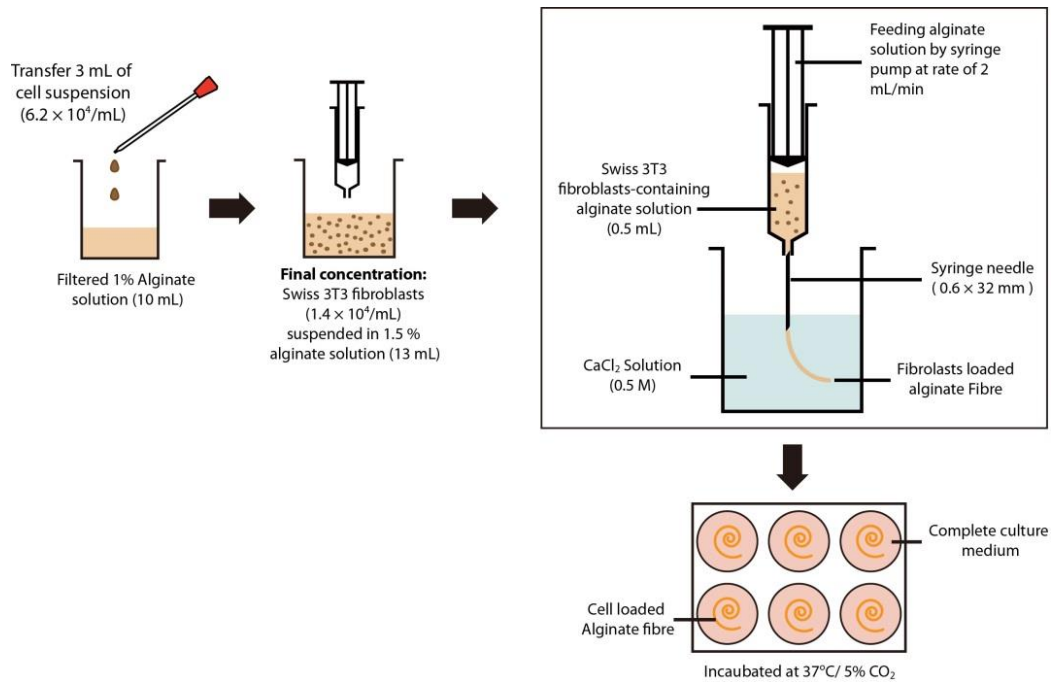


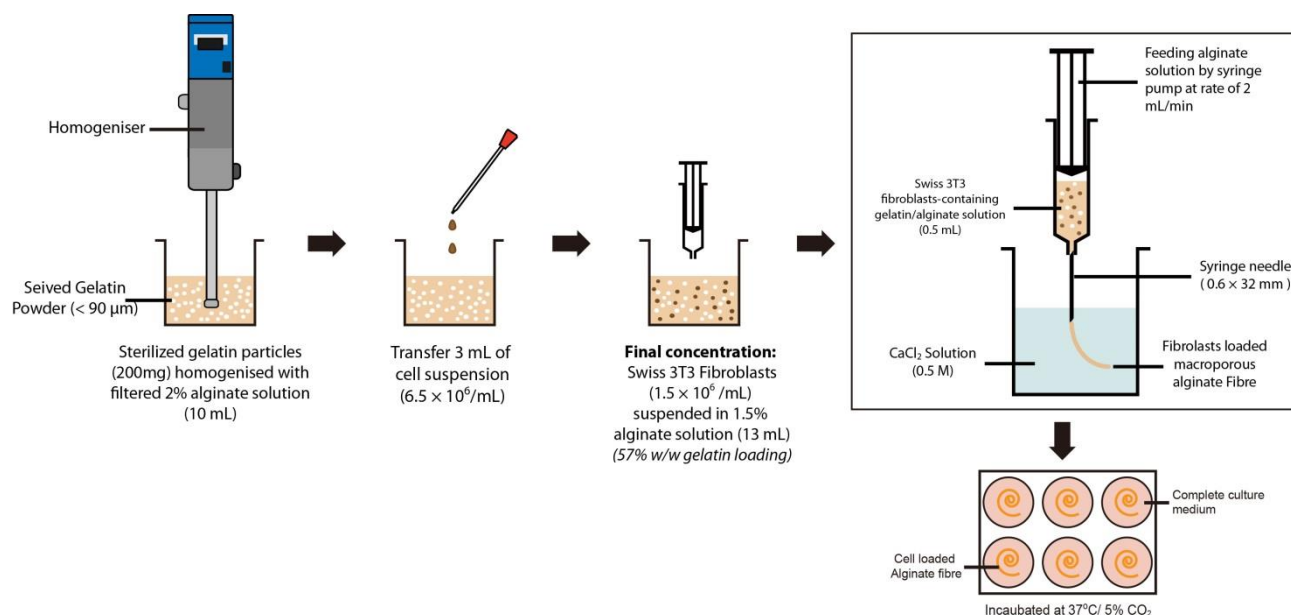
Figure 4.2 Preparation of Swiss 3T3 fibroblast-loaded alginate hydrogel fibres by wet spinning.

The effect of increasing cell density of the spinning solution on encapsulation of Swiss 3T3 fibroblasts in alginate fibres was investigated by dispersing fibroblasts (6.5×10^6 cells/mL, 3 mL) in filtered alginate solution (2% w/v, 10 mL) to obtain a cell density of 1.5×10^6 cells/mL in 1.5% w/v alginate solution. Cell–alginate solution (0.5 mL) was wet spun into 0.5 M filtered CaCl_2 (50 mL) as described in section 4.3.2 to produce fibroblast-loaded alginate fibres.

4.3.3 Encapsulation of Swiss 3T3 fibroblasts-in macroporous alginate fibres

Gelatin type A was sieved through a 90- μm mesh sieve. The collected powder was sterilized under UV irradiation (Philips TUV 15W/G15 T8) in a cell culture hood for 20 min. The container was agitated during sterilization to ensure that all particles were exposed to UV. A 2% w/v alginate solution (10 mL) was sterilized by filtration

through a syringe filter CA (0.2 × 33 mm Millex filter units, Millipore). Antiseptic techniques were strictly followed to prevent contamination. All instruments used,



including the homogeniser and syringe pump, were sterilized by wiping the surfaces with 70% ethanol. Glassware and tools were autoclaved. Sterilized gelatin particles (<math>< 90 \mu\text{m}</math>, 200 mg) were added to cold filtered 2% w/v alginate solution (10 mL) and homogenised using a IKA Ultra-Turrax[®] T25 Basic homogeniser in the cell culture hood. Suspensions were produced with gelatin:alginate w/w ratios of 4:3, corresponding to 57% w/w gelatin loading as a fraction of the total polymer content. Swiss 3T3 fibroblasts (6.5×10^6 cells/mL, 3 mL) were dispersed in the prepared gelatin/alginate suspension (10 mL) to achieve a final cell concentration of 1.5×10^6 cells/mL in an equivalent 1.5% w/v alginate solution. Cell–gelatin/alginate suspension (0.5 mL) was wet-spun into 0.5 M filtered CaCl_2 solution (50 mL) through a syringe needle (0.6 × 32 mm) as described in section 4.3.2 to produce fibroblast-loaded alginate fibres. A schematic of the cell encapsulation process with incorporation of gelatin particles is shown in Figure 4.3.

Figure 4.3 Preparation of Swiss 3T3 fibroblast-loaded macroporous alginate fibres.

4.3.4 Imaging of Swiss 3T3 mouse fibroblasts encapsulated in alginate fibres using confocal laser scanning microscopy

Hydrated alginate fibres incorporating fibroblasts which had been maintained in cell culture for 8 weeks were examined by confocal laser scanning microscopy (CLSM; Leica SP5). Fibre samples were cut into approximately 1-cm long segments and rinsed with D-PBS for 20 min. The samples were then fixed and stored in 4% paraformaldehyde/D-PBS (1 mL) before staining. The paraformaldehyde/D-PBS solution was prepared by dissolving paraformaldehyde (3.2 g, Sigma) in D-PBS (40 mL, Sigma) at 60 °C for 15 min at a concentration of 8% w/v. Sodium hydroxide (0.1 M) was added drop-wise (10–15 drops). The solution was stirred at 60 °C until it became clear and was then removed from heat. D-PBS (40 mL) was added to adjust the concentration to 4% paraformaldehyde/D-PBS. The fibroblast-encapsulated alginate fibres were subsequently stained with DAPI and rhodamine-phalloidin (Section 4.3.7) to label cell nuclei and actin filaments, respectively, after the cells were permeabilized with Triton. The samples were examined perpendicular to the long axis, and images were captured every 3 µm (10× magnification) using CLSM.

4.3.5 Encapsulation of human adult dermal fibroblasts (HDFa) in macroporous alginate fibres

Preparation of the gelatin powders and the required antiseptic procedures were carried out as described in section 4.3.3. Suspensions were produced with gelatin:alginate w/w ratios of 4:3, corresponding to 57% gelatin loading as a fraction of the total polymer content. HDFa cells (1.3×10^6 cells/mL, 3 mL) were dispersed in the

prepared gelatin/alginate suspension (10 mL) to achieve a final cell concentration of 3×10^5 cells/mL in an equivalent 1.5% w/v alginate solution. Cell–alginate solution (0.5 mL) was wet-spun into 0.5 M filtered CaCl_2 solution (50 mL) through a syringe needle (0.6×32 mm). A syringe pump was used to feed the cell–alginate solution to the needle tip at a rate of 2 mL/min. Alginate fibres were collected from the spinning bath, rinsed in distilled water and triplicate samples were cultured in complete culture medium (3 mL) for 12 days.

4.3.6 Viability assay of HDFa cells encapsulated in macroporous alginate fibres using Calcein-AM staining

Calcein-AM is a cell-permeant dye that can be used to determine cell viability in most eukaryotic cells. In live cells the nonfluorescent Calcein-AM is converted to a green-fluorescent Calcein after acetoxymethyl ester hydrolysis by intracellular esterases (Figure 4.4). Calcein-AM stock solution in anhydrous DMSO (1 mg/mL, 1 μM) was prepared by adding 50 μL of anhydrous DMSO ($\geq 99.9\%$, Sigma-Aldrich) to 50 μg of Calcein-AM. The prepared stock solution was stored at -20 °C in the dark. A working solution was prepared by pipetting 10 μL of the stock solution into 9 ml of culture medium to achieve a concentration of 10 nM. Next, 1 mL of the 10 nM working solution was added to the HDFa-encapsulated alginate fibres (approximately 1-cm section), and the samples were incubated at 37 °C under a 5% CO_2 atmosphere for 45 min.

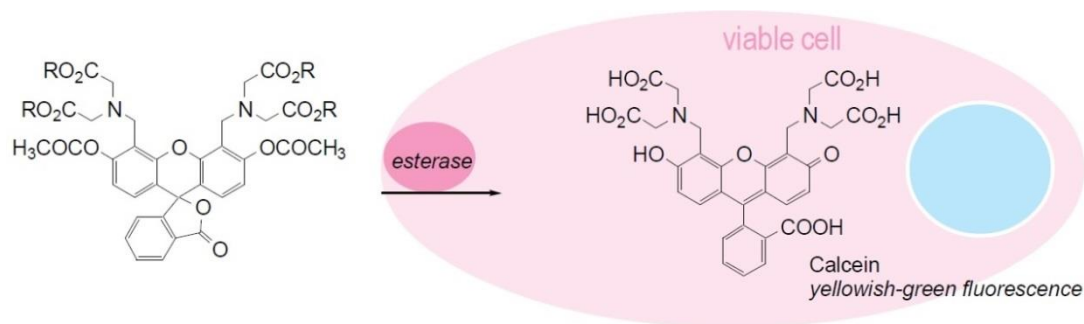


Figure 4.4 Calcein-acetoxymethyl ester (Calcein-AM) [240].

4.3.7 Cell Staining

The Swiss 3T3 fibroblast-encapsulated alginate fibres were stained with rhodamine-phalloidin and DAPI to label the actin filament and cell nuclei respectively. HDFa-encapsulated alginate fibres were stained with wheat germ agglutinin (WGA) and DAPI to label the plasma membrane and cell nuclei respectively.

Rhodamine-phalloidin staining

Phalloidin is a seven amino acid peptide toxin from the mushroom *Amanita phalloides*, which binds specifically and with high affinity (K_d 20 nM) to the polymerized form of actin (F-actin). Phalloidin lowers the critical concentration of actin polymerization to less than 1 $\mu\text{g}/\text{mL}$, thereby acting as a polymerization enhancer. Phalloidin labelled with tetramethylrhodamine B isothiocyanate [241] is widely used as an alternative to actin antibodies for specifically labelling actin filaments in tissue cultured cells and tissue sections [242] and cell-free preparations. Rhodamine phalloidin-labelled actin filaments retain many functional characteristics of unlabelled actin including their ability to interact with myosin.

A stock solution of rhodamine phalloidin was prepared by addition of 1.5 mL of methanol to Phalloidin - FluoProbes® 415 '300U' vials to yield a final concentration

of 200 units/mL (equivalent to 6.6 nmol/mL). The staining solution was prepared by addition of 100 μ L of stock solution in 25 mL PBS with 1 % BSA (250 mg BSA in 25 mL D-PBS). Staining solution (700 μ L) was added to each well of 24 well plates containing Swiss 3T3 fibroblast-encapsulated alginate fibres (approximately 1-cm), and incubated for 1 h at room temperature in the dark. Following incubation, fibres were washed twice (800 μ L/well) with D-PBS (at room temperature) for 5 min each (on a shaker) in the dark.

Wheat germ agglutinin (WGA) staining

Wheat germ agglutinin (WGA) is a carbohydrate-binding protein of approximately 36 kDa that selectively recognizes sialic acid and N-acetylglucosaminyl sugar residues which are predominantly found on the plasma membrane. Molecular probe produces WGA conjugated to fluorophores, including the Alexa Fluor fluorophores, that have excellent photostability and illumination, are pH insensitive and may be used with a wide spectrum of emission wavelengths [243].

A working solution of WGA in PBS (5 μ g/mL) was prepared by adding a WGA stock solution (5 μ L, 1 mg/mL) to PBS (1 mL). Next, 1 mL of the working solution was added to the fixed HDFa-encapsulated–alginate fibres (approximately 1-cm section) and incubated at room temperature for 30 min in the dark. Following incubation, the samples were washed twice for 5 min each with copious D-PBS.

DAPI (4',6-diamidino-2-phenylindole) staining

DAPI is a blue fluorescent nucleic acid stain that preferentially stains double-stranded DNA (dsDNA). It attaches to AT clusters in the DNA minor groove having one molecule of dye for each 3 base-pairs [244]. Binding of DAPI to dsDNA produces an approximate 20-fold fluorescence enhancement. The fluorescence is directly

proportional to the amount of DNA present, with emission maximum at approximately 460nm. A working solution of DAPI in distilled water (2.5 µg/mL) was prepared by adding a DAPI stock solution (5 µL, 5 mg/mL) to distilled water (10 mL). Then, 1 mL of the working solution was added to the fixed HDFa-encapsulated alginate fibres (approximately 1-cm sections), and incubated at room temperature for 50 min in the dark. Following incubation, the samples were washed twice for 5 min each with copious amount of D-PBS.




4.3.8 Imaging of encapsulated HDFa in alginate fibres using CLSM

Alginate fibres containing human adult dermal fibroblasts which had been maintained in cell culture for 12 days were cut into approximately 5-mm segments and rinsed with D-PBS for 20 min. Samples were routinely examined under a FluoView FV1000 confocal microscope (Olympus Corporation, Japan) in a 2-well Permanox plastic chamber slide system (Fisher Scientific) mounted in distilled water (1 mL). The samples were subsequently fixed and stored in 4% paraformaldehyde/D-PBS solution (1 mL) before staining. The paraformaldehyde/D-PBS solution was prepared as described in Section 4.3.4.

To acquire stacks of 2-dimensional parallel images, laser excitation was performed at 488 nm and 405 nm for WGA and DAPI with maximum emission detection at 535 nm and 461 nm, respectively. The image size was 640 × 640 pixels, with each pixel corresponding to 1.9884 µm in the X and Y directions. Images were acquired using a Z-axis spacing of 4 µm.

4.3.9 Image compilation and data analysis following Calcein-AM staining of

HDFa

Calcein-AM stained fibres were imaged using a FluoView FV1000 confocal microscope (Olympus Corporation, Japan). Samples (1-cm) were cut from the middle section of the spun fibre and placed in 2-well Lab-Tek chamber slides, Permanox® in contact with distilled water. To acquire stacks of 2-dimensional parallel images, laser excitation was performed at 488 nm with maximum emission detection at 498–598 nm. The image size was 640×640 pixels, with each pixel corresponding to $1.9884 \mu\text{m}$ in the X and Y directions. Images were acquired using a Z-axis spacing of $4 \mu\text{m}$. The cell distribution was analysed in 2D planes on the XY-axis and vertically through the fibre scaffold along the Z-axis. The 2D cross-sections of the fibre were used to generate 3D images using the following protocol. To visualize cell distribution in the fibre section, the low-surface-area cross sections at the top and base of the fibre were discarded and a stack of approximately 200 images was acquired. Further selection of every fifth image of the 200 images was carried out to provide an analysis depth of $800 \mu\text{m}$. The selected fibre sections were compiled using Adobe Illustrator CS4 (Figure 4.5). Cell numbers were physically counted using only those cells that were in focus on each plane (Figure 4.5A) and were subsequently compiled into 3D images via 3D-rotate (Figure 4.5C). Under “Effect > 3D > Rotation”, values were set at horizontal (x) axis  -38° , vertical (y) axis  46° , and depth (z) axis  -32° . Cells marked in green represent Calcein-AM positive (live) cells on each 2D plane. Counted cells were labelled in red to avoid double counting (Figure 4.5B). Data for total cell number/ mm^3 were acquired from the middle section of quintuplicate individual fibres for HDFa-encapsulated macroporous fibres and non-macroporous fibres (control) respectively. (Assuming a uniform distribution of cells across the fibre) A flowchart

depicting image compilation and data analysis is shown in Figure 4.5.

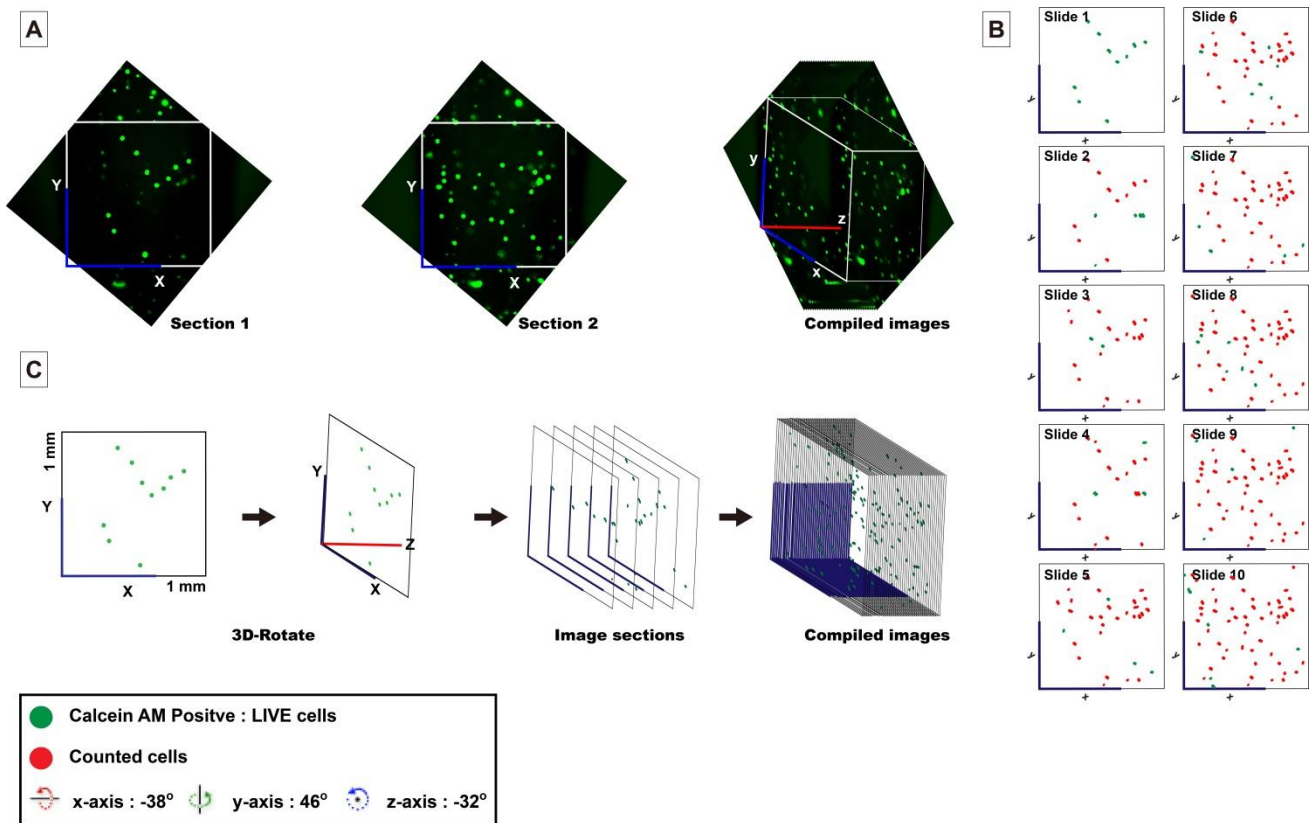


Figure 4.5 Analysis of HDFa cell distribution and density in macroporous alginate fibre after 12 days of cell culture. Cells were stained using Calcein-AM prior to analysis (viable cells emit strong green fluorescence). (A) Live cells that are in focus on each 2D plane were counted within a 1 mm^2 area in each image section and were marked in green. (B) Counted cells from each slide were labelled in different colour (red) to avoid double counting. (C) The sum of green-labelled cells in all image sections was used to determine the overall cell density.

The number of live cells (shown in green) was also counted in a 3D reconstruction of the HDFa-loaded alginate fibre (1 mm^3) and the inter-cell spacing of HDFa cells in both non-macroporous and macroporous fibres were measured directly from the reconstructed images (Figure 4.6).

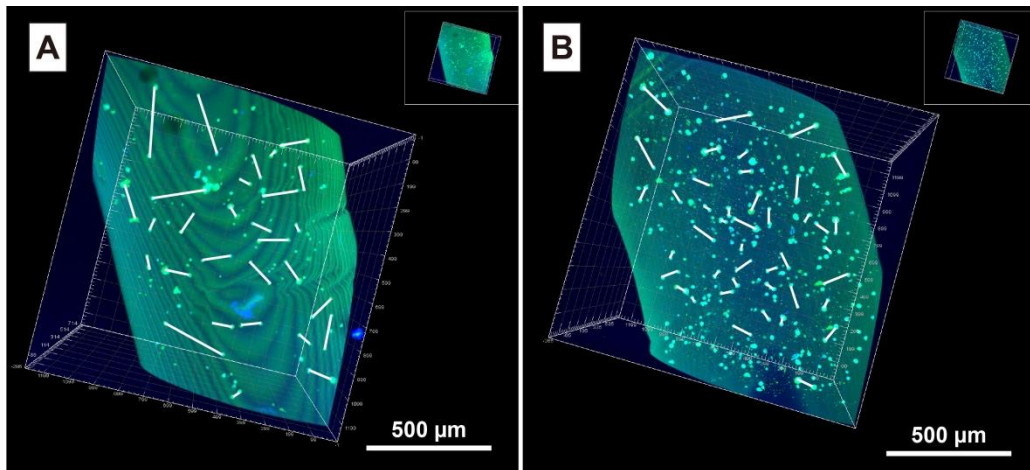


Figure 4.6 Internal cell to cell distance measured for HDFa-loaded alginate fibres (1 mm^3). (A) non-macroporous alginate fibre, (B) macroporous alginate fibre.

4.4 RESULTS AND DISCUSSION

4.4.1 Encapsulation of Swiss 3T3 fibroblasts in alginate fibres.

Experiments were conducted to establish the fibre spinning conditions required for successful encapsulation of fibroblasts in alginate fibres and the viability of encapsulated cells in the hydrogel environment. The optical micrograph of control alginate fibres (no encapsulated cells) in Figure 4.7A shows the typical translucent and longitudinal rippled texture of cell-free fibres. Optical micrographs of fibres spun using fibroblasts suspended in alginate solution at a cell density of 1.4×10^4 cells/mL, showed that the cells (arrowed) were successfully encapsulated and evenly though widely distributed in the fibres (Figure 4.7B). Encapsulation of cells was clearly demonstrated by CLSM following staining of the cells with DAPI to label the cell nucleus blue and rhodamine to label the actin filaments pink (Figure 4.8A).

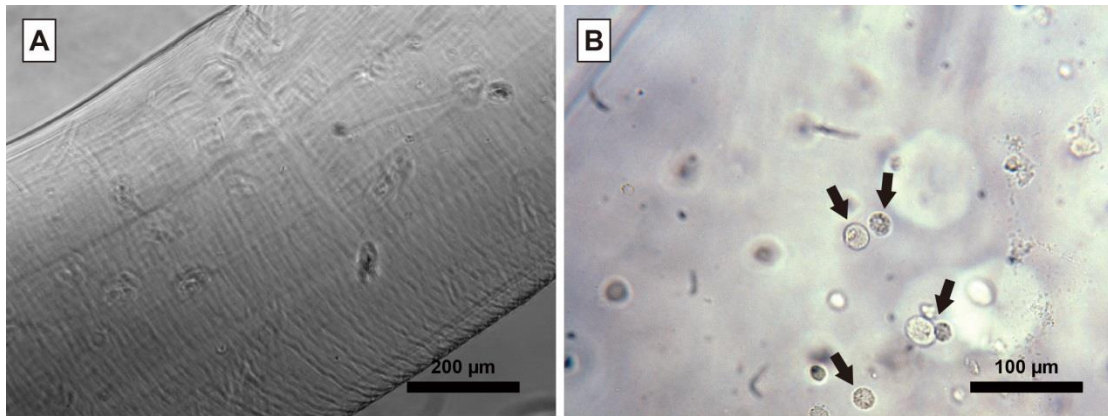


Figure 4.7 Optical micrograph of (A) control cell-free alginate fibres and (B) Swiss 3T3 fibroblasts encapsulated in alginate fibres at day 10 in culture. Fibres produced by spinning cell-alginate solution (cell density of 1.4×10^4 cells/mL in 1.5% w/v alginate solution) into 0.5 M filtered CaCl_2 solution.

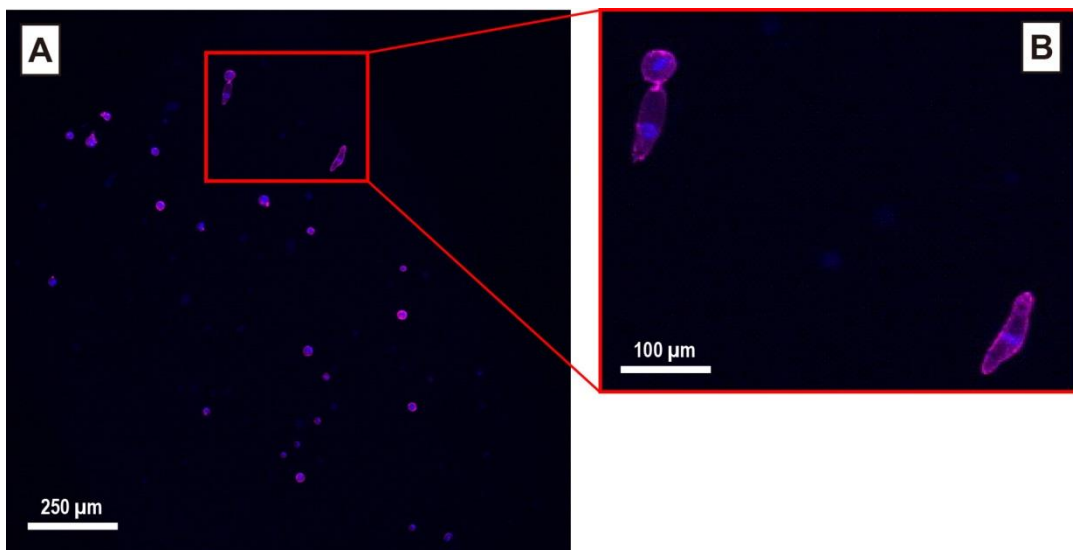


Figure 4.8 CLSM images of (A) Swiss 3T3 fibroblasts encapsulated in alginate fibres after 8 weeks in cell culture. (B) Magnified view of elongated fibroblasts in selected field of view. Fibre produced by spinning cell-alginate solution (cell density of 1.4×10^4 cells/mL in 1.5% w/v alginate solution) into 0.5 M filtered CaCl_2 solution. Cells stained with DAPI to label the cell nucleus (blue) and rhodamine to label the actin filaments (pink).

Swiss 3T3 fibroblast-encapsulated alginate fibres were incubated in complete culture medium for 8 weeks. On day 10, some fibroblasts were observed to have elongated within the fibres (Figure 4.8B), but the majority maintained a spherical morphology. It is evident that the cells are efficiently encapsulated within the alginate matrix and are sustained by efficient nutrient inflow and waste product outflow through the porous alginate microstructure. Some cells were observed at the base of the well at day 50, which had been released from fibres that had partly broken down during cell culture. The cells displayed a distinct spindle-shaped morphology characteristic of fibroblasts, providing evidence that encapsulated fibroblasts remained viable within the alginate fibres for an extended time period of 8 weeks and were capable of resuming growth outside the fibres. Thus, controlled degradation of the alginate fibre may be considered in future work to permit cell growth. Several studies have reported similar findings when seeding Schwann cells [245], chondrocytes [246], hepatocytes [247] or encapsulating perichondrium cells [248], ovine intervertebral disc nucleus pulposus (NP) cells [249] using unmodified alginate. When cultured in or on unmodified alginate, cells tend to retain their spherical morphology and show little proliferation but remain viable. Retention of the rounded form results from the absence of cell binding moieties along the polysaccharide chain which are necessary to establish cell-substrate adhesion (Chapter 1, Section 1.1.10). The inability of anchorage-dependent cells to adhere to alginate has consequences for cell growth, differentiation and gene expression.

It should be noted that the starting fibroblast concentration in the alginate solution used for fibre spinning was relatively low (1.4×10^4 cells/mL) and therefore, the cell distribution in the resultant fibres may not have been sufficient to establish cell-cell interactions. Interestingly, while the effect of scaffold material properties (e.g.

strength, adhesion, porosity) in 3D cell culture has been widely investigated [154, 235, 202], the effect of cell density, which directly influences cell–cell signalling has often been overlooked. Interactions between cells are important for cellular activities, such as cell differentiation during embryogenesis and cell survival. Moreover, cell to cell communication through paracrine signalling could also elicit changes in cell behaviour or function to other cells alongside [250, 251]. Puliafito et al. [252] and Heckman [253] reported that high cell seeding density in 2D cultures facilitated cell-cell contact and stimulated cell cycle arrest leading to ‘contact inhibition’. On the other hand, cell-cell contact has been shown to stimulate choriocarcinoma cell differentiation [254] suggesting cell-to-cell communication is ancillary to cyto-differentiation in cell aggregates on matrix gels.

Relatively few studies have examined the effect of initial cell seeding density in 3D systems, where cells are embedded within a hydrogel-like matrix. Under such conditions, cell–cell interactions may be easily hindered if cells are entrapped at too low a density [255]. The “optimal” cell seeding density for 3D culture is dependent on the type of cells and matrix. For example, Lin and Anseth [256] reported a minimum loading density of 10^7 cells/mL was necessary to maintain the survival of encapsulated pancreatic β -cells in poly(ethylene glycol) (PEG) hydrogels in the absence of material functionalities (e.g. cell adhesion ligands). Maia et al. [257] showed that a high density of human mesenchymal stem cells (hMSCs) (1.5×10^7 cells/mL) entrapped within RGD-alginate hydrogels resulted in improved cell viability and cell–cell signalling. Maguire et al. [258] described the aggregation of hepatocytes within alginate beads, a process that played a central role in controlling cell differentiation. Aggregation was dependent on the initial cell seeding density, with larger aggregates being obtained at the highest density tested (5×10^6 cells/mL). Cao et al. [259] demonstrated that viability and proliferation of pancreatic β -cells in

alginate hydrogels could depend on the concentration of the polymer and the crosslinking solution in addition to the cell density.

Swiss 3T3 fibroblasts were successfully encapsulated in alginate fibres using a cell density 1.4×10^4 cells/mL in the spinning solution and could survive for up to 50 days in cell culture. However, the encapsulated cells were essentially trapped within the alginate hydrogel and had limited space for cell elongation and proliferation. The cell density in the spinning solution was subsequently increased by approximately 100 times (1.5×10^6 cells/mL) to increase the cell density in the spun fibre and to determine its effect on cell growth. Optical micrographs obtained from fibroblast-loaded alginate fibres at day 17 and day 23 of cell culture revealed that the cells were successfully encapsulated and evenly distributed in the fibres (Figure 4.9B and 4.9C). At day 17, the first evidence of fibroblast elongation was found (arrowed in Figure 4.9B), but the majority maintained a spherical morphology as in the previous study using a lower cell density in the spinning solution (1.4×10^4 cells/mL). At day 23, some of the fibroblasts displayed the characteristic spindle-shaped structure (Figure 4.9D) which may be explained by local fracture of the hydrogel (Figure 4.9E), providing space for cell extension. Alginate is known to degrade over time by Ca^{2+} ion exchange [63] with monovalent cations such as sodium and potassium as well as phosphate ions which are present in cell culture media and the *in vivo* environment [260-262]. Swiss 3T3 fibroblasts encapsulated in 3D gelatin methacrylate (GelMA) hydrogel by Grimme & Cropek [263] also adopted elongated spindle morphology, but at earlier culture time points of 1, 3 and 5 days (Figure 4.10). Early biodegradation and dissolution of the gelatin matrix is suggested in this case, which permits cell extension.

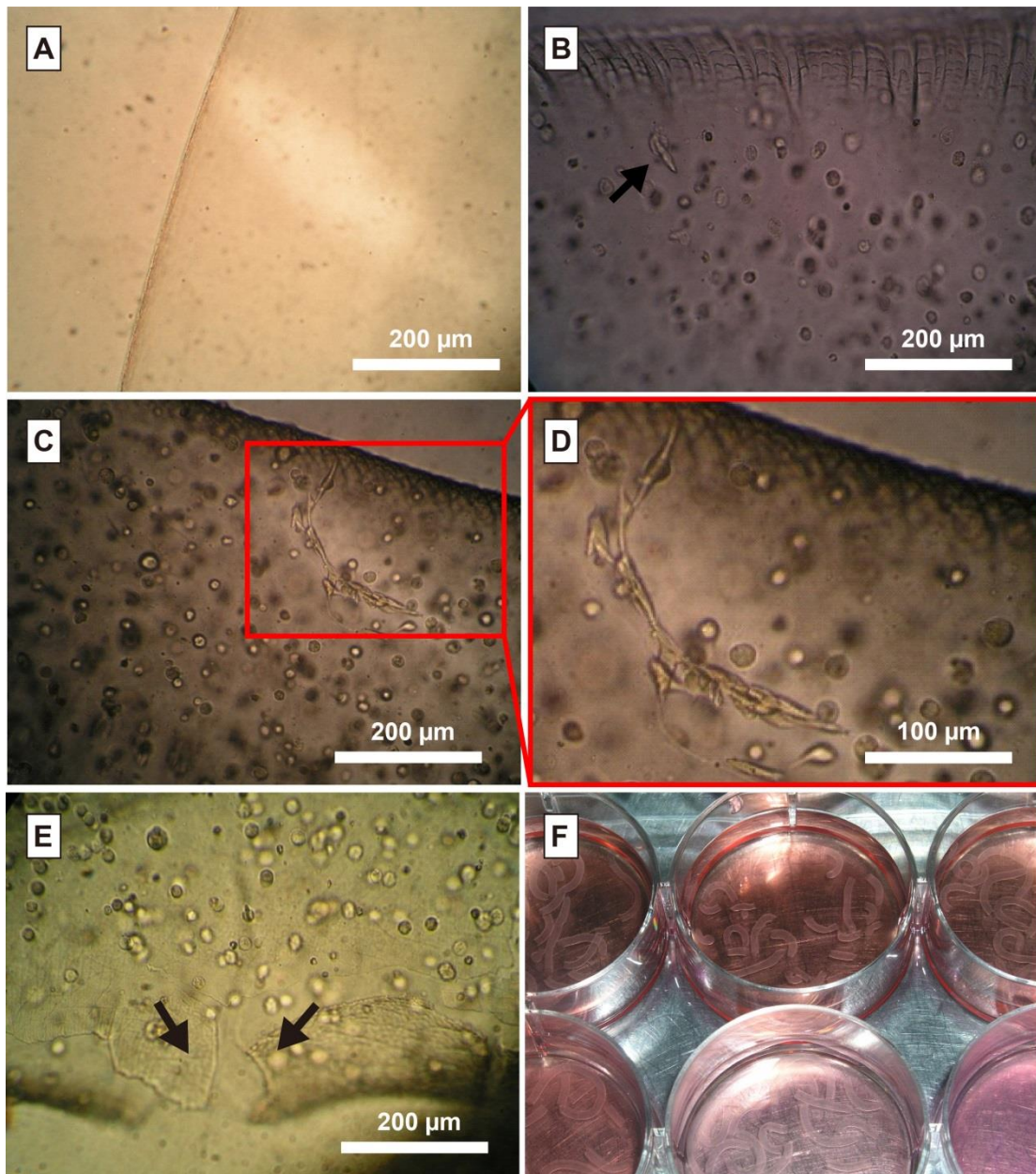


Figure 4.9 Optical micrographs of (A) hydrated cell-free alginate fibres, (B) Swiss 3T3 fibroblasts encapsulated in alginate fibres at day 17 of cell culture (C) day 23 of cell culture (D) magnified view of elongated fibroblasts (arrowed) in selected field of view. (E and F) fractured fibre at day 17 of cell culture. Alginate fibre produced by spinning suspension of fibroblasts in alginate solution (cell density 1.5×10^6 cells/mL in 1.5% w/v alginate solution) into 0.5 M CaCl_2 solution.

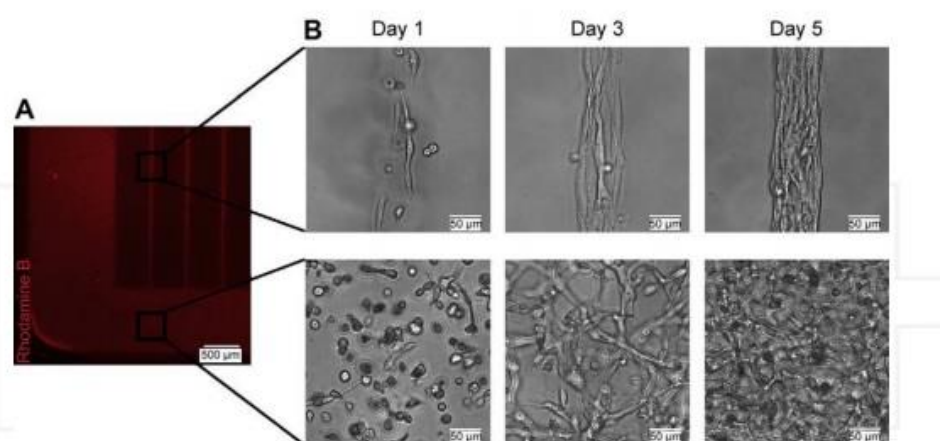


Figure 4.10 Cell morphology and organization of 3T3 Fibroblasts encapsulated in GelMA hydrogel. (A) Rhodamine B stained GelMA hydrogel construct shows patterned and unpatterned regions. (B) Representative phase contrast images of 3T3-fibroblasts (10×10^6 cells/mL) encapsulated in patterned (top row) and unpatterned regions (bottom row) of the hydrogel on days 1, 3 and 5 of culture. Cell elongation increases over time for all hydrogels, while alignment is only induced in patterned constructs [263].

4.4.2 Incorporation of Swiss 3T3 fibroblasts in macroporous alginate fibres

Swiss 3T3 fibroblasts were incorporated in macroporous alginate fibres by wet spinning alginate solutions containing both gelatin particles and suspended cells (cell concentration 1.5×10^6 cells/mL). Fibroblast elongation was observed at day 7 in cell culture (Figure 4.11C and 4.11D), approximately 10 days earlier than was observed in fibres spun from suspensions containing Swiss 3T3 fibroblasts (cell concentration 1.5×10^6 cells/mL) without gelatin particles (Figure 4.10B). Contact between fibroblasts was observed in the fibres at day 13 in cell culture (Figure 4.11E and 4.11F). Thus, the incorporation of gelatin particles in alginate fibres as a porogen appears to facilitate fibroblast elongation and cell-cell contact. This behaviour is expected to

result from two factors. Solubilisation and extraction of gelatin from the fibres over time in the culture medium provides macropores and consequently space for cell elongation. In addition, gelatin modification of the macropore surface (Chapter 3, Section 3.3.1) is expected to provide a cell adhesive surface for the fibroblasts, which enables the formation of focal contacts and cell elongation to the spindle form.

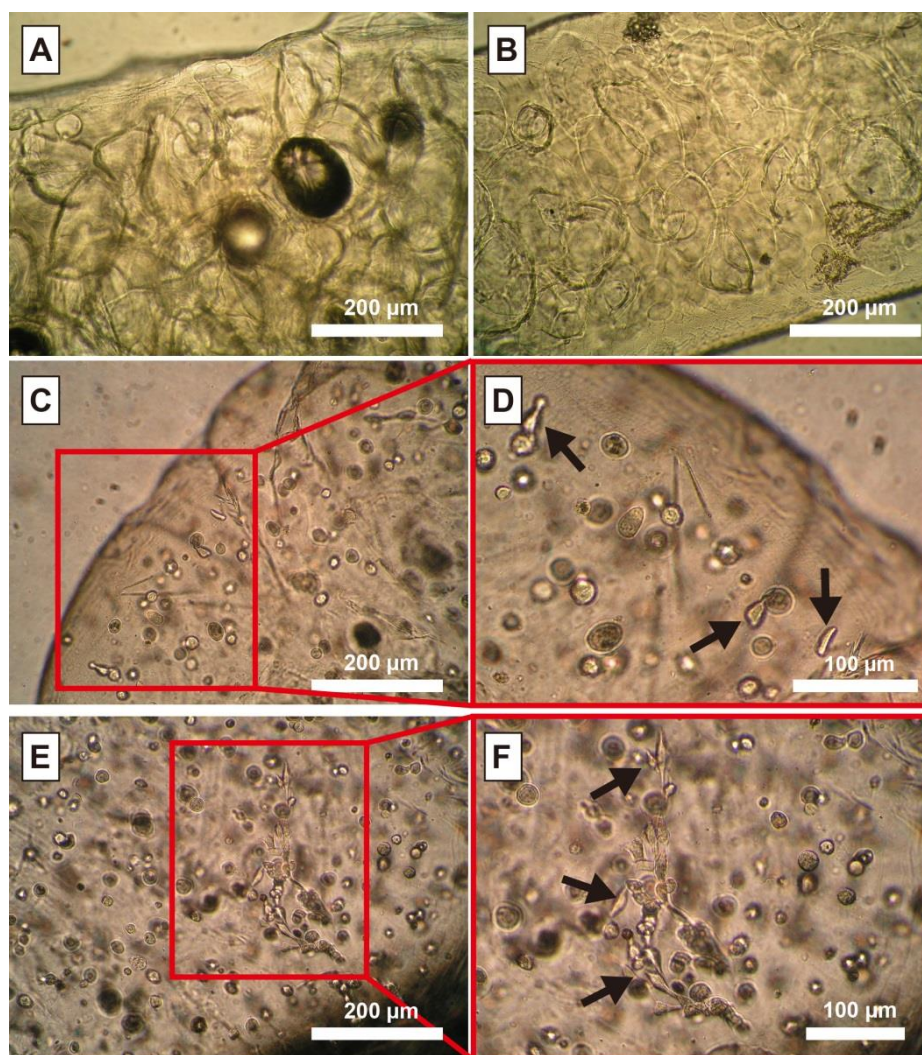


Figure 4.11 Optical micrographs of (A) cell-free gelatin particle-loaded alginate fibre before particle extraction (B) cell-free gelatin particle-loaded alginate fibres following particle extraction (C) macroporous alginate fibres incorporating Swiss 3T3 fibroblasts at day 7 of cell culture (D) magnified view of elongated fibroblasts

(arrowed) in selected field of view, (E) macroporous alginate fibres incorporating Swiss 3T3 fibroblasts at day 13 of cell culture, (F) magnified view of contacting fibroblasts (arrowed) in selected field of view. Macroporous alginate fibres produced by wet spinning suspension of Swiss 3T3 fibroblasts and gelatin particles in alginate solution into 0.5 M CaCl₂ (cell density 1.5×10^6 cells/mL, gelatin particle 57% w/w, 1.5% w/v alginate solution).

Based on observation, alginate fibres containing 3T3 mouse fibroblasts at high density weakened in cell culture at a faster rate (day 17, Figure 4.10E and F) relative to those containing cells at low density (day 40). This behaviour could be attributed to the uptake of calcium ions in alginate hydrogel by the encapsulated cells [264] and thus not being available for cross-linking of the alginate. Calcium is utilised by cells in cell signalling [265], cell proliferation and adhesion to culture substrates [266]. Work carried out by Hunt et al. [267] correlated calcium release from alginate hydrogels in culture medium with NIH 3T3 cell loading density and hydrogel degradation. Their results showed that high amounts of calcium were released from alginate hydrogels exposed to cell culture media within the first 6 days of culture resulting in weakening of the cell-scaffold construct.

4.4.3 Incorporation of HDFa in macroporous alginate fibres

Non-macroporous and macroporous alginate fibres were spun from an intermediate HDFa cell suspension concentration of 3×10^5 cells/mL in an attempt to maintain the integrity of the supporting scaffold. Assay of cell viability using Calcein-AM revealed that more than 90% of the cells encapsulated in both non-macroporous and macroporous fibres were viable after 12 days of cell culture. Calcein-AM staining

also enabled estimates to be made for cell density and inter-cell spacing in the fibres as described in Section 4.3.7.4 On day 12, the cell density in HDFa-containing macroporous alginate fibres (3.6×10^2 cells/mm³) was significantly higher (*P<0.05) than the non-macroporous control fibres (1.4×10^2 cells/mm³) (Figure 4.12) demonstrating that creation of macropores in the alginate fibres by gelatin extraction enhances cell proliferation.

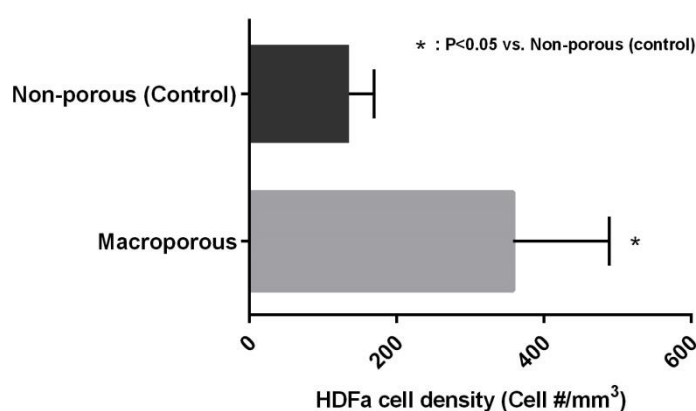


Figure 4.12 Human adult dermal fibroblast cell (HDFa) density in non-macroporous and macroporous alginate fibres. HDFa were suspended in alginate solution with or without gelatin particles at 3×10^5 cells/mL. Wet spun fibre samples subjected to Calcein-AM staining and cell density determined using CLSM. (One way ANOVA *P<0.05, n = 5).

The HDFa cell density in the fibres was estimated by two methods. In the first approach the number of live cells (shown in green) was counted in a 3D reconstruction of the fibre (1 mm³). The mean cell spacing was obtained by measuring the distance between neighbouring cells (Figure 4.6, Table 4.2). A more precise counting method was based on the model of Thevenot et al. [268] who quantified the 3D cell distribution and infiltration of 3T3-Swiss albino mouse fibroblasts in

poly(lactide-co-glycolide) (PLGA) scaffolds as illustrated in the flow chart in Figure 4.14. Images of stained cells in the scaffold (approximately 100 sections at 20 μm separation) were obtained by fluorescence microscopy then stacked and recompiled, prior to cell counting using the Volume Builder plug-in of Imaged (Figure 4.14). In the present study, HDFa cells encapsulated in macroporous fibres were imaged using CLSM to acquire stacks of 2D images at a Z-axis spacing of 4 μm (Section 4.3.9). The cell distribution was analysed in 2D planes on the XY-axis and vertically through the fibre scaffold along the Z-axis (Figure 4.5). By this means, 3.6×10^2 cells/ mm^3 were counted in HDFa -loaded macroporous alginate fibre compared with 2.0×10^2 cells/ mm^3 when counting cells directly from the 3D reconstructed image (Figure 4.13F).

Table 4.2 Cell density and inter-cell spacing of HDFa cells encapsulated in alginate fibre.

	Initial cell loading density in fibre /mL	Cell count /mm^3	Inter-cell spacing range (Mean distance \pm SEM) (μm)
Non-macroporous	$3 \times 10^5/\text{mL}$	1.4×10^2 cells/ mm^3	31-284 (111 \pm 13)
Macroporous	$3 \times 10^5/\text{mL}$	3.6×10^2 cells/ mm^3	19-144 (57 \pm 6)

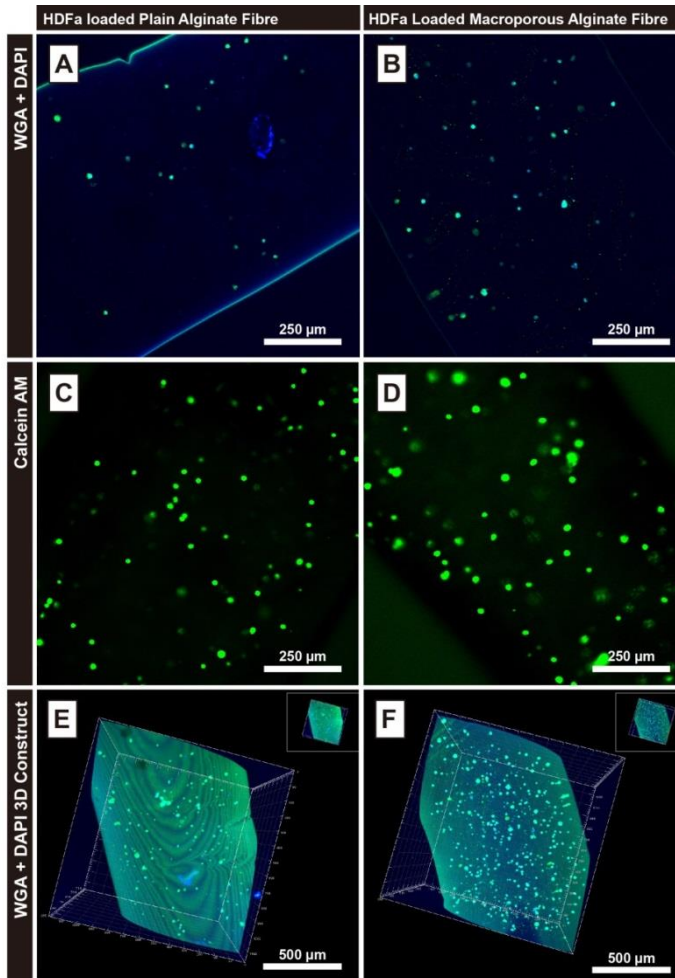


Figure 4.13 CLSM image at day 12 in cell culture of HDFa cells loaded in macroporous alginate fibres. WGA- and DAPI-labelled HDFa cells in (A) non-macroporous alginate fibre, (B) macroporous alginate fibre. Live/dead staining with Calcein-AM of HDFa cells in (C) non-macroporous alginate fibre, (D) macroporous alginate fibre. 3D visualisation of DAPI- and WGA-labelled HDFa cells in (E) non-macroporous alginate fibre, (F) macroporous alginate fibre. Non-macroporous HDFa-containing alginate fibre produced by spinning cell suspension in alginate solution (cell density of 1.3×10^6 cells/mL in 1.5% w/v alginate solution) into CaCl_2 solution. Macroporous HDFa-containing fibre produced by spinning suspension of HDFa fibroblasts and gelatin particles in alginate solution into CaCl_2 solution (cell density 1.3×10^6 cells/mL, gelatin particle 57% w/w, 1.5% w/v alginate solution).

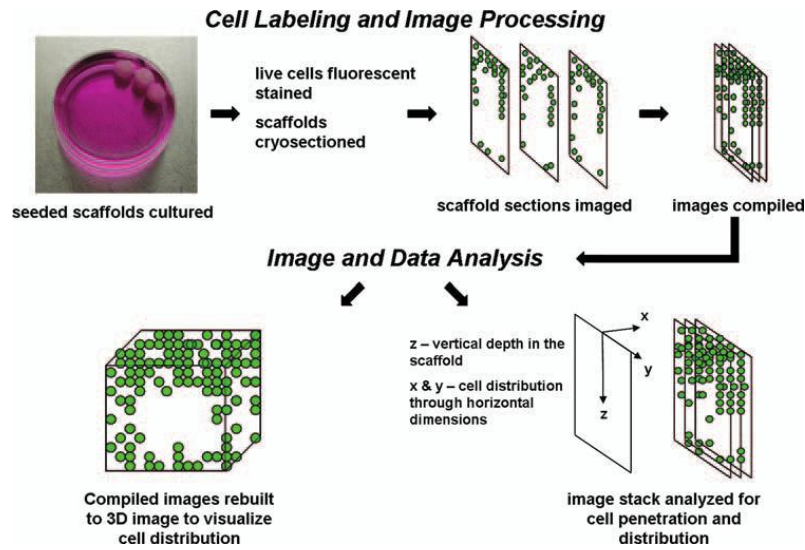


Figure 4.14. Flowchart illustrating the method of Thevenot et al. to quantify 3D cell distribution and infiltration [268].

4.5 CONCLUSION

Cell-containing alginate fibres were produced by wet spinning cell suspensions in alginate solution into CaCl_2 crosslinking solution. Swiss 3T3 mouse fibroblasts remained viable over 8 weeks in cell culture but cell elongation and cell-cell contact was hindered. The incorporation of gelatin particles in alginate fibres as a proagen facilitated Swiss 3T3 fibroblast elongation and cell-cell contact by providing macropores following gelatin extraction. Modification of the pore surface by gelatin is anticipated to produce fibroblast adhesion and permit subsequent elongation to the spindle form. On day 12 in cell culture, the cell density in HDFa-containing macroporous alginate fibres (3.6×10^2 cells/ mm^3) was significantly higher than non-macroporous fibres (1.4×10^2 cells/ mm^3) suggesting that the creation of macropores in the alginate fibres by gelatin extraction enhances cell proliferation.

CHAPTER 5

Encapsulation of Primary Rat Dorsal Root Ganglia in Macroporous Alginate Fibres for Nerve Regeneration

ABSTRACT

Macroporous alginate fibres were produced by wet spinning alginate solution containing dispersed gelatin particles and nerve cells (primary rat dorsal root ganglia (DRGs)) to investigate their potential as tissue engineering scaffolds for nerve repair. The gelatin particles were employed as porogens and simultaneously to provide cell adhesion molecules (CAM) for modification of macropore surfaces to promote nerve cell attachment and proliferation within the polysaccharide fibre structure. Marked outgrowth of DRGs was evident within the fibre at day 11 in cell culture, indicating that macropores and channels created within the alginate hydrogel by gelatin extraction were providing a favourable environment for nerve cell development. Evidence of neurite contact was obtained at day 9. These findings indicate that macroporous alginate fibres encapsulating nerve cells may provide a useful strategy for nerve repair.

5.1 INTRODUCTION

Nerve repair using tissue engineering principles seeks to regenerate the nerve fibre (Chapter 1, Figure 1.4) which is made up of neurons that transmit nerve impulses from the brain, supported and protected by glial cells (Schwann cells (SCs)) in the peripheral nervous system (PNS), astrocytes and oligodendrocytes in the central nervous system (CNS). Glial cells increase the speed of signal transmission and produce neurotrophic factors to modulate neuron growth. Nerve fibres are bundled

together to form a fascicular structure which is ensheathed by the epineurium (outermost surface layer) of the nerve. The process of natural peripheral nerve repair involves the formation of longitudinal arrangements of proliferating SCs (Büngner bands) that guide axonal growth from the damaged distal nerve segment [269] coupled with the sprouting of new axons from myelinated and non-myelinated nerve fibres in the proximal segment [270]. Nerve repair strategies in tissue engineering are generally based on a 3D scaffold or 'biological template' or artificial extracellular matrix (ECM) which is designed to support cells and guide tissue development. Refinements of this basic approach involve the incorporation of growth factors, stem cells and transfected cells, which express axon growth-promoting molecules [270, 271]

Both synthetic and natural polymer scaffolds (summarised in Table 5.1) have been utilised as guides for directing growth of nerve cells along the scaffold surface or within the scaffold [271, 272]. Poly- ϵ -caprolactone (PCL) [273], poly(L-lactic acid) (PLLA) [3, 274] and polyglycolic acid (PLGA) [28, 73] are the most commonly used synthetic polymers for nerve repair. Electrospun aligned fibres of poly(ϵ -caprolactone), for example, have been shown to produce longer oriented neurite outgrowth of PC12 cells compared with random fibres [273]. Natural polymers including ECM components (e.g. laminin, collagen and fibronectin) as well as polysaccharide materials (e.g. agarose, alginate and chitosan) have been shown to be highly effective in promoting axonal development and repair processes.

Alginate, a polysaccharide derived from brown seaweed, has been widely investigated for drug delivery and scaffold production in tissue engineering because of its good biocompatibility and low toxicity. Importantly, the material is converted to a hydrogel by exposure to divalent cations such as Ca^{2+} under mild aqueous conditions. As a result the polymer has been studied extensively for encapsulation of cells (e.g.

pancreatic islets, recombinant cells) and is also a material of interest in regeneration of neural tissue. Alginate has been fabricated in various forms including heterogeneous conduits [275], freeze-dried sponges [144, 276] and hydrogels [153, 235]. Pfister et al. [275] successfully prepared an alginate/chitosan conduit by dissolving alginate and chitosan (3:2 w/w mixture) in water and 1% acetic acid respectively, followed by addition of ethanol (44% with respect to the total amount of liquid) to both solutions. After homogenisation the dispersed alginate/chitosan complex was transferred via a syringe onto a spinning steel mandrel and solvent was allowed to evaporate under a stream of air to form a hydrogel tube. Freeze-dried alginate sponge covalently crosslinked using carbodiimide [144] was used to assess the degree of nerve regeneration from 2 weeks to 21 months in the rat sciatic nerve (10 mm defect) [276]. Early sprouting axons (100 μm) extended into the partially degraded alginate gel 4 days post implantation. Numerous Schwann cells migrated into the alginate gel at the distal lesion site over 8–14 days. The diameter of regenerated myelinated axons increased from 0 – 2 to 12 – 14 μm at 2 and 21 months post-implantation. It was also observed that regenerated axons extended through the partially degraded gel rather than through the pore structure as was anticipated, suggesting the significance of controlling the scaffold biodegradability over pore size for nerve regeneration [276]. Prang et al. [153] demonstrated axon regrowth following spinal cord injury in young rats using alginate-based, highly anisotropic capillary hydrogels (ACH). The scaffolds were produced by impinging copper nitrate solution onto the surface of alginate solution using pump spray bottles to create hexagonally structured anisotropic capillary gels. The ACH scaffolds were shown to promote oriented axon regeneration *in vivo*; across the complete length of the capillaries (500 μm) in the injured mammalian CNS and the survival of adult neural progenitor cells. Matyash et al. [235] showed that non-functionalised alginate hydrogels formed by

crosslinking with Ca^{2+} , Ba^{2+} , or Sr^{2+} support neural adhesion, and rapid and abundant neurite outgrowth on the surface and within the hydrogel *in vitro*. Furthermore, alginate hydrogel was found to exhibit neuroprotective properties against oxidative stress induced by hydrogen peroxide (H_2O_2).

The previous chapter described investigations of the ability of macroporous alginate fibres to maintain the viability of encapsulated cells and to promote cell growth. Human adult dermal fibroblasts (HDFa) were incorporated in macroporous alginate fibres by wet spinning alginate solutions containing both gelatin microparticles and suspended cells. Cell viability was maintained for time periods of at least 12 days. Incorporation of gelatin particles in the alginate fibres served as a porogen to facilitate fibroblast elongation and cell-cell contact by providing macropores, surface modified by gelatin for fibroblast adhesion and subsequent elongation to the spindle form.

In this chapter, rat dorsal root ganglion (DRG) cells were encapsulated in macroporous alginate fibres, using the method developed for HDFa, with the aim of facilitating neurite outgrowth and the formation of neuronal contacts throughout the scaffold. Growth of encapsulated DRG cells was monitored over 15 days in cell culture using optical microscopy. The neuron-specific marker TU-20 was employed to confirm neurite outgrowth from encapsulated neurons using CLSM and cell viability was assayed by Calcein-AM staining.

Table 5.1 A Summary of different approaches for nerve regeneration *in vitro*.

Materials	Fabrication methods	Cell types	Key findings	Ref.
<i>Synthetic Polymers</i>				
PCL	Polycaprolactone (PCL) aligned /random fiber meshes, electrospining	Rat pheochromocytoma 12 (PC12) cells	PC12 neurite extension on aligned PCL fibers with diameters of $3.7 \pm 0.5 \mu\text{m}$ and $5 \pm 0.9 \mu\text{m}$ were significantly longer than on randomly-orientated fibers with a diameter of $4.4 \pm 0.5 \mu\text{m}$ and neurites extended parallel to the aligned fibers for all fiber diameters studied.	[273]
PPy-PLGA	Polypyrrole-coated poly(lactic-co-glycolic acid) nanofibers (PPy-PLGA), electrospining followed by coating with PPy through in-situ polymerization to create PPy shells.	Rat pheochromocytoma 12 (PC12) cells and hippocampal neurons	Both electrospun aligned and random PPy-PLGA meshes were shown to provide electric stimulation to promote and guide neurite extension. Electrically stimulated PC12 cells had significantly longer neurites than cells on un-stimulated scaffolds.	[274]
PLLA	Poly-L-lactic acid (PLLA) scaffolds, electrospining	Neonatal mouse cerebellum C17.2 stem cells (NSCs)	Electrospun nano-sized fibers (300 nm) of PLLA enhanced neural differentiation of NSCs as compared to micron-sized ($1.25 \mu\text{m}$) fibers	[73]
<i>Natural Polymers</i>				
Alginate	Soft alginate hydrogel, produced by cross-linking low viscosity manuronic/ guluronic acid rich alginates with cations (Ca^{2+} , Ba^{2+} , and Sr^{2+}) with no >10% of gelation sites of alginate	Neuronal stem cell cultures prepared from E20 Wistar rat fetuses	Supported neural adhesion, penetration and facilitated rapid and abundant neurite outgrowth on surface as well as within the hydrogel. Alginates conferred protection to neurons against oxidative stress induced by H_2O_2 , hence prolonged cell survival up to 4 months.	[235]
Collagen	Collagen scaffolds, unidirectional freezing process followed by freeze-drying.	DRG explants from the spinal column of Lewis rats	Penetration of the axonal growth in the collagen gel ($756 \pm 318 \mu\text{m}$) was approximately 3 folds more than that in the commercially available fibrin gel ($253 \pm 131 \mu\text{m}$) over period of 21 days.	[277]
Gelatin/ alginate	Gelatin containing alginate capillary hydrogels (ACHs), ACHs with different capillary diameters and biochemically modified by introducing gelatin into the self-assembly process	DRGs from postnatal day 2–6 Wistar rats	Gelatin-containing ACHs promoted more axon elongation in comparison with ACHs without gelatin over 7 days. However, no significant difference in axon and Schwann cell density was observed. Findings suggest that gelatin provides better adhesion for DRG axons growing into the hydrogel.	[278]
Chitosan	Chitosan membrane, decetylation of chitin followed by gelation and neutralisation with 1% NaOH for 24h. The chitosan fibers, $15 \mu\text{m}$ in diameter, were purchased from Shanghai Gao Chun biomaterial Company (Shanghai, China).	Schwann cells (SCs) from Six neonatal Sprague–Dawley rats sciatic nerve fragments	Majorities of SCs migrated on to both chitosan materials after 7 days. In Comparison, SCs migrated faster onto the stereoframe of chitosan fibers than the membrane. The study showed good biological compatibility and adherence between chitosan and SCs, however, cells on the membrane retained better viability after 3–14 days than that of the corresponding groups.	[279]
Fibrin	Fibrin matrix, enzymatically-induced polymerization of fibrinogen.	DRGs from chick embryos	The rate of neurite invasion into the matrix was effected primarily by fibrin density (neurite in-growth decreased by increasing fibrin density) and not by the diameter or numbers of fibrin bundles.	[280]
Laminin	Laminin-containing cryogel scaffolds, cryogelation of dextran and gelatin linked to laminin.	Cord blood-derived stem cells (CBSCs)	laminin-rich scaffolds attracted infiltration of rats' neuroblasts (NF200+, Nestin+) indicating high neuroregeneration properties both <i>in vitro</i> and <i>in vivo</i> models.	[281]
Silk	Silk Fibers, electrospining	Rat retinal ganglion cells (RGCs)	RGCs exhibited longer axonal growth when in contact with the biofunctionalized fibers. Compared with unfunctionalized fibers ($46.9 \pm 2.4 \mu\text{m}$). The growth of neurites increases 2-fold ($82.3 \pm 2.8 \mu\text{m}$) on fibers containing BDNF, 2.5-fold ($105.2 \pm 1.3 \mu\text{m}$) on fibers containing CNTF and almost 3-fold ($117.7 \pm 2.9 \mu\text{m}$) on fibers containing both factors	[282]

5.2 MATERIALS

Sodium alginate (Protanal RF 6650, G:M 2:1) was obtained from IMCD Australia Limited. Calcium chloride (dehydrate) was purchased from UniLab. Gelatin from porcine skin (Type A, Bloom 300, average molecular mass 50-100 kDa), Dulbecco's phosphate-buffered saline (with MgCl₂ and CaCl₂, liquid, sterile filtered, suitable for cell culture, D8662) were purchased from Sigma. Cryopreserved rat DRG neurons (0.25 mL cell suspension, R-DRG-505) and primary neuron growth medium (PNGM™) BulletKit® (CC-4461) containing primary neuron basal medium (PNBM) and the primary neuron growth SingleQuots™ Kit. The PNGM™ SingleQuots™ Kit contains the necessary volumes of L-glutamine (GA-1000), and neural survival factor-1 (NSF-1), a supplement supporting neuronal growth and survival, to complement the basal medium volume provided; were purchased from Lonza. The mouse monoclonal anti- α -tubulin-III, (clone TU-20, MAB1637) was obtained from Chemicon and Cy3-conjugated AffiniPure Goat Anti-Mouse IgG (H+L) and Calcein-AM (C3100-MP) were purchased from Invitrogen. Anti-fade Vectashield mounting medium containing DAPI (1.5 μ g/mL) (H-1200, Vector) was purchased from Vector Laboratories Ltd. Dimethyl sulphoxide (anhydrous, \geq 99.9%) was purchased from Sigma-Aldrich. Mouse retinal tissue (species:7.211) was contributed by Dr Sally Firth from School of Pharmacy, University of Queensland, Australia.

5.3 METHODS

5.3.1 Preparation of cryo-sectioned mouse retinal tissue

Mouse retinal tissue (species:7.211) was fixed with 4% paraformaldehyde in 0.1 M sodium phosphate buffer (pH 7.4) for 2 h and rinsed in 0.01 M phosphate-buffered saline (PBS; pH 7.4). Prior to sectioning, the retinal tissues were cryoprotected with

30% sucrose in PBS overnight and freeze-mounted in Tissue-Tek® optimum cutting temperature (OCT) medium at -20°C . Vertical sections with a thickness of approximately $20\ \mu\text{m}$ were cut using a cryostat (Leica CM 1850) and the sections (in duplicate) were thaw-mounted onto electrostatic glass slides and allowed to dry at room temperature for 1–2 h.

5.3.2 Immunolabelling of retinal tissue

Investigations of immunolabelling of cryosectioned mouse retinal tissue were performed using anti-Tubulin, beta III isoform, C-terminus, clone TU-20 (Similar to TUJ1) to determine the suitable dilutions and sample staining protocols for DRG cell-containing alginate fibres. Class III β -tubulin is a microtubule element expressed predominantly in neurons of the central and peripheral nervous system [283], and is a popular selective marker for neurons in nervous tissue. Microtubules are one component of the cytoskeleton in neurites that serve as a scaffold for organelle transport and structural components of the neurite in neurite elongation (Figure 5.1).

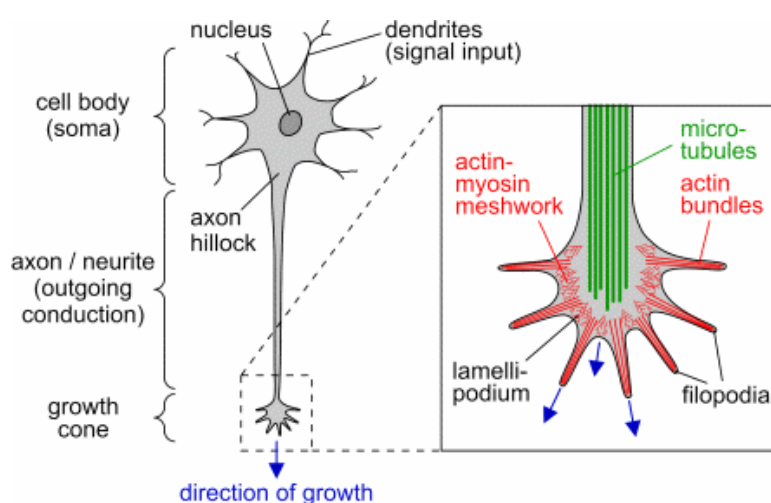


Figure 5.1 Schematic representation of a neuron and detailed view of the growth cone with its main cytoskeletal components (actin filaments and microtubules) [284].

Preparation of serial dilutions of the primary antibody (TU-20) in blocking solution

Serial dilutions of the primary antibody (clone TU-20, MAB1637; 1:100, 1:250, 1:500 and 1:1000) (Figure 5.2) were prepared in 2mL blocking solution as illustrated in Figure 1 and maintained at 2 – 4 °C. The blocking solution was prepared by adding 10% Triton-X (6 µL, 0.3% v/v, Sigma) to normal donkey serum (20 µL, 1% v/v, Jackson Immuno Research) and making up to a volume of 2 mL by adding PBS.

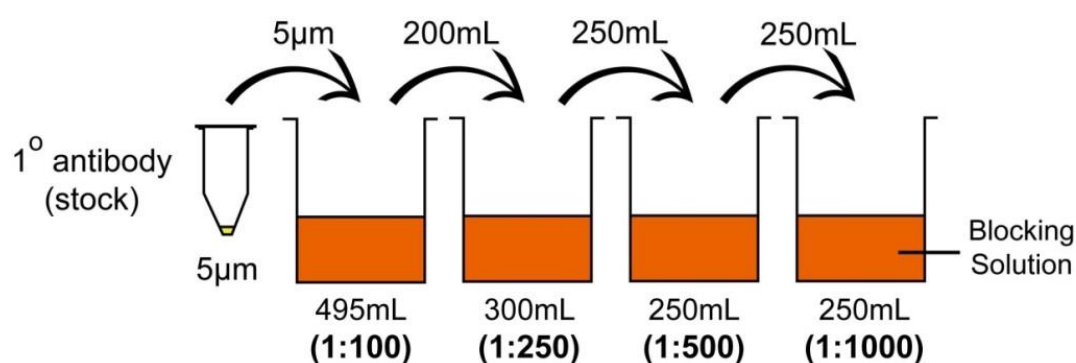


Figure 5.2 Serial dilutions of the primary antibody (TU-20) in blocking solution.

Immunolabelling with the primary antibody (TU-20)

Sections were incubated in dilutions of the primary antibody (TU-20) (1:100, 1:250, 1:500 and 1:1000) at 4 °C in a humid atmosphere for 24 h. The container was capped and carefully transferred to a 4 °C incubator. After incubation, the slides were rinsed 5 times for 10 min each in PBS at 4 °C. Next, the slides were incubated with Cy3-conjugated Affinipure Donkey Anti-Mouse IgG (dilution 1:200) for 1 h at room temperature followed by 4–5 rinses of 10 min each with copious PBS protected from light at 4 °C. Prepared sections were mounted with one drop anti-fade Vectashield mounting medium containing DAPI (1.5 µg/mL) (to label the nuclei) and kept in PBS in the dark at all times.

5.3.3 Imaging of immunolabelled mouse retinal tissue

Images of the mounted sections were acquired using a fluorescence microscope (Nikon Eclipse Ti) with an oil immersion lens (Plan Fluor 40×/1.30 Oil) and images were acquired with a digital camera (CoolSNAP HQ²). A standard rhodamine/Cy3/TRITC filter (Cy3 HYQ filter, Nikon) was used for double labelling with Alexa Fluor 488–FITC conjugated antibodies. Excitation was at 568 nm for Cy-3 with emission filters of 530–560 nm. The brightness and contrast of the images of all retina sections labelled with primary antibody dilutions (1:100, 1:250, 1:500 and 1:1000) were adjusted with Adobe Photoshop CS4 (Adobe).

5.3.4 Encapsulation of primary rat DRG cells in non-macroporous and macroporous alginate fibres

The primary DRG cell culture or explants derived from embryonic [285], post-natal [286] and adult animals [287] from the peripheral nervous system have been commonly utilised as a neuronal model to study neuron function, disease-related axonal degeneration and repair. Unlike peripheral motor neurons (Chapter 1, Figure 1.2), dorsal root ganglion, also called spinal ganglion, is the ganglion of the posterior root of each spinal segmental nerve, containing the cell bodies of the unipolar primary sensory neurons (Figure 5.3). It composes the cell body sites above the neuronal process, which extends in both directions. One axon extends centrally toward the spinal cord; the other axon extends toward the skin or muscle. It is difficult to distinguish which projections is axon or dendrite as the cell is not arranged as a typical neuron (Chapter 1, Figure 1.2).

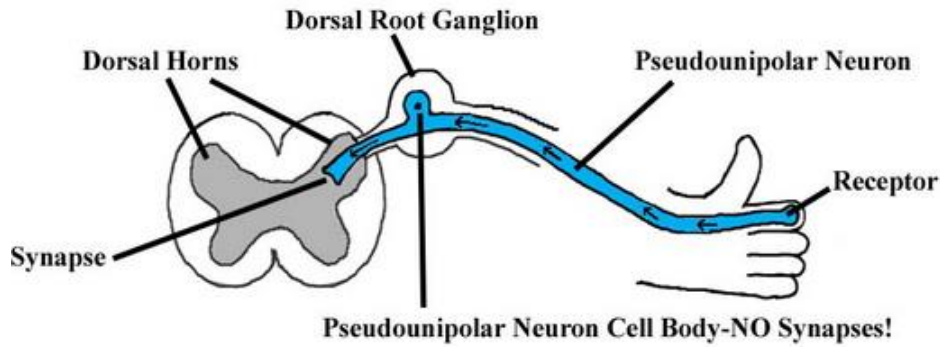


Figure 5.3 Sensory peripheral neurons are called pseudounipolar neurons [288].

Preparation of DRG cell suspensions

A vial of suspended rat DRG cells (2×10^5 cells/ 0.25 mL) was removed from liquid nitrogen and placed in a water bath preheated to 37 °C. The vial was removed after 1.5 min and immediately placed into a laminar flow hood following disinfection of the vial surface with 70% ethanol. The thawed cell suspension was gently transferred into a 15 mL centrifuge tube followed by dropwise addition of 7.75 mL of preheated (37 °C) primary neuron growth medium (PNGMTM) (contains 2mM L-glutamine, 50 µg/mL gentamicin/37ng/mL, amphotericin, and 2% NSF-1) onto the cells while rotating the tube by hand. The cells were suspended by pipetting up and down slowly with a 2 mL plastic disposable serological pipette and by carefully inverting the tube twice. One millilitre of the cell suspension (2.5×10^4 cells) was transferred to another 10 mL centrifuge tube and diluted again with preheated (37 °C) PNGMTM culture medium (3 mL) to achieve a cell concentration of 6.25×10^3 cells/mL. The diluted cell suspension (0.5 mL) was pipetted into a 6-well plate (3.13×10^3 cells/well) and cultured for 4 h at 37 °C under a 5% CO₂ atmosphere. The medium was replaced with fresh medium after 4 h [289] (*Note.* small volume of old medium was left in the plate when replacing with fresh, pre-warmed medium to ensure the cells do not dry out) and then again at 2 days. Media were changed every 2 days thereafter up to 15 days.

Assay of cell viability was carried out using Live/Dead Calcein-AM staining as described in Section 5.3.6. Cell morphology was observed using an inverted optical microscope (CKX 41; Olympus) equipped with a digital camera (DP21; Olympus) and DP Controller software (Olympus).

DRG cell encapsulation in non-macroporous alginate fibres

The prepared DRG cell suspension (1 mL, cell density 2.5×10^4 cells/mL) derived from the above method was added to 3 mL of filtered (syringe filter (0.2 μ m 33 mm) Millex Filter Units, Millipore), alginate solution (2% w/v) to achieve a final cell concentration of 6.25×10^3 cells/mL in a 1.5% w/v alginate solution. The cells were mixed with the alginate solution by pipetting slowly up and down with a 3 mL disposable plastic syringe. The cell suspension in alginate solution (0.5 mL) was wet spun into 50 mL of 0.5 M CaCl₂ solution. The resulting fibre was rinsed with distilled water and cut into 3 sections (approximately 5-cm each) that were each placed into individual wells of a 6-well plate. The cell-containing fibre samples were then cultured in 5 mL of PNGMTM culture medium for 4 h at 37 °C under a 5% CO₂ atmosphere. The medium was replaced with fresh medium after 4 h and then every day up to 15 days (Figure 5.4 – blue arrowed).

DRG cell encapsulation in macroporous alginate fibres

Gelatin powder was sieved through a 90 μ m mesh sieve. The collected powder was sterilized under UV irradiation in a cell culture hood for 20 min. The container was agitated during sterilization to ensure that all particles were exposed to UV. A 2% w/v alginate solution (10 mL) was sterilized by filtration using a syringe filter (0.2 \times 33 mm Millex filter units, Millipore). All equipment (homogeniser, syringe pump) was sterilized by wiping the surfaces with 70% ethanol. Glassware and tools were

autoclaved. Antiseptic techniques were strictly followed to prevent contamination. Sterilized gelatin particles ($90\ \mu\text{m}$, 200 mg) were added to cold filtered 2% w/v alginate solution (10 mL) and homogenised using a IKA Ultra-Turrax® T25 Basic homogeniser in the cell culture hood. A gelatin:alginate w/w ratios of 4:3 was employed, corresponding to 57% w/w gelatin particle loading as a fraction of the total polymer content. DRG cell suspension (1 mL, cell density 2.5×10^4 cells/mL) was added to the gelatin particle/alginate solution (3 mL) to achieve a final cell concentration of 6.25×10^3 cells/mL in a 1.5% w/v alginate solution. Cells were mixed in the gelatin/alginate solution by pipetting slowly up and down with a 3-mL disposable plastic syringe. The suspension of cells and gelatin particles in /alginate solution (0.5 mL) was wet spun into 50 mL of 0.5 M CaCl_2 solution. The resulting fibre was rinsed with distilled water and cut into 3 equivalent sections (approximately 5-cm each) prior to incubation in primary neuron basal medium (5 mL) for 4 h at 37°C under a 5% CO_2 atmosphere. The medium was replaced by fresh medium after 4 h and then every day up to 15 days (Figure 5.4 – black arrowed).

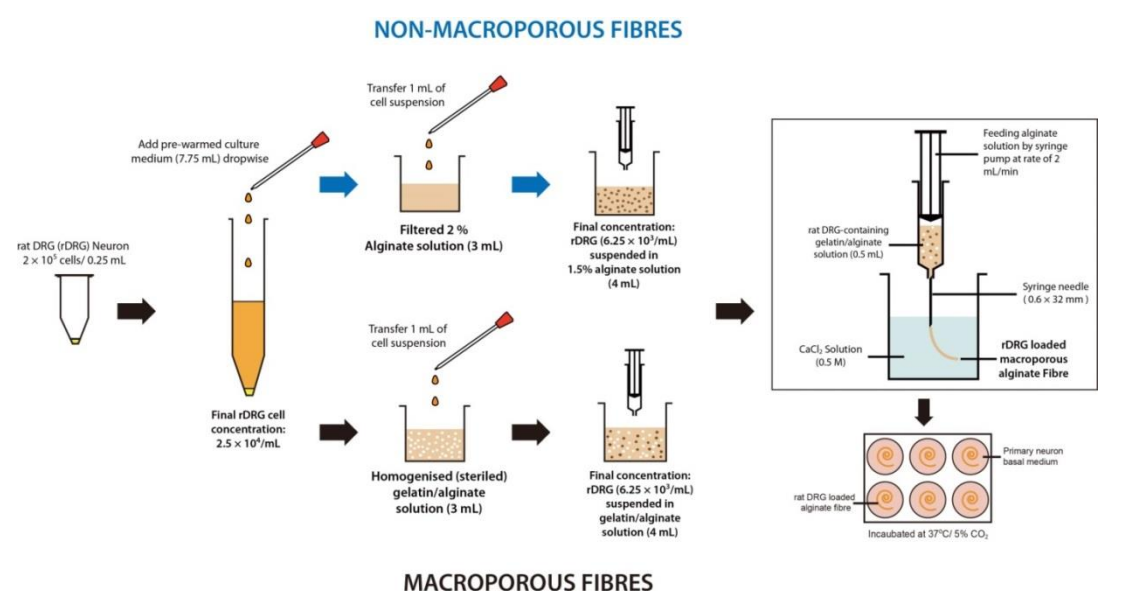


Figure 5.4 Preparation of non-macroporous (blue arrowed) and macroporous (black arrowed) alginate fibres encapsulating primary rat DRG cells.

5.3.5 Immunolabelling of DRG cells encapsulated in alginate fibres

Hydrated alginate fibres encapsulating DRG cells which had been retained in culture medium for 15 days were fixed in 1 mL of 4% paraformaldehyde/D-PBS solution (prepared as described in Chapter 4, Section 4.3.4) for 15 min.

Immunolabelling of DRGs encapsulated in the alginate fibres was carried out with the primary antibody (neuron-specific mouse monoclonal anti-tubulin-III (clone TU-20, MAB1637; 1:250)). Fixed fibre samples (approximately 0.5-cm in length) were rinsed with copious D-PBS and then transferred into 1-mL Eppendorf tubes. The fibre samples were incubated with 200 μ L of the primary antibody solution for 48 h at 4 °C in a humid atmosphere. The primary antibody solution was prepared in blocking solution as described in Section 5.3.2. After incubation, the fibre samples were rinsed 5 times for 10 min each with copious cold D-PBS at 4 °C.

Immunolabelling of encapsulated DRGs with the secondary antibody (Cy3-conjugated Affinipure Donkey Anti-Mouse IgG (H+L)) was performed by adding 7.5 μ L of the antibody solution to D-PBS (1.5 mL) to achieve a dilution of 1:200. Fibre samples were incubated with the prepared solution at room temperature for 50 min in the dark. Following incubation, fibre samples were rinsed 5 times for 10 min each with copious D-PBS. Washing was performed in the dark to prevent the fluorescence from fading. Fibre samples were then washed with copious cold D-PBS and preserved in one drop anti-fade Vectashield mounting medium with DAPI (1.5 μ g/mL). Prior to imaging, the samples were stored at 4 °C in the dark.

5.3.6 Assay of viability of primary rat DRG cells encapsulated in alginate fibres using Calcein-AM staining

The viability of DRGs encapsulated in both non-macroporous and macroporous

alginate fibres by wet spinning were evaluated using Calcein-AM staining. Calcein-AM stock solution in anhydrous DMSO (1 mg/mL, 1 μ M) was prepared by adding 50 μ L of anhydrous DMSO (\geq 99.9%, Sigma-Aldrich) to 50 μ g of Calcein-AM. The prepared stock solution was stored at -20 °C in the dark. A working solution was prepared by pipetting 10 μ L of the stock solution into 9 mL of PNGMTM culture medium to achieve a concentration of 10 nM. Then, 1 mL of working solution was added to DRG-containing –alginate fibre samples (approximately 1-cm long sections) and incubated at 37 °C under a 5% CO₂ atmosphere for 45 min.

Following Calcein-AM staining, a FluoView FV1000 confocal microscope (Olympus Corporation, Japan) was used to image DRG containing alginate fibre sections placed in a 2-well Permax Plastic Chamber Slide System (Fisher Scientific) and mounted in anti-fade mounting medium containing n-propyl gallate. The anti-fade medium was prepared from a stock solution of 20% w/v n-propyl gallate (Sigma P3130) in DMSO by first thoroughly mixing 1 part of D-PBS with 9 parts of glycerol (ACS grade, 99%–100% purity), after which 0.1 part of the n-propyl gallate solution was slowly added (drop-wise) with rapid stirring. Stacks of 2-dimensional parallel longitudinal images of the fibres (i.e. parallel to the fibre axis), were acquired using laser excitation at 405 nm and emission detection at 461 nm in conjunction with a 10 \times objective lens with numerical aperture of 0.4.

Imaging of immunolabelled of DRG-loaded alginate fibres was performed using laser excitation at 559 nm for Cy-3 with emission detection at 564 – 664 nm. The image size was 640 \times 640 pixels, with each pixel corresponding to 1.9884 μ m in the X and Y directions. Images were acquired using a Z-axis spacing of 8 μ m.

5.4 RESULTS AND DISCUSSION

Primary rat DRG cells were successfully encapsulated in alginate fibres using wet

spinning wherein a suspension of cells (6.25×10^3 cells/mL) and gelatin particles ($<90 \mu\text{m}$, 57% w/w) in alginate solution (1.5% w/w), was extruded through a syringe needle into 0.5 M CaCl_2 solution used as a crosslinking/gel forming agent for the alginate phase. The gelatin particles were employed as porogens to provide a macroporous fibre structure and simultaneously to provide cell adhesion molecules (CAM) for modification of macropore surfaces. The aim was to provide space and a favourable adhesive pore surface to promote nerve cell attachment and growth within the polysaccharide fibre structure. DRG-containing non-macroporous alginate fibres were produced by spinning DRG suspensions in alginate solution without gelatin particles and showed no significant cell growth up to day 15 (Figure 5.5). Magnified images of the fibre showed the translucent appearance of the alginate fibre with characteristic ‘chevron-like’ flow markings (Figure 5.5A) and the presence of rounded, highly separated cells. An isolated example of neurite extension and network formation (arrowed) by DRG cells was observed at day 5 (Figure 5.5B and 5.5C). During “neuritogenesis” (formation of neurites), spherical neurons differentiate and form membrane projections or dynamic extensions (outgrowths) called neurites that could later become dendrites or axons. Neuronal axons elongate from the growth cone at the axon tip and subsequently form synaptic contacts with other neurons. Matyash et al. showed that non-functionalised alginate hydrogel supports neural adhesion, and abundant neurite outgrowth (on the surface) and penetration into the hydrogel (up to $1000 \mu\text{m}$), creating a three-dimensional network by day 10 *in vitro* [235]. Krantis et al. [290] reported extensive neurite outgrowth from cryopreserved DRG neurons on day 2 – 3 culture on micro-ruled Cellattice™ coverslips in 96-well plate. Likewise, adult mouse DRG neurons (cell size up to $50 \mu\text{m}$) were also shown to generate long myelinated axons ($100 - 200 \mu\text{m}$) at day 3 in cell culture [287]. The virtual absence of neurite outgrowth in the present study indicates that nerve cells are

efficiently encapsulated within the alginate hydrogel matrix and there is no pore and channel structure of dimensions sufficient to accommodate neurite growth. In addition, biodegradation of the matrix is not adequately advanced at day 15 to allow neurite growth through a weakened hydrogel structure.

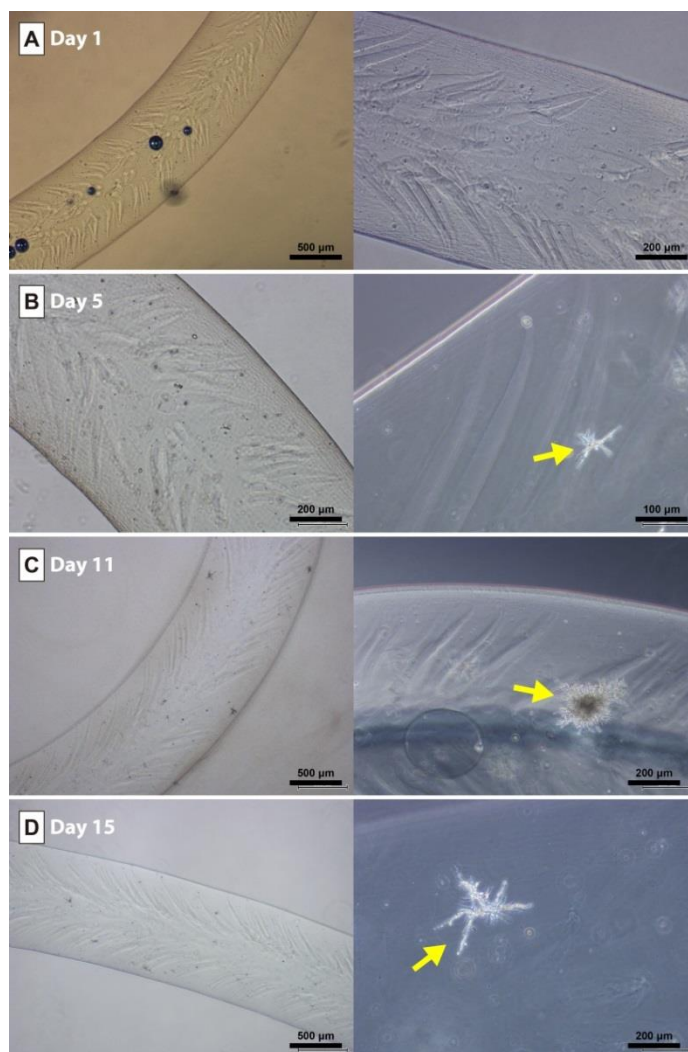


Figure 5.5 Bright field microscopy images of DRGs encapsulated in a non-macroporous alginate fibre at Day 1 (A), Day 5 (B), Day 11 (C) and Day 15 (D) in cell culture.

In contrast, DRG cells encapsulated in alginate fibres that developed macroporosity on extraction of incorporated gelatin particles developed a branched neurite structure,

and cell–cell contact was observed at day 9 (Figure 5.6). On day 1, undissolved gelatin particles, approximately 50 – 200 μm in size are evident in the fibres (Figure 5.6A). By day 2 (Figure 5.6B), the majority of the gelatin particles had been extracted, which would have served to increase the internal macroporosity. Rapid gelatin release from alginate fibres was discussed in Chapter 2. On day 5 (Figure 5.6C) and similar to non-macroporous fibres, the first evidence of neurite outgrowth and branching was observed over a distance of around 40 μm (arrowed). By day 9 (Figure 5.6D), cell–cell contact was evident, and at day 11 (Figure 5.6E), extensive neurite outgrowth and spreading within the alginate fibre was confirmed. This behaviour indicates formation of a channel structure within the alginate hydrogel which supports neurite extension.

Alginate hydrogels are known to be non-adhesive for cultured cells in general and have thus been functionalised with molecules, such as fibronectin [291] or peptides (i.e. Tyr-Ile-Gly-Ser-Arg (YIGSR) [109] to enhance neuron growth. In the present study, extensive neurite outgrowth was observed in macroporous alginate fibres produced by wet spinning alginate solution containing DRGs and gelatin particles. The gelatin particles were employed as porogens to provide a macroporous fibre structure and simultaneously to provide cell adhesion molecules (CAM) for modification of macropore surfaces to promote nerve cell attachment and growth. The investigations described in Chapter 3 revealed protein residues lining the macropore cavities formed by gelatin extraction (Chapter 3, Figure 3.12B). However the extensive dendrite outgrowth observed at day 11 (Figure 5.6E), suggests that the pores and channels in the alginate hydrogel phase, external to the macropores have also been modified by cell adhesion molecules. This condition may have been accomplished by adsorption of CAMs from the culture medium (e.g. fibronectin) and gelatin molecules during extraction of the gelatin particles. The release experiments reported in Chapter 2 demonstrated that 50% of the original gelatin content of the

fibres was retained following 2 days in release medium.

Further observations of the morphology of DRGs encapsulated in alginate fibre are presented in Figure 5.7. The early stage of neurite outgrowth (day 1 – 5) appears to show a pseudounipolar-DRG-like neuron (Figure 5.7 A-C). DRGs aggregate in balls and extend multiple neurites becoming a densely branching network after 9 days (Figure 5.7 E and F). Evidence of neuronal contacts is shown in Figure 5.7G and 5.7I. Flavin coenzymes and reduced nicotinamide adenine dinucleotide (NADH) are the most commonly observed autofluorescent molecules in mammalian cells. NADH and flavin adenine dinucleotide (FAD) have been found to contribute in major part to rat DRG neuron autofluorescence excited by UV (~365 nm) and blue (~435 nm) excitation light respectively, through modulation of the cellular metabolism with cyanide (CN) and carbonyl cyanide 4-(trifluoromethoxy)phenyl-hydrazone (FCCP) [292]. In the present study, DRG cells encapsulated within the alginate fibre were autofluorescent when excited with UV at wavelength 350 nm and emission maximum at 460 nm, Regions of dendrite branching and extension over a distance of approximately 150 μm in the alginate fibre, at day 15 in cell culture, are clearly visible in Figure 5.8.

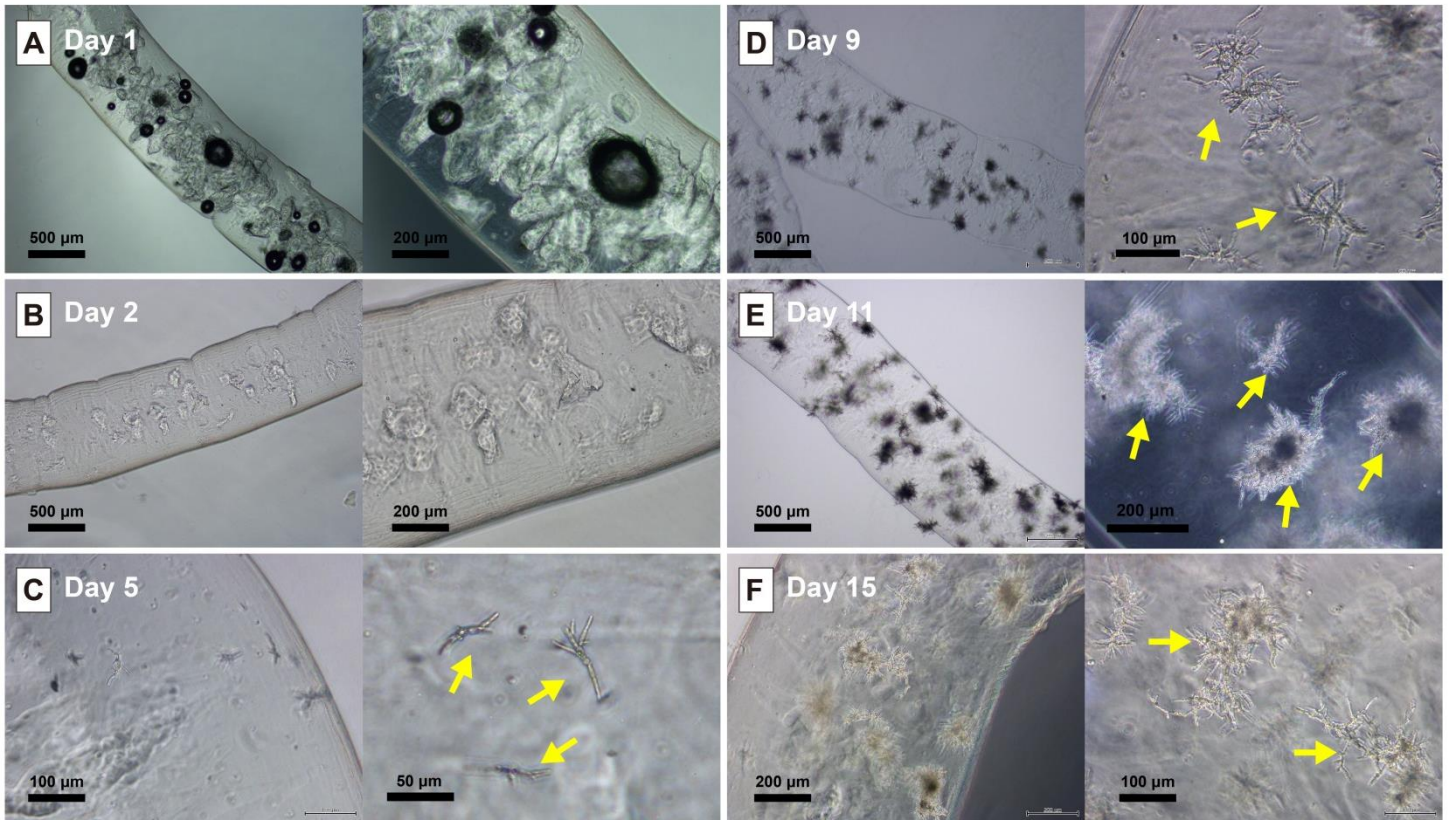


Figure 5.6 Bright field microscopy of DRGs encapsulated in a alginate fibre by wet spinning suspensions of cells and gelatin particles in alginate solution at Day 1 (A), Day 2 (B), Day 5 (C), Day 9 (D), Day 11 (E) and Day 15 (F) in cell culture.

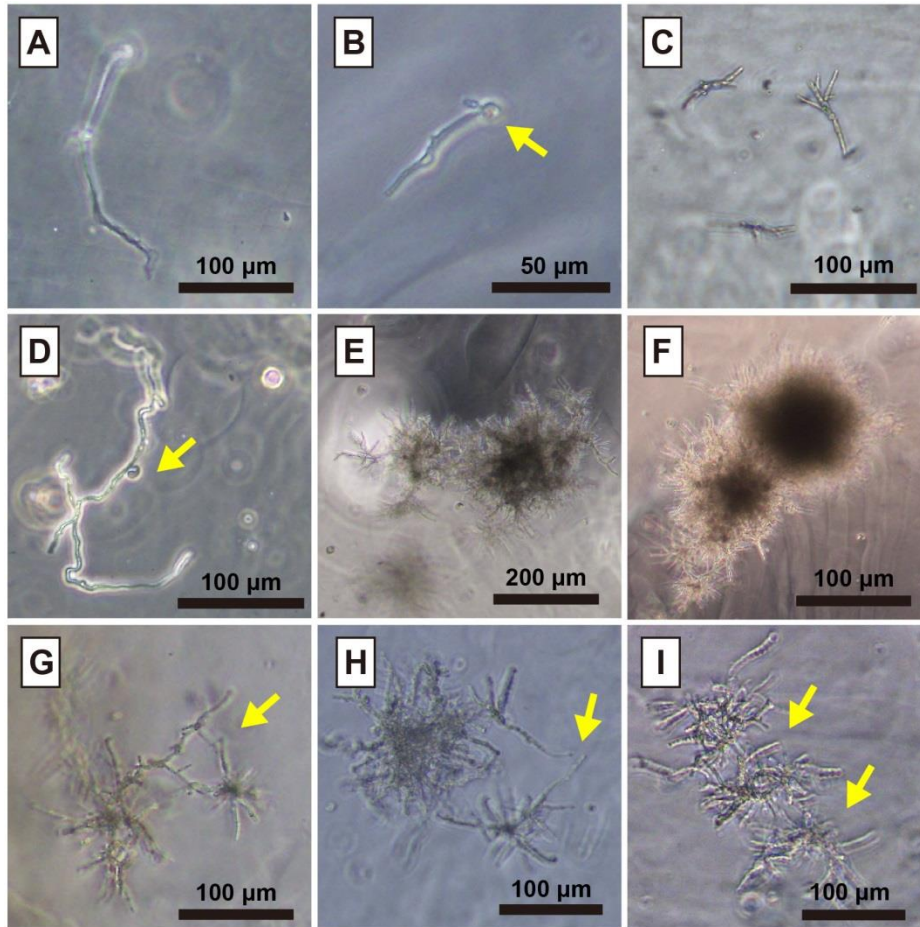


Figure 5.7 Morphology of DRGs encapsulated in alginate fibre and observed using inverted microscopy. (A–C) Early stage of neurite outgrowth at day 1 – 5, (D) a pseudounipolar-DRG-like neuron (E–F) DRGs aggregate in balls and extend multiple neurites becoming a densely branching network after 9 days, (G–I) evidence of neuronal contacts.

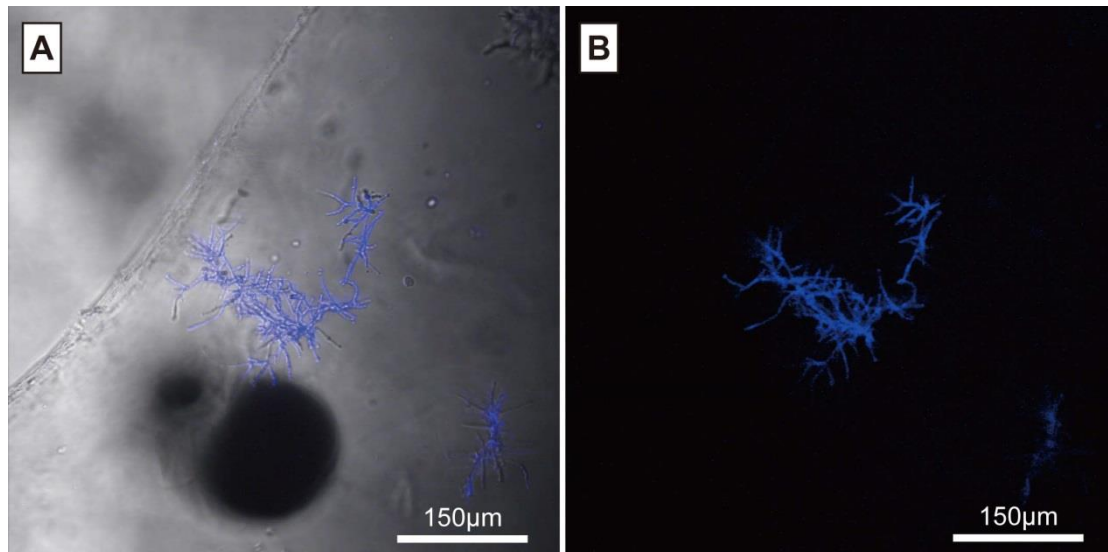


Figure 5.8 CLSM characterisation of dendritic outgrowth from rat DRG cells contained in a macroporous alginate fibre at day 15 in cell culture. (A) Superimposed DIC/autofluorescent and (B) autofluorescent images of the neurites.

DRG-containing fibre produced by wet spinning 1.5% w/v alginate solution containing DRGs (cell density 6.25×10^3 cells/mL) and gelatin particles (57% w/w) into 0.5 M CaCl_2 solution. Autofluorescence produced using UV at excitation wavelength 350 nm and emission maximum 460 nm.

Non-fluorescent Calcein-AM is converted to green-fluorescent calcein, after acetoxymethyl ester hydrolysis by intracellular esterases within viable cells. At day 2, DRG cells displayed outgrowth and varied cell soma (cell body) size (7 – 20 μm) when cultured by conventional 2D methods on tissue culture plastic (Figure 5.9). Live/dead staining with Calcein-AM of DRG-containing non-macroporous and macroporous alginate fibres were carried out on day 2 and day 5. Aggregates of DRGs were occasionally visible in non-macroporous alginate fibres at day 5 and outgrowths were generally absent (Figure 5.9B). The low DRG cell density within the macroporous alginate fibres is evident from Figure 5.10C, which reveals that the cells are widely distributed with a spacing of around 500–1000 μm . Calcein AM staining

revealed outgrowths or extensions from DRGs in macroporous alginate fibres at day 5 in culture (Figure 5.10D). However further studies described in Chapter 6, which included staining of cell nuclei, suggest that these outgrowths may consist of aggregates of DRG cells rather than neurite extension.

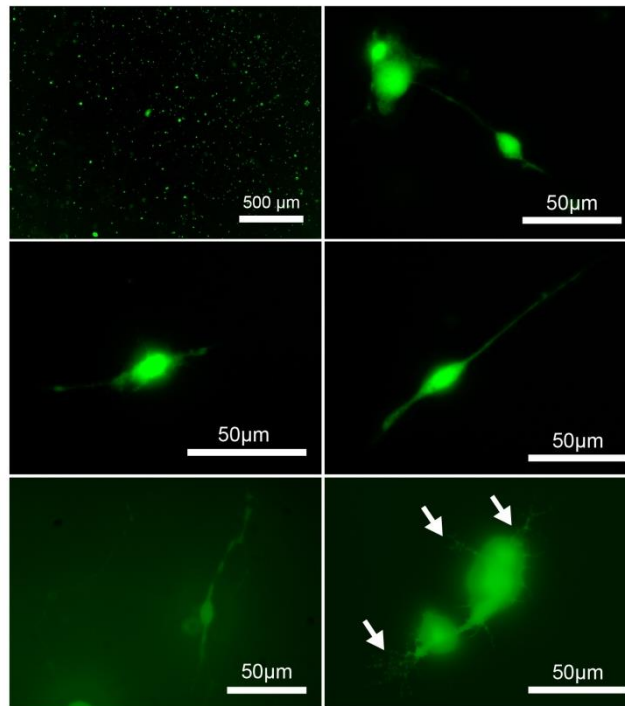


Figure 5.9 Rat dorsal root ganglion cells at 5 days in cell culture, subjected to live/dead assay by staining with Calcein-AM. Cells were seeded on 6-well plate at densities of 6.25×10^3 cells/mL. The DRG cells display outgrowth and varied cell soma size (7 – 20 μm).

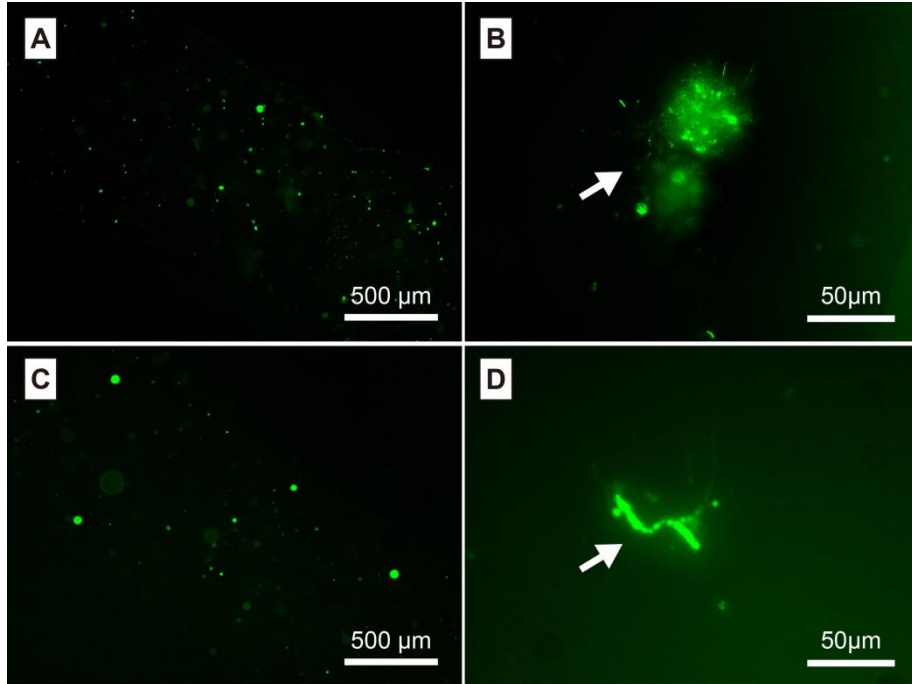


Figure 5.10 Live/dead staining assay using Calcein-AM of rat DRGs encapsulated in non-macroporous alginate fibre at (A) day 2, (B) day 5 in culture. Rat DRGs encapsulated in macroporous alginate fibre at (C) day 2 and (D) day 5 in culture.

DRG-containing macroporous alginate fibre produced by wet spinning alginate solution (1.5% w/v) containing DRG (cell density 6.25×10^3 cells/mL) and gelatin particles (57% w/w) into 0.5 M CaCl_2 solution. Gelatin particles omitted for production of DRG-containing non-macroporous fibres.

Investigations of immunolabelling of cryosectioned mouse retinal tissue were performed to determine the suitable dilutions and sample staining protocols for DRG cell-containing alginate fibres. Fluorescence micrographs for each dilution (1:100, 1:250, 1:500 and 1:1000) were acquired under the same settings and conditions for comparison. Mouse retina tissue presenting the ganglion cell layer was used as a positive control for the neuronal selective marker TU-20 antibody to ascertain the titer and specificity before applying to the DRG-loaded fibre sample. Immunolabelling using dilution of 1:1000 revealed that the concentration was too high, resulting high

background interference and possible non-specific binding of antibody. Dilution 1:100 on the other hand, was insufficient to yield a satisfactory signal for detection of neurons, especially when considering the thickness of the DRG loaded-alginate fibre (~800 μm). A dilution of 1:250 was found to be optimal for labelling (Figure 5.11B); the image showed clearly visible labelled cells and no sign of over exposure from background interference. Stained mouse retinal tissue (Figure 5.12) showed the axonal extension (green arrowed) of a ganglion cell (yellow arrowed) present in ganglion cell layer (stained red) for neuronal beta III tubulin.

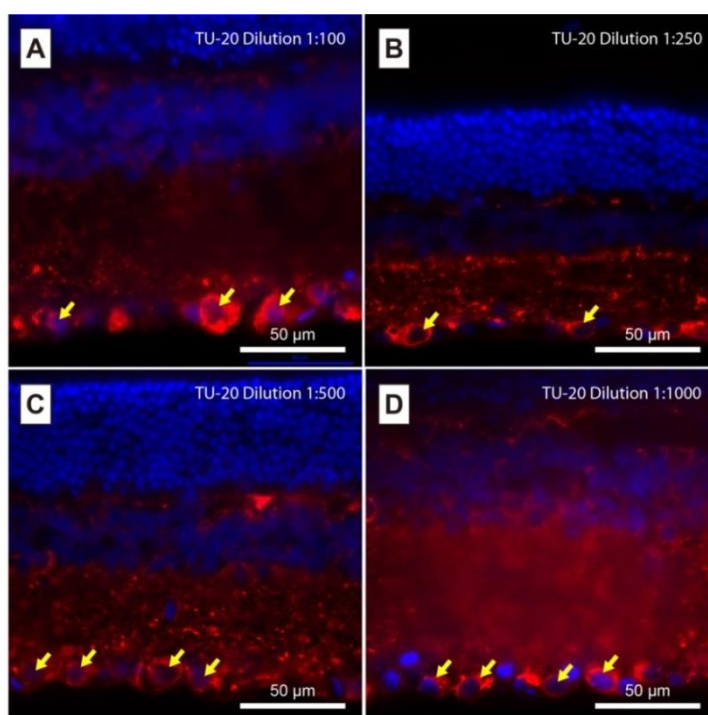


Figure 5.11 Imaging of mouse retinal tissues, labelled with Vectashield Anti-fade containing DAPI and TU-20, using fluorescence microscopy. Cryosections of mouse retina tissue were incubated for 24 h at 4 °C with anti- β -tubulin (TU-20) at dilution (A) 1:100, (B) 1:250, (C) 1:500 and (D) 1:1000. Cryosections were fixed in 4% paraformaldehyde for 15 min. and washed with copious D-PBS followed by incubation with primary antibodies (TU-20) for 24 h at 4 °C and with the secondary antibody (Cy3-conjugated Affinipure Donkey Anti-Mouse IgG) for 1 h at room temperature.

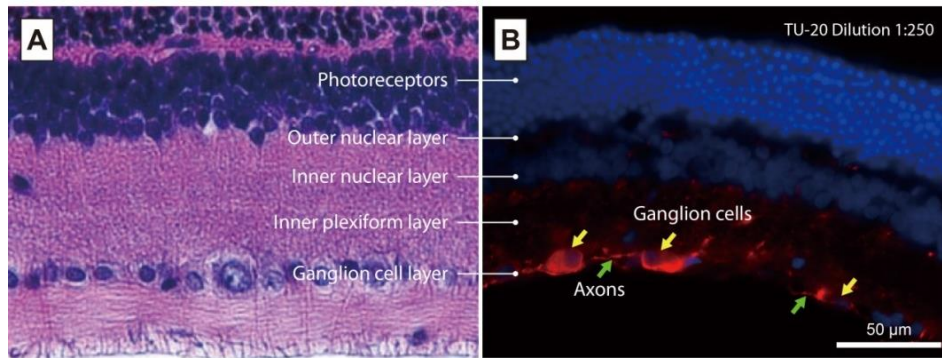


Figure 5.12 TU-20 was used as a marker to differentiate encapsulated neurons from glia. (A) Hematoxylin and eosin stain of normal rat retina [293]. (B) Cryosections of mouse retinal tissue labelled with anti- β -tubulin (TU-20) 1:250 dilution).

Prior to immunolabelling, alginate fibre cryosections were prepared using the method described in Section 5.3.1. However, the fibre sections became detached from the slides during rinsing with PBS. Furthermore, the labelling method for alginate fibre samples requires that the rinsing medium contains CaCl_2 (Dulbecco's (D) PBS was used) to avoid dissolution in normal PBS. Immunolabelling with TU-20 was therefore performed by soaking the fibre sections (approximately 0.5 cm) directly in the primary antibody for 48 h.

Immunolabelling of DRG cells in a macroporous alginate fibre at day 15 of cell culture with the neuronal selective marker, TU-20 (mouse monoclonal anti-tubulin-III antibody) is shown in Figure 5.13B. Neurite outgrowth is identified from DRG cells forming a network that extends approximately 200 μm in the hydrogel structure (white arrows). The DIC and fluorescence image (Figure 5.13A) corresponds with the specific TU-20 labelled neurites and provides a further measure of the spacing of such networks of around 500 μm . These observations suggest that nerve cell density within the alginate fibres should be increased by a factor of at least two to increase the probability of neurite contact.

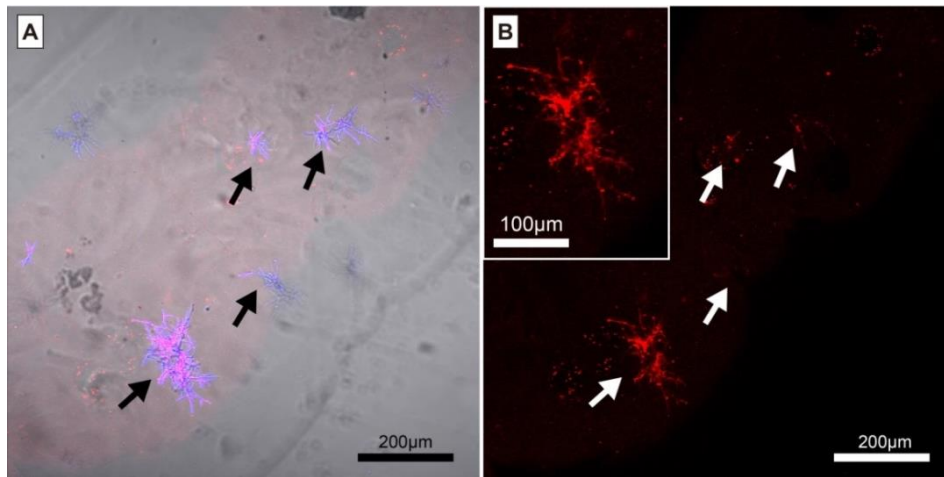


Figure 5.13 TU-20 (mouse monoclonal anti-tubulin-III antibody)-labelled DRG cells in a macroporous alginate fibre at day 15 of cell culture. (A) Superimposed DIC and fluorescence (arrowed black) and (B) TU-20 labelled images revealed neurites (arrowed white) encapsulated in the alginate fibre. Magnified view of highly branched neurite displayed in the selected field. DRG-containing alginate fibre produced by wet spinning 1.5% w/v alginate solution containing DRGs (cell density 6.25×10^3 cells/mL and gelatin particles 57% w/w) into 0.5 M CaCl_2 solution.

5.5 CONCLUSION

Rat DRG cells were encapsulated in macroporous alginate fibres for applications in nerve regeneration by wet spinning alginate solution containing a suspension of DRGs and gelatin particles. At day 5 in cell culture neurite outgrowth and branching was observed over a distance of around 40 μm. By day 9 cell–cell contact was evident, and at day 11 extensive neurite spreading was confirmed, indicating formation of a connected pore and channel structure within the alginate hydrogel. These findings indicate that macroporous alginate fibres encapsulating nerve cells may provide a useful strategy for nerve repair.

CHAPTER 6

Encapsulation of 661W Cone Photoreceptor Cells in Macroporous Alginate Fibre Scaffolds for Retinal Regeneration

ABSTRACT

Retinal degeneration including retinitis pigmentosa (RP) and age related macular degeneration (AMD) caused by progressive and eventual death of photoreceptor cells can eventually lead to blindness. Macroporous alginate fibres were produced by wet spinning alginate solution containing dispersed gelatin particles and cone photoreceptor-derived (661W) cells to investigate their potential as tissue engineering scaffolds for retinal repair. The gelatin particles were employed both as porogens and to provide cell adhesion molecules (CAM) for modification of macropore surfaces to promote photoreceptor cell attachment and proliferation within the poorly cell adhesive polysaccharide fibre structure. Significantly higher cell proliferation (* $P < 0.05$) was evident within macroporous fibres at day 14 in cell culture compared with non-macroporous fibres. Cell flattening and elongation with formation of cell extensions/projections was extensive in 2D culture on tissue culture plastic (TCP) but was not observed in 3D culture within the fibres, indicating that a suitable pore/channel structure for photoreceptor cell development was not created within the alginate hydrogel at 14 days in cell culture.

6.1 INTRODUCTION

The photoreceptor layer located at the back of the retina adjacent to the pigmented

epithelium comprises rods and cones whose function is to absorb light. Visual information produced by changes in photoreceptor cell membrane potential is processed in turn by bipolar, amacrine and horizontal cells and finally ganglion retinal cells that connect with the optic nerve (Figure 6.1).

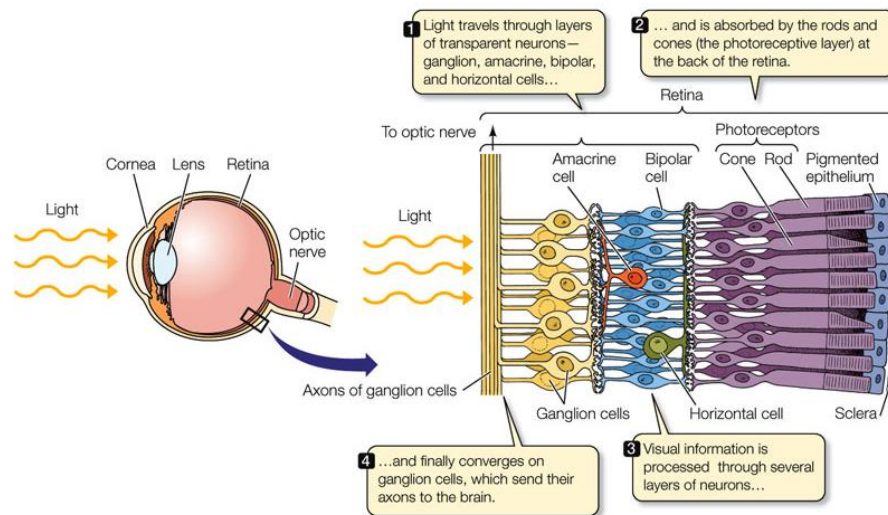


Figure 6.1 Photoreceptor cells in the retina of the eye [294].

Retinal degeneration including retinitis pigmentosa (RP) and age related macular degeneration (AMD) caused by progressive and eventual death of photoreceptor cells can eventually lead to blindness. Conventional treatments for AMD have focused on neuroprotective therapies, for example, using neurotrophic factors (e.g. brain-derived neurotrophic factor (BDNF)) [295], stem cells [296] or gene therapy (via subretinal injection) [297]. However, these approaches are confined to patients diagnosed at early stages of the disease with the aim of preventing further progression and functional deterioration. In the case of patients diagnosed at later stages of the disease, where loss of photoreceptor cells has occurred, cell transplantation has emerged as a key strategy to re-establish synapses with host retinal neurons and restore light-evoked electrical responses to regain retinal function [298]. However,

transplantation of photoreceptor precursor cells via bolus injection into the sub-retinal space (between the sensory retina and the retinal pigment epithelium) in animal models has shown lack of cell engraftment, limited cell integration and relatively low cell survival (less than 1% of the injected cells) [299] due to excessive shear forces generated during injection and movement of cells away from the injection site.

The application of tissue engineering principles whereby photoreceptor cells are integrated with a support structure or scaffold and exposed to growth (or neurotrophic) factors provides a means of addressing the problems of photoreceptor cell injection at defect sites in the retina. In line with general scaffold design criteria, the ideal scaffold material for retinal repair must be biocompatible, biodegradable and mechanically stable while not inducing immunogenic responses [300]. Earlier studies [301-303] have recommended that the scaffold should be relatively thin, less than 150 μm (compare the thickness of the photoreceptor layer of $155.6 \pm 12.6 \mu\text{m}$ in normal adults) [304] to avoid physical distortion of the overlying retina after transplantation. For example, Tomita et al. [301] fabricated a polymer scaffold from PLLA/PLGA ($10 \times 10 \text{ mm} \times 150 \mu\text{m}$) using a solid-liquid-phase separation technique to obtain a pore size of 35 – 50 μm and porosity of 95%. Prior to transplantation, retinal progenitor cells (RPCs) were seeded on upper and lower surfaces of the scaffold; one side was seeded for 3 days in culture followed by the reverse side for an additional 4 days. Scaffold/RPC composites were then cut into $500 \times 300 \mu\text{m}$ segments and transplanted into the subretinal space of rhodopsin knockout mice. The results showed enhanced RPC survival (by 10-fold) as well as improved cell delivery (by 16-fold) compared with a single injection of cells. Redenti et al. [303] fabricated thin laminin-coated poly(ϵ -caprolactone) (PCL) films ($6.00 \pm 0.70 \mu\text{m}$ thick) of vertically aligned nanowires by casting PCL solution onto nanoporous aluminum oxide (AAO) membranes using a spin coater followed by incubation in mouse laminin in PBS for

12 h to enhance adhesion of RPCs. The laminin coated-nanowire PCL films (1.0 × 0.5 mm), seeded with RPCs for 7 days in cell culture were transplanted into the subretinal space of rhodopsin knockout mice. High numbers of RPCs were observed to have differentiated and migrated into the inner nuclear layer (INL) and ganglion cell layer (GCL) of host retinal tissue directly adjacent to the site of transplantation [303].

In this chapter, mouse photoreceptor-derived (661W) cells were encapsulated in macroporous alginate fibres to investigate the potential for retina regeneration following AMD for example. 661W cells cloned from retinal tumours of a transgenic mouse line that expresses the simian virus (SV) 40 T antigen were shown to express photoreceptor-specific proteins such as cone blue opsin (SWS1), cone red or green opsin (L/MWS), transducin (G α T1), and cone arrestin (cArr) exhibited by cone photoreceptor cells [305]. Spindle-like processes displayed by 661W cells resemble neuronal cells. Cell viability in the fibre scaffolds was investigated by Calcein-AM staining and cell proliferation was monitored over 14 days in cell culture. The neuron-specific marker TUJ-1 was employed in combination with fluorescence microscopy to further identify morphological changes during cell development and proliferation.

6.2 MATERIALS

Sodium alginate (Protanal RF 6650, G:M 2:1) was obtained from IMCD Australia Limited. Calcium Chloride dihydrate (ReagentPlus®, $\geq 99.0\%$, C3881), Gelatin from porcine skin (Type A, Bloom 300, average molecular mass 50-100 kDa, G2500), Resazurin sodium salt (powder, BioReagent, suitable for cell culture, MW: 251.17, R7017-5G), Dimethyl sulphoxide (DMSO, anhydrous, $\geq 99.9\%$, 276855), Dulbecco's

phosphate-buffered saline (D-PBS; with MgCl₂ and CaCl₂, liquid, sterile filtered, suitable for cell culture, D8662) were purchased from Sigma-Aldrich Australia. Blue fluorescent Hoechst dye 33342 (cell permeable nucleic acid stain, H1399-100mg), Dulbecco's Modified Eagle Medium, Low Glucose (DMEM, containing 1 g/L D-Glucose, 11885-092), Calcein, AM (Special Packaging 20 × 50 µg, C3100MP), Penicillin-Streptomycin, Liquid (15140-122), Fungizone® Antimycotic, Liquid (15290-018), 0.25% Trypsin (1X), phenol red (15050-065) and Hank's balanced salt solution (HBSS, Calcium, Magnesium, no Phenol Red, 14025-092) were purchased from Invitrogen Australia. HyClone* Fetal Bovine Serum (GVD0074) was purchased from Thermo Scientific. Anti-β-Tubulin III (Anti-Tuj1) antibody produced in rabbit (T2200-200 µL), Formalin solution, neutral buffered, 10% (HT501128-4 L), Triton-X 100 (BioXtra, T9284-100 mL) were purchased from Sigma-Aldrich Australia. Goat anti-rabbit IgG (H+L) Secondary Antibody, Alexa Fluor® 594 conjugate (A11012-500 µL), Goat Serum, New Zealand origin (16210-064-100 mL) were purchased from Invitrogen Australia. Photoreceptor-derived cell line (661W) was provided by Dr John Wood, Ophthalmic Research Laboratories, Institute of Medical and Veterinary Science, Adelaide, SA.

6.3 METHODS

6.3.1 661W cell growth on tissue culture plastic (TCP)

661W cells growth medium was prepared using Dulbecco's modified Eagle medium (DMEM); containing 5mM glucose (440 mL), supplemented with 10% fetal bovine serum (FBS) (50 mL), 1% penicillin/ streptomycin solution (5 mL) and 1% fungizone (amphotericin B) (5 mL). The medium was stored at 4 °C until required.

Aliquots (1 mL) of 661W cells at a seeding density 4.5×10^3 cells/mL were added to

each well of 6-well plates. A further 1 mL of growth medium was added in each well and the cells were cultured for 4 h at 37 °C under a 5% CO₂ atmosphere. The growth medium was replaced with fresh medium after 4 h and then every 3 days up to 14 days.

6.3.2 Encapsulation of 661W cells in non-macroporous alginate fibres

Antiseptic techniques were strictly followed to prevent contamination. All instruments used (e.g. homogeniser, syringe pump) were sterilized by wiping the surfaces with 70% ethanol. Glassware and tools were autoclaved. 661W cell suspension (1×10^5 cells/mL, 1 mL) was added to 3 mL of 2% w/v alginate solution to achieve a final cell concentration of 2.5×10^4 cells/mL and alginate solution concentration of 1.5% w/v. Cells were mixed with the alginate solution by pipetting slowly up and down with a 3-mL disposable plastic syringe. The suspended cell/alginate solution (0.5 ml) was wet spun into 50 mL of 0.5 M CaCl₂ solution. The wet spun fibre was rinsed with D-PBS and then cut into 3 equivalent sections (5.5-cm length) that were each placed into a well of a 6-well plate. The cell loaded fibres were then cultured in 2 mL of culture medium (prepared as described in Section 6.3.1) for 4 h at 37 °C under a 5% CO₂ atmosphere. The medium was replaced with fresh medium after 4 h and then every day during the first 3 days and every second day thereafter, up to 14 days.

6.3.3 Encapsulation of 661W cells in macroporous alginate fibres

Gelatin type A (Porcine, Bloom 300, Sigma) was sieved through a 90- μ m mesh sieve. The powder was collected into a glass vial and sterilized by gamma irradiation at 1.25 kiloGray (kGy) for 3.5 hours [306]. Sterilized gelatin particles (<90 μ m, 200 mg) were added to cold (4 °C) filtered 2% w/v alginate solution (10 mL) followed by

homogenisation for 30 s using a homogeniser (IKA Ultra-Turrax® T25 Basic) under the cell culture hood to produce suspensions with gelatin:alginate w/w ratios of 4:3 (corresponding to 57% gelatin loading as a fraction of the total polymer content). 661W cell suspensions (1×10^5 cells/mL, 1 mL) were added to the suspension of gelatin particles in alginate solution (3 mL) to achieve a final cell concentration of 2.5×10^4 cells/mL and alginate solution concentration of 1.5% w/v. Cells were mixed in the gelatin particle/alginate solution by pipetting slowly up and down using a 3-mL disposable plastic syringe. The resulting suspension (0.5 mL) was wet spun into 50 mL of 0.5 M CaCl₂ solution. The wet spun fibre was rinsed with distilled water and cut into 3 equivalent sections (5.5-cm in length) that were each placed into separate wells of a 6-well plate. Cell-containing fibres were cultured in 2 mL of culture medium for 4 h at 37 °C under a 5% CO₂ atmosphere. The medium was replaced with fresh medium after 4 h and then every day in the first 3 days then every second day thereafter, up to 14 days.

6.3.4 Measurement of cell viability using the alamarBlue® Assay

Viable cells maintain a reducing environment within the cytoplasm. Alamar Blue reagent, resazurin dye (7-Hydroxy-3H-phenoxazin-3-one 10-oxide) is an oxidized form of redox indicator that is blue in colour and non-fluorescent. When incubated with viable cells, the reagent undergoes reduction of resazurin to resorufin by transferring electrons from NADPH+ H⁺ to resazurin. Post-reduction the blue resazurin colour changes into pink to highly red fluorescent resorufin which is consequently used as an oxidation-reduction indicator in cell viability and proliferation assays (Figure 6.2).

Resazurin powder (1.76 g) was dissolved in Hank's balanced salt solution (HBSS) (Ca⁺/Mg⁺, 100 mL) followed by filtration using a 0.2 µm syringe filter to sterilize the

solution. Stock solution (70 mM) was divided into 1.5mL aliquots and stored at - 20 °C. An aliquot of 70 mM stock resazurin was thawed and 20 µL was added to each well (containing samples in 2 mL culture medium) to produce a final concentration of 700 µM. Samples were incubated with resazurin dye for 3 hrs at 37 °C in a 5% CO₂ atmosphere and analyzed using a spectrophotometer AD200C microplate reader (Beckman Coulter). The level of reduction was quantified by spectrophotometry as resazurin exhibits an absorption peak at 600 nm and resorufin at 570 nm wavelength. The detected absorption values of test samples at each wavelength were corrected by deduction of the absorption values obtained from blank culture medium. The % reduction of alamarBlue® for each test sample was calculated using the following formula [307].

$$\% \text{ Reduction of resazurin} = \frac{(E_{oxi600} \times A_{570}) - (E_{oxi570} \times A_{600})}{(E_{red570} \times C_{600}) - (E_{red600} \times C_{570})}$$

E_{oxi570} : Molar extinction coefficient (E) of oxidized alamarBlue Reagent at 570nm = 80586

E_{oxi600} : E of oxidized alamarBlue Reagent at 600nm = 117216

A_{570} : Absorbance of test wells at 570nm

A_{600} : Absorbance of test wells at 600nm

E_{red570} : E of reduced alamarBlue at 570nm = 155677

E_{red600} : E of reduced alamarBlue at 600nm = 14652

C_{570} : Absorbance of negative control well (media, alamarBlue Reagent, no cells) at 570nm

C_{600} : Absorbance of negative control well (media, alamarBlue Reagent, no cells) at 600nm

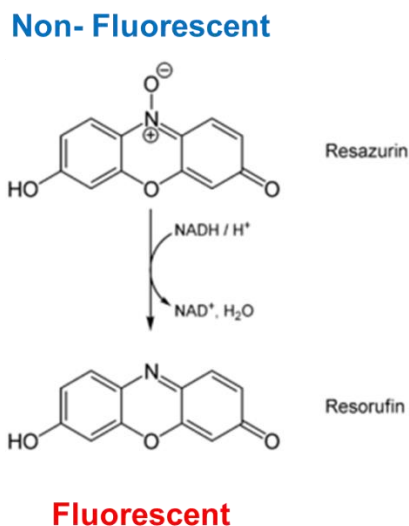


Figure 6.2 The reduction reaction of resazurin dye.

6.3.5 Immunolabelling of 661W cells grown on TCP or encapsulated in alginate fibres using β -tubulin III antibody

0.1% (v/v) Triton-X 100 buffer in D-PBS (DPBS-T 0.1%) was prepared by addition of 500 μ L Triton-X 100 to D-PBS (499.5 mL). Blocking buffer, 5% Normal Goat Serum (NGS) in DPBS-T 0.1%, was prepared by addition of NGS (5 mL) to DPBS-T 0.1% (95 mL). Preparation of 1% Normal Goat Serum for antibody dilution involved the addition of NGS (1 mL) to DPBS-T 0.1% (99 mL).

Immunolabelling of 661W cell cultured in 2D on tissue culture plastic (TCP) and cultured in 3D in alginate fibres was performed using neuronal class III β -tubulin (TUJ-1) rabbit monoclonal antibody. Class III β -tubulin is a microtubule element expressed predominantly in neurons of the central and peripheral nervous system [307], and is a popular selective marker for neurons in nervous tissue.

661W cells cultured on TCP and alginate fibres encapsulating 661W cells that had been cultured for 7 and 14 days were fixed by addition of 2 mL 10% neutral buffered formalin to each sample well of a 6-well plate for 20 minutes at room temperature. Samples were rinsed three times in D-PBS followed by addition of 0.1% Triton-X 100

buffer in D-PBS (2mL) to each well for 15 minutes then rinsed with D-PBS three times. This was followed by the addition of 2 mL 5% NGS in DPBS-T 0.1% for 15 minutes and rinsed with D-PBS three times. Primary antibody solution (rabbit anti- β -tubulin III, 1.5 mL, dilution 1:200 in 1% NGS) was added to each sample and incubated at 4 °C overnight. The next day, the antibody solution was removed and samples were rinsed with blocking buffer (5% Normal Goat Serum in DPBS-T 0.1%) three times.

Secondary antibody (goat anti-rabbit IgG (H+L), Alexa Fluor® 594 conjugate, 1.5 mL, dilution 1:500 in 1% NGS) was added to each well followed by incubation for 1 hour at room temperature in the dark. Post incubation, the secondary antibody solution was removed and samples were rinsed with D-PBS three times. D-PBS (1 mL) was added to each well prior to examination of samples using fluorescence microscopy (Nikon Eclipse TE2000-U). The instrument was equipped with CoolSNAP_{ES} camera and super high pressure mercury lamp (100 W). A standard filter set was utilised for image acquisition UV-2A (Alexa Fluor 594, Exc. 590 Emi 617).

6.3.6 Fluorescent labelling of 661W cell nuclei

Hoechst 33342 dye (2'-[4-ethoxyphenyl]-5-[4-methyl-1-piperazinyl]-2,5'-bi-1H-benzimidazole trihydrochloride trihydrate) (Figure 6.3) is a cell-permeable DNA stain that is excited by ultraviolet light and emits blue fluorescence at 460-490 nm. Hoechst 33342 dye binds preferentially to adenine-thymine (A-T) regions of DNA and exhibits fluorescence emission spectra that are dependent on dye:base pair ratios [308].

661W cells grown on TCP or encapsulated in alginate fibres were counterstained with Hoechst 33342 dye which was prepared by making a dilution of 1:500 from the stock solution (10 μ L added to 5 mL D-PBS). Samples were incubated for 15 minutes at room temperature in the dark following the addition of 1.5 mL dye solution to each

sample well. Post incubation, cells grown on TCP and cell-containing alginate fibres were rinsed with D-PBS 3 times prior to examination using a fluorescence microscope (Nikon Eclipse TE2000–U). The instrument was equipped with CoolSNAP_{ES} camera and super high pressure mercury lamp (100 W). A standard filter set was utilised for image acquisition G-2A (Hoechst 33342, Exc. 347, Emi. 483).

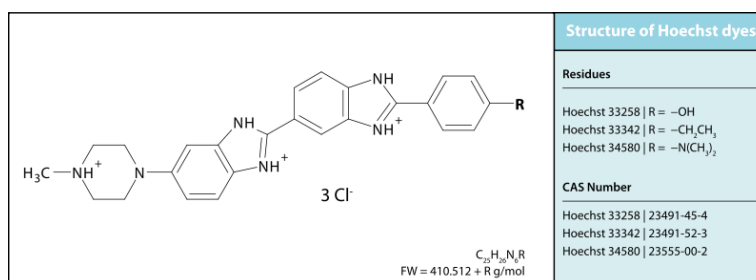


Figure 6.3 Hoechst 33342 stain for nucleic acid [309].

6.3.7 Assay of viability of 661W cells encapsulated in alginate fibres using Calcein-AM staining

Calcein acetoxymethyl ester (Calcein-AM) is a cell-permeating dye that may be used to determine the viability of most eukaryotic cells. In live cells the non-fluorescent Calcein-AM is converted to green-fluorescent calcein after acetoxymethyl ester hydrolysis by intracellular esterases (Chapter 4, Figure 4.4). Calcein-AM stock solution in anhydrous DMSO (1 mg/mL, 1 μ M) was prepared by adding 50 μ L of anhydrous DMSO ($\geq 99.9\%$) to 50 μ g of Calcein-AM. The prepared stock solution was stored at -20 $^{\circ}$ C in the dark. A working solution was prepared by pipetting 10 μ L of the stock solution into 9 mL of culture medium to achieve a concentration of 10 nM and 1 mL was added to alginate fibre samples containing 661W cells (approximately 1-cm sections). Samples were incubated at 37 $^{\circ}$ C under a 5% CO₂ atmosphere for 45 min followed by examination using fluorescence microscopy (Nikon Eclipse TE2000–U). The instrument was equipped with CoolSNAP_{ES} camera

and super high pressure mercury lamp (100 W). A standard filter set was utilised for image acquisition comprising B-2A (Calcein-AM, Exc. 494, Emi. 517).

6.4 RESULTS AND DISCUSSION

The growth characteristics of mouse photoreceptor-derived cell line (661W) in conventional 2D culture on TCP over 6 days (initial seeding density 4.5×10^3 cells/mL) are shown in Figure 6.4. 661W cells exhibited a rounded or ovular form at day 0 and transformed into a distinct flattened and spread morphology at day 3, characterised by spindle-like elongated central axes and cell contact via projected extensions (arrowed) [16]. Such extensions are anticipated to form connections with the bipolar, amacrine and horizontal cells in adjacent layers of the retina (Figure 6.1). The results of 661W cell immunolabelling with TUJ-1 and nuclear staining using Hoechst 33342 dye are shown in Figure 6.5. Positive staining with TUJ-1 provides a strong indication of the neuronal characteristics of the photoreceptor-derived cell line used in these studies and is consistent with the study reported by Wood et al. [310] showing 661W cells expressing the neuronal markers tau, β -III-tubulin, microtubule-associated protein (MAP)-1b, microtubule-associated protein 2 (MAP2), and PGP9.5.

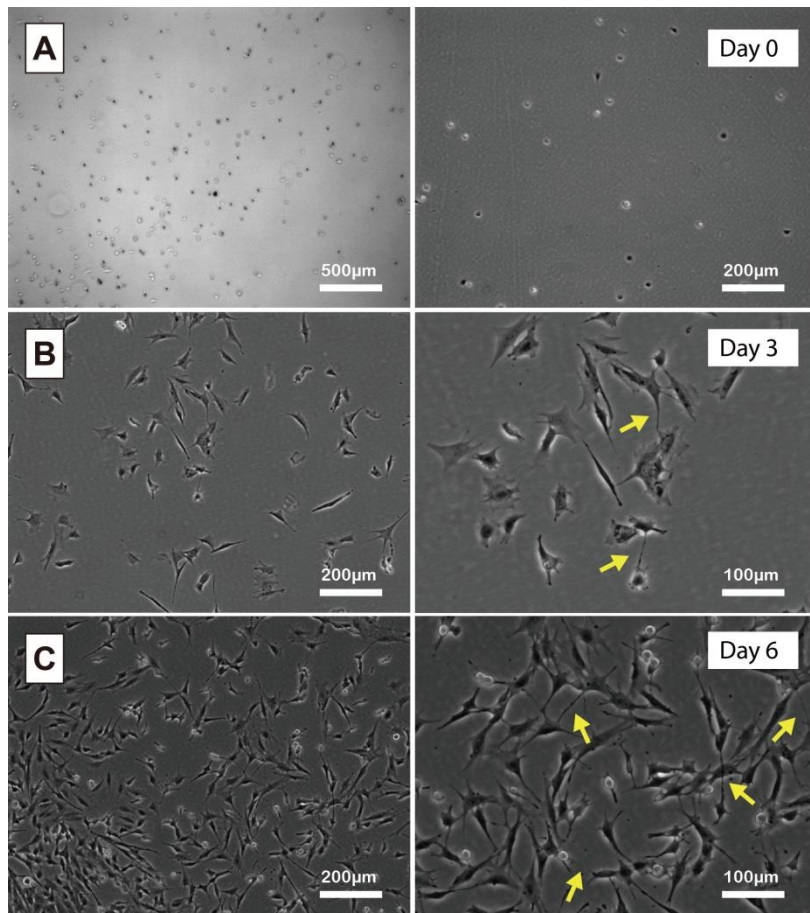


Figure 6.4 Phase contrast microscopy images of 661W culture on TCP at Day 0 (A), Day 3 (B) and Day 6 (C) in cell culture. Cells were seeded on 6-well plates at a density of 4.5×10^3 cells/mL.

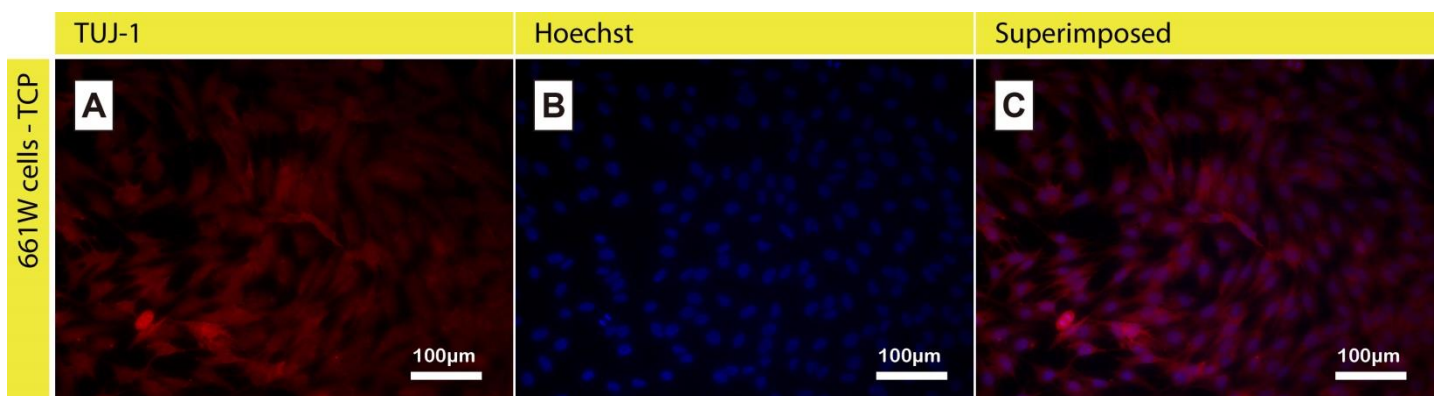


Figure 6.5 Fluorescence imaging of 661W cells cultured on TCP labelled with TUJ-1 (A) Hoechst dye reveals nuclear DNA in blue (B) resulting composite image (C) at day 7 in culture. Cells were seeded on 6-well plates at a density of 4.5×10^3 cells/mL.

Formalin fixed 661-W cells were permeabilized with 0.1% Triton X-100 in D-PBS for 15 minutes at room temperature and blocked with 5% NGS + 0.1% Triton X-100 for 15 minutes at room temperature. Cells were probed with primary antibody (TUJ-1) at 1:200 dilution for 24 h at 4 °C and with the secondary antibody (goat anti-rabbit IgG (H+L), Alexa Fluor® 594 conjugate) at 1:500 dilution for 1 h at room temperature. Nuclei (blue) were stained with Hoechst 33342 dye at 1:500 dilution for 15 minutes.

Photoreceptor-derived cells (661W) were successfully encapsulated in macroporous alginate fibres by addition of cell suspension to a pre-homogenised suspension of gelatin particles in alginate solution, followed by wet spinning into CaCl₂ solution. Cell encapsulated non-macroporous alginate fibres were produced by omitting the gelatin particles. Non-macroporous alginate fibres essentially entrapped 661W cells (Figure 6.6), in a hydrogel matrix and generally prevented cell growth and elongation to the spindle-like form, in contrast to 661W cells grown on TCP (Figures 6.4). Cells within the fibres retained the rounded form over 13 days in culture, similar to the behaviour of HDFa fibroblasts encapsulated in non-macroporous alginate fibres reported in Chapter 4 (Figure 4.13).

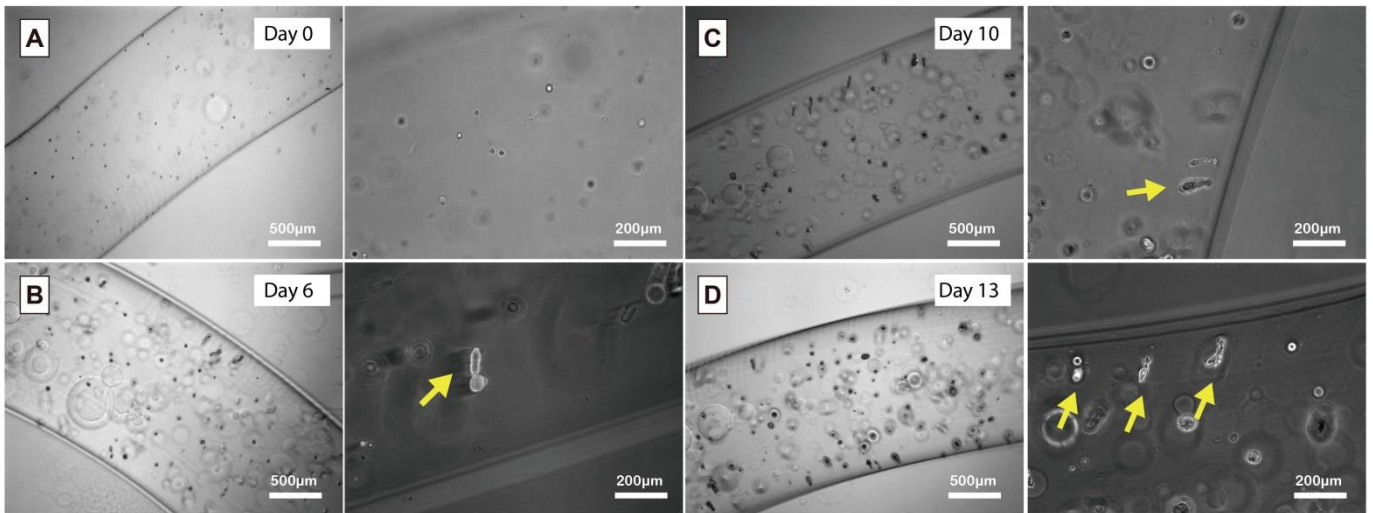


Figure 6.6 Differential interference contrast (DIC) images of 661W cells encapsulated in a non-macroporous alginate fibre at Day 0 (A), Day 6 (B), Day 10 (C) and Day 13 (D) in cell culture. Cell concentration of alginate spinning solution 2.5×10^4 cells/mL.

661W cells encapsulated in alginate fibres that developed macroporosity on extraction of incorporated gelatin particles also showed restricted cell growth. Formation of macropores (approximately 100-250 μm) in a translucent hydrogel matrix due to extraction of incorporated gelatin particles is indicated by day 1. In contrast to non-macroporous fibres, more cell clusters were observed at day 10 in macroporous samples (Figure 6.7C) indicating that the macropores, surface modified by gelatin (discussed in Chapter 3, Section 3.4) promote cell adhesion and localised proliferation. Clusters of proliferating 661W cells within a macropore in a macroporous alginate fibre are revealed by TUJ-1 and Hoechst 33342 staining in Figure 6.8D, E and F.

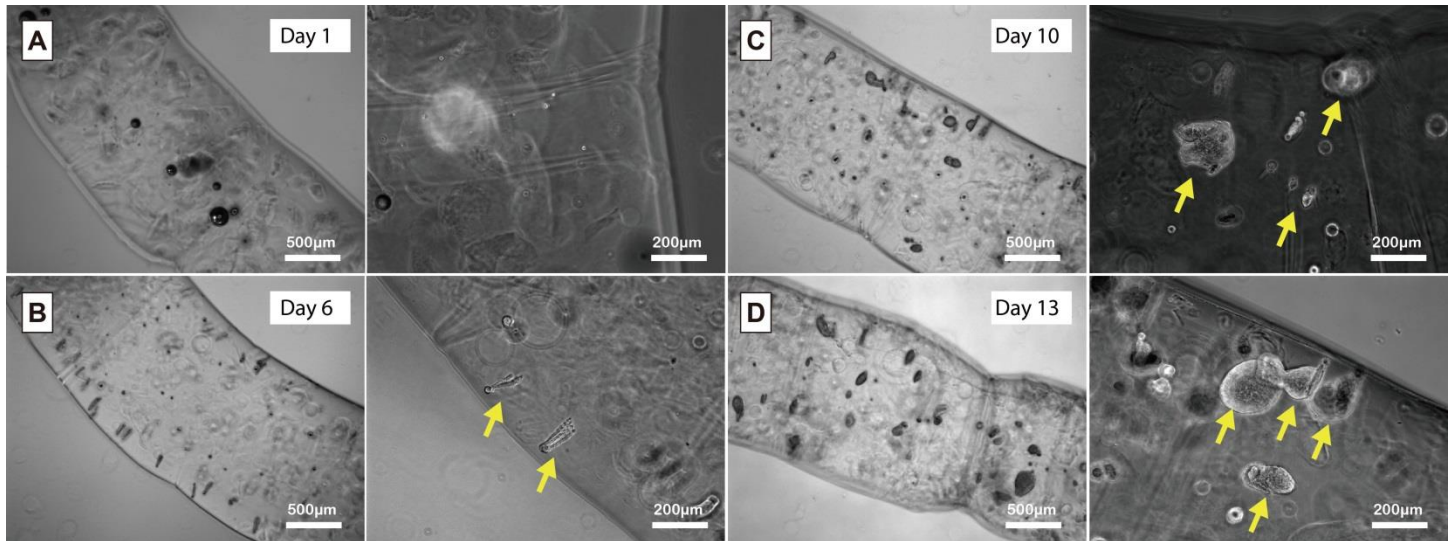


Figure 6.7 Differential interference contrast (DIC) images of 661W cells encapsulated in a macroporous alginate fibre at Day 1 (A), Day 6 (B), Day 10 (C) and Day 13 (D) in cell culture. Cell concentration of alginate spinning solution 2.5×10^4 cells/mL.

Non-macroporous and macroporous fibres both showed regions of elongated cell morphology at day 6 in culture (Figure 6.6B and 6.7B), which were initially thought to be single elongated cells similar to that observed with 3T3 fibroblasts encapsulated in alginate fibres (Chapter 4, Figure 4.8). However, counterstaining of cell nuclei with Hoechst 33342 dye revealed strings of proliferating cells within elongated pores or channels (Figure 6.8A, B and C).

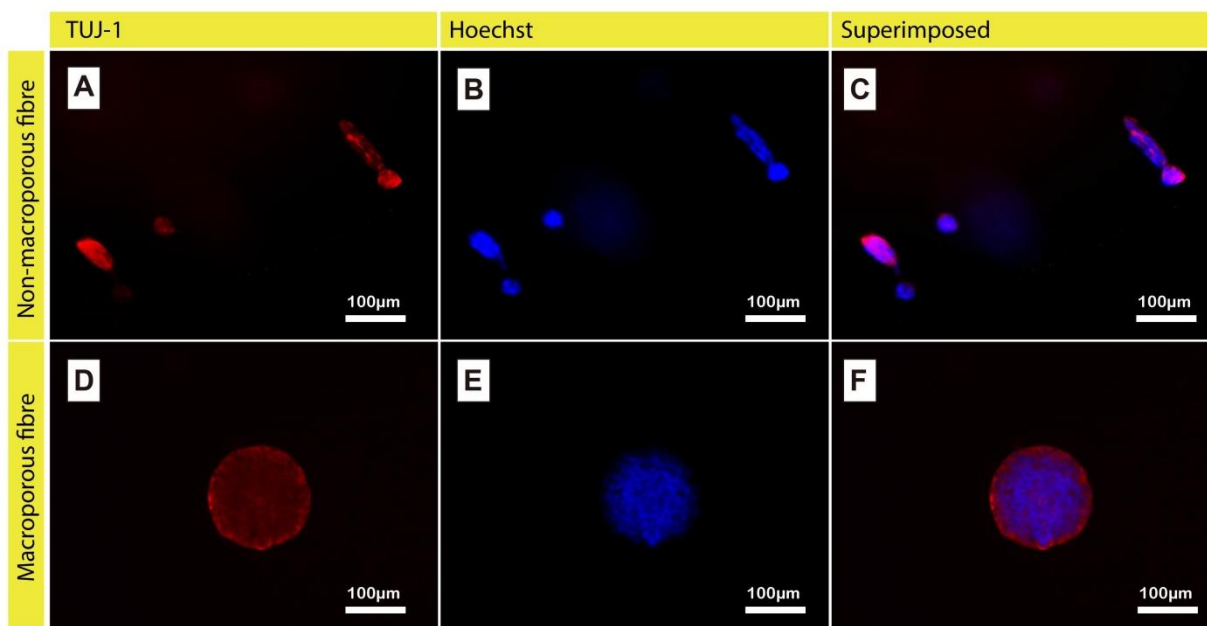


Figure 6.8 Fluorescence imaging of 661W cells encapsulated in non-macroporous fibre labelled with TUJ-1 (A) Hoechst 33342 dye (B) superimposed image (C) and in macroporous fibre labelled with TUJ-1 (D) Hoechst dye (E) superimposed image (F). 661W-containing macroporous alginate fibre produced by wet spinning 1.5% w/v alginate solution containing 661W cells (density 2.5×10^4 cells/mL) and gelatin particles 57% (w/w) into 0.5 M CaCl_2 solution. Non-macroporous fibres produced by omitting the gelatin particles.

Positive staining of 661W cells with Calcein-AM in non-macroporous and macroporous alginate fibres (Figure 6.9) showed that cell viability was maintained for 14 days in culture medium, highlighting the known capacity of alginate hydrogel matrices for permitting efficient transfer of nutrients and oxygen to encapsulated cells. Clustering of proliferating cells within macropores in both fibre types was observed. However there was no evidence of cell elongation to the spindle shape with formation of projections or extensions in contrast to the cells cultured on TCP (arrowed in Figure 6.4), indicating that a system of interconnected pores and channels suitable for

cell elongation had not been formed at 14 days in cell culture. Breakdown of the alginate hydrogel matrix would seem to be required to permit development of encapsulated photoreceptor cells. However it is interesting to note that extensive neurite outgrowth was observed for DRGs in macroporous fibres (Chapter 5, Section 5.4, Figure 5.6), highlighting the different response of cells to scaffold structure depending on cell type.

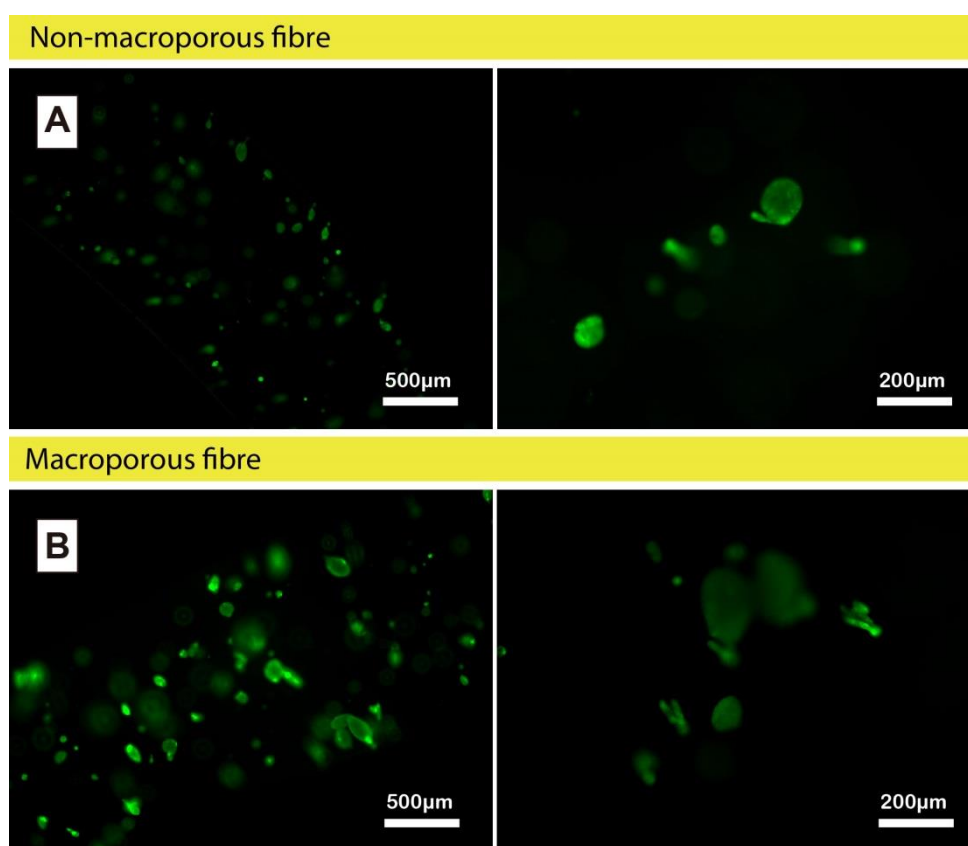


Figure 6.9 Live/dead staining assay using Calcein-AM of 661W cells encapsulated in non-macroporous alginate fibre (A) and macroporous alginate fibre (B) at day 14 in culture. 661W-containing macroporous alginate fibre produced by spinning alginate solution (1.5% w/v) containing 661W cells (density 2.5×10^4 cells/mL) and gelatin particles (57% w/w) into 0.5 M CaCl_2 solution. Gelatin particles omitted for production of 661W-containing non-macroporous fibres.

At day 1 in cell culture the reduction (%) of resazurin to resorufin by mitochondria (thus providing a measure of cell number) for (i) cells cultured on TCP (ii) cells encapsulated in non-macroporous fibre and (iii) cells encapsulated in macroporous fibre was $0.7 \pm 0.3\%$, $1.7 \pm 0.6\%$ and $0.3 \pm 0.5\%$ respectively. The initial cell seeding density on TCP (1 mL per well) was 4.5×10^3 cells. The cell density in the fibre spinning solution was 2.5×10^4 cells/mL and 0.5 mL (containing 1.3×10^4 cells) was wet spun into CaCl_2 solution to produce a fibre length of approximately 16.5 cm of fibre. Assuming no loss of cells during fibre spinning, the estimated number of cells per 5.5-cm sample used for cell culture equates to 4×10^3 cells. Thus the cell numbers cultured on TCP and encapsulated within the alginate fibre samples should be comparable. The differences in resazurin reduction at day 1 suggest that the cell numbers in the macroporous fibre are lower than in the non-macroporous fibres and compared with cell culture on TCP.

The increased level of resazurin reduction measured for 661W cells on day 14 in macroporous alginate fibres ($16.8 \pm 2.9\%$) compared with non-macroporous ($8.8 \pm 0.5\%$) fibre samples (Figure 6.10) indicates significantly higher cell proliferation (* $P < 0.05$) in the former samples. The inclusion of gelatin particles in the fibre as porogens followed by rapid protein extraction during the first day of cell culture was designed to increase the macroporosity of the fibres and facilitate cell growth. However, the low particle content of the fibres resulting in large inter-particle separation and low macroporosity of the fibres (around 14%) precludes the formation of interconnections between macropores due to initial particle-particle contact. Thus extensive cell growth throughout the fibre would not be expected. However, clustering of proliferating cells within macropores was evident (Figures 6.7, 6.8, 6.9) and probably explains the higher cell proliferation in macroporous fibres. The protein residues which were observed to line the macropore surfaces or pore cavities (Chapter

3, Figure 3.12B) are also expected to provide a cell adhesion property and enhance the attachment of encapsulated 661W cells to the alginate hydrogel matrix. It should be noted that the cell numbers in non-macroporous and macroporous fibres may be different and the above explanation may be invalid. The differences in % resazurin reduction at day 1 indicate that the cell numbers in the macroporous fibre are lower than in the non-macroporous fibres, suggesting cell loss during fibre spinning. Further work is required, therefore, to determine 661W cell numbers within the fibres (e.g. by cell extraction and counting or quantification of DNA or CLSM analysis of image stacks (Chapter 4, Figure 4.5) in order to clarify this issue.

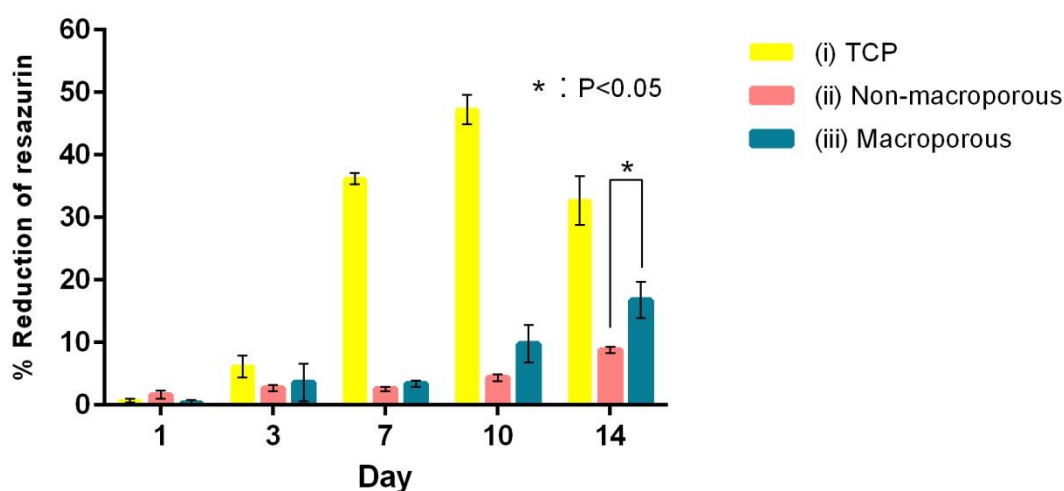


Figure 6.10 Resazurin assay of 661W cell proliferation in culture on TCP (cells were seeded on 6-well plates at a density of 4.5×10^3 cells/mL) (i) encapsulated in non-macroporous alginate fibre (ii) and encapsulated in macroporous alginate fibre (iii) (cell concentration of spinning solution 2.5×10^4 cells/mL). (Mean \pm SEM, One way ANOVA * $P < 0.05$, $n = 6$).

6.5 CONCLUSIONS

Mouse photoreceptor-derived (661W) cells were successfully encapsulated within macroporous alginate fibres using a technique based on wet spinning a suspension of cells and gelatin particle porogens in alginate solution. Cell-containing non-macroporous fibres were produced by wet spinning cell suspensions in alginate solution. Encapsulated 661W cells remained viable for 14 days in cell culture. Significantly higher cell proliferation was measured in macroporous fibres compared with non-macroporous fibres due to the formation of cell clusters within macropores, probably surface modified by gelatin residues. Formation of cell extensions/projections was extensive in 2D culture on TCP but was restricted in 3D culture within the fibres, indicating that a suitable pore/channel structure for photoreceptor cell development was not created within the alginate hydrogel at 14 days in cell culture.

CHAPTER 7

Overall Conclusions and Future Work

The overall aim of the research presented in this thesis was to develop an advanced nerve substitute based on tissue engineering principles by encapsulating nerve cells in an alginate hydrogel fibre scaffold. The production techniques established during the project could be widely applied in soft tissue engineering, for example for encapsulating genetically modified, growth factor-secreting cells. The research is also expected to provide strategies for developing “model” nerves for studying the causes and determinants of disease progression (e.g. multiple sclerosis) and for screening new drugs.

Alginate fibres were successfully produced by wet spinning and modified by gelatin by a) protein adsorption b) wet spinning into gelatin/CaCl₂ solution c) wet spinning from a mixed alginate/gelatin solution and d) suspending gelatin particles in the alginate spinning solution (Chapter 2). The first three approaches were intended to improve nerve cell adhesion to the alginate scaffold since polysaccharides inherently exhibit poor cell adhesion properties. Gelatin modification of hydrated and dried alginate fibres by adsorption from gelatin solution resulted in retention of 50% and 90% respectively of the protein content after incubation in distilled water at 37 °C for 3 – 4 days, indicating the potential for provision of a cell-adhesive surface. Alginate fibres incorporating gelatin particles as porogens up to a loading of 24% w/w were successfully produced by wet spinning suspensions of gelatin particles in alginate solution. Around 45 – 60% of the gelatin content of hydrated fibres was released in 1 h in distilled water at 37 °C, suggesting that a macroporous structure, potentially advantageous for nerve cell growth, would be rapidly established in cell culture.

Furthermore the residual gelatin was expected to form a favourable surface for nerve cell adhesion and axonal extension.

Macroporous alginate fibres for application in nerve tissue engineering were produced by wet spinning suspensions of gelatin particles in alginate solution followed by extraction of gelatin (Chapter 3). CLSM image analysis exploited the autofluorescence properties of alginate and gelatin to provide detailed 3D reconstructions of the pore structure, macropore dimensions, pore size distribution, porosity and pore connectivity for correlation with fibre spinning conditions and subsequent cell ingrowth behaviour. A maximum macroporosity of 14.6% was obtained following particle extraction from 21% w/w gelatin-loaded alginate fibres. Importantly, CLSM revealed modification of the macropore surface by gelatin, which is expected to be advantageous for nerve cell adhesion and axonal extension.

Further work is recommended to investigate the influence of gelatin particle size and concentration on fibre macroporosity with the aim of optimising the pore structure and connectivity for neurite outgrowth and axonal development. Further study is also required to correlate pore interconnectivity with fibre spinning conditions and neurite extension. The image analysis method described in this chapter for measuring pore connectivity provides a useful basis for this study. However, future work would be suggested to validate the developed pore analysis method with the conventional technique such as Brunauer–Emmett–Teller (BET) surface area analysis.

Cell-containing alginate fibres were produced by wet spinning cell suspensions in alginate solution into CaCl₂ crosslinking solution as a precursor to investigations using nerve cells (Chapter 4). Swiss 3T3 mouse fibroblasts remained viable within non-macroporous fibres over 8 weeks in cell culture but cell elongation and cell-cell

contact was largely prevented. These findings recommend future work on encapsulation of genetically engineered cells within alginate fibres to secrete growth factors or hormones. The creation of macropores in alginate fibres by extraction of gelatin particles facilitated fibroblast elongation and cell-cell contact. On day 12 in cell culture, the density of adult human dermal fibroblasts in macroporous alginate fibres (3.6×10^2 cells/mm³) was significantly higher than non-macroporous fibres (1.4×10^2 cells/mm³) demonstrating that the macropores, probably surface modified by residual gelatin, enhance cell proliferation.

Controlled biodegradation of the alginate fibre could be investigated in future work to increase cell proliferation. Cell density influences cell–cell signalling and subsequently cell function including for differentiation and cell survival. Hence it is important to determine the optimal cell seeding density in the fibre for the cell type of interest in future studies. Moreover, quantification of dead cells could be carried out by Calcein-AM staining in combination with Ethidium Homodimer-1 (ETHD-1) in future work to differentiate between cell proliferation and viability.

Rat dorsal root ganglion (DRG) cells were encapsulated in macroporous alginate fibres for applications in nerve regeneration by wet spinning alginate solution containing a suspension of DRGs and gelatin particles (Chapter 5). At day 5 in cell culture neurite outgrowth and branching was observed over a distance of around 40 μ m. By day 9 cell–cell contact was evident, and at day 11 extensive neurite spreading was confirmed, indicating formation of a favourable connected pore and channel structure within the alginate hydrogel. These findings indicate that macroporous alginate fibres encapsulating nerve cells may provide a useful strategy for nerve repair but observations suggest that nerve cell density within the alginate fibres should be increased by a factor of at least two to increase the probability of neurite contact.

Photoreceptor-derived (661W) cells were successfully encapsulated within macroporous alginate fibres by wet spinning a suspension of cells plus gelatin particle porogens in alginate solution to investigate their potential as tissue engineering scaffolds for retinal repair (Chapter 6). Significantly higher cell proliferation was evident within macroporous fibres at day 14 in cell culture compared with non-macroporous fibres. Cell flattening and elongation with formation of cell extensions/projections was extensive in 2D culture on tissue culture plastic but was not observed in 3D culture within the fibres, indicating that a suitable pore/channel structure for photoreceptor cell development was not created within the alginate hydrogel at 14 days in cell culture. Future work is recommended to produce alginate fibres with a transverse pore structure and addition of neurotrophin that permits photoreceptor cell development and contact with adjacent bipolar, amacrine and horizontal neurons in the retina.

Future work is recommended to develop an advanced biomimetic nerve substitute based on alginate hydrogel fibres.

Incorporation of both neurons and glia in the fibres during fibre spinning is suggested such that they develop in close association (as in the natural axon growth cone/Schwann cell interaction) prior to insertion in the injury site (e.g. rat sciatic nerve model). A major advantage is that sustained cell viability within the fibre guide would avoid the need for nerve cell migration into and along the guide from damaged nerve ends following implantation. In the event of cell death within the nerve guide a repair process is expected to be triggered, similar to the response to transplanted autografts which lose viability.

Applying a layer of collagen to the outer surface of an alginate fibre nerve guide is suggested to model the epineurium. The epineurium (connective tissue cell layer comprising fibrocollagenous tissue formed from epineural cells) constitutes the outermost layer of peripheral nerves and provides structural support and protection to nerve fascicles. The applied collagen coating on the alginate fibres is designed to be remodelled by myofibroblast action in culture pre-implantation or *in vivo* and replaced by ECM.

Investigation of the effect of growth factors (e.g. NGF, glial-derived neurotrophic factor (GDNF)) on nerve cell development within alginate fibres is recommended by addition of growth factor to the cell-alginate spinning solution or prior encapsulation within the gelatin porogens.

REFERENCES

1. Tabata Y. Significance of release technology in tissue engineering. *Drug Discov Today*. 10(23-24): 1639-1646, 2000.
2. van Dijk J. G., Pondaag W., and Malessy M. J. Obstetric lesions of the brachial plexus. *Muscle Nerve*. 24(11): 1450-1461, 2001.
3. Huang Y. C., and Huang Y. Y. Biomaterials and strategies for nerve regeneration. *Artif Organs*. 30(7): 514-522, 2006.
4. Murugan R., and Ramakrishna S. Design strategies of tissue engineering scaffolds with controlled fibre orientation. *Tissue Eng*. 3(8): 1845-1846, 2007.
5. Heichelk, Peripheral motor neuron (n.d.) [Online image]. Retrieved June 21, 2015 from <http://heichelk.wikispaces.com/09.+Nervous+System>. Copyright 2015 Tangient LLC.
6. Kalat, James W. *Biological Psychology*, 9th ed. USA: Thompson Learning, 2007
7. Gamble H., Eames R. An electron microscope study of the connective tissues of human peripheral nerve. *J Anat*. 98:655–663, 1964.
8. Sunderland S., Bradley K. The cross-sectional area of peripheral nerve trunks devoted to nerve fibres. *Brain*. 72:428 – 449, 1949.
9. Sunderland S., Bradley K. Stress-strain phenomena in denervated peripheral nerve trunks. *Brain*. 84:125–127, 1961.
10. Rydevik B. L., Kwan M. K., Myers R. R., Brown R. A., Triggs K. J., Woo S. L., Garfin S. R. An in vitro mechanical and histological study of acute stretching on rabbit tibial nerve *J Orthop Res*. 8 (5): 694-701. 1990.
11. Stolinski C. Structure and composition of the outer connective tissue sheaths of peripheral nerve. *J Anat*. 186:123–130, 1995.
12. Bow K. Understanding nerve injury and recovery (July, 2014) [Online image].

Retrieved June 21, 2015 from

<http://www.klintneuro.com.au/insights/2014/7/29/understanding-nerve-injury-and-recovery>.

13. Griffin J. W., Hogan M. V., Chhabra A. B., Deal D. N. Peripheral nerve repair and reconstruction. *J Bone Joint Surg Am.* 95(23):2144-2151, 2013.
14. Nervous system (n.d.) [Online image]. Retrieved June 21, 2015 from http://intranet.tdmu.edu.ua/data/kafedra/internal/histolog/classes_stud/en/med/lik/pptn/1/09%20Nerve%20tissue.%20Nerve%20cells.%20Glial%20cells.%20Nerve%20fibers.%20Nerve%20endings..htm.
15. American medical forensic specialists. Acute nerve injuries (n.d.) [Online image]. Retrieved June 21, 2015 from <http://www.bailey-law.com/docs/acute-nerve-injuries.htm>.
16. Schnell E., Klinkhammer K., Balzer S., Brook G., Klee D., Dalton P., Mey J. Guidance of glial cell migration and axonal growth on electrospun nanofibres of poly- ϵ -caprolactone and a collagen/poly- ϵ -caprolactone blend. *Biomaterials.* 28(19): 3012-3025, 2005.
17. Bellamkonda R. V., "Peripheral nerve regeneration: an opinion on channels, scaffolds and anisotropy," *Biomaterials*, 27(19): 3515–3518, 2006.
18. Belkas J. S., Shoichet M. S., Midha R. Peripheral nerve regeneration through guidance tubes, *Neurological Research*, 26(2): 151–160, 2004.
19. Noble J., Munro C. A., Prasad V. S. S. V., Midha R. Analysis of upper and lower extremity peripheral nerve injuries in a population of patients with multiple injuries, *J Trauma.* 45(1):116-22, 1998.
20. Gartner L. P., Hiatt J. L: *Color textbook of histology*, 3rd ed. Philadelphia, Saunders. p 217, 2007
21. Kannan R. Y., Salacinski H. J., Butler P. E., Seifalian A. M. Artificial nerve

- conduits in peripheral-nerve repair. *J Biotechnol Appl Biochem.* 41(3):193-200, 2005.
22. Madison R. D., da Silva C., Dikkes P., Sidman R. L., Chiu T. H. Peripheral nerve regeneration with entubulation repair: comparison of biodegradable nerve guides versus polyethylene tubes and the effects of a laminin-containing gel. *Exp Neurol.* 95(2):378-90, 1987.
 23. Luciano R. M., de Carvalho Zavaglia C. A., de Rezende Duek E. A. Preparation of bioabsorbable nerve guide tubes. *Artif Organs.* 24(3): 206-208, 2000.
 24. Yang F., Murugan R., Ramakrishna S., Wang X., Ma Y. X., Wang S. Fabrication of nano-structured porous PLLA scaffold intended for nerve tissue engineering. *Biomaterials.* 25(10): 1891-1900, 2004.
 25. Nakamura T., Inada Y., Fukuda S., Yoshitani M., Nakada A., Itoi S., Kanemaru S., Endo K., and Shimizu Y. Experimental study on the regeneration of peripheral nerve gaps through a polyglycolic acid-collagen (PGA-collagen) tube. *Brain Res.* 1027(1-2): 18-29, 2004.
 26. Bender M. D., Bennett J. M., Waddell R. L., Doctor J. S., Marra K. G. Multi-channeled biodegradable polymer/CultiSpher composite nerve guides. *Biomaterials.* 25(7-8): 1269-1278, 2004.
 27. Verreck G., Chun I., Li Y., Kataria R., Zhang Q., Rosenblatt J., Decorte A., Heymans K., Adriaensen J., Bruining M., Remoortere M. V., Borghys H., Meert M., Peeters J., Brewster M. E. Preparation and physicochemical characterisation of biodegradable nerve guides containing the nerve growth agent sabeluzole. *Biomaterials.* 26(11): 1307-1315, 2005.
 28. Ciardelli G., Chiono V. Materials for peripheral nerve regeneration. *Macromol Biosci.* 6(1): 13-26, 2005.
 29. Huang Y-C., Huang Y-Y. Tissue engineering for nerve repair. *Biomed Eng Appl*

- Basis Comm. 18(3): 100-110, 2006.
30. Letourneau P. C., Condic M. L., Snow D. M. Interactions of developing neurons with the extracellular matrix. *J Neurosci.* 14(3): 915-928, 1994.
 31. Isabelle V, Lan T. Biodegradable Polymers. *Materials* 2: 307-344, 2009
 32. Letourneau P. C., Condic M. L., Snow D. M. Interactions of developing neurons with the extracellular matrix. *J Neurosci.* 14(3): 915-928, 1994.
 33. Klein C. L., Scholl M., Maelicke A. Neuronal networks in vitro: formation and organization on biofunctionalized surfaces. *J Mater Sci Mater Med.* 10(12): 721-727, 1999.
 34. Kato K., Utani A., Suzuki N., Mochizuki M., Yamada M., Nishi N., Matsuura H., Shinkai H., Nomizu M. Identification of neurite outgrowth promoting sites on the laminin alpha 3 chain G domain. *Biochemistry.* 41(35): 10747-10753, 2002.
 35. Shin H., Jo S., Mikos A. G. Biomimetic materials for tissue engineering. *Biomaterials.* 24(24): 4353-4364, 2003.
 36. Labrador R. O., Buti M., Navarro X. Influence of collagen and laminin gels concentration on nerve regeneration after resection and tube repair. *Exp Neurol.* 149(1): 243-252, 1998.
 37. Miller C., Shanks H., Witt A., Rutkowski G., Mallapragada S. Oriented Schwann cell growth on micropatterned biodegradable polymer substrates. *Biomaterials.* 22(11): 1263-1269, 2001.
 38. Zhang J., Oswald T. M., Lineaweaver W. C., Chen Z. R., Zhang G. J., Chen Z. W., Zhang F. Enhancement of rat sciatic nerve regeneration by fibronectin and laminin through a silicone chamber. *J Reconstr Microsurg.* 19(7): 467-472, 2003.
 39. Zhang Z., Yoo R., Wells M., Beebe T. P. Jr, Biran R., Tresco P. Neurite outgrowth on well-characterised surfaces: preparation and characterisation of chemically and spatially controlled fibronectin and RGD substrates with good bioactivity.

- Biomaterials. 26(1): 47-61, 2005.
40. Sigma Aldrich. Laminin [Online image]. Retrieved June 21, 2015 from <http://www.sigmaaldrich.com/life-science/biochemicals/biochemical-products.html?TablePage=21735645>). Copyright © 2015 Sigma-Aldrich Co. LLC.
 41. Fibronectin (October, 2008) [Online image]. Retrieved June 21, 2015 from <http://en.wikipedia.org/wiki/Fibronectin>. Copyright © 2008 CC BY-SA 3.0.
 42. IJkema-Paassen J., Jansen K., Gramsbergen A., Meek M. F. Transection of peripheral nerves, bridging strategies and effect evaluation. *Biomaterials*. 25(9): 1583-1592, 2004.
 43. Hanthamrongwit M., Reid W. H., Grant M. H. Chondroitin-6-sulphate incorporated into collagen gels for the growth of human keratinocytes: the effect of cross-linking agents and diamines. *Biomaterials*. 17(8): 775-780, 1996.
 44. Laemmel E., Penhoat J., Warocquier-Clerout R., Sigot-Luizard M. F. Heparin immobilized on proteins usable for arterial prosthesis coating: growth inhibition of smooth-muscle cells. *J Biomed Mater Res*. 39(3): 446-452, 1998.
 45. Pieper J. S., Oosterhof A., Dijkstra P. J., Veerkamp J. H., van Kuppevelt T. H. Preparation and characterisation of porous crosslinked collagenous matrices containing bioavailable chondroitin sulphate. *Biomaterials*. 20(9): 847-858, 1999.
 46. Chen P. R., Chen M. H., Sun J. S., Chen M. H., Tsai C. C., Lin F. H. Biocompatibility of NGF-grafted GTG membranes for peripheral nerve repair using cultured Schwann cells. *Biomaterials*. 25(25): 5667-5673, 2004.
 47. Kato Y., Onishi H., Machida Y. N-succinyl-chitosan as a drug carrier: water-insoluble and water-soluble conjugates. *Biomaterials*. 25(5): 907-915, 2003.
 48. Shi Z. Neoh K. G., Kang E. T., Wang W. Antibacterial and mechanical properties

- of bone cement impregnated with chitosan nanoparticles. *Biomaterials*. 27(11): 2440-2449, 2005.
49. Bunge R. P. The role of the Schwann cell in trophic support and regeneration. *J Neurol*. 242(1): S19-S21, 1994.
 50. Itoh S., Yamaguchi I., Suzuki M., Ichinose S., Takakuda K., Kobayashi H., Shinomiya K., Tanaka J. Hydroxyapatite-coated tendon chitosan tubes with adsorbed laminin peptides facilitate nerve regeneration in vivo. *Brain Res*. 993(1-2): 111-123, 2003.
 51. The Food Chemical Codex, (Source: <http://www.usp.org/food-ingredients/food-chemicals-codex>).
 52. King A. H. Brown seaweed extracts (alginates). Florida, CRC Press, 1983.
 53. Grasdalen S., Larsen S., Smidsrød, O. ¹³C-NMR studies of monomeric composition and sequence in alginate. *Carbohydr Res*. 68(1): 23-31, 1981.
 54. Haug A., Larsen B., Smidsrød O. A study of the constitution of alginic acid by partial acid hydrolysis. *Acta Chem Scand*. 20: 183-190, 1966.
 55. Haug A., Larsen B., Smidsrød O. Uronic acid sequence in alginate from different sources. *Carbohydr Res*. 32(2): 217-225, 1974.
 56. Haug A., Myklestad S., Larsen B., Smidsrød O. Correlation between chemical structure and physical properties of alginate. *Acta Chem Scand*. 21: 768-778, 1967.
 57. Penman A., Sanderson G. R. A method for the determination of uronic acid sequence in alginates. 25(2): 273-282, 1972.
 58. Smidsrød O., Haug A. Dependence upon the gel-sol state of the ion-exchange properties of alginates. *Acta Chem Scand*. 26(5): 2063-2074, 1972.
 59. Smidsrød O., Haug A., Whittington S. G. The molecular basis for some physical properties of polyuronides. *Acta Chem Scand*. 26: 2563-2564, 1972.

60. McDowell, R.H., 1977. Properties of alginates. London, Alginate Industries Ltd., 67 p. 4th ed.
61. Protan. Alginates. Chilton's Food Eng. Int. 11(2): 60, 1986a.
62. Kelco A. Hydrophilic derivatives of alginic acid for scientific water control. San Diego, Division of Merck and Co. Inc., 1976.
63. Guisan J. M. Immobilization of enzymes and cells. (Encapsulation of cells in alginate gels). Madrid, Institute of Catalysis, CSIC, Humana Press, 2006.
64. Grant G. T., Morris E. R., Rees D. A., Smith P. J. C., Thom D. Biological interactions between polysaccharides and divalent cations: The egg-box model. 32(1): 195–198, 1973.
65. McHugh D. J. (ed.) FAO Fisheries Technical Paper - Production and Utilization of Products from Commercial Seaweeds, Chapter 2 – Production, Properties and Uses of Alginate, Food and Agriculture Organization, Rome, 1987
66. Martinsen A., Skjåk-Bræk G., Smidsrød O. Alginate as immobilization material: I. Correlation between chemical and physical properties of alginate gel beads. Biotechnol Bioeng. 33(1): 79-89, 1992.
67. Agrawal C. M., Ong, J. L., Appleford M. R., Mani G. Introduction to biomaterials: Basic theory with engineering applications, Cambridge University Press, United Kingdom, 2013.
68. Constantinidis I., Rask I., Long R. C. Jr., Sambanis A. Effects of alginate composition on the metabolic, secretory, and growth characteristics of entrapped β TC3 mouse insulinoma cells. Biomaterials. 20(21): 2019-2027, 1999.
69. Stabler C. L., Sambanis A., Constantinidis I. Effects of alginate composition on the growth and overall metabolic activity of betaTC3 cells. Ann N Y Acad Sci. 961: 130-133, 2002.
70. Stabler C. Wilks K., Sambanis A., Constantinidis I. The effects of alginate

- composition on encapsulated beta TC3 cells. *Biomaterials*. 22(1): 1301-310, 2001.
71. Simpson N. E., Stabler C. L., Simpson C. P., Sambanis A., Constantinidis I. The role of the CaCl₂-guluronic acid interaction on alginate encapsulated betaTC3 cells. *Biomaterials*. 25(13): 2603-2610, 2004.
 72. Gu B., Cao Y., Du Q., Yang Y. Morphology of fibrefibres formed via thermally induced phase separation of polypropylene and liquid paraffin blend in stress-field. *Polymer Bulletin*. 43(2-3): 291-296, 1999.
 73. Yang F., Murugan R., Wang S., Ramakrishna S. Electrospinning of nano/micro scale poly(L-lactic acid) aligned fibrefibres and their potential in neural tissue engineering. *Biomaterials*. 26(15): 2603-2610, 2005.
 74. Yang S., Leong K. F., Du Z, Chua CK. The design of scaffolds for use in tissue engineering. Part I. Traditional factors. *Tissue Eng*. 7(6): 2001.
 75. Hou Q., Grijpma D. W., Feijen, J. Porous polymeric structures for tissue engineering prepared by a coagulation, compression moulding and salt leaching technique. *Biomaterials*. 24(11): 1937-1947, 2000. (FDM)
 76. Melchels F. P. W., Domingos M. A. N., Klein T. J., Malda J., Bartolo P. J., Hutmacher D. W. Additive manufacturing of tissues and organs. *Prog Polym Sci* 37:1079–1104, 2012.
 77. Leong K. F., Cheah C. M., Chua C. K. Solid freeform fabrication of three-dimensional scaffolds for engineering replacement tissues and organs. *Biomaterials* 24:2363–2378, 2003.
 78. Dalton P. D., Woodfield T., Hutmacher D. W. Snapshot: polymer scaffolds for tissue engineering. *Biomaterials* 30:701–702, 2009.
 79. Mota C., Puppi D., Chiellini F., Chiellini E. Additive manufacturing techniques for the production of tissue engineering constructs. *J Tissue Eng Regenerat Med*,

- 2012.
80. Swift K. G., Booker J. D. Rapid prototyping processes. In: Manufacturing process selection handbook. Butterworth-Heinemann, Oxford, pp 227–241, 2013.
 81. Xiong Z., Yan Y., Zhang R., Sun L. Fabrication of porous poly(L-lactic acid) scaffolds for bone tissue engineering via precise extrusion. *Scripta Materialia*. 45(11): 771-776, 2001.
 82. Gurr M., Mülhaupt R. Rapid prototyping. In: Krzysztof M, Martin M (eds) *Polymer science: a comprehensive reference*. Elsevier, Amsterdam, pp 77–99, 2012.
 83. Bose S., Suguira S., Bandyopadhyay A. Processing of controlled porosity ceramic structures via fused deposition. *Scripta Materialia*. 41(9): 1009-1014, 1999
 84. Shor L., Gucer S., Chang R., Gordon J., Kang Q., Hartsock L., An Y., Sun W. Precision extruding deposition (PED) fabrication of poly(ϵ -caprolactone) (PCL) scaffolds for bone tissue engineering. *Biofabrication* 1:015003, 2009.
 85. Arafat M.T., Lam C. X. F., Ekaputra A. K., Wong S. Y., Li X., Gibson I. Biomimetic composite coating on rapid prototyped scaffolds for bone tissue engineering. *Acta Biomater* 7:809–820, 2011.
 86. Seidi A., Ramalingam M., Elloumi-Hannachi I., Ostrovidov S., Khademhosseini A. Gradient biomaterials for soft-to-hard interface tissue engineering. *Acta Biomater*. 7(4):1441-51, 2011.
 87. Flynn L., Dalton P. D., Shoichet M. S. Fibre templating of poly(2-hydroxyethyl methacrylate) for neural tissue engineering. *Biomaterials*. 24(23): 4265-4272, 2003.
 88. Tong X., Hirai I. K., Shimada H., Mizutani Y., Izumi T., Toda N., and Yu P.

- Sciatic nerve regeneration navigated by laminin-fibronectin double coated biodegradable collagen grafts in rats. *Brain Res.* 663(1): 155-162, 1994.
89. Ceballos D., Navarro X., Dubey N., Wendelschafer-Crabb G., Kennedy W. R., and Tranquillo R. T. Magnetically aligned collagen gel filling a collagen nerve guide improves peripheral nerve regeneration. *Exp Neurol.* 158(2): 290-300, 1999.
 90. Dubey N., Letourneau P. C., Tranquillo R. T. Guided neurite elongation and schwann cell invasion into magnetically aligned collagen in simulated peripheral nerve regeneration. *Exp Neurol.* 158(2): 338-350, 1999.
 91. Hadlock T., Sundback C., Hunter D., Cheney M., Vacanti J. P. A polymer foam conduit seeded with Schwann cells promotes guided peripheral nerve regeneration. *Tissue Eng.* 6(2): 119-127, 2000.
 92. Sundback C., Hadlock T., Cheney M., Vacanti J. Manufacture of porous polymer nerve conduits by a novel low-pressure injection molding process. *Biomaterials.* 24(5): 819-830, 2003.
 93. Teng Y. D., Lavik E. B., Qu X., Park K. I., Ourednik J., Zurakowski D., Langer R., and Snyder E. Y. Functional recovery following traumatic spinal cord injury mediated by a unique polymer scaffold seeded with neural stem cells. *Proc Natl Acad Sci U S A.* 99(5): 3024-3029, 2002.
 94. Stokols S., Tuszynski M. H. The fabrication and characterisation of linearly oriented nerve guidance scaffolds for spinal cord injury. *Biomaterials.* 25(27): 5839-5846, 2004.
 95. Valentini R. F., Aebischer P., Winn S. R., Galletti P. M. Collagen- and laminin-containing gels impede peripheral nerve regeneration through semipermeable nerve guidance channels. *Exp Neurol.* 98(2): 350-356, 1987.
 96. Labrador R. O., Buti M., Navarro X. Peripheral nerve repair: Role of agarose

- matrix density on functional recovery. *Neuroreport*. 6(15): 2022-2026, 1995.
97. Saltzman W. M. *Tissue engineering (Principles for the design of replacement organs and tissues)*. New York, Oxford University Press, Inc., 2004.
 98. Tamada Y., Ikada Y. Fibroblasts growth on polymer surfaces and biosynthesis of collagen. *J Biomed Mater Res*. 28(7): 783-789, 1994.
 99. van Wachem P. B., Hogt A. H., Beugeling T., Feijen J., Bantjes A., Detmers J. P., van Aken W. G. Adhesion of cultured human endothelial cells onto methacrylate polymers with varying surface wettability and charge. *Biomaterials*. 8(5): 323-328, 1987.
 100. Curtis A. S., Forrester J. V., McInnes C., Lawrie F. Adhesion of cells to polystyrene surfaces. *J Cell Biol*. 1983(5 Pt 1): 1500-1506, 1983.
 101. Lydon M. J., Minett T. W., Tighe B. J. Cellular interactions with synthetic polymer surfaces in culture. *Biomaterials*. 6(6): 396-402, 1985.
 102. Chinn J., Horbett T., Ratner B., Schway M., Haque Y., Hauschka S. Enhancement of serum fibronectin adsorption and the clonal plating efficiencies of Swiss mouse 3T3 fibroblast and MM14 mouse myoblast cells on polymer substrates modified by radiofrequency plasma deposition. *J Colloid Interface Sci*. 127(1): 67-87, 1986.
 103. Horbett T. A., Schway M. B. Correlations between mouse 3T3 cell spreading and serum fibronectin adsorption on glass and hydroxyethylmethacrylate-ethylmethacrylate copolymers. *J Biomed Mater Res*. 22(9): 763-793, 1988.
 104. Weiss P. Experiments on cell and axon orientation in vitro: The role of colloidal exudates in tissue organization. *J Exp Zool*. 100(3): 353-386, 2005.
 105. Meyle J., Gültig K., Nisch W. Variation in contact guidance by human cells on a microstructured surface. *J Biomed Mater Res*. 29(1): 81-88, 1995.

106. Campos D. M., Gritsch K., Salles V., Attik G. N., Grosogeat B. Surface entrapment of fibronectin on electrospun PLGA scaffolds for periodontal tissue engineering. *Biores Open Access*. 3(3):117-26, 2014.
107. Yao L., Wang S., Cui W., Sherlock R., O'Connell C., Damodaran G., Gorman A., Windebank A., Pandit A. Effect of functionalized micropatterned PLGA on guided neurite growth. *Acta Biomater*. 5(2):580-588, 2009.
108. Liu X., Won Y., Ma P. X. Surface modification of interconnected porous scaffolds. *J Biomed Mater Res A*. 74(1):84-91, 2005.
109. Dhoot N. O., Tobias C. A., Fischer I., Wheatley M. A. Peptide-modified alginate surfaces as a growth permissive substrate for neurite outgrowth. *J Biomed Mater Res A*. 71(2):191-200, 2004.
110. Massia S. P., Hubbell J. A. An RGD spacing of 440 nm is sufficient for integrin alpha V beta 3-mediated fibroblast spreading and 140 nm for focal contact and stress fibre formation. *J Cell Biol*. 114(5): 1089-1100, 1991.
111. Shin H., Jo S., Mikos A. G. Modulation of marrow stromal osteoblast adhesion on biomimetic oligo[poly(ethylene glycol) fumarate] hydrogels modified with Arg-Gly-Asp peptides and a poly(ethyleneglycol) spacer. *J Biomed Mater Res*. 61(2): 169-179, 2002.
112. Shin H., Jo S., Mikos A. G. Modulation of marrow stromal osteoblast adhesion on biomimetic oligo(poly(ethylene glycol) fumarate) hydrogels modified with Arg-Gly-Asp peptides and a poly(ethylene glycol) spacer. *J Biomed Mater Res*. 61: 169-79, 2002.
113. Massia S. P., Hubbell J. A. An RGD spacing of 440 nm is sufficient for integrin alpha V beta 3-mediated fibroblast spreading and 140 nm for focal contact and stress fibre formation. *J Cell Biol*. 114: 1089-1100, 1991.
114. Mann B. K., Schmedlen R. H., West J. L. Tethered TGF-beta increases extracellular

- matrix production of vascular smooth muscle cells. *Biomaterials*. 22:439–44, 2001.
115. Ranieri J. P., Bellamkonda R., Bekos E. J., Vargo Jr. T. G., Aebischer J. A. G. Neuronal cell attachment to fluorinated ethylene propylene films with covalently immobilized laminin oligopeptides YIGSR and IKVAV. II. *J Biomed Mater Res*. 29:779–85, 1995.
116. Bellamkonda R., Ranieri J. P., Aebischer P. Laminin oligopeptide derivatized agarose gels allow three dimensional neurite extension in vitro. *J Neurosci Res*. 41:501–9, 1995.
117. Hubbell J. A., Massia S. P., Desai N. P., Drumheller P. D. Endothelial cell-selective materials for tissue engineering in the vascular graft via a new receptor. *Biotechnology*. 9:568–72, 1991
118. Panitch A., Yamaoka T., Fournier M. J., Mason T. L., Tirrell D. A. Design and biosynthesis of elastin-like artificial extracellular matrix proteins containing periodically spaced fibronectin CS5 domains. *Macromolecules*. 32:1701–3, 1999.
119. Schense J. C., Bloch J., Aebischer P., Hubbell J. A. Enzymatic incorporation of bioactive peptides into fibrin matrices enhances neurite extension. *Nature Biotech*. 18:415–9, 2000.
120. Kam L., Shain W., Turner J. N., Bizios R. Selective adhesion of astrocytes to surfaces modified with immobilized peptides. *Biomaterials*. 23:511–5, 2002.
121. Rezanian A., Healy K. E. Biomimetic peptide surfaces that regulate adhesion, spreading, cytoskeletal organization, and mineralization of the matrix deposited by osteoblast-like cells. *Biotechnol Prog*. 15:19–32, 1999.
122. Rezanian A., Healy K. E. Biomimetic peptide surfaces that regulate adhesion, spreading, cytoskeletal organization, and mineralization of the matrix deposited

- by osteoblast-like cells. *Biotechnol Prog.* 15:19–32, 1999.
123. Suzuki Y., Tanihara M., Suzuki K., Saitou A., Sufan W., Nishimura Y. Alginate hydrogel linked with synthetic oligopeptide derived from BMP-2 allows ectopic osteoinduction in vivo. *J Biomed Mater Res.* 50:405–9, 2000.
124. West J. L., Hubbell J. A. Polymeric biomaterials with degradation sites for proteases involved in cell migration. *Macromolecules.* 32:241–4, 1999.
125. Mann B. K., Gobin A. S., Tsai A. T., Schmedlen R. H., West J. L. Smooth muscle cell growth in photopolymerized hydrogels with cell adhesive and proteolytically degradable domains: synthetic ECM analogs for tissue engineering. *Biomaterials.* 22: 3045–51, 2001.
126. Bunge M. B. Bridging areas of injury in the spinal cord. *Neuroscientist.* 7(4): 325-339, 2001.
127. Geller H. M., Fawcett J. W. Building a bridge: engineering spinal cord repair. *Exp Neurol.* 174(2): 125-136, 2002.
128. Alexander M., Bendas G. The Role of Adhesion Receptors in Melanoma Metastasis and Therapeutic Intervention Thereof, *Research on Melanoma - A Glimpse into Current Directions and Future Trends*, Prof. Mandi Murph (Ed.), 2011.
129. Blesch A., Lu P., Tuszynski M. H. Neurotrophic factors, gene therapy, and neural stem cells for spinal cord repair. *Brain Res Bull.* 57(6): 833-838, 2002.
130. Lundborg G. A 25-year perspective of peripheral nerve surgery: evolving neuroscientific concepts and clinical significance. *J Hand Surg.* 25(3): 391-414, 2005.
131. Terenghi G. Peripheral nerve regeneration and neurotrophic factors. *J Anat.* 194(1): 1-14, 1999.
132. Cavalcanti-Adam E. A., Shapiro I. M., Composto R. J., Macarak E. J., Adams, C.

- S. RGD peptides immobilized on a mechanically deformable surface promote osteoblast differentiation. *J Bone Miner Res.* 17(12): 2130-2140, 2002.
133. Cao X., Schoichet M. S. Delivering neuroactive molecules from biodegradable microspheres for application in central nervous system disorders. *Biomaterials.* 20(4): 329-339, 1999.
134. Maysinger D., Krieglstein K., Filipovic-Grcic J., Sendtner M., Unsicker K., Richardson P. Microencapsulated ciliary neurotrophic factor: physical properties and biological activities. *Exp Neurol.* 138(2): 177-188, 1996.
135. Berry M., Barrett L., Seymour L., Baird A., and Logan A. Gene therapy for central nervous system repair. *Curr Opin Mol Ther.* 3(4): 338-349, 2001.
136. Hermens W. T., Verhaagen J. Viral vectors, tools for gene transfer in the nervous system. *Prog Neurobiol.* 55(4): 399-432, 1998.
137. Smith G. M., Romero M. I. Adenoviral-mediated gene transfer to enhance neuronal survival, growth, and regeneration. *J Neurosci Res.* 55(2): 147-157, 1999.
138. Prabhakaran M. P., Venugopal J., Chan C. K., Ramakrishna S. Surface modified electrospun nanofibrous scaffolds for nerve tissue engineering. *Nanotechnology.* 19(45): 1-8, 2008.
139. Ueyama Y., Ishikawa K., Mano T., Koyama T., Nagatsuka H., Suzuki K., Ryoike K. Usefulness as guided bone regeneration membrane of the alginate membrane. *Biomaterials.* 23(9):2027-2033, 2002
140. Sarker B., Singh R., Silva R., Roether J. A., Kaschta J., Detsch R., Schubert D. W., Cicha I., Boccaccini A. R. Evaluation of fibroblasts adhesion and proliferation on alginate-gelatin crosslinked hydrogel. *PLoS One.* 9(9): e107952, 2014.
141. Khanna O., Larson J. C., Moya M. L., Opara E.C., Brey E. M. Generation of

- alginate microspheres for biomedical applications. *J Vis Exp.* (66). pii: 3388, 2012.
142. Hariyadi D. M., Lin S. C., Wang Y., Bostrom T., Turner M. S., Bhandari B., Coombes A. G. Diffusion loading and drug delivery characteristics of alginate gel microparticles produced by a novel impinging aerosols method. *J Drug Target.* 18(10):831-41, 2010.
143. Hariyadi D. M., Wang Y., Lin S. C., Bostrom T., Bhandari B., Coombes A. G. Novel alginate gel microspheres produced by impinging aerosols for oral delivery of proteins. *J Microencapsul.* 29(3):250-261, 2012.
144. Kataoka K., Suzuki Y., Kitada M., Ohnishi K., Suzuki K., Tanihara M., Ide C., Endo K., Nishimura Y. Alginate, a bioresorbable material derived from brown seaweed, enhances elongation of amputated axons of spinal cord in infant rats. *J Biomed Mater Res.* 54(3):373-84, 2001.
145. Hegge A. B., Andersen T., Melvik J. E., Bruzell E., Kristensen S., Tønnesen H. H. Formulation and bacterial phototoxicity of curcumin loaded alginate foams for wound treatment applications: studies on curcumin and curcuminoides XLII. *J Pharm Sci.* 100(1):174-85, 2011.
146. Qin Y. Ion-Exchange Properties of Alginate Fibers. *Textile Res J.* 75:165-168, 2005.
147. Le Y., Anand S. C., Horrocks A, R. Using alginate fiber as drug carrier for wound dressing, in *Medical Textiles '96*. Woodhead Publishing, Cambridge, 1997.
148. Fan L., Du Y., Huang R., Wang Q., Wang H., Zhang L. Preparation and characterisation of alginate/gelatin blend fibers. *J Appl Polym Sci* 96:1625 (2005).
149. Kobayashi Y., Matsuo R., Ohya T., Yokoi N., Enzyme-entrapping behaviours in alginate fibers and their papers. *Biotechnol Bioeng.* 30:451, 1987.

150. Sun J., Tan H. Alginate-based biomaterials for regenerative medicine applications. *Materials*. 6:1285-1309, 2013.
151. Mosahebi A., Wiberg M., Terenghi G. Addition of fibronectin to alginate matrix improves peripheral nerve regeneration in tissue-engineered conduits. *Tissue Eng.* 9(2):209-18, 2003.
152. Dhoot N. O., Tobias C. A., Fischer I., Wheatley M. A. Peptide-modified alginate surfaces as a growth permissive substrate for neurite outgrowth. *Biomed Mater Res A*. 71A(2):191-2004.
153. Prang P., Müller R., Eljaouhari A., Heckmann K., Kunz W., Weber T., Faber C., Vroemen M., Bogdahn U., Weidner N. The promotion of oriented axonal regrowth in the injured spinal cord by alginate-based anisotropic capillary hydrogels. *Biomaterials*. 27(19):3560-3569, 2006.
154. Drury, J. L., Mooney, D. J. Hydrogels for tissue engineering: scaffold design variables and applications. *Biomaterials*. 24:4337–4351, 2003.
155. Smith P. K., Krohn R. I., Hermanson G. T., Mallia A. K., Gartner F. H., Provenzano M. D., Fujimoto E. K., Goeke N. M., Olson B. J., Klenk D. C. Measurement of protein using bicinchoninic acid. *Anal. Biochem.* 150(1):76–85, 1985.
156. Olson B. J., Markwell J. Assays for determination of protein concentration. *Curr Protoc Protein Sci*. Chapter 3: Unit 3.4, 2007.
157. IUPAC, Compendium of Chemical Terminology, 2nd ed. (the "Gold Book") (1997). Online corrected version: (2006–) "modulus of elasticity (Young's modulus), E".
158. Kononen M., Hormia M., Kivilahti J., Haotaniemi J., Theless I. Effect of surface processing on the attachment, orientation, and proliferation of human gingival fibroblasts on titanium. *J Biomed Mater Res*. 26:1325–41, 1992.

159. Schwartz Z., Martin J. Y., Daen D. D., Simpson J., Cochran D. L., Boyan B. D. Effect of titanium surface roughness on chondrocyte proliferation, matrix production, and differentiation depends on the state of cell maturation. *J Biomed Mater Res.* 30:145–55, 1996.
160. Draget K., Myhre S., Skjak-Break G, Ostgaard K. Regeneration, cultivation and differentiation of plant protoplasts immobilized in Ca-alginate beads. *J Plant Physiol.* 132:552-6, 1988.
161. Wong M., Siegrist M., Wang X., Hunziker E. Development of mechanically stable alginate/chondrocyte constructs: effects of guluronic acid content and matrix synthesis. *J Orthop Res.* 19(3):493-9, 2001.
162. Bohari S. P., Hukins D. W., Grover L. M. Effect of calcium alginate concentration on viability and proliferation of encapsulated fibroblasts. *Biomed Mater Eng.* 21(3):159-70, 2011.
163. Kong H. J., Smith M. K., Mooney D. J. Designing alginate hydrogels to maintain viability of immobilized cells, *Biomaterials.* 24(22): 4023–4029, 2003.
164. Kononen M., Hormia M., Kivilahti J., Haotaniemi J., Theless I. Effect of surface processing on the attachment, orientation, and proliferation of human gingival fibroblasts on titanium. *J Biomed Mater Res.* 26:1325–41, 1992.
165. Boyan B. D., Hummert T. W., Daen D. D., Schwartz Z. Role of material surfaces in regulating bone and cartilage cell response. *Biomaterials.* 17:137–46, 1996.
166. Schwartz Z., Martin J. Y., Daen D. D., Simpson J., Cochran D. L., Boyan B. D. Effect of titanium surface roughness on chondrocyte proliferation, matrix production, and differentiation depends on the state of cell maturation. *J Biomed Mater Res.* 30:145–55, 1996.
167. Pan J., Liao H., Leygraf C., Thierry D., Li J. Variation of oxide films on titanium induced by osteoblast-like the cell culture and the influence of an H₂O₂

- pretreatment. *J Biomed Mater Res.* 40:244–56, 1998.
168. Curtis A., Wilkinson C. Topographical control of cells. *Biomaterials.* 18(24):1573-1583, 1997.
169. Boby J. D., Wilson G. J., MacGregor D. C., Pilliar R. M., Weatherly G. C. Effect of pore size on the peel strength of attachment of fibrous tissue to porous-surfaced implants. *J Biomed Mater Res.* 16(5):571-84, 1982.
170. Pilliar R. M. Powder metal-made orthopedic implants with porous surface for fixation by tissue ingrowth. *Clin Orthop Relat Res.* 176:42-51, 1983.
171. Zhang M. *Biomaterials and Tissue Engineering – Biocompatibility of Materials.* Shi D. (Ed.), Berlin ; New York : Springer-Verlag Berlin Heidelberg, 2004.
172. Wen X., Wang X., Zhang N. Microrough surface of metallic biomaterials: a literature review. *Biomed Mater Eng.* 6(3):173-189, 1996.
173. Borenstein J. T., Weinberg E. J., Orrick B. K., Sundback C., Kaazempur-Mofrad MR, Vacanti JP. Microfabrication of three-dimensional engineered scaffolds. *Tissue Eng.* 13(8):1837-44, 2007.
174. Yang J, Shi G., Bei J., Wang S., Cao Y., Shang Q., Yang G., and Wang W. Fabrication and surface modification of macroporous poly(L-lactic acid) and poly(L-lactic co-glycolic acid) (70/30) cell scaffolds for human skin fibroblasts cell culture. *J Biomed Mater Res.* 62, 438-446, 2002.
175. Ashman A., and Moss M. L. Implantation of porous polymethylmethacrylate resin for tooth and bone replacement. *J Prosthe Dent.* 37, 657-665, 1977.
176. Jones J. R., Poologasundarampillai G., Atwood R. C., Bernard D., and Lee P. D. Non-destructive quantitative 3D analysis for the optimisation of tissue scaffolds. *Biomaterials.* 28, 1404-1413, 2007.
177. deGroot J. H., de Vrijer R., Pennings A. J., Klomp maker J., Veth R. P. H., and Jansen H. W. B. Use of porous polyurethanes for meniscal reconstruction and

- meniscal prostheses. *Biomaterials*. 17, 163-173, 1996.
178. Yannas I. V., Lee E., Orgill D. P., Skrabut E. M., Murphy G. F. Synthesis and characterisation of a model extracellular matrix that induces partial regeneration of adult mammalian skin. *Proc Natl Acad Sci USA*. 86, 933-937, 1989.
179. O'Brien F. J., Harley B. A., Yannas I. V., Gibson L. J. The effect of pore size on cell-adhesion in collagen-GAG scaffolds. *Biomaterials*. 26, 433-441, 2005.
180. Zeltinger J., Sherwood, J. K., Graham, D. A., Mueller, R., Griffith L. G. Effect of pore size and void fraction on cellular adhesion, proliferation, and matrix deposition. *Tissue Eng*. 7, 557-572, 2001.
181. Salem A. K., Stevens R., Pearson R. G., Davies M. C., Tendler S. J. and Roberts C. J. Interactions of 3T3 fibroblasts and endothelial cells with defined pore features. *J Biomed Mater Res*. 61, 212-217, 2002.
182. Lee J., Cuddihy M. J., Kotov N. A. Three-dimensional cell culture matrices: state of the art. *Tissue Eng Part B Rev*. (14): 61-86, 2008.
183. Zhong S. P., Zhang Y. Z., Lim C. T. Fabrication of large pores in electrospun nanofibrous scaffolds for cellular infiltration: A review. *Tissue Eng Part B Rev*. (in press)
184. Rnjak-Kovacina J., Weiss A. S. Increasing the pore size of electrospun scaffolds. *Tissue Eng Part B Rev*. (17): 365-372, 2011.
185. Tai H., Mather M. L., Howard D., Wang W., White L. J., Crowe J. A., Morgan S. P., Chandra A., Williams D. J., Howdle S. M., Shakesheff K. M. Control of pore size and structure of tissue engineering scaffolds produced by supercritical fluid processing. *Eur Cell Mater*. 14:64-77, 2007.
186. Borenstein J. T., Weinberg E. J., Orrick B. K., Sundback C., Kaazempur-Mofrad MR, Vacanti JP. Microfabrication of three-dimensional engineered scaffolds. *Tissue Eng*. 13(8):1837-44, 2007.

187. Moroni L., de Wijn J. R., van Blitterswijk C. A. Integrating novel technologies to fabricate smart scaffolds. *J Biomater Sci Polym Ed.* 19(5):543-572, 2008.
188. Zohora F. J., Azim A. Y. M. A. Biomaterials as porous scaffolds for tissue engineering applications: A review. *ESJ.* 10(21):186-209, 2014.
189. Ramalingam M., Jabbari E., Ramakrishna S., Khademhosseini A. *Micro and Nanotechnologies in Engineering Stem Cells and Tissues.* Wiley-IEEE Press, New Jersey, 2013
190. Nam J., Huang Y., Agarwal S., Lannutti J. Improved cellular infiltration in electrospun fiber via engineered porosity. *Tissue Eng.* 13, 2249, 2007.
191. Yang J, Shi G., Bei J., Wang S., Cao Y., Shang Q., Yang G., Wang W. Fabrication and surface modification of macroporous poly(L-lactic acid) and poly(L-lactic co-glycolic acid) (70/30) cell scaffolds for human skin fibroblasts cell culture. *J Biomed Mater Res.* 62, 438-446, 2002.
192. Ashman A., Moss M. L. Implantation of porous polymethylmethacrylate resin for tooth and bone replacement. *J Prosthe Dent.* 37, 657-665, 1977.
193. Ma P. X., Choi J. W. Biodegradable polymer scaffolds with well-defined interconnected spherical pore network. *Tissue Eng.* 7(1):23-33, 2001.
194. Jones J. R., Gentleman E., Polak J. Bioactive glass scaffolds for bone regeneration. *Elements* 3, 393-399, 2007.
195. Jones J. R., Poologasundarampillai G., Atwood R. C., Bernard D., Lee P. D. Non-destructive quantitative 3D analysis for the optimisation of tissue scaffolds. *Biomaterials.* 28, 1404-1413, 2007.
196. Soliman S., Pagliari S., Rinaldi A., Forte G., Fiaccavento R., Pagliari F. Multiscale three-dimensional scaffolds for soft tissue engineering via multimodal electrospinning. *Acta Biomater* 6, 1227, 2010.
197. Partap S., Muthutantri A., Rehman I. U, Davis G. R., Darr J. A. Preparation and

- characterisation of controlled porosity alginate hydrogels made via a simultaneous micelle templating and internal gelation process. *J Mater Sci.* (42): 3502-3507, 2007.
198. Klein J., Stock J., Vorlop K. -D. Pore size and properties of spherical Ca-alginate biocatalysts. *Eur J Appl Microbiol Biotechnol.* 18: 86-91, 1983.
199. Simidsrod O. Molecular basis for some physical properties of alginates in the gel state. *Faraday Disc Chem Soc.* 57: 263-267, 1974.
200. Martinsen A. Alginate as immobilization material: III. Diffusional Properties. *Biotechnol Bioeng.* 36: 186-194, 1992.
201. de Vos P., Faas M. M., Strand B., Calafiore R. Alginate-based microcapsules for immunoisolation of pancreatic islets. *Biomaterials.* (27): 5603-5617, 2006.
202. Rowley J. A., Madlambayan G., Mooney D. J.: Alginate hydrogels as synthetic extracellular matrix materials. *Biomaterials.* 20(1):45-53, 1999.
203. Nuttelman C. R., Mortisen D. J., Henry S. M., Anseth K. S. Attachment of fibronectin to poly(vinyl alcohol) hydrogels promotes NIH3T3 cell adhesion, proliferation and migration. *J Biomed Mater Res.* 57: 217-223, 2001.
204. Zhang Y., Ouyang H., Lim C. T., Ramakrishna S., Huang Z. M. Electrospinning of gelatin fibers and gelatin/PCL composite fibrous scaffolds. *J Biomed Mater Res Part B: Appl Biomater.* (72B): 156-165, 2005.
205. Brynda E., Houska M., Kysilka J., Prádný M., Lesný P., Jendelová P., Michálek J., Syková E. Surface modification of hydrogels based on poly(2-hydroxyethyl methacrylate) with extracellular matrix proteins. *J Mater Sci Mater Med.* (20): 909-915, 2009.
206. Wang Y., Wertheim D. F., Jones A. S., Chang H. I., Coombes A. G. Micro-CT analysis of matrix-type drug delivery devices and correlation with protein release behaviour. *J Pharm Sci.* 99(6): 2854-2862, 2010.

207. G2500® - Gelatin Product Information, Sigma-Aldrich Pty. Ltd.
208. Monici M. Cell and tissue autofluorescence research and diagnostic applications. *Biotechnol Ann Rev.* (11): 227-256, 2005.
209. Azar F. S., Intes X., editors, *Translational Multimodality Optical imaging*, Fred S. Azar, Siemens Corporate Research and Xavier Intes, Rensselaer Polytechnic Institute, (2008). p4-5
210. Lakowicz J. R. *Principles of fluorescence spectroscopy*. New York– London: Plenum Press, (1983). p342
211. Li M., Mondrinos M. J., Gandhi M. R., Ko F. K., Weiss A. S., Lelkes P. I. Electrospun protein fibers as matrices for tissue engineering. *Biomaterials* (26): 5999-6008, 2005.
212. Anderson S. O. Characterisation of a new type of cross-linkage in resilin, a rubber-like protein. *Biochim Biophys Acta.* (69): 249-262, 1963.
213. Young H. H. In: Herman F. M, Norbert M. B., Charles G. O., Georg M., Jacqueline I., editors. *Gelatin in encyclopedia of polymer science and engineering*, vol. 7. New York: Interscience., p446, 1967.
214. Liu W. G., Yao K. D., Wang G. C., Li H. X. Intrinsic fluorescence investigation on the change in conformation of cross-linked gelatin gel during volume phase transition. *Polymer* (41): 7589-7592, 2000.
215. Skjåk-Bræk G., Murano E., Paoletti S. Alginate as immobilization material. II: Determination of polyphenol contaminants by fluorescence spectroscopy, and evaluation of methods for their removal. *Biotechnol Bioeng.* (33): 90-94, 2004.
216. Le Gloahec V. C. E., Herter J. B. Method of treating seaweed. U.S. Patent 2,128,551. (1938).
217. Kuhlreiber W. M., Lanza R. P., Chick W. L., editors. In: *Cell encapsulation technology and therapeutics*. Publisher Birkhauser, Boston, p43, 1999.

218. Shinde U. A., Nagarsenker M. S. Characterisation of Gelatin-Sodium Alginate Complex Coacervation System. *Indian J Pharm Sci.* 71(3): 313–317, 2009.
219. Gelatin manufacturers institute of America (2012) Gelatin handbook – Physical & chemical properties [Online]. Available:
http://www.gelatin-gmia.com/images/GMIA_Gelatin_Manual_2012.pdf
[Accessed 1 January 2014]
220. Velings N. M., Mestdagh M. M. Protein adsorption in calcium alginate gel beads. *J. Bioactive Compatible Polym.* 9: 133–141, 1994.
221. O’Connell B. M., McGloughlin T. M., Walsh M. T. Factors that affect mass transport from drug eluting stents into the artery wall. *Biomed Eng Online.* 9: 15, 2010.
222. Fodor L. W. Tissue engineering and cell based therapies, from the bench to the clinic: The potential to replace, repair and regenerate. *Reprod Biol Endocrinol.* 1(102): 1-6, 2003.
223. Bryant S. J., Anseth K. S. The effects of scaffold thickness on tissue engineered cartilage in photocrosslinked poly(ethylene oxide) hydrogels. *Biomaterials.* 22(6):619-26, 2001
224. Kobayashi M., Hyu H. S. Development and Evaluation of Polyvinyl Alcohol-Hydrogels as an Artificial Articular Cartilage for Orthopedic Implants. *Materials.* 3(4): 2753-2771, 2010.
225. Elisseeff J., McIntosh W., Fu K., Blunk T., Langer R. Controlled-release of IGF-I and TGF-beta1 in a photopolymerizing hydrogel for cartilage tissue engineering. *J Orthop Res.* 19:1098– 1104, 2001.
226. Suh J. K., Matthew H. W. Application of chitosan-based polysaccharide biomaterials in cartilage tissue engineering: a review. *Biomaterials.* 21(24):2589-98, 2000.

227. Ahearne M., Yang Y., El Haj A. J., Then K. Y., Liu K. K. Characterizing the viscoelastic properties of thin hydrogel-based constructs for tissue engineering applications. *J R Soc Interface* 2005; 2:455-463.
228. Ghosh K. K., Ren X. D., Shu X. Z., Prestwich G. D., Clark R. A. F. Fibronectin functional domains coupled to hyaluronan stimulate adult human dermal fibroblast responses critical for wound healing. *Tissue Eng.* 12:601–613, 2006.
229. Black A. F, Bouez C., Perrier E., Schlotmann K., Chapuis F., Damour O. Optimization and characterisation of an engineered human skin equivalent. *Tissue Eng* 11:723-733, 2005.
230. Longo U. G., Lamberti A., Petrillo S., Maffulli N., Denaro V. Scaffolds in tendon tissue engineering. *Stem Cells Int.* 2012:517165, 2012.
231. Tabata Y., Hijikata S., Ikada Y. Enhanced vascularization and tissue granulation by basic fibroblast growth factor impregnated in gelatin hydrogels. *J Control Release.* 31:189–199, 1994.
232. Zusiak S. P., Pubill S., Ribeiro A., Leach J. B. Hydrolytically degradable poly(ethyleneglycol) hydrogel scaffolds as a cell delivery vehicle: characterisation of PC12 cell response. *Biotechnol Prog.* 29(5): 1255–1264, 2013.
233. Crompton, K.E., Goud, J.D., Bellamkonda, R.V., Gengenbach, T.R., Finkelstein, D.I., Horne, M.K., et al. Polylysine- functionalised thermoresponsive chitosan hydrogel for neural tissue engineering. *Biomaterials.* 28(3):441-499, 2007.
234. Itoh S., Takakuda K., Kawabata S., Aso Y., Kasai K., Itoh H., Shinomiya K. Evaluation of cross-linking procedures of collagen tubes used in peripheral nerve repair. *Biomaterials.* 23:4475–4481, 2002.

235. Matyash M., Despong F., Mandal R., Fiore D., Gelinsky M., Ikonomidou C. Novel soft alginate hydrogel strongly supports neurite growth and protects neurons against oxidative stress. *Tissue Eng Part A*. 18(1-2):55-66, 2012.
236. Nicodemus G. D., Bryant S. J. Cell encapsulation in biodegradable hydrogels for tissue. Engineering applications. *Tissue Eng Part B Rev*. 14(2): 149–165, 2008.
237. Lim F., Sun A. M. Microencapsulated islets as bioartificial endocrine pancreas. *Science*. 210(4472):908-910, 1980.
238. Maysinger D., Piccardo P., Filipovic-Grcic J., Cuello A. C. Microencapsulation of genetically engineered fibroblasts secreting nerve growth factor. *Neurochem Int*. 23(2):123-129, 1993.
239. Peirone M., Ross C. J. D., Horteland G., Brash J. L., Change P. L. Encapsulation of various recombinant mammalian cell types in different alginate microcapsules. *J Biomed Mater Res*. 42: 587–596, 1998.
240. Dojindo Molecular Technologies, Cellstain-Calcein-AM [Online image]. Retrieved June 21, 2015 from <http://www.dojindo.com/store/p/162-Cellstain-Calcein-AM-Solution.html>. Copyright © 2015 Dojindo Molecular Technologies, Inc.
241. Wulf E., Debohen A., Bautz F. A., Faulstich H., Wieland T. Fluorescent phallotoxin, a tool for the visualization of cellular actin. *Proc Natl Acad Sci U S A*. 76(9):4498-502, 1979.
242. Kron S. J., Toyoshima Y. Y., Uyeda T. Q., Spudich J. A. Assays for actin sliding movement over myosin-coated surfaces. *Methods Enzymol*. 196:399-416, 1991.
243. Wright C. S. Structural comparison of the two distinct sugar binding sites in wheat germ agglutinin isolectin II. *J Mol Biol*. 178(1):91-104, 1984.
244. Kapuściński J., Szer W. Interactions of 4', 6-diamidine-2-phenylindole with synthetic polynucleotides. *Nucleic Acids Res*. 6(11):3519-34, 1979.

245. Mosahebi A., Simon M., Wiberg M., Terenghi G. A novel use of alginate hydrogel as Schwann cell matrix. *Tissue Eng.* 7(5):525-34, 2001.
246. Genes N. G., Rowley J. A., Mooney D. J., Bonassar L. J. Effect of substrate mechanics on chondrocyte adhesion to modified alginate surfaces. *Arch Biochem Biophys.* 422(2):161-167, 2004.
247. Glicklis R., Shapiro L., Agbaria R., Merchuk J. C., Cohen S. Hepatocyte behaviour within three-dimensional porous alginate scaffolds. *Biotechnol Bioeng.* 67(3):344-53, 2000.
248. Van Osch G. J., Van Der Veen S. W., Burger E. H., Verwoerd-Verhoef H. L. Chondrogenic potential of in vitro multiplied rabbit perichondrium cells cultured in alginate beads in defined medium. *Tissue Eng.* 6(4):321-30, 2000.
249. Pattison S. T., Melrose J., Ghosh P., Taylor T. K. Regulation of gelatinase-A (MMP-2) production by ovine intervertebral disc nucleus pulposus cells grown in alginate bead culture by Transforming Growth Factor-beta(1) and insulin like growth factor-I. *Cell Biol Int.* 25(7):679-89, 2001.
250. Beck L., Damore P. A. Vascular development: Cellular and molecular regulation. *Faseb J.* 11:365-373, 1997.
251. Brogi E., Schatteman G., Wu T., Kim E. A., Varticovski L., Keyt B., Isner J. M. Hypoxia-induced paracrine regulation of vascular endothelial growth factor receptor expression. *J Clin Invest.* 97:469-476, 1996.
252. Puliafito A., Hufnagel L., Neveu P., Streichan S., Sigal A., Fygenon D. K., Shraiman B. I. Collective and single cell behaviour in epithelial contact inhibition. *Proc Natl Acad Sci U S A.* 109(3):739-44, 2012.
253. Heckman C. A. Contact inhibition revisited. *J Cell Physiol.* 220(3):574-5, 2009.

254. Hohn H. P., Grümmer R., Bosserhoff S., Graf-Lingnau S., Reuss B., Bäcker C., Denker H. W. The role of matrix contact and of cell-cell interactions in choriocarcinoma cell differentiation. *Eur J Cell Biol.* 69(1):76-85, 1996.
255. Cukierman E., Pankov R., Stevens D. R., Yamada K. M. Taking cell-matrix adhesions to the third dimension. *Science.* 294(5547):1708-1712, 2001.
256. Lin C. C., Anseth K. S. Cell-cell communication mimicry with poly(ethylene glycol) hydrogels for enhancing beta-cell function. *Proc Natl Acad Sci U S A.* 108(16):6380-6385, 2011.
257. Maia F. R., Lourenço A. H., Granja P. L., Gonçalves R. M., Barrias C. C. Effect of cell density on mesenchymal stem cells aggregation in RGD-alginate 3D matrices under osteoinductive conditions. *Macromol Biosci.* 14(6):759-71, 2014.
258. Maguire T., Davidovich A. E., Wallenstein E. J., Novik E., Sharma N., Pedersen H., Androulakis I. P., Schloss R., Yarmush M. Control of hepatic differentiation via cellular aggregation in an alginate microenvironment. *Biotechnol Bioeng.* 98(3):631-44, 2007.
259. Cao N., Chen X. B., Schreyer D. J. Influence of calcium ions on cell survival and proliferation in the context of an alginate hydrogel. *ISRN Chem. Eng.* 516461-516469, 2012.
260. Smidsrod O., Haug A., Larsen B. Degradation of alginate in the presence of reducing compounds. *Acta Chem Scand*, 17:2628–2637, 1963.
261. Donati I., Asaro F., Paoletti S. Experimental evidence of counterion affinity in alginates: the case of nongelling ion Mg^{2+} . *J Phys Chem B.* 113(39):12877-12886, 2009.
262. Smidsrød O., Skjåk-Braek G. Alginate as immobilization matrix for cells. *Trends Biotechnol.* 8(3):71-78, 1990.

263. Grimme J. M., Cropek D. M. Biomimetic sensors for rapid testing of water resources, state of the art in biosensors - environmental and medical applications, rinkin T. (Ed.), 2013. ISBN: 978-953-51-1035-4, InTech, DOI: 10.5772/52438.
Available from:
<http://www.intechopen.com/books/state-of-the-art-in-biosensors-environmental-and-medical-applications/biomimetic-sensors-for-rapid-testing-of-water-resources>
ON
264. Moore P. B., Dedman J. R. Calcium binding proteins and cellular regulation. *Life Sci.* 31(26):2937-2946, 1982.
265. Berridge M. J., Lipp P., Bootman M. D. The versatility and universality of calcium signalling. *Nat Rev Mol Cell Biol.* 1(1):11-21, 2000.
266. Rouzair-Dubois B., Dubois J. M. Calcium-dependent proliferation of NG108-15 neuroblastoma cells. *Gen Physiol Biophys.* 23(2):231-239, 2004.
267. Hunt N. C., Smith A. M., Gbureck U., Shelton R. M., Grover L. M. Encapsulation of fibroblasts causes accelerated alginate hydrogel degradation. *Acta Biomater.* 6(9):3649-3656, 2010.
268. Thevenot P., Nair A., Dey J., Yang J., and Tang L. Method to analyze three-dimensional cell distribution and infiltration in degradable scaffolds. *Tissue Eng Part C Methods.* 14(4): 319-331, 2008.
269. Dodla M. C., Mukhatyar V. and Bellamkonda R. "Peripheral nerve regeneration". *Principles of Regenerative medicine.* 2nd Edition. 1047-1062, 2010.
270. Fine E., Valentini R., Aebischer P. Nerve regeneration. In: *Principles of tissue engineering.* Lanza R. P., Langer R., Vacanti J. (Eds.) Academic Press. 785-797, 2000.
271. Yoshi. S., and Oka M., Collagen filaments as a scaffold for nerve regeneration. *J. Biomed. Mater. Res.* 56, 400-405, 2001.

272. Rangappa N., Romero A., Nelson K. D., Eberhart R. C. and Smith G. M.
Laminin coated poly(L-lactide) filaments induce robust neurite growth while providing directional orientation. *J. Biomed. Mater. Res.* 51, 625-634, 2000.
273. Yao L., O'Brien N., Windebank A. and Pandit A. Orienting neurite growth in electrospun fibrous neural conduits. *J. Biomed. Mater. Res. B Appl. Biomater.* 90, 483-491, 2009.
274. Lee J. Y., Bashur C. A., Goldstein A. S. and Schmidt C. E. Polypyrrole-coated electrospun PLGA nanofibers for neural tissue applications. *Biomaterials.* 30, 4325-4335, 2009.
275. Pfister L. A., Papaliozios M., Merkle H. P., Gander B. Hydrogel nerve conduits produced from alginate/chitosan complexes. *J Biomed Mater Res A.* 80(4):932-937, 2007.
276. Hashimoto T., Suzuki Y., Kitada M., Kataoka K., Wu S., Suzuki K., Endo K., Nishimura Y., Ide C. Peripheral nerve regeneration through alginate gel: analysis of early outgrowth and late increase in diameter of regenerating axons. *Exp Brain Res.* 146(3):356-368, 2002.
277. Bozkurt A., Brook G. A., Moellers S., Lassner F., Sellhaus B., Weis J., Woeltje M., Tank J., Beckmann C., Fuchs P., Damink L.O., Schügner F., Heschel I. Pallua N. In vitro assessment of axonal growth using dorsal root ganglia explants in a novel three-dimensional collagen matrix. *Tissue Eng.* 13, 2971-2979, 2007.
278. Pawar K., Mueller R., Caioni M., Prang P., Bogdahn U., Kunz W. Weidner N. Increasing capillary diameter and the incorporation of gelatin enhance axon outgrowth in alginate-based anisotropic hydrogels. *Acta Biomaterialia.* 7, 2826-2834, 2011.
279. Yuan Y., Zhang P., Yang Y., Wang X. Gu X. The interaction of Schwann cells with chitosan membranes and fibers in vitro. *Biomaterials.* 25, 4273-4278, 2004.

280. Herbert C. B., Nagaswami C., Bittner G. D., Hubbell J. A., Weisel J. W. Effects of fibrin micromorphology on neurite growth from dorsal root ganglia cultured in three-dimensional fibrin gels. *J Biomed Mater Res.* 40, 551-559, 1998.
281. Jurga M., Dainiak M. B., Sarnowska A., Jablonska A., Tripathi A., Plieva F. M., Savina I. N., Strojek L., Jungvid H., Kumar A., Lukomska B., Domanska-Janik K., Forraz N. McGuckin C. P. The performance of laminin-containing cryogel scaffolds in neural tissue regeneration. *Biomaterials.* 32, 3423-3434, 2011.
282. Wittmer C.R., Claudepierre T., Reber M., Wiedemann P., Garlick J. A., Kaplan D. Egles C. Multifunctionalized electrospun silk fibers promote axon regeneration in the central nervous system. *Adv Funct Mater.* 21, 4232–4242, 2011.
283. Karki R., Mariani M., Andreoli M., He S., Scambia G., Shahabi S., Ferlini C. β III-Tubulin: biomarker of taxane resistance or drug target? *Expert Opin Ther Targets.* 17(4):461-472, 2013.
284. Pawlizak S. Neurons and neuronal signalling (2009) [Online image]. Retrieved June 21, 2015 from <http://www.uni-leipzig.de/~pwm/web/?section=introduction&page=neurons>. Copyright 2009 © Soft Matter Physics Division, University of Leipzig.
285. Wood P. M., Bunge R. P. Myelination of cultured dorsal root ganglion neurons by oligodendrocytes obtained from adult rats. *J Neurol Sci.* 74(2-3):153-169, 1986.
286. Horie H., Kim S. U. Improved survival and differentiation of newborn and adult mouse neurons in F12 defined medium by fibronectin. *Brain Res.* 294(1):178-181, 1984.
287. Scott B. S. Adult mouse dorsal root ganglia neurons in cell culture. *J Neurobiol.* 8(5):417-427, 1977.
288. The University of Michigan. Learning modules - Medical gross anatomy spinal

- cord and spinal nerve (n.d.) [Online image]. Retrieved June 21, 2015 from http://www.med.umich.edu/lrc/coursepages/m1/anatomy2010/html/modules/spinal_cord_module/spinalcord_10.html. Copyright© 2002 The University of Michiga.
289. Lonza Walkersville, Inc. Rat dorsal root ganglion neurons (Instruction for use).
Source:
http://bio.lonza.com/uploads/tx_mwaxmarketingmaterial/Lonza_ManualsProductInstructions_Instructions_-_Rat_Neonatal_DRG_Neuronal_Cell_System.pdf.
290. Krantis A. (Lonza Walkersville, Inc.) Cryopreserved Rat Primary Dorsal Root Ganglion Cells: Simply Thaw and Culture. Source:
http://bio.lonza.com/fileadmin/groups/marketing/Mailings/2010/eNews/eNews_03/DRG_Cambrex.pdf.
291. Novikova L.N., Mosahebi A., Wiberg M., Terenghi G., Kellerth J.O., Novikov, L.N. Alginate hydrogel and matrigel as potential cell carriers for neurotransplantation. *J Biomed Mater Res A*. 77, 242-252, 2006.
292. De Beule P. A. A., Development of multidimensional fluorescence instrumentation for biomedical applications. Published PhD thesis, University of London, Imperial Collage London, United Kingdom. 2007.
293. IHC World Image Gallery. H&E stains of normal tissues (n.d.) [Online image]. Retrieved June 21, 2015 from <http://www.ihcworld.com/imagegallery/he-stain.htm>. Copyright © 2003-2011 IHC WORLD, LLC.
294. Life: The science of biology. 8th ed. Chapter 45: Sensory systems [Online image]. Retrieved June 21, 2015 from http://bcs.whfreeman.com/thelifewire8e/content/cat_010/f45021.jpg. Copyright © 2007 Sinauer Associates, Inc and W. H. Freeman & Co.

295. Zeng A., Xu H. The neuroprotection of brain-derived neurotrophic factor in experimental retinal detachment reattached. *Zhonghua Yan Ke Za Zhi.* 50(11):820-825, 2014.
296. Huang Y., Enzmann V., Ildstad S. T. Stem cell-based therapeutic applications in retinal degenerative diseases. *Stem Cell Rev.* 7(2):434-445, 2011.
297. Stieger K., Cronin T., Bennett J., Rolling F. Adeno-associated virus mediated gene therapy for retinal degenerative diseases. *Methods Mol Biol.* 807:179-218, 2011.
298. MacLaren R. E., Pearson R. A., MacNeil A., Douglas R. H., Salt T. E., Akimoto M., Swaroop A., Sowden J. C., Ali R. R. Retinal repair by transplantation of photoreceptor precursors. *Nature.* 444(7116):203-207, 2006.
299. Mizumoto H., Mizumoto K., Shatos M. A., Klassen H., Young M. J. Retinal transplantation of neural progenitor cells derived from the brain of GFP transgenic mice. *Vision Res.* 43(16):1699-1708, 2003.
300. Huhtala A., Pohjonen T., Salminen L., Salminen A., Kaarniranta K., Uusitalo H. In vitro biocompatibility of degradable biopolymers in cell line cultures from various ocular tissues: direct contact studies. *J Biomed Mater Res A.* 83(2):407-413, 2007.
301. Tomita M., Lavik E., Klassen H., Zahir T., Langer R., Young M. J. Biodegradable polymer composite grafts promote the survival and differentiation of retinal progenitor cells. *Stem Cells.* 23(10):1579-1588, 2005.
302. Redenti S., Neeley W. L., Rompani S., Saigal S., Yang J., Klassen H., Langer R., Young M. J. Engineering retinal progenitor cell and scrollable poly(glycerol-sebacate) composites for expansion and subretinal transplantation. *Biomaterials.* 30(20):3405-3414, 2009.
303. Redenti, S., Tao, S., Yang, J., Gu, P., Klassen, H., Saigal, S., Desai, T., Young,

- M.J. Retinal tissue engineering using mouse retinal progenitor cells and a novel biodegradable, thin-film poly(ϵ -caprolactone) nanowire scaffold. *J. Ocul. Biol. Dis. Infor.* 1:19-29, 2008.
304. Fan N., Huang N., Lam D. S., Leung C. K. Measurement of photoreceptor layer in glaucoma: a spectral-domain optical coherence tomography study. *J Ophthalmol.* 2011:264803, 2011.
305. Tan E., Ding X. Q., Saadi A., Agarwal N., Naash M. I., Al-Ubaidi M. R. Expression of cone-photoreceptor-specific antigens in a cell line derived from retinal tumors in transgenic mice. *Invest Ophthalmol Vis Sci.* 45(3):764-768, 2004.
306. Fu J. J., Shen W. Q., Bao J. S., Chen Q. L. The decontamination effects of gamma irradiation on the edible gelatin. *Radiat Phys & Chem.* 57(3-6): 345–348, 2000.
307. Karki R., Mariani M., Andreoli M., He S., Scambia G., Shahabi S., Ferlini C. β III-Tubulin: biomarker of taxane resistance or drug target? *Expert Opin Ther Targets.* 17(4):461-472, 2013.
308. ThermoScientific: alamarBlue™ Cell Viability Assay Reagent, Source: <http://www.piercenet.com/instructions/2162502.pdf>.
309. Structure of Hoechst dyes (September, 2011) [Online image]. Retrieved June 21, 2015 from https://en.wikipedia.org/wiki/Hoechst_stain. Copyright © 2011 CC0 1.0 Universal.
310. Wood J. P., Chidlow G., Tran T., Crowston J. G., Casson R. J. A comparison of differentiation protocols for RGC-5 cells. *Invest Ophthalmol Vis Sci.* 51(7):3774-3783, 2010.